Volodymyr G. TKACHENKO

is head of the Physical Metallurgy Department at the I.M. Frantsevich Institute for Problems of Materials Sciences of the NAS of Ukraine, Director of the International Center for Electronic Materials Science and Applied Problems of Airspace Technology (ICEMS), Academician of Ukrainian Academy of Sciences.

Dr. V.G. Tkachenko was graduated from Kyiv Polytechnic Institute in 1961 in metallurgical engineering and from Kyiv National University in 1970 in metal physics; received a ScD in solid state physics in 1982 from the Institute for Problems of Materials Science.

Author of 400 scientific publications, 21 patents (with co-workers), and 3 monographs. Member of the FEMS Society, EU. Ukrainian State Prize Laureate and NAS of Ukraine Prize Winner.

He is presently involved in the thermoactivation analysis of creep rate-controlling mechanisms in advanced rapid-hardened crystals and cluster-induced nanophase materials.

ВИДАВНИЧИЙ ДІМ АКАДЕМПЕРІОДИКА

V.G. TKACHENKO DISLOCATION MECHANISMS AND STRENGTHENING METHODS IN METAL CRYSTALS

V.G. TKACHENKO

DISLOCATION MECHANISMS AND STRENGTHENING METHODS IN METAL CRYSTALS

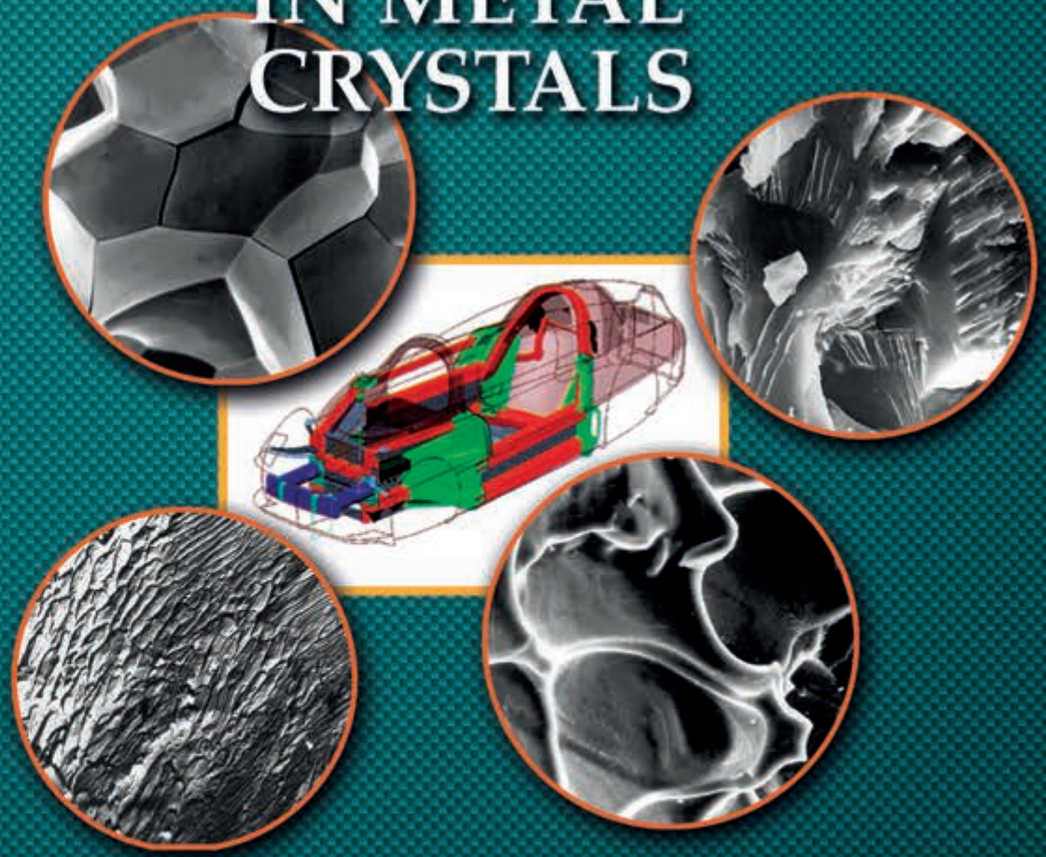

NATIONAL ACADEMY OF SCIENCES OF UKRAINE
I.M. FRANTSEVICH INSTITUTE FOR PROBLEMS
OF MATERIALS SCIENCES OF THE NAS OF UKRAINE

НАЦІОНАЛЬНА АКАДЕМІЯ НАУК УКРАЇНИ
ІНСТИТУТ ПРОБЛЕМ МАТЕРІАЛОЗНАВСТВА
ім. І.М. ФРАНЦЕВИЧА НАН УКРАЇНИ

В.Г. ТКАЧЕНКО

ДИСЛОКАЦІЙНІ МЕХАНІЗМИ ТА МЕТОДИ ЗМІЦНЕННЯ МЕТАЛЕВИХ КРИСТАЛІВ

ПРОЄКТ
«УКРАЇНСЬКА НАУКОВА КНИГА»
ІНОЗЕМНОЮ МОВОЮ

КИЇВ
АКАДЕМПЕРІОДИКА
2021

V.G. TKACHENKO

DISLOCATION MECHANISMS AND STRENGTHENING METHODS IN METAL CRYSTALS

PROJECT
«UKRAINIAN SCIENTIFIC BOOK»
IN A FOREIGN LANGUAGE

KYIV
AKADEMPERIODYKA
2021

https://doi.org/10.15407/akademperiodyka.439.298
UDC 669.018:539.21
T66

Reviewers:

O.I. DEKHTYAR,
Dr. Sci. (Phys. & Math.), Professor. G.V. Kurdyumov Institute
for Metal Physics of the NAS of Ukraine

M.V. KARPETS, Dr. Sci. (Phys. & Math.), Professor. I.M. Frantsevich
Institute for Problems of Materials Sciences of the NAS of Ukraine

The publication was funded within the framework of the Targeted Complex Program of the NAS of Ukraine "Scientific Bases of Functioning and Providing for Conditions for the Development of the Scientific and Publishing Complex of the NAS of Ukraine"

*Approved to press by the Scientific Council of I.M. Frantsevich Institute
for Problems of Materials Sciences of the NAS of Ukraine
(July 21, 2020, Protocol No. 4)*

Tkachenko V.G.

T66 Dislocation mechanisms and strengthening methods in metal crystals / V.G. Tkachenko; I.M. Frantsevich Institute for Problems of Materials Sciences of the NAS of Ukraine. — Kyiv: Akademperiodyka, 2021. — 298 p.

ISBN 978-966-360-439-8

The world advances in the fields of strength physics, physical metallurgy, and materials science are analyzed and summarized with the primary objective of exploring the potential of different dislocation strengthening mechanisms in rare earth and superlight metals, their ordered alloys, cluster-assembled nanophase, and rapid-hardening materials. Besides, the monograph aims to provide a vehicle for exchange and dissemination of basic ideas in the fields. The volume is intended for scientists, engineering, and technical workers specializing in solid state physics and physical metallurgy as well as for educational use by students and postgraduates of relevant specialties.

UDC 669.018:539.21

ISBN 978-966-360-439-8

CONTENTS

Section 2

RATE-CONTROLLING STRENGTHENING MECHANISMS

Section 3
EVOLUTION OF STRENGTH PHYSICS CONCEPT

Chapter 11 **NANOPHASE STRENGTHENING OF HEXAGONAL METAL ALLOY CRYSTALS**

Section 4

SCOPES OF STRUCTURAL APPLICATIONS FOR CRYSTALLINE MATERIALS

Chapter 12 **METAL MATRIX COMPOSITES**

PREFACE

In memory of Academician
Viktor I. TREFILOV

World Tendencies in Development of National Economies on Modern Technologies of Alloys

Currently automobile industries of the USA, Japan, and Western Europe are basic customers of cast Al-based alloys, including obtained by process engineering (die and squeeze casting) that appropriates needs of quantity production. Under the data [1], resistance to creep is one of the key factors limiting conditions of service of high temperature aluminum alloys of a new generation. The analysis of mechanisms of dimensional instability of Al-based alloys confirms expediency of development of more effective methods of heat treatment for dimensional stabilization of structural-homogeneous materials with a necessary combination of properties at increased temperatures (493-723 K). Over the last decade by anticipating rates the new approach has been developing at designing of parts and units of automobiles with taking into account a capability of increase in their micromechanical properties. Though Al saves the privileged position, the problem of a drop of automobile weight of the gains is still of large urgency. In this context, Mg and its light alloys are considered as perspective and competitive structural materials for use in modern areas of engineering due to their good foundry properties, so low cost of manufacturing from them of precision parts and units for automobile industry, commercial aviation, electronics engineering. Under the specific characteristics of strength Mg exceeds a number of new materials (on the basis of aluminium and steel) but requires increase of resistance to creep at least in the temperature interval 423-493 K.

Magnesium is the lightest metal used for structural applications. Due to its low density the specific strength and stiffness of the materials have been attractive to designers and magnesium alloys have historically been used in a number of high-performance aerospace structural applications. Improvements in properties and

castability (casting quality and complexity for thin walls) achieved by magnesium in the last 30 years make magnesium alloys a prime choice for further application within the aerospace industry. However, because of low (poor) corrosion resistance and formability at room temperature as well as the moderate mechanical properties compared to aluminum alloys having been improved the metal has not seen extensive use (market niches have decreased rather than increased).

The main reasons of slow introduction of advanced know-how and new sorts of magnesium alloys are high prices and insufficient reproducibility of their properties. To address these problems and increase the use of light magnesium alloys, the following important development work has been carried out by Lockheed and Allied Signal in North America, MEL/Metalloys/Shell in the United Kingdom, Norsk — Hydro/Pechiney in Europe (Norway, France).

Thereby, with appropriate protection techniques (high corrosion resistance) magnesium alloys offers the aerospace engineers a valuable material choice now and during the 21st century. As aerospace designers continue to strive for overall efficiencies and power system improved performance, the requirement is made for the manufacturers to reduce weight, improve elevated temperature properties, and provide more complex thin wall castings.

The demands on mechanical properties and temperature of application being satisfied the designers requirements for light high-performance alloys are ever increasing. To meet these demands, Magnesium Electron Ltd. (MEL) has developed a new family of alloys based upon the Mg—Y—Nd, RE system.

Two groups of structural magnesium alloys are being developed in industrial use to meet requirements for further developments of technical progress: (i) high creep-resistant, light and cheaper magnesium alloys for automobile, radio engineering and other dynamic applications; (ii) high-temperature-strength magnesium based alloys containing Y, Sc, RE as alloying elements for high-loaded parts applications in industrial use (aircrafts, helicopters, and automobile engines). Taking into consideration seller's prices for RE, which restrict their adoption in a mass production, aerospace, acoustician, and car designers are interested in development of lower cost, high creep-resistant and light structural materials in order to use them in dynamic applications where a low moment of inertia, good static stiffness and high resistance to deformation at evaluated temperatures are essential. In the present research the main attention is paid to magnesium alloys of the Mg—Al—Ca, X system of eutectic origin as well as to discontinuous nanoparticle-reinforced magnesium matrix composites produced by different routes of advanced processing. The evaluated temperature creep and strength properties should be significantly better than ones of the commercially available hcp MgAZ91D alloy with divorced eutectics (Dow Chemical Corp., USA). The various space programs, realized in the USA, present increased requirements to heat resistant Ti based alloys, which are concerned mainly with increase in the resistance to creep, stability against oxidation, and improvement of operating characteristics at working temperatures up to 873 K. So, on the basis of the

existing alloys such as Ti-6242S and Ti-1100, a number of their modifications are intended for compressors, units, systems of afterburning, exhaust pipelines, besides perspective as matrix high-temperature materials in chemical and petrochemical industry. Thus, the ability of metal materials and items to spontaneously changing the shape and size becomes a significant obstacle for maintenance of continuously growing requirements for accuracy and reliability of precise devices, machines, and optically precise designs. For many of them the dimensional instability should not exceed 10^{-6}-10^{-7} mm/mm.

New generation superlight alloys of the hcp Be—Al, Mg, Si system can be successfully used in precision aerospace navigational instrumentation such as gyroscope components requiring materials with high microyield strength and good dimensional stability as well as precision optical components for high quality metal optic mirrors with extremely high stiffness-to-weight ratio and thermal conductivity.

The market becomes opener to competition of novel consolidation processes, which ensure cost effective mass production or effective individual parts manufacture under improved quality standards with accelerated realization of the products. A significant amount of effort has been expended during the past decade to give detailed account of contributions to the field of advanced magnesium technology. The growing product quality requirements, especially in an automobile and aerospace industry, stimulate further searching for lighter and cheaper structural materials of a new generation ensuring an optimum combination macro- and micromechanical properties with allowance for the cost of their production.

The competitive global posture of automakers will increase if they can design and manufacture vehicles that offer greater consumer value. This could improve the nation's trade balance with countries producing more fuel-efficient vehicles than those produced in the world up to now. Health and environmental issues for workers are reduced during light metal casting operations, compared with such problems in ferrous foundries and polymer molding operations. The national laboratories will gain valuable manufacturing development and product application experience. They will gain an opportunity to develop math-based simulation models and technologies that benefit both the auto industry and technology programs.

Nanomaterials are cornerstones of nanoscience and nanotechnology. Nanostructure science and technology is a broad and interdisciplinary area of research and development activity which has been growing explosively worldwide in the past few years [2]. It has the potential for revolutionizing the ways on which materials and products are created and the range and nature of functionalities can be accessed. It is already having a significant commercial impact, which will assuredly increase in the future (Figure).

Nanotechnology has emerged as an important field of modern scientific research due to its diverse range of applications in the areas of electronic, material sciences, biomedical engineering, and medicine on the nanolevel such as energy science, optoelectronics, catalysis, chemical industries, light emitters, and other applications.

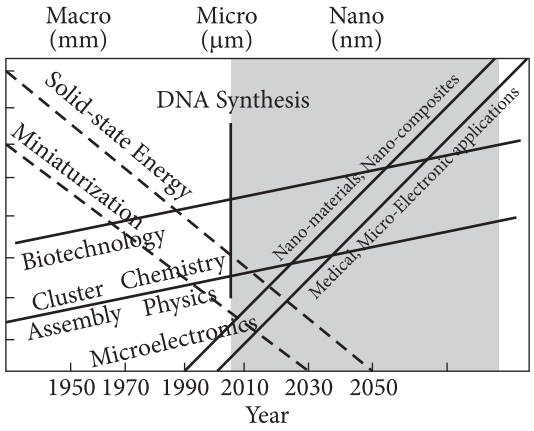

Evolution of science and technology in the future (adapted from Ref. [2])

The increased interest of designers and customers in development of light structural materials (on the basis of aluminum, magnesium, and titanium) intended for production of components, units and items in automobile, electron space, and other technical industries is stipulated by their attractive specific characteristics of strength and rigidity, and also other important advantages of metal alloys systems. However, to these materials and their items usually working below a macroscopic yield point in conditions of relaxation of stresses and cyclical loading, the preservation of dimensional stability is required, i.e. abilities to save the shape and sizes with specific accuracy under static and dynamic loads (change of temperature, vibrations, acceleration) or during long time of service (storage). The dimensional (structural) stability is usually characterized by a precision elasticity limit (σ_{PEL}) or microscopic yield stress (σ_{MYS}), resistance to microcreep or conditional limit of relaxations (σ_r), i.e. maximum level of stresses, which do not relax during hundreds and thousands of hours. Resistance to microplastic deformation (R_{MPD}) already for a long time issued for evaluation of quality of a number of major structural materials, for example, spring alloys. The R_{MPD} value determines the main working characteristics of items made of them (elastic elements).

Scope of Structural Applications for Crystalline Materials

At present, different research programs on strength physics are running in various highly-industrial countries. Research efforts have resulted in establishment of appropriate processing methods that improve the product performance. It is now generally accepted that less stressed components (chambers, turbochargers for diesel engine) are more likely to be introduced into the market in the near future. However, the application feasibility demonstration program has made very considerable progress. Main application problems for high stressed components with complicated shapes include component design, service life, reliability, and joining. On the other hand, component performance is strictly related to structural homogeneity and reproducibility of the material properties after processing as well as to material degradation during use (oxidation, sub-critical crack growth, etc.). This calls for a better understanding of the processes occurring during strength and microstructure formation.

The most important work in this respect is performed in the USA by Lange and Clarke, in the UK by Jack et al. and especially in Germany by Petzow and co-workers at Max Plank Institute in Stuttgart. Much information has been produced which is extremely useful in selecting proper compositional fields in a number of multicomponent systems with a view to improving the sintering capability or the material properties. Nevertheless, the severe limitations that often are encountered when making use of the above information should be pointed out. These are mainly related to: i) difficulty in realizing equilibrium conditions during the consolidation process; ii) composition changes occurring during sintering as a consequence of nitride volatilization; iii) the presence of various kinds of impurity elements which cannot be taken into full consideration when constructing equilibrium phase diagrams.

Therefore, it seems worthwhile to consider them as "behavioral" phase equilibrium diagrams which give an indication to the possible results that one may expect from the gross composition of the grain boundary phase in dense materials.

The value R_{MPD} determines the main working characteristics of the items made of them (elastic elements). The behavior of materials in he field of microyielding and resistance to plastic deformations are linked not only with dimensional stability, but also with such properties as mechanical hysteresis, resistance to fatigue fracture and wear. Nevertheless, assimilation in industrial scales of light structural materials and modernization of existing process engineering of their production frequently restrained in mainly because of origin dimensional (thermal or time) instability due to relaxation of elastic energy localized on structural defects and prices for the RE which are now used as strengthening components.

We would like to give only one example underlining vital importance of the actual problem of dimensional (structural) stabilization. As known, beryllium is rather promising material for optical industry and military engineering. The designers and developers of optical systems for the first time were interested in beryllium, possessing high rigidity and low density, after its successful use in gyroscopes to engineering and high-frequency navigational systems. However, in a number of cases beryllium even with high optical characteristics does not satisfy the new requirements for spatial optical systems with more rigid tolerances because of time instability due to constant deformation of mirror surface within several months. A number of mechanisms for explanation of an unstable behavior of Be mirrors is offered, however all attempts to remove undesirable properties have failed because of complexity of the problem. Moreover, the price and toxicity of Be alongside with its weak resistance to corrosion (in environment of chlorides), high coefficient and anisotropy of the thermal extension are the main shortages hindering it to broad use in modern engineering as a major structural material with a complex of unique properties.

The idea of gaining the technological market in this case contacts to creation of special methods and process engineering of dimensional (structural) stabilization of items on the basis of cheaper RE-free metal alloys combining high specific strength and low density with increased microyielding resistance (with a deformation

tolerance of 10^{-5}-10^{-6}) at short-term loads and high creep resistance at long-term loads and temperatures.

Taking into account connection of the dimensional stability with the alloy structure, the capability of preservation of an initial specific structure and related properties, i.e., stability of microstructure, becomes one of the major problems of physical material science, and capability of preservation of structural stability during the service life becomes fundamentals of further searching and perfecting mass production process of structural materials and items working in conditions of long service at increased temperatures and stresses below the macroscopic yield point.

The requirement of a high constancy of the sizes also stimulates developments of relaxation-stable materials with high microyielding resistance and creation on this basis of items with improved characteristics of dimensional stability (temperature and time).

Over the last fifty years or so, there has been a significant increase in our knowledge of the dislocation aspects of strength. Extensive fundamental research on high-temperature strength properties of promising metal alloy systems contributes to a much greater understanding of the microyield and creep processes from the atomistic viewpoint. The physical nature of dislocation movement produced by external stress in deformed solid solutions is a basic problem of a more comprehensive understanding of plastic strain in the pre-yield region of the load-elongation tensile curves. Such information can be obtained of the short-range obstacles which prevent the motion and of the means by which dislocations overcome these barriers. Current models concern largely the structural sensitivity and structure-related properties associated with long-range order. However, the coefficient of rate sensitivity, $m = \partial \ell n \sigma / \partial \ell n \dot{\varepsilon}$, can only be attributed to the long-range (athermal) internal stress τ_G [3], while the velocity of dislocations is controlled by the thermally activated short-range component τ^* of the applied stress.

Activation analysis of the known diffusion concepts shows dispersion of the data and proves the necessity of continuing the work involving more precise structure-sensitive measuring techniques for analyzing the activated diffusion of point defects and estimating bcc lattice in a wide range of temperatures to reveal the most probable mechanisms. In the monograph we try to review some recent trends and developments in the field of high-strength materials rather than to give a detailed description of the present state of the art and the way of its developing.

In this monograph, a brief review of original results and published literature data, current research in the field performed to analyze the known physical results and to assess their interpretation with an emphasis on elucidating the true dislocation mechanisms of pre-yield, plastic deformation and strengthening. Chemical dynamics and diffusion in solid-state crystalline structure is at present technology-oriented. For example, hydrogen migration in steels is followed by forming fixed traps in the lattice of so-called clusters.

Our work is dedicated to an in-depth understanding of the dislocation strengthening mechanisms and describing the means and strengthening methods for the existing and new developed alloys in the binary, ternary and quaternary metal systems including those with a cluster site-forming structure.

Presently and in future directions, generic programs for light metals will continue, with the emphasis, as in the past, on doing challenging work aimed at understanding mechanisms thus allowing science-based development of new materials.

Proper thermomechanical treatment of Zr_3Al based alloys having a substantially ordered $L1_2$ structure is found to provide the optimal combination of their unique strength and excellent ductility in a wide range of stresses and temperatures. In summary, atom, dislocation, and cluster physics is sure to have a potential for providing insight into the rate-controlling mechanisms responsible for further advances in metal crystal strengthening.

Acknowledgements. I am pleased to thank Prof. Arnuld Maeland (Norway, Energiteknikk Insitite*)*, Prof. Dr. Michail D. Hampton (USA, University of Central Florida), and President of International Magnesium Association Helmut Brandt (USA, Lunt Manufacturing Co. Inc.) for useful discussions. The author is indebted to Academician B.A. Movchan (Ukraine, Institute of Electric Welding), Prof. V.A. Tatarenko, Dr. A.I. Dekhtiar (Ukraine, Institute for Metal Physics), and Dr. V.F. Britun (Ukraine, Institute for Problems of Materials Science) for their continual interest in the problems considered.

I would like to thank my colleagues Dr. I.M. Maksymchuk, Dr. O.M. Malka, Dr. O.I. Kondrashev, Dr. P.M. Romanko, and Dr. V.S. Slyusareva for advancing throughout the course of this research by supplying the necessary materials, typing the manuscript, etc. at the Institute for Problems of Materials Science, NAS of Ukraine.

INTRODUCTION

Over the last fifty years, there has been a significant increase in our understanding of strengthening mechanisms and deformation behavior of metal crystals. An understanding of the basic concepts is aiding in the development of new high strength alloys with attractive combination of properties [4, 5]. The strengthening of metals and alloys is associated with impeding mobile dislocations by certain components of their microstructure. Understanding the effectiveness of many of these components has led to the development of reliable theories governing strengthening mechanisms [6, 7]. Since we are unable to calculate mechanical properties from first principles [8], the fundamental concepts serve as guidelines for alloy development and design is only based on experience.

In the present monograph, recent approach to alloy design of high-strength high-temperature zirconium and titanium alloys as well as high-strength low-density magnesium and aluminum alloys are discussed in terms of the fundamentals of strengthening mechanisms for solid solutions, precipitates, dispersoids and grain/subgrain boundary effects. A brief overview of the basic and applied research is given to explore the potential of strengthening mechanisms for metallic crystals with hcp, fcc, and bcc lattice.

Many theories of the structure of solid solutions provide relations between the mean square of displacements and the change in lattice parameter with composition [9, 10]. Considering the uncertainties in the parameters and the limitations of theoretical models, we found very few analytical treatments that show excellent agreement with experiment [11, 12]. Although the experiments provide a test of theories and confirm qualitative predictions, they tend to discredit the physical basis of pure elastic models for displacements in solid solutions. Attempts have been made through the years to improve the cognitive situation [13, 14]. Numerical experimental results have been reported [15, 16] but unfortunately many of them seem to be based on the athermal (long-range) mechanisms re-

sponsible for the structural sensitivity to an applied stress. Moreover, current models of long-term strength concern mainly structure-related effects and phenomena.

In any events, current theory does not appeal for microyield/creep resistance to evaluate the origin of the rate-controlling mechanisms. Therefore, it would be expedient to examine reliably the temperature variation of the thermal component τ^* of an applied stress and to compare the predictions with the experimental observations in terms of the short-range mechanisms responsible for the strain rate sensitivity to temperature variation of τ^*. Such an approach will contribute to providing more general insights into the dynamic resistance to the dislocation microyield in many aspects of long-term strength formation. Very few investigations of this type have made, and up to now none has been with polycrystalline magnesium and other hcp crystals.

We present a brief overview concerning the short-term and long-term strength properties of hcp, fcc and bcc metals and their binary, ternary and quaternary alloys with the objective of assess recent advances in materials science in terms of in-depth understanding of rate-controlling mechanisms (Fig. 1). The main purpose of the monograph is to explore the potential of different strengthening mechanisms needed for choice of chemical composition, development and application of a series of high temperature alloys having desirable combination of mechanical properties (strength, ductility, fracture toughness, etc.) during long-term service (Fig. 1).

Considerable experimental effort in the world is being expended on developing long-term strength of aluminum and magnesium alloys containing light elements and on improving structural materials made of them to operate in the transport (automobile, powertrain) industry at higher useful temperatures and larger stresses [17, 18]. For this reason, sound theoretical and thermoactivation analyses have been carried out to account for the fundamental characteristics of long-term strength and microyield (creep) resistance and to acquire a more complete understanding of the strain rate-controlling mechanisms [19, 20]. In order to use the better relaxation

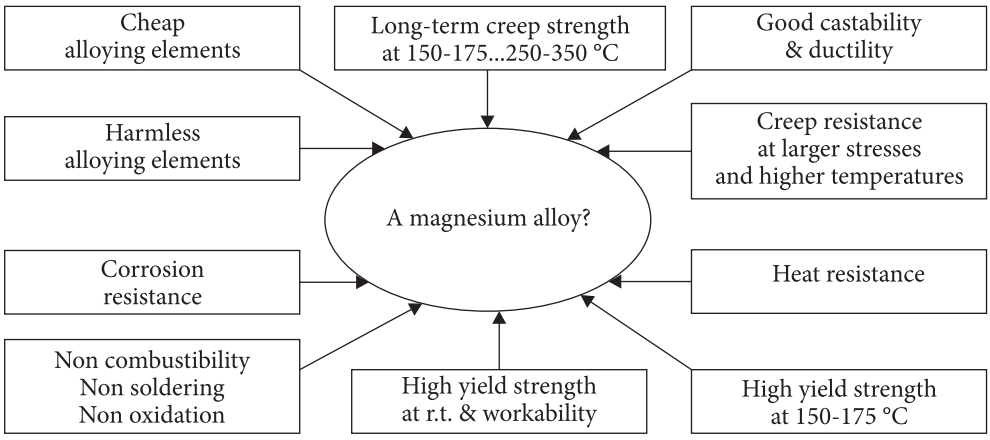

Fig. 1. Requirements for development and application of the best metal alloy systems

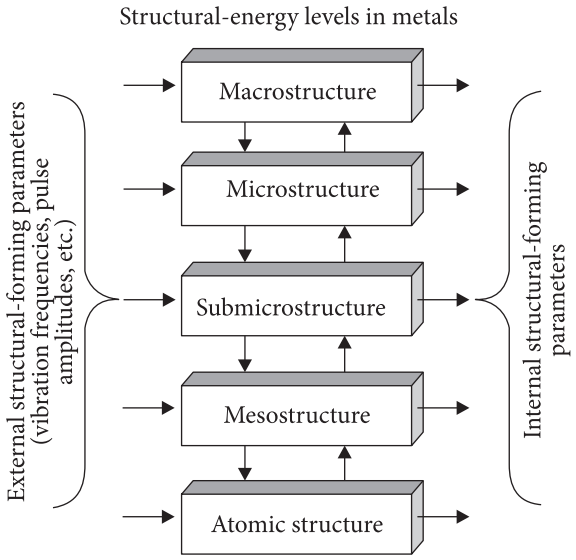

Fig. 2. Structural-energy levels in metals

strength properties of RE-containing and RE-free magnesium alloys, a family of die castable, creep-resistance and long-term strength experimental and industrial alloys is being developed for higher temperature dynamical applications where low moment of inertia, excellent stiffness and high resistance to time-dependent deformation are essential. The useful RE-effect in the expensive prototypes should be compensated by addition of alloying elements to the cheaper RE-free alloys. An ongoing study provides for development of new experimental alloys for various dynamic applications including high creep-resistant and light magnesium alloys for automobile industry, and high temperature-strength magnesium and aluminum based alloys, their particulate-reinforced composite materials for high-loaded parts in aviation and automobile production as well as magnesium-based alloys with improved damping characteristics and high sound quality in the audible range of 20 Hz to 35 kHz for driver and tweeter diaphragms production in radio engineering.

Research teams over the world have great potential to continue the work by using computer modeling, TEM, SEM, XRD examinations, Auger-electron and mechanical spectroscopy as well as all-the-round creep and short-term tensile tests [21-24]. Nevertheless, there is no faintest chance to develop further the conventional alloying methods. Their possibilities are exhausted completely, and for this reason, newly developed physicochemical principles of segregation alloying for so called immiscible systems should be required. The experimental data are presented in some detail and are discussed as thoroughly as possible.

There is an experimental correlation among the activation energies calculated at atomistic, mesoscopic, and microstructural levels (Fig. 2).

This argument implies, as proposed in [25], that all the processes are correlated phenomena. In particular, the dislocation creep and the amplitude dependence of internal friction (ADIF) are different aspects of the same phenomenon of microyielding attributed to dislocations. Besides, the study is concerned with analysis of inelastic, microyield and creep behavior of precise metal alloy systems below the macroscopic yield stress to reveal the processing — chemistry — structure — property relations responsible for dislocation resistance and strength.

The State-of-the-Art Research

Although the change in external shape is the only parameter available for the measurements of strain, it may always be equated with internal microscopic changes associated with dislocation motion. Thus, the parameter expansion by even one dislocation loop within a crystal constitutes of plastic strain may be spoken of as a manifestation of microscopic yielding or pre-yield "microyielding". The nature of the effect is examined in terms of the mechanisms involved in processes of tensile, compression and cyclic loading at stresses far below the upper yield stress. In the past, studies of microyielding phenomena were retarded by the lack of strain measuring techniques of adequate sensitivity. In recent years, however, new techniques have permitted a number of workers to make progress in the area. According to [20], the microplastic response of commercially available Mg, Al and Ti based alloys at low (room) temperatures depends strongly on the type of the dislocation substructure. In general, the greater number of mobile edge segments, the larger the plastic strain produced in the microstrain range. Under these conditions, the steep slope of the stress-microstrain curves of the systems, at low temperatures, could be interpreted in the terms of the dynamics of dislocation motion [26]. Apart from attempting to understand the dislocation mechanisms that control deformation, our interest in the microstrain region of the above alloys is motivated by its potential application in precision components and products. Knowledge of the stress levels which give rise to small permanent strains provides a useful measure of dimensional stability. In the case, the microscopic yield stress (σ_{MYS}) is defined as the stress required to cause a permanent strain of $2 \cdot 10^{-6}$ in./in.

Traditionally, one may expect poor creep resistance in small-grained materials according to the well-known $\dot{\varepsilon} - d^{-2}$ relationship [27]. Refinement of the grain structure and the absence of stable dispersoids result in poor creep resistance of Al and Mg based alloys at elevated temperatures [28]. For example, particles in the conventional Mg alloys AZ91 (nominal composition 9 mass% Al; 0.7 mass% Zn; 0.15 mass% Mn) are coarse (~0.5 μm) and have most likely weak effect on the creep behavior.

As reported in [29], the fine particles (about 10^{11} particles per mm^3, with a mean diameter of 0.05 μm) are very stable at 423K and pin the grain boundaries thus impeding dislocation motion inside the grain in improved Mg alloys. With the addition of calcium a high density of small stable dispersoids may be formed. Impeding the dislocation movement increases the creep resistance of Ca-added Mg alloys produced by rapid solidification. Although the alloy has a smaller grain size and hence from the above could be expected to show poor creep properties: the creep rate $\dot{\varepsilon}$ is 5 times smaller than that of the conventional Mg alloys AZ91. In the Mg alloys tested at temperatures from RT to 423 K there is observed a big difference in the creep resistance and stress relaxation depending on their microstructure [28] In some rapidly solidified Al-based alloys the creep resistance is good, due to fine particle pining grain boundaries and impeding dislocation movement as well [28]. The small stable

particles pin the grain boundaries making the advanced Mg and Al based alloys less sensitive to exposure to elevated temperatures.

Dislocation-impurity interaction in metal alloy systems includes the solute atmosphere formation round a moving dislocation, the effect of dragging and the appearance of Portevin-Le Chatelier's effects expected from solute atmosphere dragging at the dynamic deformation aging mode. Efforts are continually being made to improve fundamental understanding of their rate-controlling mechanisms.

Topical Problems in Strength Physics and Materials Science

Historically, the first principal difficulty in the theory of dislocations arose in attempts to explain the low macroscopic yield stress (σ_Y) of metals and the phenomenon of strain hardening. Moreover, in many cases it was not possible for a long time to smooth out the large discrepancy between microscopic theory and macroscopic observations. However, new results obtained in recent years [30] show such striking agreement with experimental data that the validity of the concept of a dislocation taken from the nature of a defect crystal structure is no longer in doubt. For example, the growth of crystals from vapour is associated with the presence of screw dislocations.

Traditionally, mechanical properties are associated with the initial structure, however, according to modern concepts, these properties are determined by the dynamic structure which is formed in the process of plastic deformation in a stress field (tension, creep, etc.). Under the thermodynamically nonequilibrium conditions, pressure, temperature and chemical potential become interconnected. Dislocation (homogeneous), cellular, cluster and nanosized structures are modifications of dissipative structures self-organized as a result of density fluctuations (atoms, dislocations, pair defects, and clusters). In particular, the cellular structure can be regarded as an energetically favorable distribution of dislocations, which is characteristic of intermediate dissipative structures that retain their dislocation sources of relaxation. Its further self-organization leads to a more ordered nanostructure. At the same time, it has been established that, in contrast to rather misoriented cell boundaries, which function as grain boundaries, the nanoboundaries do not obey the Hall-Petch barrier criterion based on the formation of dislocation pile-ups across boundaries. Coherent precipitates of phases as a result of the solid solution decomposition can be cut by mobile dislocations. Incoherent zones and particles are an exception in this respect. It is generally accepted that in this case dislocations bypass particles according to the Orowan athermal mechanism. However, at elevated temperatures and stresses below the Orowan stress, thermally activated bypass of solid particles and strong barriers (up to 2.0 Gb^3) by mobile dislocations is believed to be possible.

Hydrogen is known to diffuse as an interstitial element without any deviation from the classical (Arrhenius) behavior. According to [31], the published discussion considers the possibility of hydrogen capture by thermally equilibrium vacancies.

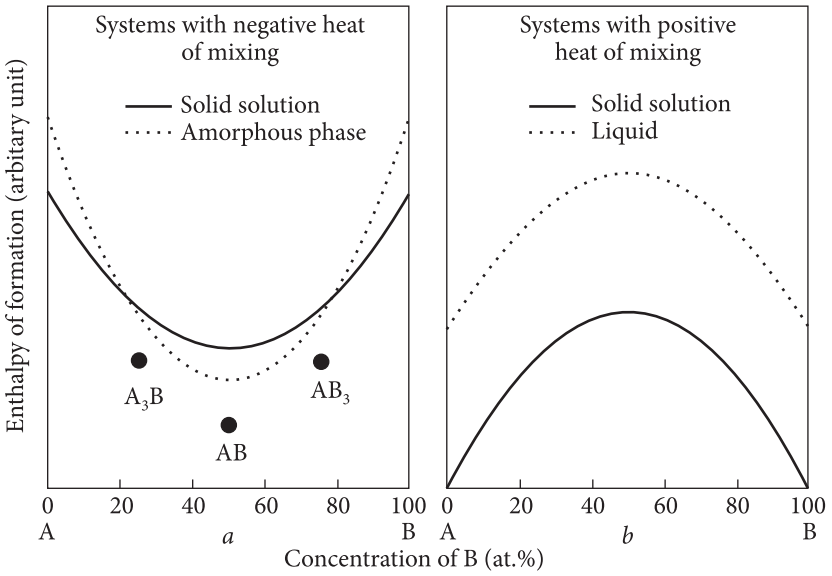

Fig. 3. Schematic diagrams of enthalpy of formation ΔH for A—B systems with negative heat of mixing *(a)* and positive heat of mixing *(b)* as a function of chemical composition at 300 K [33]

However, their concentration C is insignificant even at melting temperature T_m ($C \sim 10^{-4}$-10^{-5}). Nevertheless, in the stress field, mobile hydrogen atoms generate excess site vacancies, the concentration of which is several orders of magnitude higher than that of thermally equilibrium point defects. Elucidation of the role of these vacancies in the defect crystal structure requires additional data.

Identification of metal hardening mechanisms up to now remains one of the most important problems of dislocation theory [32]. Besides, the relative importance of thermally activated obstacles (solutes, dislocations of forest, jogs) and more strong barriers slowing down the movement of gliding dislocations are still subject to speculation. Nevertheless, they have fundamental differences in the following features: a) short-range obstacles can be overcome using thermal fluctuations; b) when dislocations move outside thermal fluctuations (at distances greater than 5-10 interatomic spacings), long-range (athermal) stresses become virtually independent of the rate, $\dot{\varepsilon}$, and deformation temperature, T_d. In the literature, researchers try to eliminate difficulties associated with interpretation of hardening mechanisms by identifying and classifying thermal obstacles and athermal barriers along the radius of interaction of dislocations. In this monograph, an attempt is made to separate the strengthening effects caused by the activation of short-range thermally activated mechanisms on the basis of a thermoactivation analysis concerning the dependence of the thermal component of the applied stress τ^* ($\dot{\varepsilon}$, T) on thermal obstacles. This approach opens up new possibilities for determining the thermal activation energy, a.e. U^*, effective activation volume, a.v., and other activation parameters.

There are two major points, which in the author opinion need clarifying. One of them is concerned with macroscopic changes in the strain responsible for the appearance of the Portevin-Le Chatelier effect and jerky flow. The other is related to the model calculations of the enthalpy formation for metal systems with negative and positive heat of mixing ΔH (Fig. 3). Metastable amorphous alloys with negative ΔH are defined by a free energy close to the free energy of equilibrium compounds (A_3B_2, AB_3) due to the existence of chemical and topological (short-range) order (Fig. 3, *a*). Clustering or other types of local structures (of short and middle order) remains unexplored (Fig. 3, *b*).

Physical Premises and Background

It is generally accepted that in physical metallurgy the mechanical properties are available with microstructure, chemistry, and processing methods of metal alloy systems and structural materials made of them. The properties appear now necessary to define the newly developed technologies of alloys and their metal matrix composites (MMC). The multicomponent alloys exhibit optimum strength due to commercial developments in practice. In particular, yield strength in excess over 500 MPa are fairly common and promising in production scale. Besides, light metal alloy systems, i.e., magnesium, aluminum and titanium based alloys, appear attractive for their potential of large scale economic production required for the development of their technological applications. Nevertheless, ductility and toughness tend to be unpredictable. In spite of numerical studies on the conventional alloys, there is still uncertainty as to the sources of ductility and toughness variations. Moreover, the main source of the rapid increase in the macroscopic yield stress in bcc metals and their interstitial solid solutions is still a matter of controversy as well, moreover in hcp crystals (Ti, Zr, H_f) impurity interstitials amplify the covalence of their bonds and cause an embrittlement of these metals. Despite the commercial developments in technical practice, it is only within the two-three last decades that fundamental studies of strength physics have been performed and analyzed [33]. The wealth of work that has been done in the past 10 years on atomistic and dislocation dynamic simulations in line with clean and clear experiments on strain localization via microstructural observations [34-36]. However, these research works bear a relation to the Portevin-Le Chatelier effect and serrated yielding near the yield point or above macroscopic flow stress. The sole subject of the discussion is an analysis of the yielding evolution as a macroscopic phenomenon in terms of strain rate sensitivity of flow stress connected with activation of long-range diffusion mechanism. As to the Portevin-Le Chatelier (PLC) effect, dynamic strain aging and serrated yielding a maximum stress drop $\Delta\sigma$ occurs near the ultimate stress during localized necking, just prior to fracture. This type of discontinuous and repeated yielding is commonly referred to as the PLC effect. However, it is not possible with the present evidence to explain rapid strengthening at stresses below macroscopic yield stress and microyield/creep strain which do not exceed 0.5% at long-term tests. In spite of

considerable research efforts over the past few years, the subject of the pinning dislocation effects in metals and alloys still requires clarification.

Although great amount of work has been done on creep deformation, creep strength and material properties of precipitate-hardening alloys, little has been reported on creep/microyield resistance and long-term strength of rapid-hardening alloys, and what has been reported is contradictory [37, 38]. Long-term strength of these metal alloy systems remains an unsolved problem, although limited progress has been achieved with their processing. Its clear-cut explanation, however, has not been given so far, because experimental results are insufficient to clarify the phenomenon of rapid strengthening.

Moreover, the Cottrell drag accounts satisfactorily for the enhanced resistance to the dislocation movement in the stress region of 10^{-5} cm/sec. With this provision, enrichment of the ordered atmosphere occurs by long-range diffusion, thereby increasing the dragging effect above the level predicted by Snoeck in terms of a short-range mechanism [39].

Because of the inherent difficulties in determining the concentration of vacancies by TEM [12], original experimental techniques should be developed to detect any systematic variation in the maximum vacancy concentration for different alloys with equivalent solute contents. Besides, from the experimental observations of clusters by TEM it is impossible to determine which solute atoms are most strongly bound to vacancies.

One of the basic questions concerning microplastic deformation of metal alloys below macroscopic yield stress is the mechanism of dislocation creep resistance at elevated temperatures. It would, therefore, be expedient to assess the creep resistance of rapid-hardening alloys, to specify the dislocation nature of their rate-controlling mechanisms and to resolve controversies and augments of the limited information available in the literature.

Structural analysis is aimed at characterizing the microstructure and micromechanical properties relations in eutectic alloys to be investigated with and without RE to compare them using compositional and microstructural data on their microyield and creep behavior at elevated temperatures of stabilization. It would be also expedient to investigate the physical nature of microyielding in the matrix (crystalline lattice), structural defects (grain and cell boundaries) and crystalline interfaces using thermoactivation analysis of pair defects, grain boundaries and eutectic phase relaxation as well as internal friction background after different processing.

At this stage Research Program aims to reveal the controlling mechanisms responsible for the creep rate in RE-free Mg, Al and Ti alloys on the basis of comparative structural and thermoactivation analyses of their solid solution (segregation), age-hardening (intermetallic), dispersion and grain boundary strengthening by additional alloying them. Although a small grain structure is believed to be undesirable for high temperature applications, the formation of nanoparticles along the grain boundaries at high temperature is expected to increase the dislocation creep resistance.

EXPERIMENTAL TECHNIQUES

For phase identification, XRD analysis was performed using a Siemens diffractometer with a CuK_{α} radiation. The phases were identified by comparing the experimentally determined 2θ values with those of the published standard diffraction data. Lattice parameter measurements were carried out using XRD procedures. The large diffuse background intensities of the XRD spectra can be explained by the existence of large number of vacancies or ordered atomic displacements in the interface region. Quantitative results were obtained after instrument calibration by using a pure Si standard specimen. Repeated measurements of the diffraction line positions resulted in an error of ±0.05 for 20 values. For a substitution solid solution, the lattice parameter exhibits an increasing tendency to reduce with increasing solute concentration.

The integral width of the diffraction peaks was used for evaluation of the mean size of the coherent diffraction domains and the microstrain in deformed specimens by the Williamson-Hall method [40]. The volume portion of the second phase was approximately estimated by the peak intensity comparison approach. Energy-dispersive X-ray spectrometry (EDX) was used for chemical microanalysis.

Microstructures of alloys obtained were characterized by employing scanning (SEM) and transmission (TEM) electron microscopy and analyzed by electron diffraction pattern evaluation. The volume fraction of second phase was determined by selected area diffraction (SAD) patterns taken from a selected area of 22 μm^2 by the movement of the selected area along the foil.

Electron diffraction shows Debye ring patterns due to the polycrystalline nature of the sample. Phase analysis was performed by comparing the theoretical electron diffraction patterns calculated by EMS with those experimentally obtained.

ESCA studies (N (E), E is the binding energy) and XRD patterns, in contrast to electron diffraction, did not reveal any lines

from the surface oxide layer. Generally, X-ray scattering in a material is much weaker than electron scattering. Accordingly, electrons do not penetrate deeply into a solid, which makes electron diffraction more sensitive to surfaces than XRD.

The density measurements by the Archimedes method were performed using methylene iodide as a liquid. A minimum of three meaningful measurements are considered to be an average value.

Thin foils for TEM examination were prepared by mechanical grinding and ion milling. Vickers microhardness was measured using 100 g load for 15 sec on polished sample surface to reduce variability. An analysis of variance was carried out to account for statistically significant differences in density and hardness values. The typical standard deviation was ± 0.02 g/cm^3 for density, and ± 9 for Vickers values. The particle size in the nm-range was revealed by high resolution electron microscopy using lattice contrast evidence.

Nanostructure in alloys subjected to severe plastic deformation [41] was formed by torsional deformation under a quasi hydrostatic pressure of 6 GPa with the true logarithmic strain to be 7. The sample structure was studied using a JEM-2000 EX transmission electron microscope with acceleration voltage of 200 kV, using SAGD pattern, bright field and dark field images. Nanocrystalline samples were prepared by an isothermal annealing of an amorphous ribbon below the conventional crystallization temperature using a scanning calorimeter (DSC-II, Perkin-Elmer) so that the annealing process stopped after the exothermal crystallization peak, i.e., complete crystallization. Electron probe compositional analysis of amorphous and crystallized samples indicates the overall composition preservation. Amorphous alloys with different chemical compositions were made by melt-quenching using a single roller melt-spinning apparatus.

Mechanical alloying has been recently used to synthesize a variety of inorganic solids including intermetallic compounds and composites. An advantage of this processing route is that synthesis of fairly high melting materials takes place at room temperature. Another advantage is that the structures generated are often nanocrystalline, with interesting properties.

The average nanograin size is measured by XRD in CuK_α radiation. To evaluate the effective grain size and the mean square strain, we used a double peak Warren-Averbach analysis based on determination of the X-ray diffraction line broadening. Herein rolled samples were continuously rotated during the measurement to decrease the effect of the deformation texture.

A relatively large uncertainty is expected to be due to the brooding diffraction lines because of small size of crystalline. The appearance of both a typical amorphous halo and the point reflection on the SAD patterns provides the evidence of the existence of a phase-mixture of amorphous and crystalline states in the structure. A mean crystallite size defined by dark field images is 10-30 nm.

The average nanoparticle size can be obtained by TEM and/or XRD analyses. Scanning probe microscopy was used to study the nanometer-scale morphological

changes in metal alloys. Average (mean) grain size in nanocrystals was determined using XRD approach, the so-called area-averaging Warren-Averbach method, from the mean coherent scattering length normal to the diffraction direction after removing instrumental broadening (with error about 25%).

Microhardness was determined by the Vickers method using a 0.5 N load applied for 30 sec. Each hardness value represents the average of 10 such measurements.

The effective elastic modulus was estimated on the basis of sound wave velocity measurements using a pulse-echo method of 5 MHz frequency. Velocities of longitudinal ($\nu_1 = \sqrt{c_1 / \rho}$) and transversal ($\nu_t = \sqrt{G / \rho}$) ultrasound ($10^5$ cm/sec) waves were measured. Here ρ is the sample density, c_1 is the longitudinal elastic modulus, and G is the shear elastic modulus. The direction of the wave propagation vector coincides with the vector parallel to the sample thickness. Isochronous annealing of the nm-crystallites was carried out at sequentially increasing temperatures.

Positron annihilation technique is a power and promising tool in the study of vacancy-sized defects in solids, and it was applied to examine the defective structure in cluster-forming and nanocrystalline metals and alloys. Since nano-sizes are much smaller than the mean diffusion way of positrons (~100 nm), positrons may diffuse rapidly across undistorted crystals into the interfaces to be trapped and annihilated with high probability. So, the positron lifetime and intensity reflect the volume and density of the interfacial defects. There are two types of defects including free-volume-size defects (point defects) and nanovoids (clusters of free volume) in the interface boundaries of nanostructured alloys [42]. Additionally, microgravimetry and positron annihilation are used to characterize the reduction of surface oxide layers and some impurities on ultrafine powder, if these effects are at least not revealed by TEM.

Section 1

FEATURES OF SUBSTRUCTURAL TRANSFORMATIONS IN METAL ALLOY SYSTEMS

The large-scale formalism of the entire set of formulas should not obscure the physical essence of phenomena.

Niels BOHR

Chapter

1 CLUSTER STRUCTURE OF A MELT

1.1. Physics of Liquid State: Modeling Clusters in Liquid Metals and Alloys

Existing experimental procedures for studying the structure of disordered systems can give averaged characteristics only. Therefore, to obtain detailed structural information, models are required to be constructed, which could describe the available data. There are a number of algorithms for simulation of atomic structure of liquid and amorphous metals based on evidence derived from diffraction experiments such as structure factors as well as atomic radial distribution functions. Using the experimental atomic pair correlation function, a modeling approach is suggested to reconstruct the structural state of a disordered system on the basis of diffraction evidence applied to liquid magnesium and aluminum [43]. Results obtained are consistent with the fact that clusters responsible for hcp- and fcc-like ordering exist in pure liquid metals (Fig. 1.1).

These crystal-like clusters combined in the distorted fcc structure are treated as nuclei of the fcc phase in liquid, then the result obtained suggests the existence of regions with crystal-like structure at temperatures close to the melting temperature, and the decrease in their concentration and sizes during heating.

Binary and liquid phases show strong ordering tendencies around their stoichiometric composition. In order to account for the strong ordering tendency in the liquid phase, the modified elastic and quasichemical models [44-48] consider the short-range ordering of nearest neighbor atoms in the liquid as liquid solutions. Such an approach gives a more realistic description of short-range ordering in liquid solutions, compared with the conventional simple random-mixing polynomial model. In the case, the energy of nearest-neighbour pair formation is expanded as a polynomial in the pair function instead of the component function of the previous model.

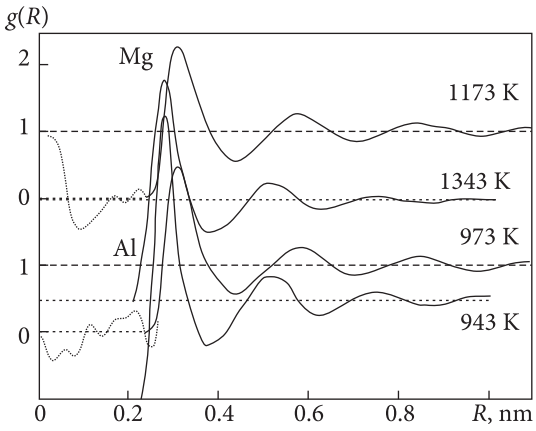

Fig. 1.1. Crystal-like liquid clusters in melts of pure metals [43]

Under certain kinetic and thermodynamic conditions, far from equilibrium, crystallization and melting of metal, semiconductor and ion crystals, by data from digital DTA (Fig. 1.2) are followed by forming self-organized nanosystems with a clusterized structure in mesoscopic areas below and above T_m (approximately by 30-60 K) [48].

Local (short-range) order is certain to arise if the number of short-range unlike atom pairs is greater than that in a random solution [44]. The existence of chemical short-range order in liquid alloys is also supported by neutron diffraction which is considered to be direct experimental evidence [45-47].

Additional research of non-equilibrium crystallization [49] shows that this phenomenon is quite common, connected to intensification of cooperative (dissipative) processes and instability of thermodynamic parameters. General concept of "in situ" diffusion nano-clustering of melt structures and their solid solutions is being developed, according to which a cluster should be considered as a source of crystal nuclei in matrix of eutectic alloy. Similar genetic structure of "liquid" and solid matrix clusters is confirmed not only by experimental data, but also by calculation of the cluster electron structure from the first principles with usage of ab-initio FLAPW method with full approach to cluster potential [50]. Size of primary nanoclusters calculated by the Frenkel-Hight method is in good agreement with data of mechanical spectroscopy. Besides, their size for Mg-1%Ba alloy melt reduces (from 4.7 nm to 1.5 nm) in the region of pre-

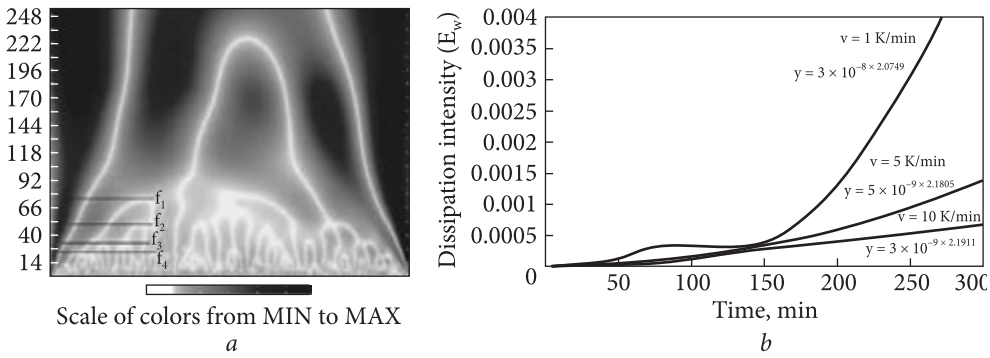

Fig. 1.2. Digital differential thermal analysis of Mg-1% Ba alloy melt: Wavelet-diagram of heat flows of premelting dissipation upon heating with a rate of 10 K/min (*a*) and change in intensity E_w of premelting dissipation processes in various kinetic modes (*b*) for nanocluster-induced premelting [48]

melting with increasing heat rate, but in the region of post-melting slightly increases (at 5 K/min). Process of structure nano-clustering is accelerated by introducing cluster-forming elements like Ba, Gd, Y to α-Mg and Al, especially with melting of alloys with restricted mutual component solubility in stationary dynamic modes of pre-melting with different kinetics of crystallization (1 K/min, 5 K/min, 10 K/min).

Process of nano-clustering is facilitated with imposition of weak magnetic and pulse electromagnetic fields (0.03-0.5 Tesla [51]). Formation of electron structure and coherent interfaces in nano-clusters (5-12 nm of size and $10^{10}/cm^2$ of density) [49, 52] causes effects of additional light-adsorption with higher quantum yield of photoemission, as well as solid-solution strengthening of matrix by new cluster-induced mechanism [53], thus opening perspectives for the creation of new generations of functional materials of vacuum nano-electronics, and light constructive alloys with a clusterized matrix structure.

1.2. Liquid Cluster Compound Formation

In the present work, an attempt has been made to investigate characteristics of solute clustering in a liquid atomic structure by recording the weak heat effects that could be caused by the short-range ordering in liquid solutions of the magnesium alloys containing cluster-forming additions such as Gd, Ba, Ti, and Y. Such thermal effects were first revealed in the hcp Mg—Al—Ca—Y (Gd) system by using DSC technique which enables the alternative exo- and endothermal reactions to be measured with a high accuracy of 0.01 J/g (Fig. 1.3). It is important to underline that the same DSC effects were also revealed in the liquid Mg—Ba and Mg—Al—Ca—Ti systems. The observed exo- and endothermal chemical reactions are most likely associated with the appearance of the binary cluster A_mB_n compounds. The same shape of the primary heating and cooling curves demonstrate the occurrence of cluster-induced A and B regions in a macroscopically uniform melt (Fig. 1.3). Suitable DSC peaks with a small specific enthalpy represent the energy expended in the liquid when forming the cluster chemical bonds (A region) and the energy absorbed

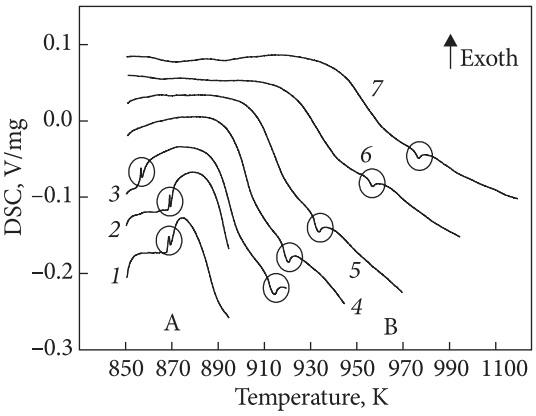

Fig. 1.3. Thermographs produced by differential scanning calorimetry technique for Mg12.5Al1.4Ca0.3Y0.2Gd after the first three remelts (region A) and after the following four remelts (region B). The corresponding peak temperatures and enthalpies are: (*1*) 870.8 K and 0.05 J/g, (*2*) 871.5 K and 0.02 J/g, (*3*) 859.1 K and 0.03 J/g, (*4*) 921.0 K and –0.24 J/g, (*5*) 926.9 K and –0.24 J/g, (*6*) –941.5 K and –0.25 J/g, (*7*) 963.4 K and –0.1 J/g

in the liquid when breaking the chemical bonds during the dissolution of the cluster separations (B region).

The atomic distribution in cluster solutions of liquid eutectic alloys shows both topological and chemical short-range order with the tendency to form self-associated atom groups and chemically ordered clusters of unlike kind atoms [54].

DSC observations of the liquid solutions register the weak thermal effects of chemical reactions at short-range (atomic) distances. They support the appearance of weak exothermic peaks with association heat of up to 0.05 J/g as well as weak endothermic peaks with the reversed sign and a dissolution heat of up to 0.25 J/g. The values of reaction heat measured in the Mg—Gd system appear to be by four orders of magnitude lower than those for melting (234.1...255.6 J/g) and crystallization (243.1...254.8 J/g) Besides, DSC peak areas on the calorimetric curves correspond to the heats of reactions caused by positive absorption and negative generation of thermal energy during the Mg_nGd_m clusters formation and their dissolution, respectively. Furthermore, A and B regions are zones of their formation and dissolution in the melt under overheating. It follows that it is A_mB_n non-crystallizing clusters with more dense packing that must be embedded in the primary solid solution during melt solidification. For this reason, a genetic relation between A_mB_n clusters formed in the atomic liquid and embedded into the primary solid solution is likely to take place. Liquid clusters have been revealed in many alloy systems [55-57]. However, the physicochemical principles of cluster-forming alloying can be formulated on the basis of the findings (Fig. 1.3) and more obvious physical interpretation of their behavior to indicate that A_mB_n chemically bound cluster compounds arise in the liquid.

A genetic relation between solid and liquid states, i.e. structures of short-range ordered clusters in a melt and primary solid solutions, facilitates introducing modifiers such as Al_3Zr in the fcc Al as well as refractory alloying elements such as Ti having a large enthalpy of mixing in the hcp Mg. Heat effect characteristics emanate from solute clustering in a liquid atomic structure to form A_mB_n solid-state cluster compounds such as $Mg_{16}Ba_2$ in the Mg—2.1Ba system and $Al_{18}Ba_9$ in the Al—1.0Li—2.1Ba system. The method enables the pre-cluster complexes and pre-phase cluster compounds to be formed by a self-supported mechanism. Besides, these results are the first indication that A_mB_n cluster compounds under investigation can be formed directly from a melt.

Concluding Remarks

The evidence derived from diffraction, neutron, and digital DSC/DTA measurements brings a larger volume of available information on the melt structure of metals and their alloys based on crystal-like clusters at temperatures close to the melting temperatures. Elastic and quasi-chemical models indicate that the atomic pair correlation functions and structure factors are consistent with the experimental observations in liquid alloys studied.

Chapter

2 FORMATION OF SOLID CLUSTER COMPOUNDS

2.1. The State-of-the-Art Research

Describing a wide variety of so-called multi-level solute-defect structures in α-primary solid solutions systems is a longstanding problem in material science. At first glance, the structures seem rather uninteresting but they are much richer than commonly appreciated. The structural transformations in solid solutions in the early stage of their evolution were summarized and systematized in terms of trapping hydrogen by thermally equilibrium vacancies (10^{-4} at T_m of fcc Al) [58]. However, purely vacancy diffusion mechanism modeling based on the surface-sensitive techniques such as absorption, desorption and permeation, in this case, produces the data confusion when measuring solute atom diffusivity. Besides, new data obtained show evidence of generating excess (non-intrinsic, structural) vacancies by the stress field of mobile hydrogen [59-60]. With this condition, the concentration of excess vacancies is found to exceed that of thermally equilibrium ones by two-three orders of magnitude. Moreover, their short-range ordering has length scales that are difficult to study with the above conventional techniques.

On this view, the introduction of more precise and highly structure-sensitive techniques such as positron annihilation, Auger-electron, mechanical spectroscopy (internal friction) and electric resistance is believed to facilitate the study of short-range interactions between structural defects and solutes to analyze their behavior as cooperative phenomena. Such an approach has a significant potential for providing more general insights into clustering a structure that occurs during the mesoscopic evolution of the phenomena in many aspects of precision alloying and related casting technology. Many aspects of the effects have been reasonably well interpreted [61-63]. At the same time, the physical interpretation of the structural transformations is being hindered by a lack of modeling and experimental information, in particular, for the metal alloy systems enriched with excess vacancies. It is well known that mobile vacancies efficiently restore the chemical short-range order as they mi-

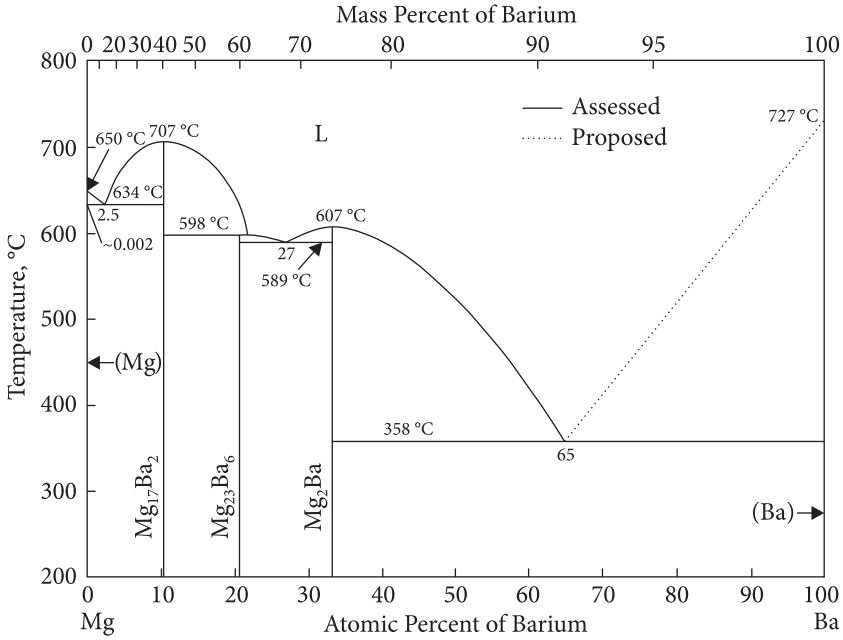

Fig. 2.1. Assessed Mg—Ba phase diagram [77]

grate by thermally-induced mechanism in disordered solid solutions [64]. Much work remains to be done for a better understanding of the cluster-forming alloying mechanism. Its thermally activated analysis appears to be a complex sophisticated problem of basic physic researches [65]. The cluster-forming metal alloy systems have been an object of extensive investigations considering their technological importance as a basis for different applications. It is generally recognized that nanocluster-induced optical properties of metal alloy systems are of great interest for high-current electronics, first of all, due to the highest relaxation rate for electrons [66, 67]. Novel approaches in preceding theory of alloys associated with recent progress in nanophysics [68-69] have promoted the development of a new class of promising photoemissive materials in terms of nanocluster-forming alloying [66]. The electronic structure of the clusters and their chemical reactivity, magnetic and optical properties are among the most important issues in cluster physics [70-73]. Photoemission techniques have proven to be a very powerful tool in elucidating the electronic structure of supported clusters. Using available data of X-ray and UV-photoelectron spectroscopy, as well as Auger-electron spectroscopy and bulk paramagnetic susceptibility, there has been for the first time established the reliable correlation between the improving quantum yield of photoemission and the increasing local density of states near the Fermi energy for hcp and fcc solid solutions to be considered as open systems with the destroyed long-range order [66]. The essential improvement in quantum efficiency for promising metal alloy systems is expected to speed up works in developing photoemit-

ters as key components of photoelectron guns. Nevertheless, basic information on the physical nature of the phenomenon is still scarce. Besides, the sequential interpretation of binary cluster compound properties is restrained, first of all, due to unsatisfactorily describing their electronic structure. Since details of the cluster compound formation are impossible to be completely controlled, the exact nature of their chemical bonding strength compounds is not yet completely understood.

The main purpose of the present study is to work out a problem of the paired and collective short-range interactions between solutes and structural defects aimed at elucidating their physical origin and evolution in metal alloy systems enriched with excess vacancies. It therefore seems appropriate to give an idea of solute clustering in the liquid and solid-state solutions as well as to gain some insight into the nature of the short-range interactions between solutes and structural defects. In this contribution, we present the most salient features of the A_mB_n-type binary cluster compounds in terms of a detailed analysis of their electron-sensitive properties. A number of metal alloys with hcp and fcc structure were studied to obtain data required for better understanding of their fundamental properties in solid-solution alloys enriched with excess vacancies.

2.2. Experimental Procedure

Cast magnesium, aluminium and titanium-based alloys of given chemical composition were made using the ingot manufacturing methods described elsewhere [74]. Cluster compounds of the A_mB_n* type were produced using a physical method of melt treatment by a pulsed magnetic field [75] aimed at embedding the chemically bound compounds in the primary solid solution to be suitable for such a case. Characteristics of solute clustering in a liquid atomic structure were generated by thermal reactions and calculated from differential scanning calorimetry (DSC) thermographs obtained from suitably designed experiments to identify DSC peaks [76]. Magnesium alloy of hypoeutectic origin was chosen as a reference material to explore the possibility of chemical reaction synthesis in liquid solutions (Fig. 2.1). Pre-cluster separations (complexes) and pre-phase cluster compounds were also generated by isothermal heat treatment followed by quenching with increased undercooling temperatures and subsequent ageing.

To form more stable configurations, the excess vacancies of high density tend to clusterize with alloying elements (AE) and to act as deep traps with sufficient binding energy, which requires higher temperature for the onset of core vacancy migration. Hydrogen to be useful as a probe for structural analysis was added to generate excess concentration of non-intrinsic (structural) vacancies exceeding that of thermally equilibrium ones by two-three orders of magnitude. The hydrogen vacancies facilitate the formation and evolution of atomic groups in solute-defect structures. The experiment procedure relates to introducing excess vacancies by the stress field of

* A_m is the number of solvent lattice atoms; B_n is the number of solute atoms.

mobile hydrogen atoms which are certain to be a source of point defects. In this study, alloys in the hcp Mg—Ba—H, hcp Ti—H and fcc Al—H systems were investigated using the electrochemical introduction of hydrogen into samples in order to check on and support a concept of the paired inelastic relaxation and cluster-induced structural transformations in the hydrogenous solid solutions with known amount of hydrogen C_H [78].

A possibility of pairing the alloying constituents consisting of a solute and a vacancy was evaluated by using the electron-positron annihilation technique. The capture (in the potential wells) and annihilation of the thermalized positrons with conductivity electrons are certain to occur on the structural defects (vacancies and dislocation cores) providing a non-uniform distribution of electron density. Therefore, the values of parameter S, which characterizes a probability of the annihilation as well as the range of the positron wave function, were calculated from a spectrum of the angular distribution of photons. Positrons as the lightest chemical analogs of protons can be regarded as a probe of atomic localization sites due to their ability to be trapped at the open-volume type defects. The sizes of positron localization sites in a specific alloy were calculated from the measurements of the angular distribution of annihilation photons by using a conventional long-slit spectrometer with a ^{22}Na radioactive positron source of about m Ci activity. The dispersion of angular resolution function estimated from positronium narrow component width in single-crystalline silica constitutes of about 0.55 mrad (standard deviation). The positron localization radius is assumed to be proportional to the defect size.

Internal friction (Q^{-1}) values have been measured by using the inverse torsion pendulum technique [79, 80] at the stress amplitude of 10^{-5} G typical for the low-frequency range of 0.5-3.5 Hz. Activation parameters of paired relaxation and activation energies (a.e) E for the short-range reorientation of the paired point defects in the cyclic stress field were determined by the well-known method of Wert-Marx as well as by the peak half-width measurements under the data of the discrete temperature spectra of internal friction (mechanical spectroscopy). Frequency factor τ_0^{-1} (short-range atom jumps) was calculated from an equation for the inelastic time $\tau = \tau_0 \exp [E(kT)^{-1}]$. Ultraviolet (UV) photoelectron and Auger electron spectroscopy (AES) were used as advanced short-pulse methods not only for the thorough physicochemical analysis but also for examination of pre-phase transformations [81, 82]. AES spectra were taken under ultrahigh vacuum conditions, with Ar^+ sputtering required for in situ sample cleaning [23]. Electron spectra induced by the photo- and Auger electron transitions were recorded with the relative spectral sensitivity of about 0.3% and 0.01%, respectively, with the energy resolution better than 0.1 eV (in a UV spectral range). AES and TEM-observations were carried out with instruments JAMP-100, JEOL C and JSEM-200. Electrical resistivity data were obtained and processed with the use of the experimental procedure described elsewhere [83]. Densities of states (DOS) for magnesium and the Mg_nBa_m cluster compound were calculated with the use of the Full Potential Linearized Augmented Plane Wave (FLAPW) package

representing the well-documented and well-recognized forecasting technique for ab-initio theoretical analysis of cluster electronic structures [84].

2.3. Pre-Cluster Solid-State Complexes

The effect of inducing the excess (non-intrinsic, structural) vacancies, (V_e), by the stress field of mobile solutes (hydrogen and the like) was predicted theoretically and then explained in a series of our works for metal alloy systems of hypoeutectic origin having regions of extended substitutional solid solutions [59, 78, 85]. The excess concentration of vacancies in the hydrogen-charged alloys is found to exceed their thermal equilibrium one in pure metals by two-three orders of magnitude.

Annihilation of positrons is believed to occur with a probability of S in the regions having a low electron density typical of the crystalline defects (excess vacancies and dislocation cores) which act as traps for the capture and localization of elementary particles. Following the data, the behavior of excess vacancies generated by the stress field of hydrogen atoms suggestive of B_nV_e complexes is first detected in the Mg—Ba—H alloys. Owing to the accepted approximation for positron wave function (superposition of a parabola and a gaussian) [84] we succeeded in obtaining the calculated values of the localization range for defects in magnesium and its alloy with barium (Table 2.1). The almost two-fold decrease in positron localization radius, i.e., mean open-volume defect size, is recorded for hcp Mg—2.1Ba—1.1H as against with hcp Mg. It appears from this that Ba atoms are really localized near excess vacancies by means of contracting the localization range for positrons. This suggestion is strongly supported by the data of mechanical spectroscopy for magnesium alloy in the hcp Mg-Ba-H system enriched with excess vacancies (Fig. 2.2). An isolated solute atom and a node monovacancy in the anisotropic hcp lattice cannot be inelastic relaxation centers due to the low crystal symmetry to be maintained. The appearance of the relaxation maximum A of vacancy origin in the discrete temperature spectrum of internal friction is attributed to the paired inelastic relaxation caused by the Ba—V_e dipoles in the cyclic stress field (curve *1* — quenching) and enhanced by the grain boundary (GB) relaxation (B). Thermally activated recovery of the defect structure is accompanied by suppressing the GB-induced relaxation (B) and appearing the peak

Table. 2.1. **Parameters of electron-positron annihilation for magnesium and its alloy with barium**

Composition of alloys	Parabolic component S_p, %	Gaussian component S_g, %	Angular distribution function*, Θ_p, mrad	Positron localization radius, R_m, nm	Positron wave function range, nm
Hcp Mg	75.4	24.6	5.32	0.060	0.156
Mg—2.1Ba—1.1H	78.1	21.9	5.09	0.063	0.079

* With standard deviation of 0.55 mrad.

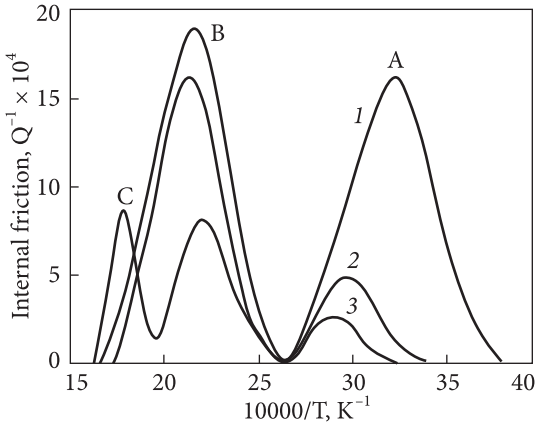

Fig. 2.2. The discrete temperature spectra of internal friction $Q^{-1}(T)$ at 1Hz with measured damping components (above background) for Mg—2.1Ba—1.1H in which are: first revealed: the Ba–V_e paired defect-induced inelastic relaxation maximum A of vacancy origin with a.e. of 0.8 eV at 310 K; grain-boundary inelastic relaxation maximum B with a.e. of 1.2 eV at 455 K and the Ba-H paired defect-induced inelastic relaxation maximum C with a.e. of 1.5eV at 565 K with segregation at grain boundaries (*1* — quenching; *2* — annealing at 673 K for 1 hr; *3* — the same heat treatment (at slow cooling)

C which is associated with the segregation of activation of alloying elements at the GBs (curves *2* — annealing and *3* — slow cooling). Internal friction data (Fig. 2.2) give the first clear evidence for the presence of the B_nV_e-type complexes in the hcp Mg—Ba—H system.

These separations relax the lattice strain in the α-Mg matrix by stress-induced reorientation of elastic dipoles oscillating in the cyclic stress fields.

The pairing of solutes with excess vacancies provides the anisotropic fields of internal deformation with symmetry different from that of the crystal. In other words, they represent inelastic (time-dependent) relaxation by reason of the reorientation of the B_nV_e elastic dipole in the cyclic stress field. Solute ions are expected to be paired with positive ion vacancies, which attract them strongly and produce large lattice distortions. In magnesium alloys with strong chemical interaction, it is more likely that the excess vacancies will remain in solution associated with solute alloying elements in the form of the B_nV_E pre-cluster complexes which are termed sometimes as primary separations. The comparatively large values of the solute-vacancy binding energy implicate that it is possible to suppress the precipitation phenomena. The atom size difference in binary solid solutions, as a rule, induces short-range ordering, as suggested by Rudman [86]. As a result, local stress fields of the mobile dissolve atoms generating the excess vacancies [59] cause unsymmetrical strains and statistical atomic shifts. This leads to the partial relaxation of the pre-cluster separations energy. Therefore, at this point, these become diffusion traps for excess vacancies to be captured.

At higher temperatures the thermally activated clustering of solutes and excess vacancies in the structure of solid solutions causes in two standard curve noticeable deviations from linearity $\Delta R_T(T)$, the positive or negative sign of which depends on the nature of crystalline matrix (Fig. 2.3). Because of different electronegativities and valences, they are of the positive sign for fcc Al—H, $\Delta R_T(T, C_H) > 0$ and the negative sign for hcp Ti—H and other hydride-forming metal alloy systems, $\Delta R_T(T, C_H) < 0$.

Measuring electric resistivity increments in the wide range of quenching temperatures for pure magnesium, aluminum and titanium and their alloys with hydro-

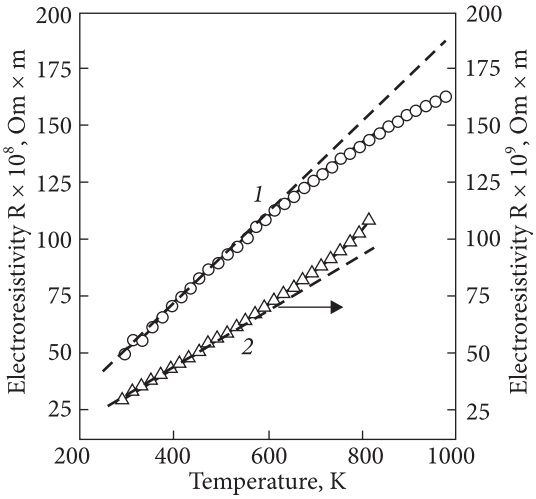

Fig. 2.3. Electric resistivity, R, as a function of temperature, T, with deviations from their linear relationship at higher temperatures for α-Ti—0.5H (*1*) and Al— 0.5H (*2*) alloys. (Arrow indicates measured R values for Al—0.5 H)

gen enables the effective a.e. for the formation of a vacancy to be evaluated, and indicates the existence of the binding energy (E_b) between vacancy and hydrogen. The calculated values of binding energy between V_e and hydrogen atom make up of about 0.5 eV/atom and 0.2 eV/atom for the Al—H and α-Ti—H systems, respectively. Positive deviation, ΔR_T (T, $C_{V,H}$) > 0 is observed in the Al—H non-hydride-forming system which stimulates the formation of the V_e—H complexes with high binding energy (E_b ~ 0.5 eV/atom) due to the less electronegative fcc Al. The probability of H-trapping vacancy in the fcc Al—H system was postulated by Hashimoto and Kino [87]. The hydrogen diffusivity measurements in metal crystals reveal the deviation from classical (Arrhenius) behavior due to the activation of the immobile trapping centers — substitutional solutes [63]. Negative deviation, ΔR_T (T, $C_{V,H}$) < 0, characterizes the Ti—H hydride-forming system due to the more electronegative hcp Ti. Nucleation of the hydride phase appears to be dependent upon the excess vacancies concentration and binding energy E_b responsible for the strength of the complexes. While the strong thermally activated dissociation of the V_e—H pairs suppresses the hydride nucleation in the Al—H system, on the contrary, weak thermally activated dissociation of the pairs in the Ti—H system encourages the hydride nucleation at significantly lower temperatures when the atomic redistribution and vacancy mobility become increasingly difficult.

Thus, the short-range interaction of an excess vacancy with a solute atom to form the chemically bound complexes is considered to be one of the most probable rate-controlling mechanisms which cause the anomalous deviations of solute diffusivity from the classical (Arrhenius) correlation in solid solutions. This effect has been detected in many hcp and fcc binary and ternary alloys with increasing temperature [59].

2.4. Solid-State Cluster Compounds

According to the Mott-Nabarro theory [88], the solute atom clusters, as well as Guinier-Preston nanosized zones cause the internal stresses in a matrix prior to coherent precipitation. Transformation of nanoclusters into nanoparticles, on the contrary, may be fixed only, for example, in water solutions transparent

for radiation by X-ray absorption spectroscopy technique. Such an approach is not available for metal solid solutions that are non-transparent for the spectral examination. The phase particles as small as 5 nm may be identified by proper electron microscopic technique. However, clusters crystallographically ordered with the matrix are not resolved by TEM observation, e.g., in a dark field micrograph being the integral part for primary solid solution.

In order to attack the problem of revealing the cluster-induced microstructural changes in deformed matrix lattice and adapt them to a selected area-diffraction (SAD) technique, cluster compounds were grown up to the appearance of nanoparticles (≤100 nm) by diffusion-controlled encounter mechanism. This method was certain to be enough for observing the residual features and traces of clustering a crystalline structure in the primary α-solid solution after short-term annealing at 423 K. Selected-area electron diffraction patterns for the hcp Mg—2.1Ba and fcc Al—1Li—2.1Ba alloys are presented in Fig. 2.4, *b*. It is seen that SAD patterns taken from the phases of cluster origin are characterized by the streak-like reflections which are closely associated with the matrix spots and indicative of the nucleation of the $Mg_{16}Ba_2$ cluster compound in the hcp Mg—Ba alloy and the $Al_{18}Ba_9$ cluster compound in the fcc Al—1Li—2.1Ba alloy respectively. As a rule, these cluster compounds reflections are found out in reflections of the $Mg_{17}Ba_2$ and Al_4Ba phase thereby testifying to the affinity of their lattice parameters.

The matrix reflections of arc-like shape and their fuzziness indicate the clustering of solute atoms in a solid solution structure representing the pre-phase compounds that resemble the Guinier-Preston zones. The results obtained are consistent with the well-known Curie's symmetry principle [89] according to which the crystal nucleus shape maintains only those intrinsic symmetry elements that coincide with the superposed symmetry elements of surroundings. Weak distortion of the crystal-

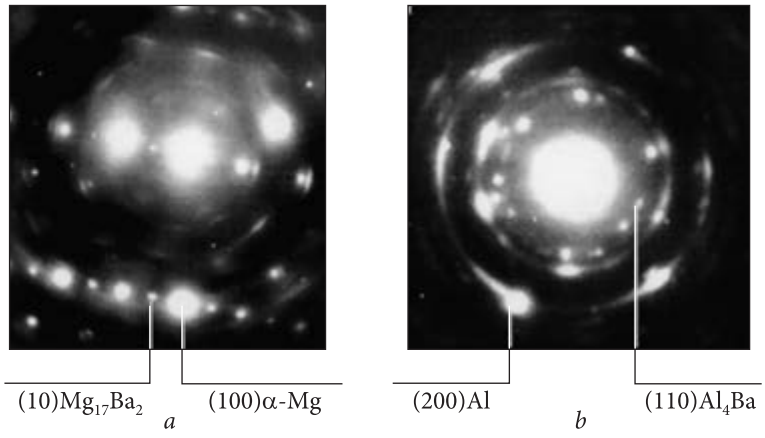

Fig. 2.4. Selected area diffraction patterns taken from $Mg_{17}Ba_2$ (*a*) and Al_4Ba (*b*) phases of nanocluster compound origin

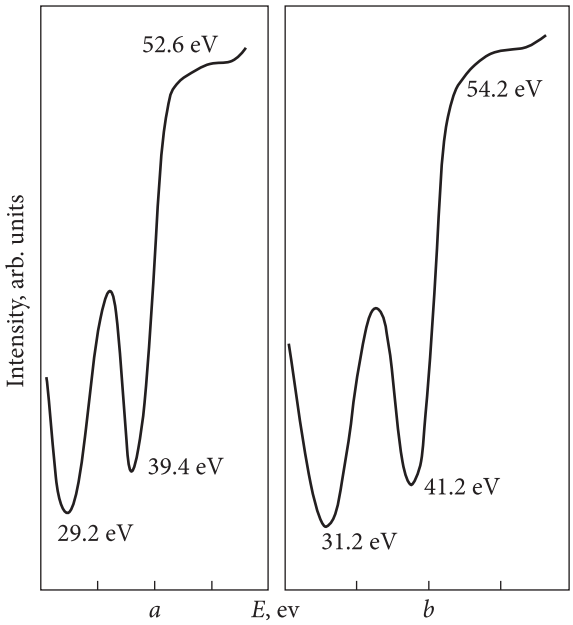

Fig. 2.5. Cluster-induced chemical (energy-dependent) shift of LVV-transition in Auger electron spectrum in going from hcp Mg (*a*) to Mg—2.1Ba alloy (*b*)

line structure of a solid solution by embedded nanoclusters is thought to maintain the main elements of a bulk crystal. The weak lattice distortions observed in the Mg—Ba, as well as in Al—Li, Ba systems (Fig. 2.4, *a*, *b*) give rise to measurable effects of the clusters presence. Since nanocluster compounds cannot be resolved by diffraction analysis absolutely, the various features of the cluster compound formation are believed to become clear after further evaluation. Additional support for the mechanism proposed can be seen in Figs 2.4.-2.6. So-called chemical shifts (to higher binding energy) are observed in the low energy region of Auger-electron spectrum for magnesium alloys with cluster-forming additions such as barium (Fig. 2.5). These energy shifts indicate the occurrence of the bond-dissociation energy which is a measure of the binding energy between the atoms in a chemical bond. Under the data of Auger spectral analysis, the shifts are certain to be caused by the valence electrons within the maximum density of states suggestive of the $Mg_{16}Ba_2$ cluster. Various displacements of LVV — electron transitions detected in a fine structure of the Auger spectra for Mg—Ba and Al—Li systems demonstrate increase in the binding energy E_b for internal electrons, which appears to be significant for the Mg—2.1Ba substitutional solid solution (up to 2.0 eV/atom) (Fig. 2.5) and small for the Al—1.0Li interstitial solid solutions (up to 0.4 eV/atom). Introduction of the cluster-forming AE of Ba in the matrix of Al—Li alloy also increases E_b from 0.4 to 1.4 eV/atom.

Possibility to investigate a continuous change of electron states from the atom orbits to the bands in bulk matter is one of the important aspects of cluster physics. Such a cluster electronic structure could not be clarified without ab-initio calculations. Therefore, decoding of the photoelectron spectra with and without embedded clusters is considered as an effective means for identification of their electronic structure [90]. To illustrate, the first-principle theoretical calculations of the $Mg_{16}Ba_2$ cluster-induced electron configurations in the Mg—Ba system (Figs 2.6-2.8) predict increasing the local density of the engaged electron states near the Fermi energy inside cluster sites formed by the short-range mechanism. Theoretical calculations of the

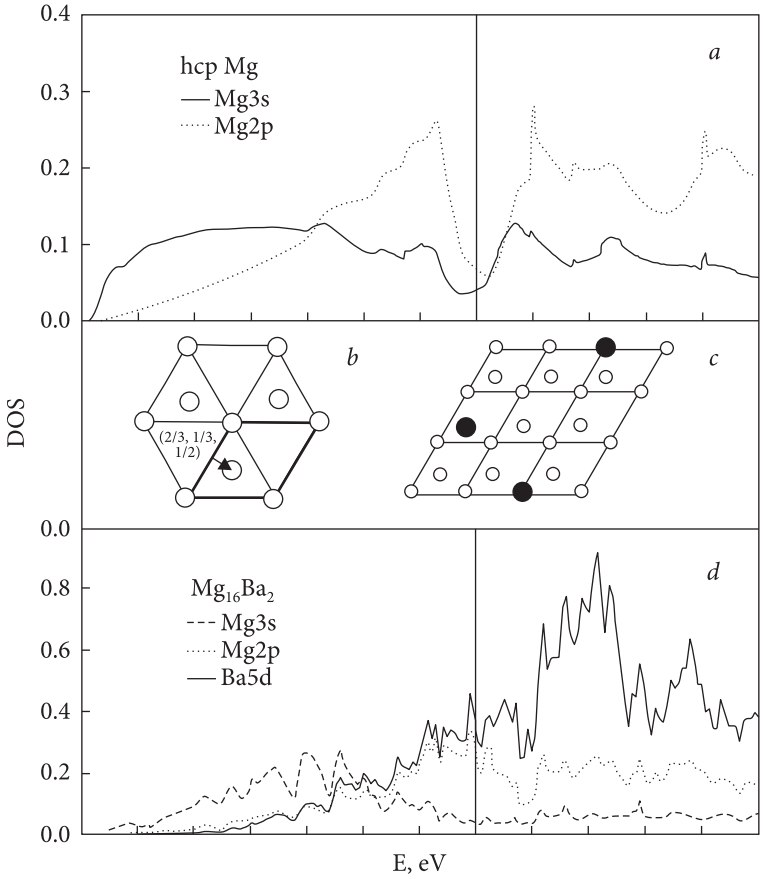

Fig. 2.6. Theoretical calculations of partial electron densities of 3s-2p-states for Mg atom (*a*) in terms of model hcp cell used to be transformed into model atom cluster configuration $Mg_{16}Ba_2$ (*b, c*), as well as of partial electron densities of 3s-2pstates for Mg atom and 5d-state for Ba atom in the $Mg_{16}Ba_2$ cluster (*d*)

partial DOS for hcp Mg and $Mg_{16}Ba_2$ are in a reasonable agreement with the experimentally observed distribution of DOS measured for hcp Mg and bulk Mg—2.1Ba alloy (Figs. 2.6 and 2.7). The well-resolved spectrum $Mg_{16}Ba_2$ is found to exhibit a bulk-like behavior. In particular, the fine structure of the theoretical spectrum for $Mg_{16}Ba_2$ nanocluster calculated with the use of the FLAPW approximation approaches that of the experimental spectrum for bulk Mg—2.1Ba observed in the UV photoelectron spectrum range at a photon energy of 8.4 eV (Fig. 2.7). As seen, maximum positions in DOS distribution for Mg—2.1Ba shifted towards the Fermi energy with respect to positions for hcp Mg due to the cluster-induced *s-*, *p-*, *d*-hybridization (Figs 2.6, *a*, *d*).

Change in the fine structure of energy levels in the UV spectral range, occurrence of chemical shifts in Auger electron spectra (Fig. 2.5), and amplification of

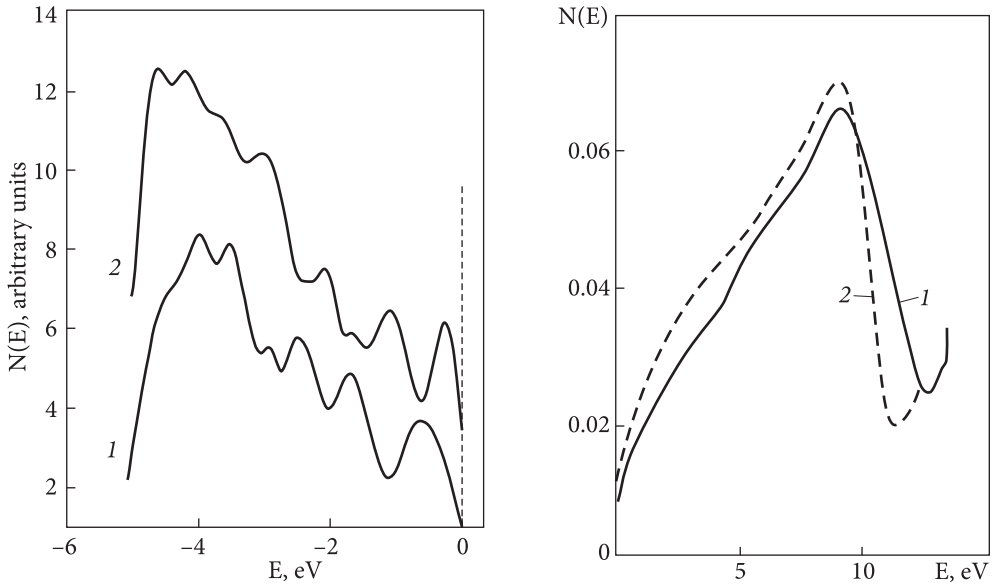

Fig. 2.7. Distribution of the density of states near the Fermi energy in hcp Mg (*1*) and cluster-forming Mg—2.1Ba alloy (*2*) at a photon energy of 8.4 eV

Fig. 2.8. Electron density of states for hcp Be and other metals of subgroup IIA: *1* — theory; *2* — experimental data

paramagnetic susceptibility of Mg—Ba alloys [60] show that Ba as a cluster-forming alkaline-earth AE liquidates minimum on the curve of density of electronic states N(E) by hybridizing *s, p*-states of Mg and *d*-state of Ba (Fig. 2.6, *d*) and really raises the local density of engaged states near the Fermi energy of the $Mg_{16}Ba_2$ cluster. Since metal clusters possess high absorption coefficient for photons in the short-range UV spectrum range, it is evident that cluster-induced *s, p, d*-hybrid electronic structure reveals itself as a system with isolable properties that enables the cluster compounds to be operated as emission-active centers. The latter are responsible for the high quantum efficiency which raises a stable quantum yield of photoemission by three orders of magnitude for the Mg—Ba and Al—Li, Ba systems [60, 91].

2.5. Topical Problems in Cluster Physics

It is very difficult to identify the occurrence of pre-cluster and pre-phase constituents especially within the crystalline structure of a primary solid solution. Therefore, metals physics is often entangled in the attempts to correctly describe the interaction between all types of structural defects conditioning metal alloy properties. To illustrate, some alloys pass through a pre-precipitation stage at which the pairing of solute atoms occurs in the form of Guinier-Preston zones having the internal structure which is coherent with that of the solvent lattice. Following the supposi-

tions of Ferragut and co-workers [92], Guinier zones or pre-precipitate solute clusters are likely to be responsible for the kinetics of structural transformations with the participation of excess vacancies in the early stage. This assumption appears to be unsound. According to the Mott-Nabarro model [29], the solute atom clusters or defect-free Guinier-Preston zones are formed in the matrix prior to coherent precipitation. However, unlike the cluster-induced structure, the zones are typical for saturated solid solutions not containing vacancies and localized precipitates.

The approach and ab-initio result make it possible to predict increasing local density of electron states near the Fermi energy level inside cluster sites formed by short-range mechanism. Thin structure of theoretical spectrum for $Mg_{16}Ba_2$ cluster approximates structure experimental RPES spectrum for massive Mg—2Ba (Mg0.94Ba0.06). TEM researches of magnesium alloy thin structure confirm the presence of disperse clusters in the sizes 4-12 nm and density 5×10^{10} /cm^2. They are coherent with a magnesium matrix. As a rule, these separations are found out in the $Mg_{17}Ba_2$ reflections, which can testify to affinity of their clusterization with the solid solution structure, representing prophase separations which resemble zones of Genie-Preston, probably Mg0.96Ba0.04.

In the periodic literature [93, 94] there are two major points of view by which the pairing of solutes and excess vacancies needs clarifying. One of them believes that there is a correlation between vacancy binding energy and solute size, i.e., larger solute atoms tend to bind more favorably with vacancies to relax the strain induced by solute atoms. The other believes that ab-initio calculations by electron density function method predict positive vacancy binding energies for some commonly used solutes, e.g., elements Ca, Na, Cu, etc. in magnesium alloy systems which await experimental validation. The observations are helpful, although up to now no systematic studies have been available in this respect.

The theory of atom size difference considers clustering of solute atoms in a structure as a mode of local (short-range) ordering [95, 96] where the atoms have an excess of their own kind for first neighbors. In a binary solid solution A—B, the atom size difference will give rise to strain energy which can be partially relieved by the larger A atoms preferentially surrounding themselves by the smaller B atoms, and vice versa for the B atoms. Thus, size difference always stimulates short-range ordering in contrast to the other possible mode of local ordering.

Our results strongly support the model of the clustering-type local order proposed by Rudman [97] for describing the short-range mechanism of solid solution strengthening in bcc Group A metal alloy systems. Since details of the pairing of a solute with an excess vacancy and cluster formation are impossible to control, the validity of this model should be tested for experience. When an excess vacancy is trapped forming a solute-vacancy complex, its apparent migration energy is reduced by a measure of their binding energy. One should expect the thermally activated deviation of the self-diffusivity in the α-Ti—H system from the classical Arrhenius behavior, as predicted by the authors [93]. Our experimental results (Fig. 2.2) are

consistent with the published data for the hcp Ti—H system. As a by-product of the binding energy calculations, we succeeded in obtaining the vacancy formation energy in magnesium solid solutions [98]. By reason of its physical sense, the trapping level of the solute-vacancy binding energy gives rise to a considerable impact on determining which clustering process is dominant and, in turn, which postulated precipitation process can occur. Nevertheless, when the initial solute atoms interact preferentially with excess vacancies, their binding energy, E_b, becomes large enough to maintain the complexes at higher temperatures and to suppress the premature precipitation process. Further, larger solute atoms, more favorably binding with neighboring vacancies, relax the strain induced by the solutes [94].

In disordered alloys, according to [86], about half of the atom size difference and elastic strain energy can be relaxed by short-range ordering, so that the strain energy is not the only local order driving force. Although the clustering of point defects and solute atoms is certain to be another possible mode of local ordering (Table 2.1, Figs. 2.2 and 2.6), the strain relaxation calculations being a good elastic approximation could not take into account the effect of electronic interaction (chemical approximation). There are several model calculations explaining the origin of local order based on electronic structure [99, 100]. In particular, the analytical approaches [40] predict elastic and electronic effects due to the filling of electronic states at the Fermi energy of a metal as a result of its electron charging and lattice distortion by its long-range interaction with solute atoms of hydrogen. However, the results obtained do not affect the problem of embedding the A_mB_n clusters in the crystalline structure of a primary solid solution as elastic interaction lowers the enthalpy of solution, and, on the contrary, filling of the electronic states increases it. Furthermore, the long-range interaction is shown to be independent of the chemical reaction course. These results are far from being conclusive at least for solid solutions enriched with excess vacancies, so most these calculations are clearly not in agreement with the idea of short-range interaction. Nevertheless, all the data published in the literature are theoretical premises for developing a unified concept of the short-range clustering inherent in a solute-defect-vacancy structure.

The observed inelastic stress paired relaxation (Fig. 2.2) and other evidence of the pairing of solutes with excess vacancies (Fig. 2.3, Table 2.1) demonstrate that a different mechanism operates in the cluster-forming solid solutions. Under the data [59, 79, 96], apparent migration energy for vacancy-solute complexes gives a good fit to experimental data compared to that for solutes. The complexes have higher mobility with smaller a.e., which differs substantially from that of isolated solute atoms and individual defects. The formation of paired defects and their complexes enables them to be relaxed by a rapid short-range mechanism with the participation of the bound vacancies. With this provision, they are shown to be stable against the thermal dissociation (Figs. 2.2 and 2.3, Table 2.1).

Much progress has been made in researches into electronic structure and optical properties of metallic clusters [70, 71]. In recent years, significant efforts have been made and will continue aimed at finding their electron shells to be atomistically cal-

culated [73]. Nevertheless, the exact nature of the chemical bonding strength in cluster compounds has not yet been completely understood. To illustrate, chemical bonding in B_nV_e complexes and the A_mB_n nanoclusters made of them are certain to depend strongly on the chemical type of the surrounding atoms. A strong atomic attraction causes the effect of short-range ordering (SRO) in the molten state lowering the configuration entropy and changing the a.e. for crystallization [96, 100]. Otherwise, the chemical SRO originates in the liquid. The nature of chemical bonding is changed at the addition of AE with higher cohesive energy.

Therefore, the chemical energy is thought to play the major role in clustering of atomic structure to nucleate chemically bonded cluster compounds A_mB_n with own hybridized electronic structure. The energy appears to be sufficient to provide all the chemical reactions as required. It is obvious that the solute-excess vacancy complexes undergo some reactions suggestive of the structural heredity connecting them with cluster compounds to be reformed in the presence of excess vacancies. It should be pointed out that the energy increase due to the generation of excess vacancies or other defects certainly contributes to the atomic self-assembly mechanism. Considerable chemical shifts (of about 2.0 eV, Fig. 10) suggestive of strong chemical bonding are observed in the $Mg_{16}Ba_2$ cluster embedded in the crystalline structure of solid solution. Additional support for the mechanism comes from measurements and calculations (Table 2.1, Figs. 2.6 and 2.7) and can be seen in Figs. 2.2 and 2.5.

Concluding Remarks

The formation and physical origin of the pre-cluster complexes and pre-phase (cluster) compounds have been studied on cast magnesium alloys in the liquid and solid states as well as other primary solutions enriched with excess (non-intrinsic, structural) vacancies. The results produced by DSC and TEM observations, Auger-electron, UV and X-ray photoelectron spectroscopy techniques were combined with positron annihilation, electric resistance and internal friction measurements to evaluate different stages of the cluster compounds formation and to examine their chemical bonding strength in terms of a detailed analysis of electron-sensitive properties. The thermally activated deviations from classical (Arrhenius) behavior in hydrogen-charged hcp and fcc metal crystals are found to be caused by the nucleation of the solute-excess vacancy complexes. Additional support for this short-range self-supported mechanism comes from data obtained by mechanical spectroscopy and positron annihilation. These pre-cluster separations are assumed to act as nuclei for the synthesis of cluster compounds such as $Mg_{16}Ba_2$ and $Al_{18}Ba_9$ with own electronic hybridized structure in hcp magnesium- and fcc aluminum alloy crystals, respectively. A unified concept of the liquid-solid conversion for condensed cluster-forming alloys is considered. This approach is particularly useful for the development of chemically combined cluster compounds with own electronic configurations as functional materials for high-current electronics.

The main conclusions based on the results of observations and calculations are summarized as follows:

• A concept of nanoclustering the structure of primary solid solutions based on the pairing of solutes with excess vacancies is advanced to explain the physical origin of these new pre-cluster type separations. A series of the experimental investigations of solid solutions are performed to confirm the presence of the primary complexes referred to as pre-cluster B_nV_e type separations consisting of an excess vacancy and a dissolved alloying element. The separations are detected by parametric measurements of electron-positron annihilation and pair inelastic relaxation in the hcp Mg—Ba, H alloy enriched with excess vacancies. The additional evidence for the pairing of solutes with excess vacancies comes from the electrical resistance measurements due to the effects indicative of the thermally activated deviations from the classical (Arrhenius) behavior in the hcp Ti—H and fcc Al—H metal alloy systems. The formation of pre-cluster complexes is the major driving force for further changes in the cluster-forming structure under both kinetically and energetically favorable conditions.

• The most precise structure-sensitive methods (electron-positron annihilation, electric resistivity and internal friction measurements) yield for the existence of hydrogen-induced lattice vacancies, and hydrogen-stimulated diffusion in hcp and fcc Me—H systems which were accompanied by the formation of "H atom-excess (non-intrinsic) vacancy" paired defects (so-called separations). A new method for analyzing the high-temperature dependence of Me—H system electric resistivity was developed in terms of a model for clustering structure in solid solutions of Me—H oversaturated with excess vacancies. It was established that partial thermally activated dissociation (decay) of clusters with low bonding energy (0.2 eV) appears to be a controlling mechanism for hydrogen-stimulated diffusion in hydride-forming systems (Ti—H, Z—H). Thermally activated association of clusters with high bonding energy (0.5-0.6 eV) was found to be a controlling mechanism for hydrogen-stimulated diffusion in non-hydride-forming systems (Al—H). Clusterization of excess defects simplifies formation of hydrides at significantly lower temperature.

• A cluster-genesis concept is advanced to provide a more general insight into the genetic relation between cluster separations produced both in liquid and solid states. The data indicates that nanoclusters embedded in the crystalline structure of a solid solution represent independent subsystems of repeating units with intrinsic electron configuration to be aimed at an every-widening range of applications. The summarized experimental data are needed to advance them for the newly developed kinetic analysis of bulk materials to be significant innovation in promising metal alloy systems.

• A new procedure is suggested to obtain these valuable A_mB_n cluster compounds directly from a melt based on a unified concept for the conversion for condensed (liquid/solid) cluster-forming metal alloy systems. The DSC evidence supports the structural heredity of liquid-state and solid-state cluster compounds during prephase transformation. When a liquid, the alloy structure is found to be clusterized with the formation of liquid-state cluster compounds A_mB_n, e.g., Mg_mBa_n and Mg_m

Gd_n in the Mg—Al—Ca systems. The thermosynthesis of liquid-state cluster compounds, their thermal conversion to a solid state and integration into a primary solid solution are attributed to the nature of the exothermal and endothermal chemical reactions.

• The solid-state cluster compound formation is found to involve two progressive stages attributed to (i) the nucleation of pre-cluster B_nV_e separations by short-range mechanism and (ii) the conversion of the pair complexes subsequent to their nucleation into a pre-phase A_mB_n cluster compounds such as $Mg_{16}Ba_2$ in the hcp Mg—Ba system and $Al_{18}Ba_9$ in the fcc Al—Li, Ba system. The occurrence of pre-phase cluster compounds is revealed by the image point (brightness) contrast in the electron diffraction pattern having streak-like reflections from Mg_mBa_n, as well as arc-like shape and fuzziness of the matrix reflections.

• So-called chemical (energy) shifts of Auger lines suggestive of chemical bonding are observed in LVV Auger electron spectra of magnesium and aluminum alloys due to the formation of pre-phase $Mg_{16}Ba_2$ and $Al_{18}Ba_9$ cluster compounds, respectively. Individual solute atoms are bound to these clusters with the energies of about 2.0 eV for the $Mg_{16}Ba_2$ cluster in hcp Mg—2.1Ba alloy and of about 1.4 eV for the $Al_{18}Ba_9$ cluster in fcc Al—1.0Li—2.1Ba. The shifts of Auger electron lines caused by the valence-band transitions in the low-energy region of Auger spectrum indicate that a stronger chemical bonding in the $Mg_{16}Ba_2$ cluster is formed by the overlap of the *s, p*-states of hcp Mg and *d*-state of Ba. The cluster compounds under investigation proved to be chemically combined due to deep changes of their electronic (hybridized) structure. The presence of bound states in the $Mg_{16}Ba_2$ cluster are in reasonable agreement with the first-principle calculation of its own electronic configurations.

According to the data at our disposal, the A_mB_n cluster compounds embedded into the crystal matrix should be considered as an integral part of solid solutions typical for open (dissipative) systems with locally disturbed long-range order and cluster-saturated chemical compositions close to stoichiometric compounds. They indicate the fundamental possibility of creating a new type of nanosystems with a newly organized cluster electronic structure, which is expected to provide new functional (electronic-sensitive) properties for the use of the mentioned metal alloy systems in nanophysics and nanoelectronics. The results obtained can be applied to create sources of intense ultraviolet light using photo-induced desorption of hydrogen from the emitter surface. The novel approach opens the excellent way of obtaining a new family of perspective photoemissive materials based on cluster-forming metal alloy systems and speeding up works on the development of higher efficiency materials and building blocks made of them for high-current electronics.

Chapter

3 STRENGTHENING EFFECTS OF SHORT-RANGE ORDER

Internal friction phenomena are caused by stress-induced ordering in the lattice. The mechanism by which this ordering occurs is closely related to bulk diffusion in normal solid solutions. The effect of Zener's relaxation arises fundamentally from a microscopic rearrangement of atoms in the field of external stress. Hcp alloys of the Cd—Mg system contain both a region of normal solid solution and ordered structure of the intermetallic compound $MgCd_3$ [101]. The damping is greatly influenced by the ordering occurring in the system. Relaxation arises from a lattice dilatation accompanying changes in the degree of order. Internal friction depends on the parameter of short-range order. Maximum values of the parameter correspond to complete long-range order. $MgCd_3$ possesses long-range order at r.t. In highly-ordered alloys the damping under stress is low or absent. The formation of short-range order is accompanied by partial destruction of the defective crystal lattice of the substitution solid solution, i.e., destruction of its long-range order, which obeys the Cottrell-Bilby law, the Arrhenius kinetic equation and the Vegard rule for normal solid solutions with linear dependence of the specific volume on the alloying elements concentration.

One of the most puzzling effects presently under study is that caused by stress-induced ordering in certain substitutional alloys. This phenomenon, first seen by Zener in a Cu—30Zn alloy [102], has been observed in many other substitutional alloys. However, even with all data so far available, it has been difficult to establish criteria for the existence and magnitude of the effect in terms of other facts known about a given alloy system. This is unfortunate, since it appears that proper understanding of the effect could lead to its successful use in the study of several physical and metallurgical processes occurring in these alloys.

3.1. Theoretical Analysis of Dislocation Damping

A quantitative theory of internal friction phenomena and modulus changes due to dislocations has been developed by A. Granato and

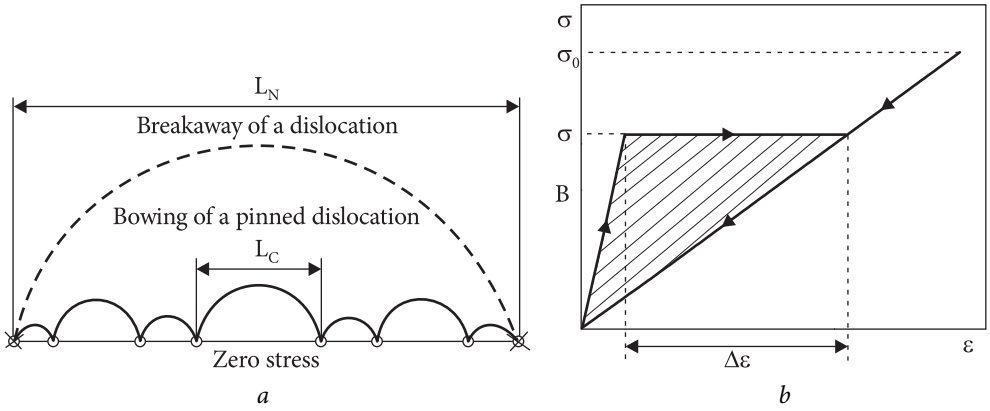

Fig. 3.1. The Granato-Lucke vibrating string model of the power breakaway of dislocation (*a*) and diagram of stress—dislocation microdeformation (*b*)

K. Lucke in a series of works [103-106]. It is based on the Kochler model of a pinned dislocation loop oscillating under the influence of an applied stress. This concept is found to lead to two kinds of loss, on frequency dependent, the other not. The frequency dependent loss is believed to have a maximum in the high megacycle range [103]. The other type of loss is a hysteresis loss which proves to be independent of frequency range which included the kilocycle range. The theory provides a quantitative interpretation of this loss. A detailed discussion of data with reference to the damping of mechanical vibrations and internal friction phenomena is given in their other paper [104].

The dependences of the decrement and modulus changes on the variables of frequency and strain amplitude are compared with predictions of the dislocation theory. Although general agreement is obtained, and many interesting quantitative results are found, it is not possible to say the theory agrees everywhere since not all the necessary parameters are known well enough theoretically. A number of new experiments are suggested which may permit a stronger conclusion to be made.

The fundamental theory of the phenomenon of internal friction based on a vibrating string model of mechanical (force) breakaway of dislocations from pinning points considers two mechanisms of energy loss (dissipation): (i) Resonant, independent of the deformation amplitude, damping of dislocations caused by the forced oscillation of a dislocation segment with length L_C between two pinning points; (ii) Force detachment of dislocations from pinning points (length L_N between nodes of the dislocation network (Fig. 3.1).

In the original Granato-Lucke concept a comprehensive theoretical treatment of energy dissipation was given. However, the proposed model of mechanical (force) breakaway of dislocations from pinning points (impurity atoms, vacancies, and other point defects) ignores the contribution of thermal activation in the process of dislocation pinning, and therefore, strictly speaking, it can be used only at 0 K. After 25

years in the modified Granato-Lucke theory [107], the temperature dependence of the amplitude-dependent (nonlinear) damping (ADD) was taken into account, within the framework of the model of thermally activated (single) breakaway of dislocations from fixed pinning points. The logarithmic decrement (1981) is described by the same equation (1956), but with a different value of the parameter.

In the Blair-Hutchison-Rogers theory [108], an analytical assessment of thermally activated depinning of dislocations is given based on the Granato-Lucke model in the approximation of cooperative breakaway of intermediate (partially fixed) dislocations. The experimental data reveal an obvious discrepancy with theoretical calculations if very long critical loops of dislocation segments (L_C from 100 b to 105 b) and the critical parameter $\beta > 1$ are used in the calculations. For short segments L_C ($\beta < 1$), the critical separation parameter is described by the relation

$$\beta = \frac{L_C \cdot E_b}{C \cdot r^2}, \tag{3.1}$$

where E_b is the maximal binding energy of dislocations with pinning points for dense atmospheres; C is the dislocation tension.

The anomalous effects and phenomena are explained on the basis of existing theoretical approaches and physical models of resistance to micro-flow (creep for slow dislocations), creep limits and long-term strength. This exploits the important advantages of the internal friction method:

- possibility of studying the fast (short-range) interaction of defects (at the interatomic distance), and the short-range ordering of solid solutions in the field of cyclic stresses;
- determining the mobility of atoms and the concentration of point defects in a wide range of temperatures (Fig. 3.2);
- measuring the parameters of the true diffusion coefficients at low temperatures (atomic jumps by 0.1 nm with a diffusion coefficient of 10^{21}-10^{22} m^2/s);
- obtaining quantitative data on the kinetics of solid solution decomposition.

It should be emphasized that the true diffusion coefficient is not related to the flow of matter, and, therefore, to the thermodynamic activity of atoms migrating in the stress field, but it is due to the height of the energy barrier between the equilibrium positions, which facilitates the physical interpretation of the results.

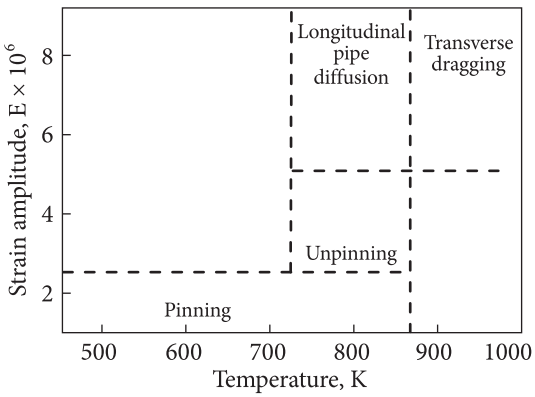

Fig. 3.2. The schematic diagram of interaction mechanisms in the strain amplitude — temperature coordinates

The high-temperature background of internal friction, independent of the deformation amplitude, is described by the expression:

$$Q_{bg}^{-1} = A \exp(-U/kT). \quad (3.2)$$

In early studies [109] a rapid exponential increase in the background of internal friction is associated with the concentration of vacancies, the a.e. for formation of which can be determined by the tangent of the straight line slope in the coordinates In Q_{bg}^{-1} — 1/T. At the same time, the a.e. for formation of vacancies increases with increasing bonding forces (strength of interatomic bonds) in solid solutions. However, the scale of this effect turns out to be too large (up to 2 eV) to be explained on the basis of the mechanism of the formation of point defects. It is also difficult to relate the background of internal friction to a specific dislocation mechanism with the e.a. Uo > U_{bg}.

Within the frame of the concept [110], diffusion-controlled and thermally activated dislocation relaxation is a rate-controlling mechanism responsible for the energy dissipation in this region (with the a.e. Uo ~ U_{bg}/n). To determine binding energy (U_b) between dislocations and dissolved impurity atoms that are technologically inevitable for many metal alloy systems, measurements of amplitude-dependent internal friction (ADIF) were carried out on unpurified hcp Mg and hcp Be containing negligible quantities of solutes such as H, C, etc. using the inverted torsion pendulum technique [111] after introducing fresh dislocations.

3.2. Data of Hysteresis (Amplitude-Dependent) Internal Friction

The Granato-Lucke approach demonstrates the linear dependence of $\ln(\delta_n \cdot \varepsilon_0^{1/2})$ on $1/\varepsilon_0$ [103, 107]. Treatment of the data in the theoretical coordinates allows one to calculate values of the minor pinning length for dislocations (L_c ~ 17-60 nm) from the logarithmic plot slope. The calculations indicate the expected composition and thermally activated unpinning of dislocations from solute atmospheres set by the physical nature of the magnesium alloy system under consideration. The low values of a.e. for sliding dislocation motion (~0.05 eV) in the dilute solid solutions also support the necessity for dragging the non-equilibrium Cottrell`s atmospheres at 423K / 60-70 MPa by the moving dislocations in the accelerating field controlled by pipe diffusion of point defects (Fig. 3.2).

The results indicate that the amplitude-dependent decrements of specimens at moderate strain amplitude (10^{-6}-10^{-5}) and the hysteretic dislocation damping data can be analyzed in terms of the Granato-Lucke theory [104] and its modifications [105, 108] to provide valuable information about the internal structure of as-cast metal alloy systems and, in particular, the solute atom-dislocation segregation process.

A solid internally dissipates energy through the induced motion of damped dislocation. Some of the applied energy is dissipated in the dislocation breakaway pro-

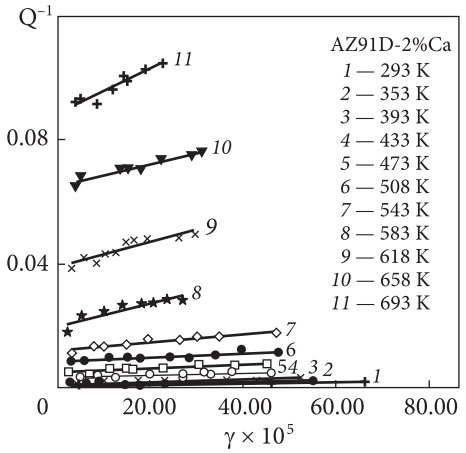

Fig. 3.3. Amplitude-dependent internal friction of AZ91D-2%Ca alloy at different temperatures

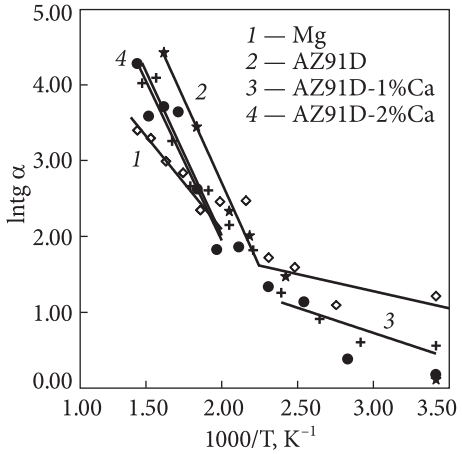

Fig. 3.4. Evaluation of binding energy E_b for different alloys

cess. As a result, internal friction loss arises which is hysteretic in nature, and therefore dependent on the amplitude of the strain resulting from oscillating stress, as predicted by the Granato-Lucke theory. Roger's modification of the analysis [108] predicts the gradual increase in the amplitude independent decrement and attributes it to the increase in the friction resistance of the lattice to dislocation motion with increasing temperature.

Measurement of the dependences of internal friction on the deformation amplitude of a sample at fixed temperatures is usually used to calculate the parameters of dislocation-impurity interaction in metals (Figs. 3.3 and 3.4). Amplitude dependences of internal friction (ADIF) were measured at different temperatures in the mode of constant increase in the deformation amplitude γ during torsional vibrations of the sample in the range from 4×10^{-5} to 60×10^{-5}.

$$Q^{-1} = K \times (\omega \cdot \exp(-U_0 / kT))^n, \tag{3.3}$$

where $\omega = 2\pi f$ is the measurement frequency; U_0 is the activation energy of diffusion climb of dislocations; k, n are constants for a given temperature range.

The damping data indicate (Table 3.1) that binding energy predominantly is governed by the elastic interaction between solute atoms and edge dislocation rather

Table 3.1. **Evaluation of binding energy E_b of dislocations with segregations and solute atmospheres**

Alloy	Mg	AZ91D	AZ91D-1Ca	AZ91D-2Ca	Mg-12Al-1.3Ca	Mg-12.5Al-1.2Ca
E_b, eV	0.21	0.38	0.37	0.36	0.5	0.32

than chemical bonding which may be responsible for the major contribution to the total solute atom-dislocation interaction in less dilute concentration range.

It is concluded that the observed in magnesium alloys amplitude-dependent decrement regularities follow the predictions of the Granato-Luke theory and its modifications in terms of the hysteretic dislocation damping mechanism. The damping property analysis is further extended for the evaluation of the binding energy between dislocations and alloying elements/impurities surrounding dislocation segments.

Unlike macrosegregation formed by reaction, which is likely to take place in higher energy input melts, microsegregation of the AE such as Ti and Sr occurs during solidification, cooling and even subsequent heat treatment by analogy with other nonequilibrium and rapidly solidified metal alloy system and melts containing well-defined short-range order. Following amplitude-dependent internal friction data such segregation effects become more pronounced in as-cast magnesium alloys with increasing temperature. The procedure reveals temperature of the Cottrell atmosphere condensation on dislocations, which separates thermally activated regions of pinning and depinning dislocations.

3.3. Linear Correlation between Residual Microplastic Deformation and ADIF

For polycrystalline magnesium (Fig. 3.5), a linear correlation is thought to be found between the amplitude-dependent internal friction (ADIF) and the direct measurement of the residual microplastic deformation, which makes it

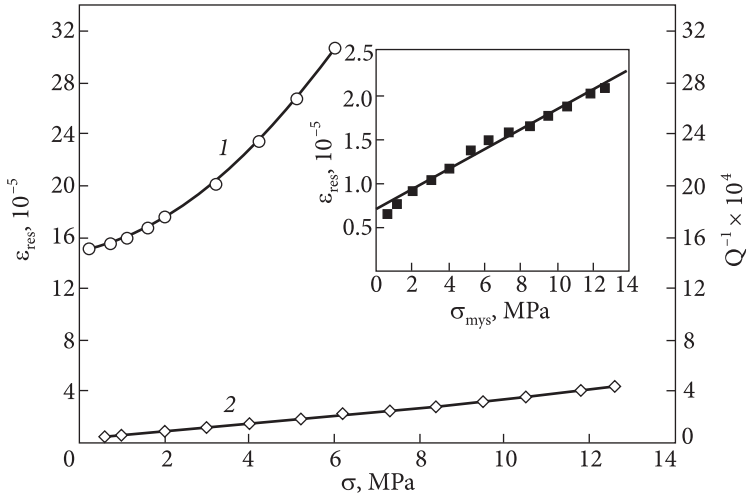

Fig. 3.5. Dependence of internal friction (1, Q^{-1}) and residual strain (2, ε_{res}) on applied stress for polycrystalline magnesium at 293 K. Insert: residual strain $\varepsilon_{res}^{1/2}$ as a function of microyield stress σ_{mys} under the data (*1*, *2*) with the correlation coefficient r_{xy}

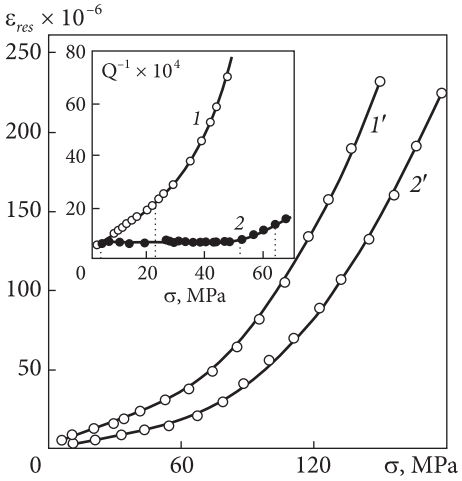

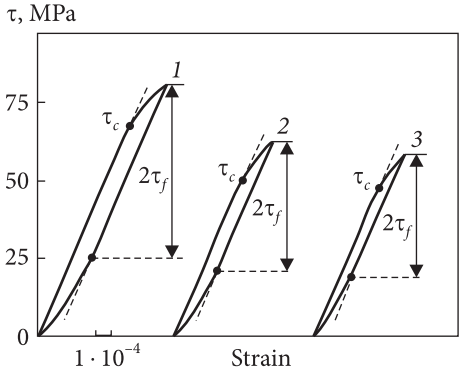

Fig. 3.7. Mechanical quasi-static hysteresis loops at temperatures of 321 (*1*), 396 (*2*), and 463 K (*3*) for Mg-0,07%Ca alloy

Fig. 3.6. Dependence of internal friction (*1*, *2*) and residual strain (*1′*, *2′*) on the applied stress for polycrystalline beryllium at 573 K (*1*, *1′*) and 293 K (*2*, *2′*)

possible to determine the corresponding critical stress for the micro-yield resistance (Fig. 3.6), the binding energy of dislocations with solutes, change in short-range order (elastic moduli) and micromechanical properties of metal crystals.

Nonlinear ADIF effects associated with dislocations were first discovered by Read [113]. Within the Koehler-Granato-L ucke approximation, these nonlinear effects of damping in the ADIF region are caused by pinned dislocations, which detach from impurity atoms at a critical stress. The suddenness of their breakaway according to Nowck's data [114] causes static hysteresis on the stress-strain curve (Fig. 3.7).

Here $2\tau_f$ is the resistance to dislocation motion; τ_C is the precise elastic limit.

The movement of dislocations is limited by linear tension (~$Gb^2/2$). Hysteresis losses (dissipation) of energy ΔE occur as a result of the breakaway of dislocations (for half cycle of oscillations).

Thus, a nonlinear dislocation damping is associated with a nonlinear increase in the dislocation segment length during bending of these linear defects.

3.4. Inelastic Relaxation and Stress-Induced Ordering

Under the data of mechanical frequency-dependent spectroscopy, in hcp metals with a low crystal lattice symmetry, an isolated atom cannot be a relaxation center. Two main types of mechanical stress relaxation of interstitial atoms (H, O, C, N) occupying octahedral or larger interstices in hcp metals have been detected by internal friction measurements. These are relaxation of intersti-

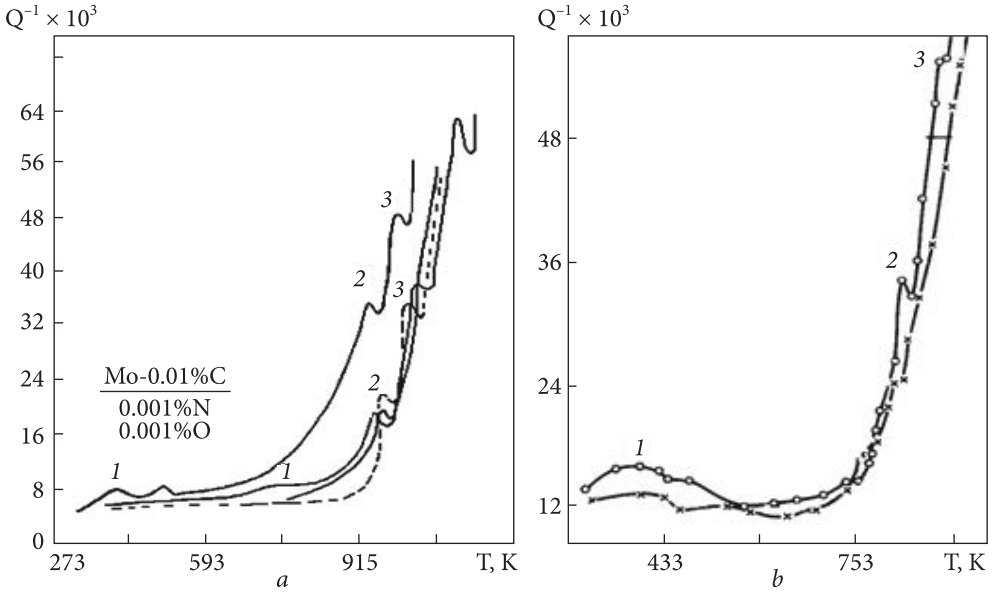

Fig. 3.8. Inelastic relaxation resonances on cell boundaries for Mo-0.01%C (*a*) and Cr-1%La-0.05%C (*b*) alloys: *1* — point defect-induced relaxation; *2* — relaxing cell boundary-induced relaxation; *3* — segregation-induced relaxation

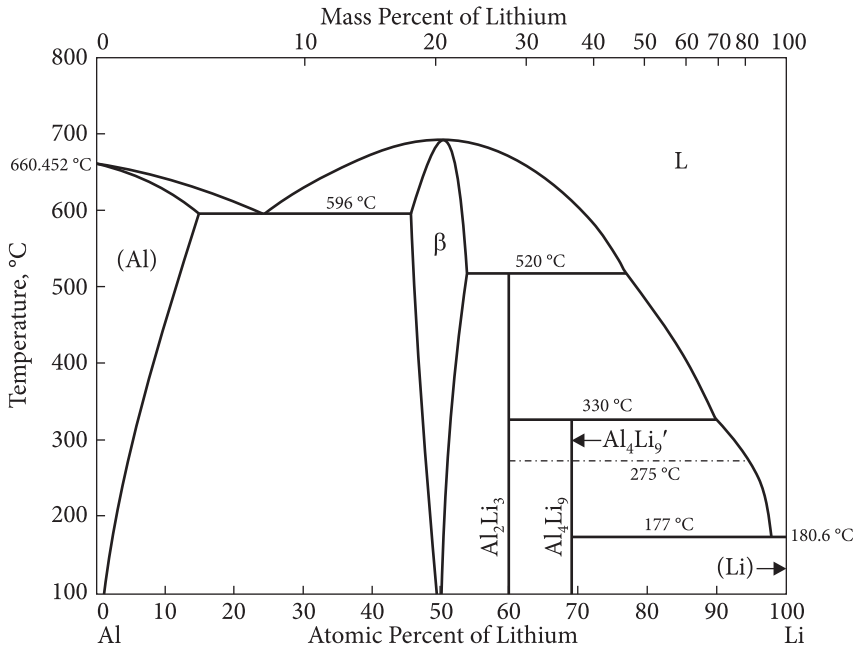

Fig. 3.9. Assessed Al-Li diagram [77]

tial-substitutional (i-s) paired defects and relaxation of interstitial-interstitial (i-i) paired defects. Relaxation modes for pair defects in hcp structures have been calculated by use of group theory methods. They involve i-i, s-i, s-s and V-V (vacancy) relaxations. In i-s pair s-atom is considered to be immobile; i-i pair differs with lower mobility and higher bonding energy than that for isolated atoms. The related migration of the defects caused by stress-induced diffusion promotes an additional time-dependent strain, especially at elevated temperatures (dynamic strain ageing, creep behavior). Mobility of these clusters is lower than that for singles at a given temperature.

The complete description is, therefore, complex in terms of the kinetics and the equilibrium constants controlling all the various possible reactions. Nevertheless, in hcp crystal interstitial atoms may exist in several different forms as isolated ones, as part of an isolated s-i defect and as precipitates. The great majority of them in the alloys are present in the form of s-i paired defects. Related solid solution hardening results from interaction between dislocation and solute atoms, Cottrell locking (by solute atom drift to dipoles) and strain interaction of solute atoms. Dislocations can be locked either by immobile precipitates or by cluster of solute atoms located at sites along the dislocation lines. One should only remark that dislocation appears to be preferential site for precipitation, but growth and solution of precipitates is observed under the influence of moving dislocations.

To obtain a far misoriented cell structure, the Cr—1La—0.05C and Mo-0.01C alloys were deformed by 90% ε at 1023 K. Their discrete temperature spectra of internal friction are shown in Fig. 3.8. In decaying solid solutions and in dilute alloys clustering of atoms and their segregation at the cell and grain boundaries occurs instead of precipitation. In this case, relaxation is caused by the motion of dislocations with their attendant atmospheres (pinning i-s and i-i defects) including atom H-substitutional atom pairs. Not so long ago some evidence has obtained that H-induced excess (non-intrinsic) vacancies are present in ordered alloys with hcp lattice, particularly in Mg alloys containing technologically inevitable (residual) H and H-like impurities (O, C, N) on the structural defects acting as reversible or irreversible traps. Effects of paired (i-i, i-s, v-s) relaxation are observed in measured discrete temperature spectra of internal friction.

The phenomenon of paired relaxation in a cast structure first observed in our laboratory as well as its experimental evidence were studied by mechanical spectroscopy which yields forming the paired defects, i.e., primary pairs of Alloying Elements (AE) — Excess Vacancy (EV) in the early (pre-precipitate) stage in segregated solid solutions of as-cast Al—Li (Fig. 3.9) and eutectic non-equilibrium casting Mg—Ba alloys oversaturated by excess vacancies (Fig. 3.10). The resonance absorption of elastic energy is certain to occur by rapid (short-range) mechanism. The resonance condition $2\pi f \cdot \tau = 1$, where f is the frequency; τ is the relaxation time, is caused by EV-AE pair reorientation in the stress field.

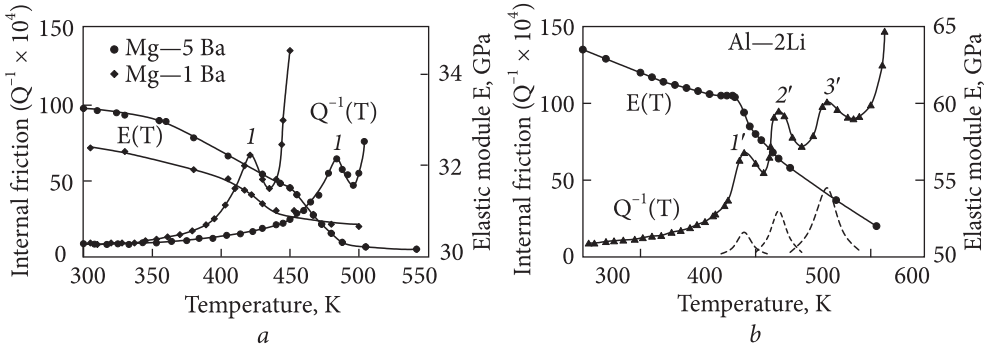

Fig. 3.10. Discrete temperature spectra of internal friction $Q^{-1}(T)$ with measured damping components (above background) and elastic modules changes E(T) for Mg—1Ba—1.1H alloy; Mg—5 Ba—1.1H alloy and Al—2Li alloy (f = 2 kHz): *a* — *1* — (Ba, excess vacancy) pair-induced relaxation peak; *b* — *1′* — (Li, excess vacancy pair) — induced relaxation peak; *2′* — grain boundary relaxation peaks; *3′* — Li segregation-induced impurity relaxation peak. (Ba — substitutional atom; Li — interstitial atom)

It is known [103, 104] that Kehler-Granato-Lucke's theory of dislocation damping connects the mechanism of energy dissipation with the vibration frequency. Usually, a change in the vibration frequency causes a shift in the temperature position of the internal friction peak of Q^{-1} (T), which indicates the relaxation nature of the thermally activated process. In this case, the frequency shift f_1/f_2 is one of the characteristics of the controlling mechanism of inelastic relaxation (Fig. 3.10, *a*, *b*). However, in the study of kinetic curves-isotherms of mono- and polycrystals irradiated with electrons, it was established [115] that $Q^{-1}(T)$ passes through a maximum proportional to the number of point defects, dependent on the deformation amplitude and independent of the vibration frequency in the low frequency range. The observed effect is accompanied by an increase in the ADIF background, which excludes the contribution of diffusion and is explained by local (short-range) fixing point defects on dislocations, thus reducing their contribution to damping (energy dissipation) by the long-range mechanism. Moreover, in the alloys of the Mg—Ba system, on the curve describing the discrete temperature range of internal friction $Q^{-1}(T)$ (Fig. 3.11), a maximum at 403 K is found, the temperature position of which is retained under changing frequency.

The appearance of a 403 K peak indicates the formation of pair defects, which can reduce hcp lattice symmetry with the formation of an associate of vacancy origin, for example, a Ba atom with an excess vacancy [116]. It is important to emphasize that such a defect structure does not cause a frequency shift in the discrete temperature spectrum (Fig. 3.11), i.e., in the Mg—Ba system of the studied composition, there is no inelastic relaxation, which is the most probable effect for solid solutions.

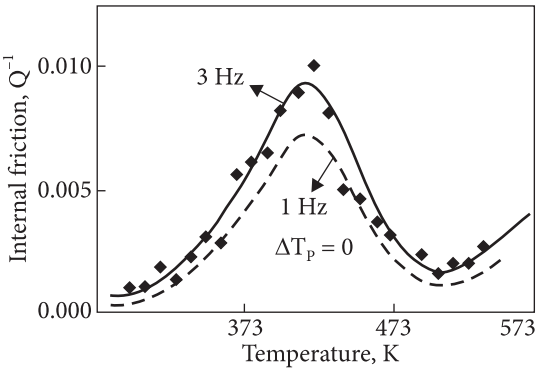

Fig. 3.11. The discrete temperature spectrum of non-relaxation origin for Mg-2.1 Ba-H alloy at two damped natural frequencies

Thus, according to [117], structural relaxation occurs on the basis of the pair defect Vi-Ba atom, which form relaxation centers in the hcp lattice of low c/a symmetry (compressed along the c axis), and thus predetermines their ordering. In this case, vacancies compensate for the difference in charges in solid solutions [135], the mechanism of structural relaxation controls the first stage of the formation of a mesoscopic (cluster-forming) structure of alloys with strong chemical interactions between the components and the process of their short-range ordering. Indeed, in real systems with distributed parameters, motion is transferred from one element (atom) to another, which is not characteristic of a fixed internal structure. In other words, in this case, density, elasticity and other properties change from point to point continuously. Therefore, such systems have an infinitely large number of degrees of freedom and an infinitely large number of normal vibrations [135]. With external excitation of the system of normal vibrations, its resonance properties are determined. Resonance occurs when the frequency of a harmonic external influence is close to one of the natural frequencies of the system or to their linear combination if the external influence changes the parameters. In this case, deviation from the kinetic Arrhenius equation for normal solid solutions should be expected. Hysteresis losses of internal friction are the result of microyielding of free damping of oscillations, independent of frequency.

One can see no change in the $Q^{-1}(T)$ peaks behavior with the frequency change (Fig. 3.11). $Q^{-1}(T)$ peak in the hcp Mg—2.1Ba internal friction spectrum will not change with the measuring frequency change under external oscillation stress. If the pinning defects, i.e. solutes, are mobile at the peak temperature (by absorption mechanism, then change in their distribution by high oscillation amplitude is possible. This means, in fact, that the observed peak Q^{-1} (T) is caused either by phase transformation of the classical type, or, most likely, by short-range ordering areas of isotherms $Q^{-1}(T)$ with the formation of metal clusters A_mB_n having own electron structure.

The absence of frequency shift of the $Q^{-1}(T)$ peak in the mechanical spectrum of the Mg-2.lBa alloy means that the relaxation process in this system could be described by a continuous spectrum of relaxation time (due to the formation of atomic groups-clusters in the process measurements) with self-organization of the structure of solid solution in thermodynamically and kinetically nonequilibrium conditions [118]. The non-relaxation behavior of Mg—2.1Ba—H alloy in the field of cycle stresses

(Fig. 3.11) is associated with the quasi-static displacements of atoms Mg and Ba having a weak binding energy (E_b ~ 0.15 eV) with dislocations in the presence of excess vacancies. In the case, such a complex is likely to present an elastic dipole of high relaxation stability due to local (short-range) ordering of the system. The weak pinning of dislocations by barium and strong interaction of Ba with excess vacancies (with the binding energy around 0.5 eV) result in the formation of the locally ordered and thermally state structure of short-range order with the participation of excess vacancies, for example, generated by hydrogen or pre-strain.

3.5. Kinetics of Cluster-Induced Age-Hardening

Isotherms of dislocation damping Δ in the Cottrell-Bilby coordinates for hcp metal crystals such as unalloyed titanium and beryllium are presented in Fig. 3.12. According to the results obtained, the dislocation damping plotted against the time obeys the traditional Cottrell-Bilby time law [119] as thermally activated kinetic process with a time exponent of 2/3. The Cottrell-Bilby relation is certain to be valid only for normal solid solutions (Fig. 3.12), e.g., technical grades of hcp metals containing free dislocations that interact with isolated solutes in early stage of aging. This means that kinetics of the Cottrell dislocation locking seems to occur provided that the isolated inevitable impurity solutes move to the free dislocations by long-range (diffusion-controlled) mechanism [120].

However, in irregular solid solutions containing excess (strain-produced) vacancies, another mechanism operates. Indeed, the occurrence of the time and temperature-dependent maximum on the kinetic curves-isotherms for some selected hcp metal alloys cannot be assessed in terms of the Cottrell-Bilby time law and Cottrell locking (Fig. 3.13). Disagreement for hcp solid solutions enriched with excess vacancies by Cottrell-Bilby concept is observed at later stage of the dislocation damping in the substitutional alloy hcp Mg—Ba, H. Kinetic curves-isotherms are characterized by long-range ordering mechanism with large diffusion length required for migration of solutes towards free dislocations, at early stage of decay.

The kinetics of the irregular damping formation in interstitial hcp Be—C, Fe, H solid solutions is similar to that observed in the substitutional hcp Mg—Ba, H solution after their high-temperature annealing at 923 K for 10 hours to neutralize the influence of substitutional Fe atoms in the hcp Be—C, Fe system. The process is controlled by bulk (long-range) diffusion of the interstitially soluble carbon with an a.e. of about 0.65 eV and its binding energy with dislocations equal to 0.34 eV in the early stage of low temperature aging in the temperature range of 393-573 K (Fig. 3.13, insert). The dislocation damping passes through temperature-dependent maximum at a later stage of aging which is likely to be due to Be_4C cluster formation [121]. It is reasonable to suppose that the origin of these maximums is attributed to the transfor-

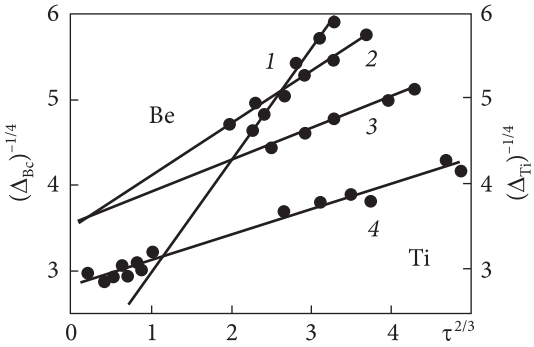

Fig. 3.12. The Cottrell-Bilby time law testing at the earliest stage of dislocation damping for hcp Be *(1, 2, 3)* and hcp Ti (*4*) at aging temperatures of 453 (*1*); 498 (*2*); 523 (*3*), and 723 K (*4*) under the data of amplitude-independent internal friction designated as Δ by the Cottrell-Bilby terminology

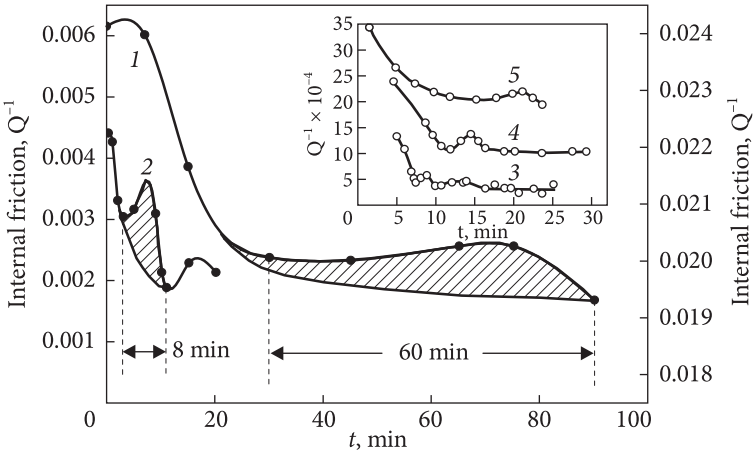

Fig. 3.13. Kinetics of decomposition of primary α-solid solutions based on the free dislocation blocking by solute segregations at the earliest stages of dislocation damping for hcp solid solutions with activation of short-range (cluster-forming) mechanism at later stages of aging (at 423 K (*1*) and 763 K (*2*)) for Mg—2.1Ba ($Mg_{0.94}Ba_{0.06}$) alloy; insert: for Be—0.1Fe—0.1C alloy at aging temperatures of 523 (*3*), 498 (*4*) and 453 K (*5*)

mation of the pre-cluster separations of vacancy-containing pair defects into prephase cluster compounds (Mg_mBa_n and Be_mC_n) by a pre-precipitation (short-range) mechanism with aid of excess vacancies at the later stage of aging. Moreover, it is important to note that in this case the temperature location of the so-called A_mB_n cluster-induced peak in the discrete temperature spectrum of internal friction $Q^{-1}(T)$ does not depend on the vibration frequency in the range of 0.5-3.5 Hz (Fig. 3.11). With this provision, the nanophase transformations in the metal alloy systems under investigation are believed to occur finally by a cluster-forming nucleation mechanism. In particular, under the data of mechanical spectroscopy and amplitude-independent internal friction there are two metastable states of nanoclusters involving primary Mg_n complexes associated with excess vacancies V_i ($n \to 2$) and resulting nanoclusters Mg_nBa_m ($n = 8, 18 \Rightarrow Mg_{16}Ba_2$).

Vacancies affect the kinetics of cluster transition, for example, fcc — bcc transition in alloys of the Fe—Ni system [122]. Vacancy clusters and other complexes of point defects create around themselves asymmetric deformations, or rather, atomic displacements in the vicinity of this defect and thus become centers of local loss of stability of the crystal lattice, providing, in particular, the diffusion-free nature of structural (martensitic) transformations [123].

New regularities of the kinetics of decomposition with clustering of the crystalline structure of solid solutions relate to the following*. When studying the kinetics of blocking of dislocations in bcc and hcp metals containing accompanying and technologically unavoidable impurities, it was found that bulk (long-range) diffusion of impurity atoms to fresh dislocations with the formation of Cottrell atmospheres is the controlling mechanism of the earliest (pre-decay) stage of aging. The activation of this mechanism obeys the Cottrell-Bilby time law for all investigated objects — normal solid solutions. However, the isotherms of the kinetic curves at the later stages of the decomposition of hcp substitutional (Mg—Ba) and interstitial (Be—C) solid solutions doped with cluster-forming elements show anomalies in the form of maxima, the time position of which (with different incubation periods) depends on temperature (Fig. 3.13).

Deviations from the Cottrell-Bilby law, $t^{2/3}$, and the Arrhenius ratio are explained by the formation of a primary cluster structure of a new local (short-range) order, which partially destroys the primary (long-range) order of the crystal structure of solid solution (Mg—Ba, Be—C). Thus, the formation of short-range order in a cluster structure is a kinetic process.

There is a group of metals prone to the formation of atomic groupings (clusters), which are an integral part of the crystal structure of the primary α-solid solution. With the introduction of the so-called cluster-forming AE (Ti, Gd, Ba, etc.) in the melts, weak (alternating) heat effects are observed, detected by the DTA method in Mg—Ba cast alloys, Mg—Al—Ca—Ti and Mg—Al—Ca —Gd systems with a high accuracy of 0.01 J/g and caused by the synthesis and decomposition of the so-called non-crystallizable cluster (chemical) compounds A_mB_n: Mg_6Ba_2, $Mg_{16}Ba_2$, Al_mTi_n. The insignificant energy required for the formation/decay of an A_mB_n cluster (~0.05 J/g) is several orders of magnitude lower than the energy of the first-order phase transition (crystallization-melting ~200-300 J/g).

Therefore, energetically favorable cluster structures are formed in the process of crystallization of a primary α-solid solution, being embedded in its crystal lattice as an irregular structure with different chemical bond lengths and aperiodic interatomic distances. In the studied solid solutions, including Mg—2.1Ba, the energy of cyclic deformation is an acting force of local order, when the first neighboring atoms reach essential own excess. The resulting clustering of the structure should be considered as one of two ways of local (short-range) ordering of a solid solution [117].

* The question is under discussion.

At 423 K, there are enough excess vacancies involved in the formation of the Mg_mBa_n cluster (8 min). Annealing these vacancies at higher temperatures (673 K) slows down the clustering reactions (from 8 to 70 min.). As a result of short-range ordering at 423 K, primary isolated associates (0.7-1.5 nm) of the Ba atom — excess vacancy type are formed with a binding energy of about 0.5 eV. After some time, depending on the temperature, they gradually (by the self-assembly mechanism) transform into stable nanoclusters 8-15 nm in size with their own electronic structure [124]. Due to over 40% of the size mismatch between the atomic volumes of Mg and Ba, their displacement occurs with the participation of excess vacancies according to one of the possible reactions $Mg_n + Ba_m + V_i \Rightarrow Ba_nV_i$: primary cluster, $Mg_6 + Ba_2 \Rightarrow Mg_6Ba_2$ metastable cluster, $Mg_{16} + Ba_2 \Rightarrow Mg_{16}Ba_2$ is a quasi-equilibrium, thermally stable cluster. It is known that the theory of dislocation damping relates the mechanism of energy dissipation to the vibration frequency.

At low temperatures (up to 423 K), the clustering process is quite rapid (up to 5 min), since it is limited by the easily activated formation of primary associates bound by excess vacancies, for example, an atom Mg-excess vacancy (n = 2). At 673 K, thermal activation makes a significant contribution to the structural rearrangement of the cluster, accompanied by self-organization (self-assembly) of primary associates "Mg atom — excess vacancy" into clusters with their own electronic structure. The binding energy increases with the growth of the cluster, $Mg_{16}Ba_2$ (n = 18), which is accompanied by the formation of a stronger (hybrid) chemical bond as a result of the overlap of electronic wave functions (*s, p*-states of Mg and *d*-states of Ba), increasing the density of electronic states near the Fermi energy. It is important to emphasize that the time for self-assembly of a cluster of critical size increases by an order of magnitude and reaches 50-70 min (Fig. 3.13).

In our studies of the Mg-Ba alloy, it was found that the stability of clusters increases with an increase in the number of atoms (n = 2, 8, 18...). Interaction of primary associates — isomers of Mg—V (n = 2) during the formation of an isolated cluster of critical size (n = 8) is accompanied by a decrease in surface energy and an increase in the time of structural rearrangement by almost an order of magnitude.

The absence of a frequency shift of the $Q^{-1}(T)$ peak in the mechanical spectrum of the Mg—2.1Ba alloy (Fig. 3.11) means that the relaxation process in this system can be described by a continuous spectrum of relaxation times (due to the formation of atomic groupings (clusters) during measurements) with self-organization of the solid solution structure under thermodynamically and kinetically nonequilibrium conditions [124]. The need for a large number of static displacements for clustering the structure of the Mg—Ba alloy with partially broken long-range order is associated with over 40% size mismatch between the Mg and Ba atoms, their negligible mutual solubility, and the elastic resistance of the α-Mg matrix. Clustering of the structure is provided by statistical displacement of atoms in the field of cyclic stresses. This displacement (in one direction) is con-

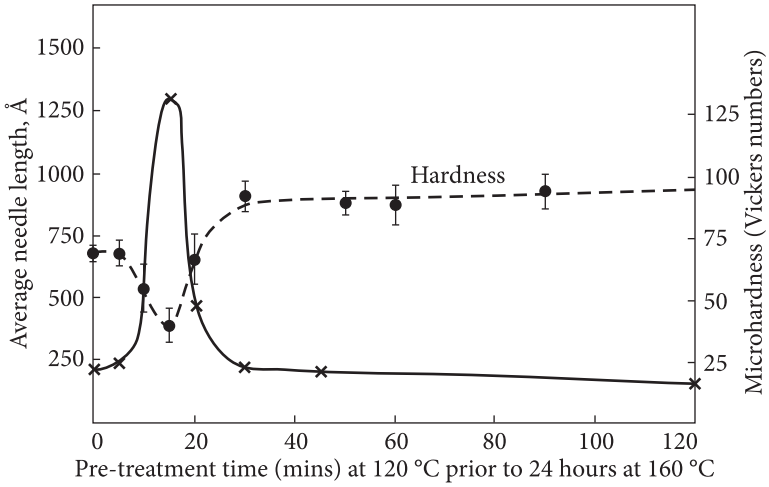

Fig. 3.14. Microhardness and nanoparticles size as functions of heat treatment time [96]

trolled by the binding energies of the primary Ba—V_i defects and Mg_mBa_n clusters. This effect manifests itself under conditions of chemical diffusion, when the redistribution of dissolved atoms and the diffusion coefficient are determined by chemical activity rather than concentration, if the energy of interacting atoms decreases. In other words, the law of such a redistribution can increase the probability of barium atoms hopping towards a high concentration for the Mg_nBa_m atomic group formation.

Therefore, in the considered metal systems with distributed parameters, i.e. with an infinitely large number of degrees of freedom, clustering of the α-Mg solid solution structure is accompanied by the formation of nuclei of primary associates Ba—an excess vacancy (n = 2) and their growth by the mechanism of self-organization of Mg_6Ba_2 inside the solid solution through metastable states n = = 8, to the cluster $Mg_{16}Ba_2$ (n = 18). Under the action of the applied cyclic stress, the phase shift between stress and strain is provided by the structural rearrangement and movement of the cluster "walls". The stable electronic structure of the valence band formed in Mg_nBa_m clusters as a result of hybridization of the *s, p*-electronic states of magnesium and *d*-electronic states of barium atoms creates a "shell" structure of the cluster (n = = 2, 8, 18...), eliminating the minimum on the density of states N (E) curve and increasing the quantum yield of photoemission in the UV spectral region by 2-3 orders of magnitude. Barium as an emission-active element in the Mg—Ba system causes a sharp absorption of laser UV radiation if the packing density of 8-10 nm nanoclusters (quasi-intermetallic compounds $Mg_{16}Ba_2$) reaches $10^{14}/m^2$.

It can be seen that the structural (cluster) transition develops with time and increases with the transformation temperature. According to the data of mechanical

spectroscopy and amplitude-independent internal friction (Fig. 3.13), two stages of the formation of a short-range order cluster structure were found in the Mg—Ba system: (a) the formation of pair defects — primary associates "Ba_n—excess vacancy V_i" at 423 K and (b) the formation of $Mg_{16}Ba_2$ nanoclusters at 673 K (near the stoichiometric composition $Mg_{17}Ba_2$). In a stable hcp α-Mg lattice, intermediate states of a nanocluster (for example, Mg_6Ba_2) gradually lose stability in the field of cyclic stresses and, as a result of short-range ordering, transform into a $Mg_{16}Ba_2$ nanocluster with an hcp crystal-like short-range order structure, which is essentially a weak distortion of the hcp lattice of α-Mg (in equilibrium conditions for the α-Mg—$Mg_{17}Ba_2$ eutectic and the $Mg_{16}Ba_2$ cluster).

Summing up, it should be emphasized that at interatomic distances, the short-range interaction in solid solutions is most likely almost instantaneous and, therefore, we can expect a deviation from the Cottrell-Bilby law $\tau^{2/3}$ for long-range AEs/impurity diffusion to "fresh" dislocations. Internal friction data confirm the formation of local short-range order in these so-called open systems with partially broken long-range order. A cluster as a crystal-like atomic group manifests itself at the mesoscopic level of collective interactions as a result of distortion of the crystal lattice and violation of the packing order. Based on the results of studies of the Mg—Ba system, there is every reason to assert that the high rate of collective interaction of defects in a stress field, i.e., fast kinetics of synthesis or decay of cluster compounds is a sign of activation of short-range controlling mechanisms. In this case, structural transformations include only short-range (0.2-0.3 nm) exchange of atoms, and not full-scale (at 300-500 interatomic distances) bulk diffusion of AE. In this regard, in contrast to the slow kinetics of the solid solution decomposition, the segregation of AEs at dislocations under conditions of short-range diffusion becomes extremely fast. Thus, a decrease in lattice (bulk) diffusion (upon introducing more refractory AEs) and a slowdown in the activity (limitation of mobility) of dislocations in slip systems are essentially the only prerequisites for a drastic decrease in the rate of dislocation microyielding (creep for slow dislocations) of the primary α-solid solutions under study. Microhardness (Hμ) measurements of an aluminum alloy with 10 nm particles indicate that the two-step aging produces a complicated structure, which contains observed coarse precipitates (at early stages) with low Hμ and the clusters nucleation (at the later stage) with increasing Hμ due to their growing contribution (Fig. 3.14).

Concluding Remarks

The great value of results obtained resides in strengthening effect of the short-range order (SRO) which is related to destroying SRO in solid state (substitutional) alloys by moving dislocations. This should lead to an additional increase in the strength of alloys by Fisher mechanism [125]. The stress τ_{SRO} to destroy short-range order is described by the following expression

$$\tau_{SRO} = \frac{\Delta\varepsilon_0 - T \cdot \Delta S_0}{fb}, \tag{3.4}$$

where $\Delta\varepsilon_0$ and ΔS_0 denote, respectively, changes in the internal energy and entropy (per atom) due to slip through a distance equal to the Burgers vector b; $f \cong \sqrt{3/4 \cdot a^2}$ is the slip surface area corresponding to one atom; a is the lattice parameter; $b \cong a/2$ for {111} <110> fcc lattice.

Section 2

RATE-CONTROLLING STRENGTHENING MECHANISMS

Everything complicated is unnecessary, but everything you need is simple.

Hryhorii SKOVORODA

Chapter

4 LATTICE STRENGTHENING

4.1. Two Alternative Approaches Based on the Contributions of Peierls Barriers and Interstitials to Temperature Dependence of Macroscopic Yield Stress

There are two commonly discussed viewpoints which attempt to explain the rapid increase of macroscopic flow stress τ in bcc metals, for example VA and VIA groups, at low temperatures [126]. According to one of them, the observed strong temperature dependence of τ (Fig. 4.1) is most likely to be caused by intrinsic lattice properties as high Peierls barrier that controls the thermally activated movement of dislocations [127]. Peierls stress as a lattice stress is the force first discovered by Peierls and modified by Frank-Nabarro [128]. It is needed to move a dislocation within a plane of atoms in the cell. The magnitude varies periodically as the dislocation moves within the plane. Peierls stress depends on the size and width of a dislocation and the distance between planes. Therefore, Peierls stress decreases with increasing distance between atomic planes. Yet since the distance between planes increases with planar atomic density, slip of the dislocation is preferred on closely packed planes. It is generally accepted that the Peierls stress also relates to the temperature sensitivity of the yield strength of a material because it too depends on both short-range atomic order and atomic bind strength. As temperature increases, the vibration of atoms increases and thus both Peierls stress and yield strength decrease as a result of weakening atomic strength at high temperatures. From a second standpoint [129-131], the cause of the observed low temperature hardening (Fig. 4.1) is interaction of mobile dislocations with tetragonal distortions due to impurity interstitials (O, N, and/or C) [129, 130]. However, there is a third standpoint which until now has not received so much attention. Accordingly, there exists an inherent lattice hardening, but interstitial impurities modify

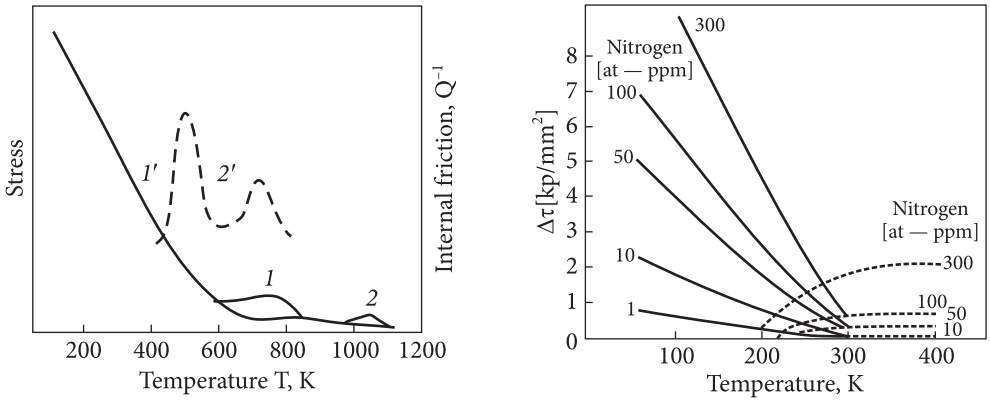

Fig. 4.1. Temperature dependence of yield stress for bcc metals having the effects of dynamic strain aging (*1*, *2*) under the data of mechanical spectroscopy (*1′*, *2′*)

Fig. 4.2. Impurity-induced increase in the flow stress $\Delta\tau$ as a function of temperature for tantalum-nitrogen system: Solid lines: $\Delta\tau_1 = \alpha_1(T) \cdot \sqrt{c}$; dashed lines: $\Delta\tau_2 = \alpha_2(T) \cdot c$ [126]

the hardening process, giving rise to an additional increase in the flow stress with decreasing temperature [131, 132].

The stress components $\alpha_1 \cdot \sqrt{c}$ and $\alpha_2 \cdot c$ formally describe the influence of impurity interstitials on the flow stress (Fig. 4.2). The impurity models by Fleisher and Frank [128, 133] predict approximately $\tau \sim \sqrt{c}$ for the solute concentration c at low temperatures and $\tau \sim c$ at higher temperature. It is noteworthy that the expressions $\tau \sim \sqrt{c}$ and $\tau \sim c$ describe the short-range interaction of mobile dislocations with impurity interstitial solute concentration in the slip planes and their long-range interaction with Snoek impurity interstitial atmospheres [128, 134].

Experiments carried out on carefully purified and doped with interstitial impurity (nitrogen) tantalum single crystals are in qualitative agreement with the predictions of the impurity hardening models [133, 135]. The equations derived by Lachenmann and Schultz [126] assume implicitly that the intrinsic and the impurity-induced stress components are additive (Fig. 4.2). Thus, there exists an inherent lattice hardening giving rise to a strong increase in the macroscopic flow stress with decreasing temperature. Impurity interstitials induce a further increase in the thermal component of the flow stress at low temperatures. Above r.t. there is also a temperature independent hardening caused by impurity interstitials.

4.2. Smoothing of the Peierls Potential Relief by Interstitials

The appearance of $(\tau_f - \tau_{fo})$ thermal component in interstitial solid solution of the Mo—C system reasons that carbon atoms as thermally activated obstacles smooth out the potential relief of Peierls ($\alpha = -1$) with the aid of

thermal fluctuations. Parameter value of $\alpha = -1$ indicates a greater width of dislocation, lesser value of Peierls' barrier and hence a higher mobility of dislocations in the bcc lattice.

As shown theoretically by Frank and Sestak [135], dynamic dragging of free (fresh, unlocked) dislocations at thermally activated obstacles [139] is the controlling mechanism responsible for low-temperature properties of bcc interstitial solid solutions. At low (cryogenic) temperatures below critical temperature ($T < T_0$) strong temperature dependence of τ^* for Mo—C alloys is determined by the strengthening dynamic braking and by the growing influence of the Peierls-Nabarro forces on the mobility of free dislocations. In this connection, variations of $\tau^*(T)$ do not depend on the carbon concentration (Fig. 4.3, *a*). Taken account of the predominant inherent (lattice) contribution, it is unlikely in such circumstances that dissolved carbon, as well as H and H-like impurities might be the source of transcrystalline brittleness of bcc Mo at low (cryogenic) temperatures.

At the same time the existence of concentration dependence of athermal stress τ_{fo} (Fig. 4.3, *b*) indicates the interaction between mobile dislocations and carbon atoms, i.e., interstitial solution hardening contribution. Monotonous growth of the τ_{fo} and $\tau(c)$ curves for Mo—C alloys is attributed to a considerable extent by the growing solid solution saturation which increases the differences between the matrix shear modulus and the tetragonal distortion of lattice domains. In this case the contact (power) interaction between mobile dislocations and dissolved carbon atoms influences only the athermal components of the flow stress and of resistance to free dislocation motion (frictional stress). Such a methodological approach allows one to separate the predominant inherent (lattice) and the predominant impurity (solutes) contributions, as well as the corresponding controlling mechanisms.

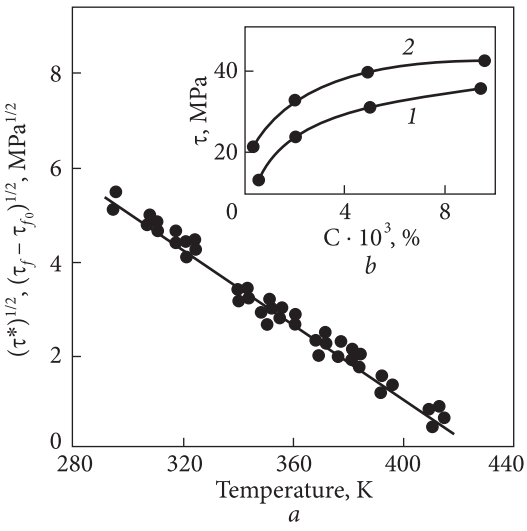

Fig. 4.3. Impurity and lattice contributions ratio in bcc interstitial solid solutions: (*a*) thermally activated contribution of the lattice resistance (Peierls-Nabarro stress) for Mo-0.001, 0.002, 0.005, and 0.1% C; (*b*) concentration dependences of the athermic components for flow stress τ (*1*), and the lattice-frictional stress or the resistance to dislocation motion x_{fo} (*2*); τ^* — thermally activated component of the flow stress; $\tau_f - \tau_{fo}$ — thermally activated component of the lattice-frictional stress for transition metals

In other words, it is significant that at $T < T_0$ the energy barrier created by forces of contact interaction appears to be less essential than the one for nucleation of double kink of critical length. Weak trend to reducing the critical temperature (T_0) with increasing carbon content demonstrates that Peierls mechanism (Seeger approximation) controls the mobility of dislocations in bcc solid solutions of the Mo—C, H system at low (cryogenic) temperatures.

First experimental evidence is obtained to indicate that interstitial solutes can smooth out a potential relief of bcc lattice with high barrier of Peierls. This effect becomes appreciable after clustering a structure reducing a number of centers of dislocation dragging and increasing the relaxation ability of matrix, but does not cause temperature impurity softening phenomenon because of prevailing influence of the Peierls barrier.

Working up and comparative analysis of the data for Mo—C, H alloys in the theoretical coordinates of Dorn and Raynak [127] and Seeger [136] for thermally activated Peierls mechanism of the plastic deformation, as well as of Feltham [137] for contact interaction of dislocations with impurities indicate that Seeger concept, more precise for bcc solid solutions, provides for the best coincidence of theoretical and experimental curves $\tau^*/\tau_{kp} = f(T/T_0)$ in the case of smoothing potential relief of Peierls ($\alpha = -1$) rather than in the case of the usual (sinusoidal) potential relief of Peierls ($\alpha = 0$). Seeger's theory based on the model of thermally activated motion of screw dislocations takes into account the interaction of the next single kinks and in this approach is presented by the following relations:

$$T \cdot f(T) = U_k - \left\{ \frac{a^3 \cdot b \cdot C_0}{2} \right\}^{1/2} \cdot \sqrt{\tau^*} \tag{4.1}$$

and

$$f(T) = H(\tau^*)/T = k \cdot \ell n \left\{ \dot{\varepsilon}_0 / \dot{\varepsilon} \right\}, \tag{4.2}$$

where $H(\tau^*)$ is the a.e. for Peierls mechanism of plastic deformation; U_k is single kink energy ($U_k \approx 0.4Gb^3$ and $U_k \approx 0.6$ eV for Mo, refined up to 99.999 %); *a* is the lattice parameter; b is the Burgers factor; $C_o \approx f(d, b)$; τ^* is the thermal component of flow stress.

Seeger approximation predicts the exponential dependence of $\tau^*/\tau_{kp} = f(T/T_0)$ and becomes valid for Mo—C, H at $\alpha = -1$ and $\tau^*/\tau_p < \bar{\tau}/\tau_p$. It should be emphasized that in the region of quasi-brittle transition and in the linear coordinates of $\sqrt{\tau - T}$ by Seeger temperature dependences of flow stress coincide with the temperature dependence of resistance to dislocation motion within the accuracy of observation. It means that Peierls' mechanism of formation of double thermal kinks in screw dislocations (Seeger approach) does operate in bcc interstitial Mo—C solid solutions. In this case temperature changes of τ^* and τ_f for Mo and its solid solutions with carbon are controlled by a single dislocation mechanism responsible for the

thermally activated overcoming of Peierls' barrier indicative of smoothing potential relief in bcc lattice by mobile screw dislocations.

Concluding Remarks

In the Mo—C, H solid solutions the dissolved interstitial atoms contribute to the change in thermal component of the resolved critical shear stress smoothing out a potential relief of bcc lattice with aid of thermal oscillations and facilitating thus thermally activated overcoming of Peierls' barriers by dislocations.

Chapter

5 GRAIN BOUNDARY AND INTERFACE STRENGTHENING

5.1. GB Glide and GB Relaxation

GBs are important because they have a controlling effect on the creep properties and premature fracture in metallic alloys. They are expected to provide the principal limit on structural cohesion and GB sliding, and hence their detailed structure consisting of GB dislocations is vitally important in understanding the creep properties of the magnesium alloys studied. GB diffusion creep regime corresponds to the Coble creep mechanism at higher temperatures.

It is considered that grain boundary diffusion in fine-grained materials is the rate controlling mechanism at elevated temperature with activation energies much lower than that for self-diffusion in Mg to be 1.35 eV [138]. Microyielding in this case takes place through a glide along the high angle grain boundaries (Fig. 5.1). Stabilizing this grain structure by means of a dense distribution of particles results only in the best superplastic behavior of metallic alloys. For example, Norsk Hydro A/S (Magnesium Divission, 3900 Porsgrunn, Norway) has successfully utilized the rapid solidification technique to produce extremely fine-grained magnesium alloy AZ91 having an elongation of up to 1000% in the temperature range of 548-573 K. However, a high density of pores developed during the process led to reduction in the strength for materials with extremely fine grain size which remains stable at the temperature deformation.

The GB-inelastic relaxation for bicrystalline Al (sliding mechanism) (Fig. 5.1) is evolved in the form of $H^* \sim \text{const} \cdot \tau_{GB}$, which is equal to resolved shear stress at GB. These results obtained are consistent with the GB-inelastic relaxation measured for hcp magnesium of high purity (Fig. 5.2). Observed relaxation occurring in grain boundaries relates to the GB dislocations having the Burgers vectors of about 1/3 that for lattice dislocations.

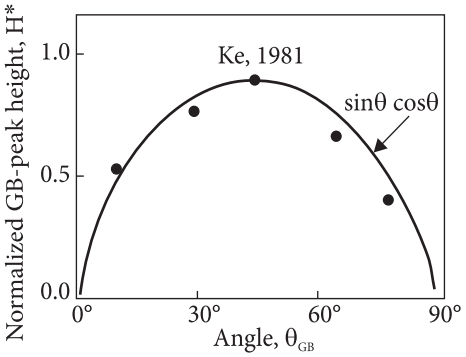

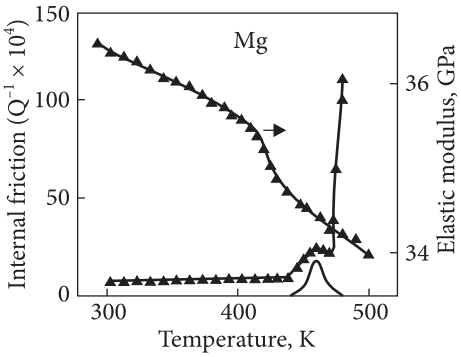

Fig. 5.1. The dependence of the normalized GB-peak height H* on the angle θ_{GB} [139]

Fig. 5.2. Grain boundary peak of internal friction and modulus change in the region of relaxation spectrum

Atomistic computer simulations have shown [140] that unlike the dispersed phase particles observed in the disintegration structure after alloy aging, the interfaces in crystallizing-out eutectics contain misfit dislocations. Interfacial energy for the boundaries is determined by sum of two components

$$\gamma_{\alpha\beta} = \gamma_{\alpha} + \gamma_{\beta}, \tag{5.1}$$

where γ_{α} is the specific energy of the misfit dislocations, γ_{β} is chemical contribution attributed by different chemical potential of the two phases. When slided into matrix, the misfit dislocations can relax part of energy intrinsic in coherent stresses. In the so-called immiscible systems (hcp Mg—Ti, fcc Al—Y, fcc Cu—Zr, etc.) the contribution of γ_{β} increases essentially to form Me_nAE_m clusters with the participation of excess vacancies V_e to be recombined.

5.2. Increment of Solubility

Enhancement of solid solubility in a solid solution can be achieved by several different methods involving non-equilibrium process such as rapid quenching, high energy ball-milling and supersaturation in nanophase/nanosolids as an extreme case for grain refinement in polycrystals. Following the Gibbs-Thomson equation [141], the increment of solubility ΔC is described by the relation

$$\Delta C = C - C_0 = \frac{4\Omega\gamma_{\text{int}}}{kTd} \cdot C_0, \tag{5.2}$$

where C_0 is the equilibrium solute solubility (in a coarse crystal); γ is the interfacial energy, $\gamma = f(\tau_{GB})$; d is the grain size (upon grinding); Ω is the atomic volume of the crystal; k is Boltzmann's constant.

The intrinsic reason for the enhancement in the solubility during grain refinement (up to nanocrystallites) is the increase in Gibbs free energy due to forming

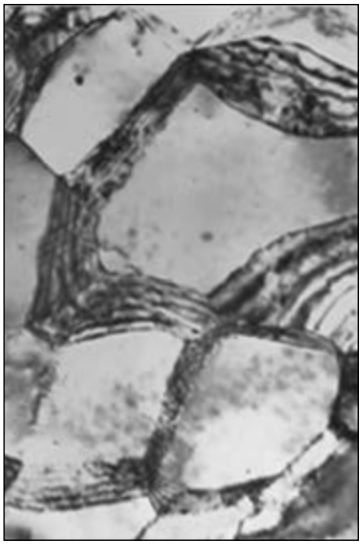

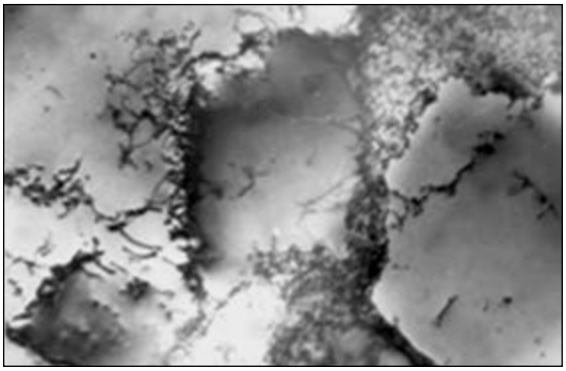

Fig. 5.4. Diffuse contrast on the grain boundaries of Cr—1Gd alloy (×15000)

◀ ***Fig. 5.3.*** Strip-like contrast on the cell boundaries of Cr—1Gd alloy (×25000)

high-energy grain boundaries (Figs. 5.3 and 5.4). In fact, the large volume fraction of the GB and/or interfaces in the nanocrystallites provides a great potential for the solubility enhancement.

The grain boundary structural transformations induced by solute segregations present a new subfield of materials science perhaps called interface science and engineering to come into use [142]. Precipitate-free zones (PFZ) along grain boundaries are often observed in age-hardening alloy systems (Fig. 5.5). Of the main interest has been the kinetic aspect of the process by which these PFZ are formed. These findings have been put together in a unifying theory [143] which seems to explain most of the metallographic observations.

Though it is generally realized that the PFZ should modify the mechanical properties in some way, there is no general agreement upon the nature of this modification, and few experiments have been done to elucidate the background of this point. Moreover, since the aging process is very often studied by hardness measurements, such investigations* could give no direct information on the variation in ductility-the property relationship.

The dislocations have never been observed within the PFZ due to high internal stresses from the slip-band and relatively low lattice friction, so that the dislocations could leave the foil prepared for TEM studies. Very little is known about the nature of the atomic mechanisms involved in the annealing-out of quenched vacancies in metals. Solute-depleted PFZs adjacent to the GBs reveal a tendency toward strain localization, since they are weaker than the matrix and therefore can be the sites of preferential deformation leading to high stress concentration at GB triple junctions and low ductility.

Impurities as well as alloying elements in highly supersaturated nanophases will be in a non-equilibrium state even relative to the nanocrystalline state and will dis-

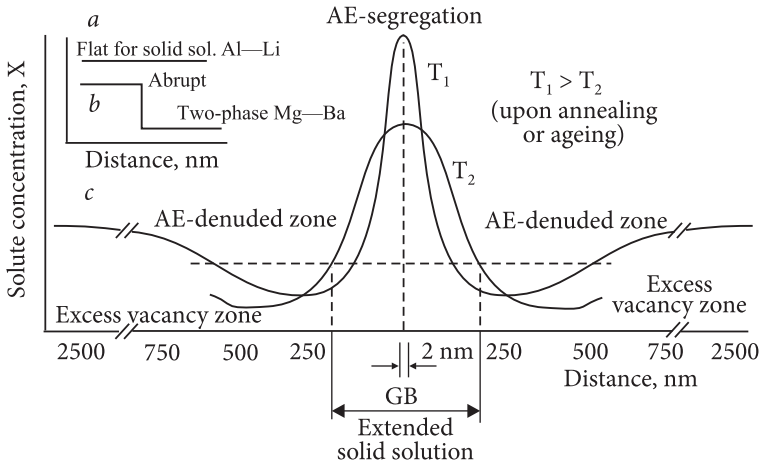

Fig. 5.5. Solid profile adjacent the GB in normal solid solution (*a*), eutectic composition (*b*), and adjacent the GB (*c*). (AE- alloying element) [142]

solve from the nanophase under proper conditions such as annealing to establish a thermodynamic equilibrium by means of solute precipitating from the solution and segregating on GBs, following the phase transformation theory and the Johnson-Mehl-Avrami analysis, in particular.

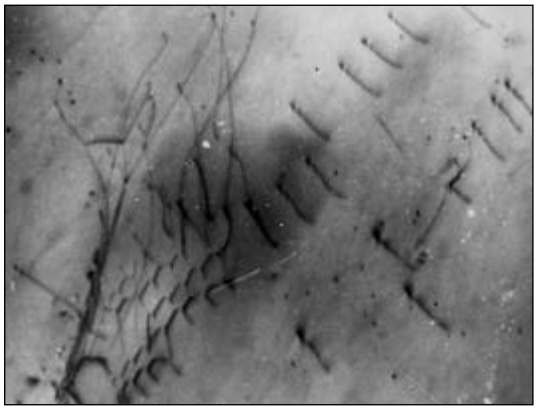

Fig. 5.6. TEM electron micrograph (×100000) of recrystallized beryllium with dislocation pile-up formation on the grain boundaries [147]

Owing to supersaturation with vacancies, the lattice cell unit of nanocrystallites will expand with an evident increment of lattice parameter in intermetallic compounds [144] as well as in metal solid solutions [145]. The P-concentration determined according to the Vegard's law by lattice parameter measurements is found to be 10-15 times that for equilibrium solubility in nanocrystalline Ni—P materials synthesized by crystallizing their amorphous state [146].

Another experimental evidence, for example, for the Pd—H nanocrystalline system [147] implies that one may expect a significant enhancement of the solid solubility in nanocrystallites relative to the equilibrium solubility in single crystals. Several other effects can influence the lattice structure of a nanophase, among which the lattice distortion and/or expansion of nanosized crystallites might play a significant role in variation of the lattice parameters.

Grain and subgrain boundaries generally inhibit dislocation motion, and their presence is a source of strength. The Petch-Hall equation describes the yielding in polycrystals with a conventional grain structure. GB strengthening is based on the interaction of dislocation pile-ups with GBs acting as long-range barriers to dislocation motion (Fig. 5.6).

The effect of GB strengthening is given by

$$\sigma_Y = \sigma_i + K_Y \cdot d_{GB}^{-1/2}, \tag{5.3}$$

where σ_i is the resistance to dislocation motion in the grain matrix, i.e. friction stress; K_Y is the measure of GB strengthening. Indeed, as can be seen from the analysis of the structural sensitivity of yield stress for the grain size ≥1 μm, the yield stress follows the Petch-Hall relation (5.3) with $K_Y = 0.35$ MN/m$^{3/2}$ for Fe and $K_Y = 0.20$ MN/m$^{3/2}$ for Ni. It has been reported that grain boundary strengthening can be very pronounced for most nanocrystalline materials [148-150].

Concluding Remarks

When deformation is continued to large enough strain for significant dynamic recovery to occur, marked increases in boundary dislocation pile-ups and disorientations are observed. These results suggest that the GB structural transformations induced by solute segregations are certain to regulate the precipitation-free zones in age-hardening alloy systems.

The nanoscale grains even in dense pure metals are thermally unstable and tend to coarsen above the recrystallization temperature. Therefore, the use of such objects is limited to relatively low temperature applications. On the other hand, it is believed that a very low impurity level is required which minimizes the potentially destructive properties associated with phase segregation at GB. Indeed, this is a promising approach for the production of sintered (consolidated) nanocrystalline oxide ceramic materials possessing, in this case, novel mechanical properties including low temperature creep and superplastic deformation at relatively low temperatures. However, for metal solid solutions with high creep resistance, an alternative process route is required based on the GB strengthening by favorable segregations.

Chapter

6 SOLID SOLUTION STRENGTHENING

The dislocation dynamics in solid solutions is interesting from a physical standpoint when point defects such as excess vacancies V_e are generated by the non-conservative motion of jogs on mobile dislocations during straining [151]. A solid solution is considered for one or more solutes in a solvent when solutes and solvent are close on the periodical table. Substitutional solute and solvent atoms are roughly of the same size, and therefore solutes will replace the solvent atoms. Interstitial solute atoms are smaller than the solvent ones, once they occupy interstitial positions in the solvent lattice. Impurity solute atoms impose lattice strain and elastic stress fields on surrounding host atoms. Lattice strain field interactions between dislocations and solutes result in restriction of dislocation movement. This is one of the most powerful reasons to make alloys which have higher strength than pure metals.

Unfortunately, large lattice distortion restricts solid solution strengthening in most commercial alloys having a high solid solubility of the alloying elements with a significant size difference from the solvent matrix. Solute element additions having high liquid solubility, low solid solubility and low diffusion rates are being used either individually or in combinations. In particular, these include Co, Fe, Ni, Ca and Cr for aluminum alloys.

6.1. Dislocation Dynamics in Solid Solutions

Yield drops and serrated yielding indicate strong effects of solid solution strengthening. It is generally excepted [152, 153] that the Portevin-Le Chatelier effect and other phenomena of dynamic strain ageing (DSA) arise from the elastic interaction of moving dislocations with mobile solutes in unordered solid solutions. The discontinuous flow implies a Portevin-Le Chatelier (P-L) effect which has been revealed in Ni-C alloys and many other solid solution-hardened alloys [154]. The P-L effect as a serrated yielding is most likely

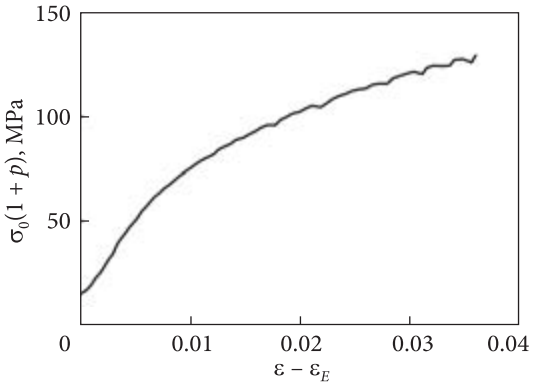

Fig. 6.1. Serrations observed on the stress-strain curve at 423 K for commercially available magnesium alloy AZ91D strengthened by 1% Ca and 0.3% Sr

to be caused by the appearance of dynamic instability due to the dragging of dislocations by nonequilibrium solute atmospheres which provides resistance to dislocation motion. However, for iron alloys with long-range order, the activation energy of the phenomenon which controls the appearance of serrations typical for the P-L effect is comparable to the vacancy migration energy, while the energy which governs the disappearance of the phenomenon is similar to the self-diffusion energy [155]. One of the reasons for structure instability within the province of DSA is the stress-induced and structure-sensitive interaction between mobile dislocations and diffusants (solute atoms). Under these conditions the P-L effect is succeeded by the sharp decrease in the creep strain, with negative strain rate and positive temperature dependence of the flow stress [156].

Observed post relaxation effect due to DSA is caused by the change in the concentration of solute atoms on dislocations with the temperature and strain rate. Unlike slow kinetics of solid solution disintegration, the kinetics of segregation of solute elements or their desegregation is extremely rapid, suggesting short-range diffusion of segregants [157]. Thus, the causes for the huge decrease in creep rate could be: (a) a decrease in the bulk (lattice) diffusion coefficient due to introducing more refractory additions, and/or (b) a slowdown in dislocation activity due to the solute-induced dragging.

The measurable effect of jerky flow is determined by the serrations on the smooth curve $\sigma - \varepsilon$ at strain rate $\dot{\varepsilon} = \text{const}$ (Fig. 6.1). This should be considered as indication of some limited dislocation activity due to pinning dislocations by Cottrell mechanism with formation of dislocation atmospheres. Strain delay to the onset of serrated yielding depends on the strain rate, while dislocations are arrested at nanoparticles. The delay time is inversely proportional to the dislocation velocity, $1/\upsilon_D$.

The initial jerks take the form of increment $\Delta\sigma$ in load. The magnitude of jerks first abruptly falls in load recorded. The test of validity of stress decrement $\Delta\sigma$ as a criterion for determination of the activation energies (a.e.) is consistent with the process of dislocation atmosphere pinning. The decrement $\Delta\sigma$ is defined as the stress differential between the breakaway stress at which dislocations escape from their atmospheres and the stress at which they move easily through the lattice before being pinned again [158]. The a.e. for solute migration was found to be 0.57 to 0.68 eV, which is consistent with the activation of solute atmosphere forming mechanism.

Nevertheless, in the course of tensile tests, serrations typical for the P-L effect are observed in magnesium alloys containing Ca, Ti, Sr, Gd additions at a strain rate of about 10^{-4} s^{-1} (Fig. 6.1). Besides, the a.e. of the phenomenon which controls the appearance of the serrations is comparable to the vacancy migration energy (~0.8 eV), while the energy governs its disappearance is similar to the self- diffusion energy (~1.35 eV) [159].

The appearance of serrations in the smooth curve (Fig. 6.1) records the onset of a jerky flow. Point defects are generated during straining by the non-conservative motion of jogs on mobile dislocations. Following the modified versions of Cottrell model for the P-L effect [160], it is deduced that repeated (serrated) yielding is caused by short-range diffusion of clusters "excess vacancy-solute" which ensure the dislocation locking with the participation of strain-produced vacancies. Annealing of the excess vacancies at appropriate sinks and their annihilation give rise to deviations of experimental data from Cottrell's model by primary cluster-induced mechanism [161].

There is an evidence that jerky flow (P-L effect) occurs while introducing alloying elements with large positive heat (enthalpy) of mixing, ΔH_m, such as Ti, etc. For the Mg—Ti system ΔH_m makes up 16 kJ/mole [162]. The measurable effect of jerky flow is determined by the serrations on the smooth curve $\sigma - \varepsilon$ at strain rate $\dot{\varepsilon} =$ = const. This should be considered as indication of some limited dislocation activity due to pinning dislocations by Cottrell's mechanism with formation of dislocation atmospheres. Jerky flow in Ti-containing magnesium is observed during tensile tests at $\dot{\varepsilon} = 10^{-3}$ s^{-1}. With this provision, regular serrations are certain to occur in the temperatures range of 403-523 K.

6.1.1. Long-Range Interactions

It is reasonable to expect that the excellent increase in creep resistance and long-term strength might be attributed to dynamic (stress-induced) dragging the dislocations by nonequilibrium Cottrell's dislocation atmospheres in full accordance with physicochemical Le Chatelier-Braun principle of mobile equilibrium shift [163]. It is noteworthy that Cottrell's model has been successfully employed for explaining the experimental data associated with the delay of plastic deformation in the region of serrated (repeated) flow as well as for evaluating the critical strain rate, $\dot{\varepsilon}_{cr}$, responsible for the appearance of serrations on the temperature curves in the $\sigma - \varepsilon$ coordinates, i.e.

$$\dot{\varepsilon}_{cr} = k\rho_D \cdot C_V \cdot \exp(-E_m / RT), \tag{6.1}$$

where k is the constant; ρ_D is the density of mobile dislocations; C_V is the concentration of vacancies; E_m is the a.e. for vacancy migration. With this provision, the long-range interaction of slow dislocations with solutes is believed to occur by Cottrell's diffusion rate-controlling mechanism. However, the results obtained do not affect the

problem of embedding the complexes and A_mB_n clusters in the crystalline structure of a primary solid solution so far as elastic interaction lowers the enthalpy of solution, and, on the contrary, filling of the electronic states increases it. Furthermore, the long-range interaction is shown to be independent of the chemical reaction course. These results are far from being conclusive at least for solid solutions enriched with excess vacancies, the more so these calculations are clearly not in agreement with the idea of short-range interaction. Nevertheless, all the data published in the literature are theoretical premises for developing a unified concept of the short-range clustering inherent in a solute-defect-vacancy structure.

The observed inelastic stress-induced pair relaxation (Fig. 2.2) and other evidences of pairing of solutes with excess vacancies (Figs. 2.3-2.6, Table 2.1) demonstrate that a different mechanism operates in the cluster-forming solid solutions. Under the data [164, 165], an apparent migration energy for vacancy/ solute complexes gives a good fit to experimental data compared to that of solutes. The complexes have a higher mobility with smaller a.e. which differs substantially from that of isolated solute atoms and individual defects. The formation of pair defects and their complexes enables them to be relaxed by rapid (short-range) mechanism with the participation of bound vacancies.

6.1.2. Short-Range Interactions

Analysis of the kinetic equations predicts that activation of the Snoek short-range order may precede activation of the Cottrell long-range diffusion-controlled mechanism with increasing strain rate, proportional to dislocation velocity. In such a case thermally activated rapid strengthening by short-range mechanism (Snoek and Schoeck approaches) appears to be energetically favorable. Thus, for slow dislocations, the interaction of solutes with moving dislocations is controlled by Cottrell locking whereas for fast dislocations, rapid (short-range) strengthening is governed by Snoek mechanism. Rapid kinetics of strong strengthening is a feature peculiar to the activation of the short-range mechanism responsible for the alloy ingredient in the stress fields of rapid dislocations. Snoek and Cottrell assumptions have similar shapes of dependence, i.e., similar and $\partial \ell n \upsilon_D / \partial \tau^*$ with the same activation energy. Besides, the serrations attributed by the activation of Snoek short-range mechanism are believed to occur at lower temperatures than that associated with Cottrell long-range (diffusion) mechanism.

The interstitial solute atmospheres are boiled out with increasing temperatures. A theory of strengthening by the fields of short-range stresses, e.g., from the dipoles consequent to intercepting forest dislocations, was put forward by Gilman [166] and then modified by Hirth [167] in terms of sitting ledges on screw dislocations.

Bcc Group A metal solid solutions exhibit indeed the clustering-type local order and, as consequence, solution strengthening by the short-range (Fisher) mechanism [168]. As the size difference increases, the phase diagrams change from the ultimate clustering limit, the solubility gap type, to the ultimate ordering limit, the intermetal-

lic compound type. While exhibiting, clusterized solid solutions also exhibit negative deviations from Vegard's law [169]. In this case, lattice parameters versus the composition behavior is not a reliable clue to the state of local order. Another measure of bond energy is the elastic (shear) modulus.

The exact nature of the chemical bonding strength in cluster compounds is not yet completely understood. Nevertheless, chemical binding in B_nV_e complexes and the A_mB_n nanoclusters made of them are certain to depend strongly on the chemical type of the surrounding atoms. A strong atomic attraction causes the effect of short-range order (SRO) in the molten state lowering the configuration entropy and changing the a.e. for crystallization. Otherwise, the chemical SRO originates in the liquid state (Fig. 1.3). The nature of chemical bonding is changed with the addition of AE with higher cohesive energy.

Therefore, the magnitude of the chemical energy is thought to play the major role in clustering of atomic structure to nucleate chemically bonded luster compounds A_mB_n with own (hybridized) electronic structure.

6.2. Rate-Controlling Dislocation Dragging Mechanisms

It is noteworthy that long-term features exhibit some correlation between creep strain rate $\dot{\varepsilon}_c$ and time to a given creep strain for all alloys under investigation [8]. Somehow the $\dot{\varepsilon}_c$ level indicates their survival probability. We abandon the idea that one should not carry out all the cycle of creep testing (up to 200 hr) to save time and resources provided single rate-controlling mechanism can operate. A analysis unambiguously displays the source data as creep strain rate rather than time interval. It might therefore be expected that solute-induced dragging is the most probable rate-controlling mechanism responsible for delaying the dislocation activity at the 10^{-9} s^{-1} level. This assumption is supported by the appearance of regular serrations on the smooth curve during tensile test of magnesium alloy containing strengthening additions (Fig. 6.1) as well as by dislocation damping investigations (Figs. 3.3 and 3.4).

By its general sense, the apparent a.e. U is not a critical event for the choice of a rate-controlling mechanism, whereas the a.v. of V is directly related to the physical mechanism. The thermal stability of structure not containing the sources of dislocation multiplication is therefore a mandatory condition for the correct theoretical calculations and experimental estimations to clear up a rate-controlling mechanism. Since the dislocation density is kept constant, such an approach makes it possible to estimate the accuracy of the above parameters, provided that the dislocation structure of a given alloy remains unchanged under investigation. Using an Arrhenius type relation which should produce straight lines, the a.e. U^* for creep involved is calculated from the line slopes.

The process of the dislocation (Cottrell) locking is accompanied by releasing the elastic energy of oscillations and, as sequence, lattice relaxation, while process of the

dislocation breaking off, being reversal, is controlled by absorbing the elastic energy of oscillations. According to current concepts, the self-adjusting synthesis of structures in the bifurcation points under system instability is attributed to the properties of absorbing and releasing energy. In our case, at lower temperatures a system which trend to stability (quasi-equilibrium) is controlled by the action of reverse-feedbacks ($-E_b$). Meantime at higher temperature the structure in bifurcation points is determined by positive feedbacks ($+E_b$) (heat of dissipation, dissociation). Thus, thermal dislocation pinning by Cottrell's mechanism is caused by energy release whereas thermal dislocation unpinning, i.e., releasing from binding is caused by thermal energy absorption. It is reasonable to suppose that the jump-like motion of dislocation under conditions of $-E_b \approx +E_b$ in the serrated yielding region is a main premise to the onset of a jerky flow by short-range mechanism. This can best be seen by an example. According to our experimental data, the values of binding energies E_b for both $-E_b$ and $+E_b$ are the same and equated to 0.45 eV for hcp Mg—H system and to 0.34 eV for hcp Be—C system [170].

The extent of smooth plastic strain preceding (by short-range mechanism) jerky flow is evaluated in the $\ln\dot{\varepsilon} - 1/T$ coordinates [171]. Besides, measured effect of serrated yielding is defined by stress oscillation amplitude, i.e., height of regulated serrations on the smooth σ-ε curves at $\dot{\varepsilon} = \text{const}$. In the case, the jump-like movement of dislocations is sure to occur by a short-range mechanism.

The mechanism of delayed discontinuous plastic flow in an age-hardened Ni-based solid solution-hardened alloy was proposed by authors [158]. It was found that there is a critical strain, $\varepsilon_{C,}$ providing an anomalous strain delay to the serrated yielding as a result of activation of a carbon atmosphere mechanism. At the same time, according to the hypothesis [172] supporting experimental approach, the stress decrement σ_D may be a more fundamental measurement of strain-aging than the strain to start of serrated flow (σ_c). It is determined as the stress differential between the breakaway stress at which dislocations escape from their atmospheres and the stress at which they move easily through the lattice before being pinned again. In terms of the stress-strain curve, σ_D is simply the height of the individual serration.

Concluding Remarks

In spite of their implication in the strength properties of structural materials, solute-induced and structure-sensitive interactions of dislocations remain a poor known mechanism. It has however been shown that:

- Under the serration yielding conditions, one should expect a huge increase in creep resistance while introducing more refractory additions and solute-induced dragging to be activated.
- The serrations are a measurable effect of jerky flow on the stress-strain curve.
- Strain delay to the onset of initial jerky flow is likely to be determined by solute-induced dislocation core dragging by a short-range mechanism.

Chapter

7 DEFORMATION (SUBSTRUCTURAL) STRENGTHENING

The process of dislocation sliding at early stages of plastic deformation has a fundamental significance for further deformation behavior of metal alloy polycrystals at higher strains (beyond the yield stress) as it often determines the subsequent microstructural evolution and, as a result, the mechanical properties of polycrystals during strengthening. It has been agreed that elastic fields of internal stresses attributed by dimension or modulus misfit, interact with dislocation cores and contribute to processes of dragging the mobile dislocation and solid solution strengthening by local ordering the structure.

7.1. Contribution of Cell Structure

Distance between misoriented enough boundaries is equal to the free path length of moving dislocation, λ, i.e.

$$L_{GB} \sim \lambda \sim K \cdot \rho^{-1/2}. \quad (7.1)$$

In other words, low-energy boundaries would be expected to be formed from dislocation density, ρ. It should be noted that the cell size is not given by Eq. (7.1) when the dislocation mobility is insufficient for a low-energy dislocation configuration to be approached or when the dislocation mobility is high enough to allow considerable dislocation annihilation with positive and negative Burgers vectors.

The so-called cellular structure presents energetically favorable configurations of dislocation densities in deformed polycrystals (Fig. 7.1, *a, b*).

During deformation of metals and their alloys, the mobile dislocations cluster into cell walls separating relatively dislocation-free regions due to decrease in the total elastic energy (Fig. 7.1, *b*). The stability of a uniformly dense dislocation distribution with respect to periodic fluctuations in dislocation density ρ was examined by Holt [173]. It was shown that an array of dislocations modeled

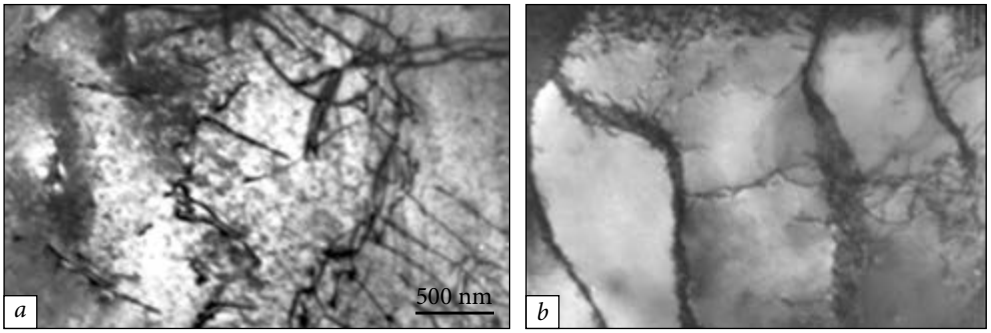

Fig. 7.1. Typical dislocation structure formed in the grain bulk and transformed in the cell configuration (×15000) (*a*) and typical cell structure formed in the Cr—0.8Y alloy (×15000) (*b*)

by parallel screw dislocations of uniform density is unstable, and the mobile dislocations move to form a structure having a modulated dislocation density. With this condition, clustering of dislocations will convert their uniform distribution into a cellular structure (Fig. 7.1, *b*) which should be considered as an energetically favorable structural state with a periodical modulation.

The study is concerned with the case in which most of the dislocations have formed themselves into cell walls. The athermal resistance to the dislocation motion contributes to the plastic flow mainly at high temperatures. At elevated temperatures, besides the athermal resistance, the thermal resistance to the dislocation motion is added to the flow stress. The athermal resistance should be considered in terms of activation by a long-term (strong barrier) mechanism whereas the thermal resistance — in terms of short-range (thermal obstacle) mechanism.

Under the data by Thompson [174] strengthening by cells or subgrains as slip barriers obeys the modified equation similar to Eq. (5.3).

7.2. Contribution of Nanosized Structure

A new category of materials, called nanocrystalline (nm) materials, containing ultrafine grains up to 100-300 nm in size gives rise to a huge number of interfaces (about 50% for 5 nm grains) which distinguish them from conventional coarse-grained polycrystalline materials. Many macroscopic properties of nm-materials (nanosolids) are therefore determined by the interfacial structure. The synthesizing procedure for bulk nanocrystalline materials proposed by Lu et al. [175] is based on the crystallization of amorphous solids and named the crystallization method. That is, upon heating amorphous ribbons, wires or powders, crystallites will nucleate and grow within the amorphous matrix. The grain size in the products can be easily controlled by different annealing procedure. Nanostructural materials have unique properties compared to conventional materials with microscale (mesoscopic)

structures. A large fraction of atoms located at interfaces is expected to play an important role in determining the unique properties of nanocrystalline materials. However, some fundamental subjects concerning their interfacial structure and structure-related properties are still controversial. So far, two major structural interface models have been proposed, i. e. the «gas-like» structure with neither long-nor short-range order by Gleiter [176] and similar to the common interfacial structure in polycrystals by Siegel [177].

7. 3. Structural Sensitivity of Yield Stress

7.3.1. Hall-Petch Relation for Traditional Crystalline Materials

It has been established experimentally and theoretically that the grain refinement increases mechanical strength and hardness in terms of pile-up-based Hall-Petch relation for polycrystalline materials [178, 179] to be considered as a modification of the Griffith concept.

The basis for this improvement is that the macroscopic yield stress/flow stress is inversely proportional to the square root of the grain diameter that is normally described by the classical Hall-Petch relation

$$\sigma = \sigma_0 + K\, d^{-1/2}, \tag{7.2}$$

where σ_0 is the resistance to dislocation movement in the matrix or the friction stress felt by a dislocation in the pile-up; K is the Hall-Petch slope or stress intensity factor (constant for the material). The dislocation model of the Hall-Petch equation describing the yielding in polycrystals with a traditional grain structure is based on the interaction of dislocation pile-ups formed by dislocation Frank-Read sources within the grain [180].

It is considered that dislocation sources inside grains can operate only down to a grain size of typically about 1 μm, since the size of a Frank-Read source cannot exceed the grain size, and the stress needed for its operation to be inversely proportional to the source size [181] Nevertheless, at grain/subgrain (cell) sizes less than 200…100 nm we observe regular Hall-Petch law manifestation (Fig. 7.2), i.e. the strength increase with decreasing grain size due to the activation of conventional dislocation-slip (pile-ups) mechanism [182]. Indeed, if subgrains (well-developed cell walls) are effective cross-barriers for dislocation pile-ups providing transmission of matrix slip (from cell to cell) by Stroch mechanism, they perform the function of grain boundaries (GBs) and obey the well-known dislocation (barrier) criteria of Hall-Petch and Mott-Stroch for macroscopic yield stress ($\sigma_\gamma \approx \sigma_o + K_\gamma d_{ef}^{-1/2}$) and true fracture stress ($\sigma_f \approx \sigma_{of} + K_f d_{ef}^{-1/2}$), respectively [183, 184].

It becomes obvious that other dominating deformation mechanisms may be operational in the nanosized grain regime, at least below 200…100 nm. If energy absorption occurs without relaxation, for instance, in brittle materials (during bull mill-

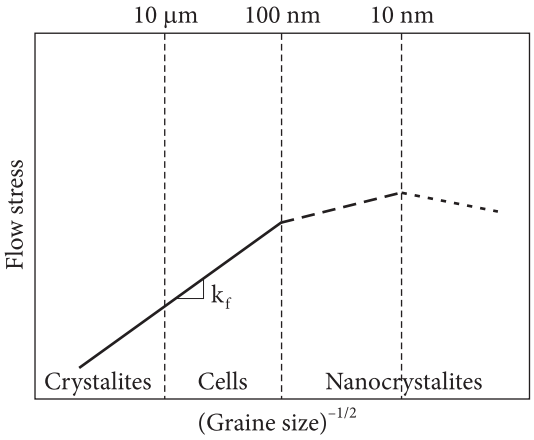

Fig. 7.2. Schematic representation of the variation of yield stress as a function of grain size in microcrystalline, cellular and nanocrystalline metals and alloys

ing), one can observe gradual evolution from a dislocation cell structure to a nanostructure. Below a critical grain size (100-50 nm) GB sliding may be responsible for the grain-size dependence of the macroscopic yield stress, according to [185].

Some appealing characteristics of nanocrystalline (nc) metals and alloys with potential significance for engineering applications include ultra-high yield and fracture strengths, decreased elongation and toughness, superior wear resistance, and the promise of enhanced superplastic formability at lower temperatures and faster strain rates compared to their microcrystalline (mc) counterparts. Consider, for example, the variation of flow stress as a function of grain size from the mc to the nc regime, which is schematically shown in Fig. 7.2. In many mc and nm metals and alloys with average grain size of 100 nm or larger, strengthening with grain refinement has traditionally been rationalized on the basis of the so-called Hall-Petch mechanism [186, 187] with pile-up of dislocation process underlying an enhanced resistance to plastic flow from grain refinement. As the microstructure is refined from the mc and ufc (ultrafine crystalline) regime into the nc regime, this process invariably breaks down, and the flow stress versus grain size relationship departs markedly from that seen at higher grain sizes (Fig. 7.3). With further grain refinement, the yield stress peaks in many cases at an average grain size of about 10 nm. Further decrease in grain size can

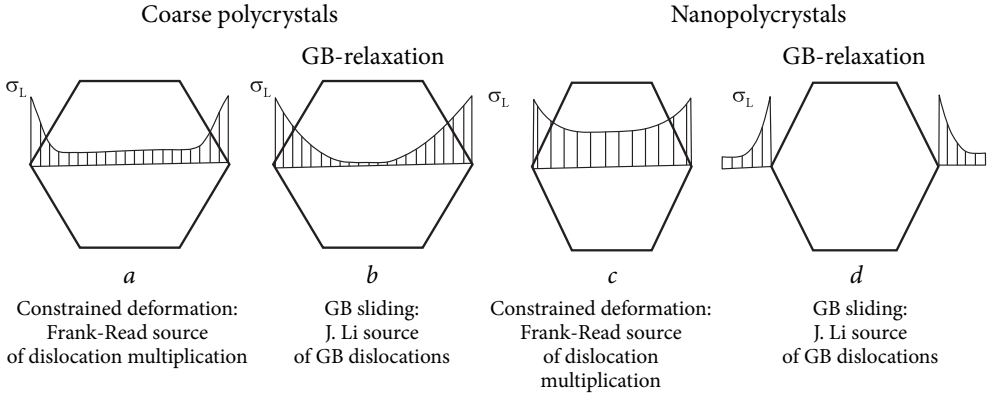

Fig. 7.3. Redistribution of the local overstresses on the boundaries of course and nano-polycrystals

cause weakening of the metal. Although there is a growing body of experimental evidence pointing to such unusual deformation responses in nc materials, the underlying mechanisms well understood. Consequently, there is a concerted global effort underway using a combination of novel processing routes, experiments and large-scale computations.

Microstructural evidence is given which shows that the well-known relations of Hall-Petch and Mott-Stroch are valid for a wide range of highly pure metals (bcc Cr, hcp Be, hcp Ti) with well-developed cellular structure (up to 200-100 nm) [188, 189]. The conventional dislocation pile-ups mechanisms responsible for observed increase in strength with decreasing grain and cell sizes (down to 20-10 nm) are further degenerated in the nanoregime where strengthening mechanism in crystal physics remains controversial because of blocking bulk dislocation sources.

GB sliding based deformation mechanisms opens the new opportunities for further strength increase even in coarse-grained polycrystalline systems (hcp Be—Co [190]). Below a critical grain size (100-50 nm) GB sliding may be responsible for the grain-size dependence of the macroscopic yield stress. According to [191-193] GB sliding involving atom shuffling and stress-induced diffusion may be also responsible for the grain–size and cell-size dependences of the macroscopic yield stress and the true fracture stress caused by activated intercrystalline failure. For example, GB sliding in hcp polycrystals such as magnesium is revealed at 77 K [191]. As GB sliding and atom diffusion are two independent types of GB process, the physical foundations, if any, of such macroscopic behavior remain to be exploited [192]. Thermally activated and stress-induced GB sliding has been shown to lead to a d^{-1} grain–size dependence of the strain rate [193, 7]. The data are in good agreement with the steady state creep rate by Coble and Nabarro-Herring mechanisms which become essentially indistinguishable in nanosolids, and the a.e. for GB sliding is equal to the a.e. for GB diffusion.

7.3.2. Deviation from Hall-Petch Law for Nanocrystalline Materials

In the available relevant literature, there is an expressed doubt as to the possibility of conventional dislocation mechanism of plastic flow being operative in nanoscale polycrystals as theoretical shear stress [177]. Indeed, it is much easier to activate the GB dislocations at the GB ledges by the James Li mechanism [194] than dislocation sources within the grain matrix. Nevertheless, some additional mechanism, for example, GB sliding enhanced by GB diffusion similar to the high temperature creep mechanism, may be operative in the plastic flow of nanocrystalline materials [195]. The mechanism may result in the softening of nanophase materials with decreasing grain size to nanoscale regime, as observed in a number of the nanocrystalline materials [196]. Therefore extrapolation of the Hall-Petch equation to nanograin size ($\leq$10 nm) not founded theoretically will result in overestimated values

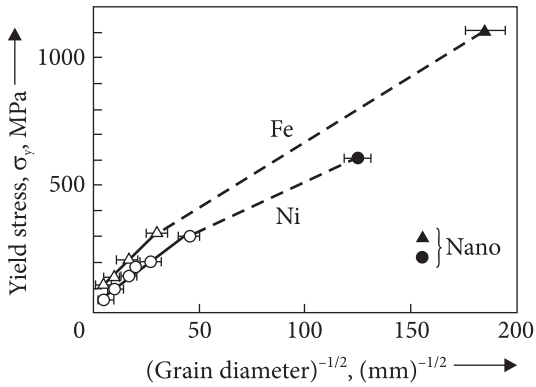

Fig. 7.4. Yield stress as a function of grain and nanograin sizes in the Hall-Petch coordinates [195]

of the yield stress for nanoscale pure metals (Al, Fe, Ni...) and their consolidated powder materials produced by the evaporation-condensation method. Thus in order to elucidate the true mechanisms of yielding and fracture to operate in pure nanocrystalline metals and their alloys, further investigations of nanograin size and temperature dependences of the yield stress and true fracture stress are required.

In view of the importance of the Hall-Petch relation in predicting material strength and the new availability of ultrafine grained materials, it is important to ascertain whether the Hall-Petch relation should be obeyed down to nanocrystal dimensions. A variety of models have been proposed to explain the grain size strengthening. It has been postulated that if the Hall-Petch relation is valid for a nanograined structure, grain refinement is expected to provide an increase in the strength which could reach the theoretical elastic limit, i.e. theoretical shear strength [197]. Nevertheless, although in most cases, the Hall-Petch relation seems to be obeyed, there have been some cases (Fig. 7.4) where different and even "inverse" Hall-Petch slopes have been reported [198]. Effective yield stresses are sometimes obtained via hardness measurement instead of directly measuring the stress-strain behavior. There is a growing body of experimental evidence pointing to such unusual deformation responses in nc materials, and the underlying mechanisms are not well understood. Consequently, there is a concerted global effort underway using a combination of novel processing routes, experiments and large-scale computations.

Indeed, as can be seen from the analysis of the yield stress dependence on the grain size ≥1μm (Fig. 7.4), the yield stress follows the Hall-Petch relation with K_y = = 0.35 MN/m$^{3/2}$ for Fe and K_y = 0.20 MN/m$^{3/2}$ for Ni, but extrapolating these dependencies to the nanometer grain size region predicts deviation from Hall-Petch law, i.e., a considerably larger increase in the yield stress than that actually observed. It is noted that some softening mechanism, e.g., the GB sliding, is involved in the plastic deformation of nanocrystalline Fe and Ni, partially neutralizing the effect of the GB strengthening. Since the GB sliding is governed by surface diffusion, it should be suppressed at lower temperature (argument to elevated temperature creep properties and transition to high temperature creep behavior). The incorporation of defects in nm-grains could activate dislocation sources other than Frank-Read's one.

So called inverse Hall-Petch relation $H_v \sim d^{-1/2}$ is observed for the Fe—Mo—Si—B nanocrystalline alloys synthesized by crystallization of an amorphous state when grain

size is less than 45 nm (Fig. 7.4) [199]. The results for the positron life time indicate great influence of nanovoids in the interfaces on the microhardness at $d < 45$ nm.

Unfortunately, up to now there has been very little information on the subject and, moreover, this information is often contradictory (Figs. 7.5 and 7.6). That is why it is necessary to have reliable experimented data in order to understand the mechanism of mechanical behavior of nanocrystalline materials.

It should be pointed out that if we extrapolate a linear function beyond the very narrow grain size range, the relationship $H_v = H_o + K^1 d_{nm}^{-1/2}$ will be violated. It means that there are different mechanisms of plastic deformation leading to the Hall-Petch relation, or for nanosized structures there are other mechanisms, for example grain sliding [200], which are not described by the Hall-Petch equation. At present, the available information is not enough to discuss the problem.

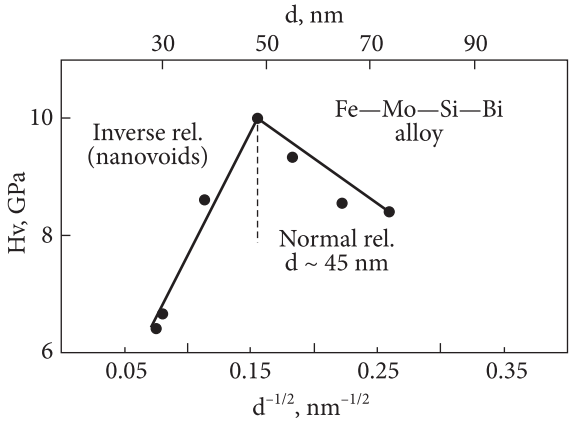

Fig. 7.5. Microhardness H_v as a function of nanograin size in the Hall-Petch coordinates where $H_v = H_{v0} + K^1 \times \times d_{nm}^{-1/2}$ and $\sigma = \sigma_0 + K \cdot d^{-1/2}$ [199]

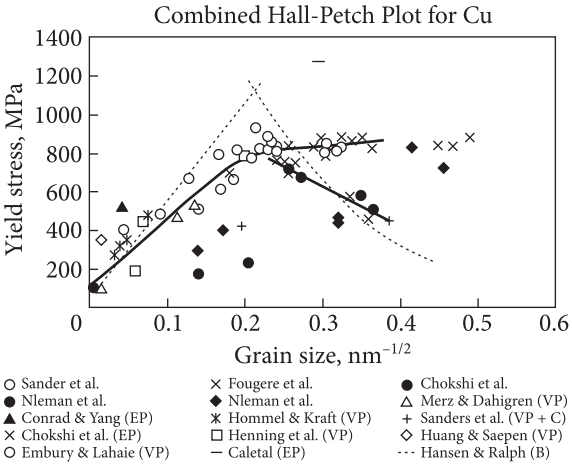

Fig. 7.6. Compiled yield stress versus the grain size plot for Cu ranging from coarse to nanograin size. The plots show different trend as the grain size falls below a critical size [205]

Decrease in the effective elastic modulus upon heating nanocrystalline solids of 5-15 nm in size is explained by contribution of disordered interfacial structure [201, 202]. The contribution becomes much smaller with increasing the nanograins during annealing. At the same time, their disordered interfacial structure is not likely to be the only cause of such modulus behavior.

An accommodation mechanism is required for GB sliding responsible for the macroscopic behavior of nanosolids. However, in this case, dislocations are unavailable to accommodate GB sliding, and thereby to ensure continuous deformation while avoiding submicrocracking, since theoretically below a threshold stress (2.3 GPa for

pure Al) mobile dislocations cannot be nucleated from GB or grain junctions [203]. Apart from partial dislocations to be inevitably nucleated from GB, GB diffusion creep seems to offer the only viable accommodation mechanism to facilitate GB sliding [204]. GB sliding and GB diffusion creep mechanisms are considered as two different aspects of the same deformation-rate controlling process. We believe that novelty of the near GB-strengthening is that the ability to GB time-dependent deformation (creep) resistance is principally controlled by impeding mechanisms with longitudinal barriers acting along the grain boundaries and correlating with a.e. for the GB diffusion of the alloying elements rather than with strengthening cross-barriers mechanisms connected with the formation of strong dislocation pile-ups against grain boundary (by Hall-Petch or Mott-Stroch models). It does mean inevitable transition from dislocation pile-ups mechanism to unconventional deformation mechanism in nanocrystalline materials to be most likely a GB based deformation mechanism.

7.4. Strain Rate Sensitivity of Yield Stress

The most important source of strain hardening is thermally activated obstacles providing the maximum force between them and gliding dislocations at a distance of the order of the Burgers vector. The main contribution to the strain hardening of fcc metal crystals is made by long-range elastic interactions between parallel lattice dislocations with the formation of pile-ups on Cottrell-Lomer barriers and reverse stress field [32], which virtually exclude the reversibility of plastic deformation.

Atomic computer simulations have shown that below a critical grain size (20-30 nm) nanograin boundary (nm GB) sliding as an accommodated process becomes the dominant deformation mechanism responsible for macroscopic behavior in pure nanometals (Ni) and in dense nanoceramics [205, 206]. If the entire macroscopic deformation arises from the GB sliding, viscosity of which is governed by stress-driven, thermally activated nm GB sliding rate transforms into the steady-state creep rate, shown to lead to the d^{-1} grain-size dependence of $\dot{\varepsilon} \sim 1/\sigma_Y$

$$\dot{\varepsilon} = \frac{d_0}{d} \cdot \exp\left(-\frac{U_{GB}}{kT}\right) \cdot \sinh\left(\frac{\sigma V_{GB}}{kT}\right), \tag{7.3}$$

where U_{GB} is the a.e. for GB sliding; V_{GB} is the GB activation volume. The experimental data are in good agreement with the well-known Coble creep mechanism for coarse-grained metals and alloys as creep resistance requires a large grain size.

According to [207], the GB sliding rate can be described by the expression:

$$\dot{\varepsilon}_{GB} = A_{GB}\sigma^{nGB} \exp(Q_{GB} / RT), \tag{7.4}$$

where the stress exponent for the GB sliding $n_{GB} = n - 1$.

A transition from low stress to high stress behavior can be observed in creep rate, time to rupture ductility and fracture mode. The stresses at the transition in creep rate and in time to rupture almost coincide with each other indicating the same change in the

fracture mechanism. The results are explained by the hypothesis that the transition is due to change in the deformation mode from one of the predominant uniform matrix deformations at high stresses to one of the localized deformations near GBs by GBs sliding, at low stresses. A higher stresses *of* GBs sliding is postulated to be negligible and constant, while at lower stresses GBs sliding is the rate controlling mechanism. Nevertheless, the strain due to the two processes are additive as they operate inconsequently. Based on all the experimental observations in the literature, the total creep deformation (ε_T) can be resolved into the matrix deformation (ε_m) and grain boundary sliding (ε_{GB}) components.

7.5. Up-to-date Analysis of Strengthening Accommodation Mechanism

To ensure continuous deformation while avoiding submicrocracking and nanopores, different deformation and diffusion processes such as dislocation emission, (GB) stress-induced atom diffusion, GB sliding, etc. have been identified in many models as viable stress accommodation mechanisms beginning from the pioneering works of Herbert Gleiter. It is widely accepted that there are at least three major accommodation mechanisms that promote grain-size and subgrain–size strengthening in solids.

Dislocation accommodation mechanism.
Bulk (Frank-Read) relaxation sources

Concerning dislocation accommodation, it is considered that dislocation sources inside grain can operate only down to a grain size of typically about 1 μm, since the size of a Frank-Read source cannot exceed the grain size and the stress needed for its operation is to be inversely proportional to the size of the source. Nevertheless, at grain/subgrain (cell) sizes less than 200...100 nm we observe regular Hall-Petch law manifestation, i.e., the strength increases with decreasing grain size due to activation of conventional dislocation-slip (pile-ups) mechanism.

Indeed, if subgrains with well-developed cell walls are effective cross-barriers for dislocation pile-ups providing transmission of matrix slip (from cell to cell) by the Stroch mechanism, they perform the function of GBs and obey the well-known dislocation (barrier) criteria of Hall-Petch and Mott-Stroch for macroscopic yield stress ($\sigma_\gamma \approx \sigma_o + K_\gamma\, d_{ef}^{-1/2}$) and true fracture stress ($\sigma_F \approx \sigma_{oF} + K_F d_{ef}^{-1/2}$), respectively. It becomes obvious that other dominating deformation mechanisms may be operational in the nanograin size regime, at least below 200...100 nm. If energy absorption occurs without relaxation, for instance, in brittle materials (during ball milling), one can observe gradual evolution from a dislocation cell structure into a nanostructure.

GB based accommodation mechanism.
GB (James Li) relaxation sources

Below a critical grain size (100-50 nm) GB sliding may be responsible for the grain-size dependence of the macroscopic yield stress. GB sliding involving atom shuffling and stress-induced diffusion may be also responsible for the grain

size and subgrain size (cell-size) dependences of the macroscopic yield stress and the true fracture stress caused by activated intercrystalline failure. For example, GB sliding in hcp polycrystals such as magnesium is revealed at 77 K. As GB sliding and atom diffusion are two independent types of GB process physical foundations, if any of such macroscopic behavior remains to be exploited. An accommodation mechanism is required for GB sliding responsible for the macroscopic behavior of nanosolids. However, in this case, dislocations are unavailable to accommodate GB sliding, and thereby to ensure continuous deformation while avoiding submicrocracking, since theoretically below a threshold stress (2.3 GPa for pure Al) mobile dislocations cannot be nucleated from the GB or grain junctions. Apart from partial dislocations to be inevitably nucleated from GB, GB diffusion creep seems to offer the only viable accommodation mechanism to facilitate GB sliding. GB sliding and GB diffusion creep mechanisms may be considered as two different aspects of the same deformation-rate controlling process. We believe that novelty of the near GBs strengthening is that the ability to the GB time-dependent deformation (creep) resistance is principally determined rather by strengthening cross-barriers mechanisms connected with the formation of strong dislocation pile-ups against GB (by Hall-Petch or Mott-Stroch models) than by impeding mechanisms with longitudinal barriers acting along the grain boundaries and correlating with a.e. for the GB diffusion of the alloying elements. It does mean inevitable transition from dislocation pile-ups mechanism to unconventional deformation mechanism in nanocrystalline materials which is most likely to be a GB based deformation mechanism.

Stress accommodation mechanism in nanocrystalline solids (metals and ceramics). Fewer relaxation sources

Microstructural evidence is presented which shows that the well-known relations of Hall-Petch and Mott-Stroch are valid for a wide range of highly pure metals (bcc Cr, hcp Be, hcp Ti) with well-developed cellular structure (up to 200-100 nm). The conventional dislocation pile-ups mechanisms responsible for observed increase in strength with decreasing grain and cell sizes are further degenerated in the nanoregime where strengthening mechanism in crystal physics remains controversial because of blocking bulk dislocation sources. GB sliding based deformation mechanisms opens the new opportunities for further strength increase even in coarse-grained polycrystalline systems. However, we believe that in the nanoregime providing a large number of surface atoms (up to 30%) more than one accommodation mechanisms is believed to need for GB sliding to operate beyond matrix-slip. It should be noted that GB diffusion is a very powerful stress-relaxation mechanism. Its potential of the true nanostructures is not used completely for structural and functional purposes. It does also mean that the inevitable transition to the other accommodation mechanisms, particularly, GB diffusion accommodated GB sliding must occur where GBs play decisive role in nanograin-size strengthening.

Thermally activated and stress-induced GB sliding has been shown to lead to a d^{-1} grain size dependence of the strain. The data are in a good agreement with steady state creep rate by Coble and Nabarro–Herring mechanisms which become essentially indistinguishable in nanosolids and the a.e. for GB sliding is equal to the a.e. for GB diffusion. Nevertheless, the above GB diffusion accommodation mechanism is thought to be activated with the participation of excess (strain-induced) vacancies, responsible for the atom shuffling and stress-induced diffusion at low temperatures.

In summary, the picture of substructural strengthening which has been developed above is as follows. Subgrain (cell) structures tend to exhibit the dependence $d^{-1/2}$. After reaching the nanosize scale, they may exhibit a transition to another dependence including function of d^{-1}. One way of rationalizing these observations is in terms of the behavior of dislocation sources which appears to be responsible for substructural strengthening mechanisms.

Concluding Remarks

The Hall-Petch relation is believed to be not enough to describe time-dependent deformation in nanocrystals; the lattice dislocations are unavailable to accommodate GB sliding. There is a competing dislocation-based deformation process attributed to the activation of dislocation sources to affect the GBs with nucleating the partial and complete dislocations.

Section 3

EVOLUTION OF STRENGTH PHYSICS CONCEPT

If the evidence has exceeded critical mass, these observations cannot be explained by coincidence.

Victor I. TREFILOV

Chapter

8 STRENGTH AGAINST FRACTURE

8.1. Fracture Mechanisms in Crystalline Materials

Modern ideas about the physical nature of fracture were formulated on the basis of the concepts of Stroch, Ioffe-Davidenkov scheme and the Hall-Petch dislocation (barrier) criteria for the macroscopic yield stress and Mott-Stroch for the macroscopic breaking stress [208-211]. For brittle failure, the sum of the kinetic and the elastic energy must be at least as large as the fracture surface energy. Methods for estimating the theoretical strength of solids (~E/10) based on a balance of the elastic strain energy and a measure of the material cohesive energy are familiar. Similar arguments are used to focus on extending similar energy concepts to be necessary for predictions of strength and failure time for brittle and ductile crystalline materials. For example, the Orowan approach is based on a sinusoidal representation of the cohesive force.

By the classic failure theory based on the Stroch-Griffith fundamental concept of brittle fracture and the Ioffe-Davidenkov schematic diagram of brittle transition, the temperature development of brittleness (under the bending or tensile testing) is accompanied by sudden (athermal) breaking of section without any plastic deformation, in particular, for isotropic crystals with one critical sliding system. According to macroscopic principles of hard to activate sliding flow stress appears to be a critical parameter at point of brittle fracture. A large stress concentration necessary for critical Griffith crack nucleation is provided by slip bands held up at grain boundaries in the form of pile-ups. Subcritical crack growth (microcracking) is believed to occur at stress intensities as low as 60% of the critical stress intensity. Particularly, cold brittleness of bcc metals (in VIA group) with high stresses of Pieirls is explained on the basis of dislocation theory of sharp temperature dependence of the flow stress due to the growing lattice resistance to the genera-

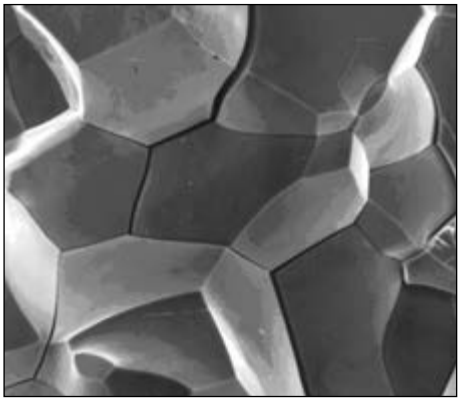

Fig. 8.1. SEM electron micrograph of fracture surface for molybdenum of high purity (~0.001% C, N, O) after tensile testing at 77 K

tion and motion of sliding dislocations at low temperatures.

True brittle fracture is modeled by the nucleation of atomic-sharp submicrocracks from dislocation pile-ups by the Stroch mechanism and their spontaneous propagation by the Griffiths mechanism. It is assumed that the fracture is a kinetic process which does not depend on the nature and conditions of fracture. Nevertheless, published discussion indicates more complicated nature of brittle transition, general universal comprehensive development and variety of the brittleness and embrittlement phenomena. First of all, the formation of an embryonic (spontaneous) Stroch submicrocrack is an insufficient criterion for the activation of general (complete) fracture due to the effective absorption of energies by stable microcracks on barriers of various physical natures. Unfortunately, all of these foundational approaches reflect or characterize the structural sensitivity of strength, measured, as a rule, by reduction in area and elongation in tensile (short-term) tests. Since long-term strength is determined by the dynamic structure which should be formed during prolonged loading rather than the initial one, it is very difficult to apply these approaches under certain temperature — strain rate conditions, especially at stresses below the macroscopic yield stress. Besides, brittle behavior and week absorption are associated with the covalent component of interatomic bond which reduces the dislocation mobility and results in the low symmetry crystalline structure formation in insufficiently active slip systems.

Starting from the unique experiments of Sargent [212], who discovered dislocation relaxation at 77 K, in the periodic literature the critical (hard-to-activate) stage of quasi-brittle fracture is considered to be the propagation of dislocation microcracks rather than their nucleation, for example, by an easily activated basic cleavage.

Intercrystalline brittleness is considered to be the main problem limiting the use of many metals and their alloys with bcc and hcp lattices (Figs. 8.1 and 8.2). The power law for creep (Fig. 8.3) in terms of GBs fracture was analyzed in a series of works by Otsuka M. and Horiuchi P. [213].

$$1/\tau_f = B\sigma^{n'} \exp(-U_f / RT), \tag{8.1}$$

where U_f is the a.e. for fracture; n is the stress exponent; τ_f is the time up to the GBs fracture [214].

Fracture occurs along the GBs, and growth and coalescence of the GB micropores is observed on the GBs facets (Fig. 8.4, *a, b*). As $\tau_f \cdot \dot{\varepsilon}_{min} = C_2/d$ law is valid for the

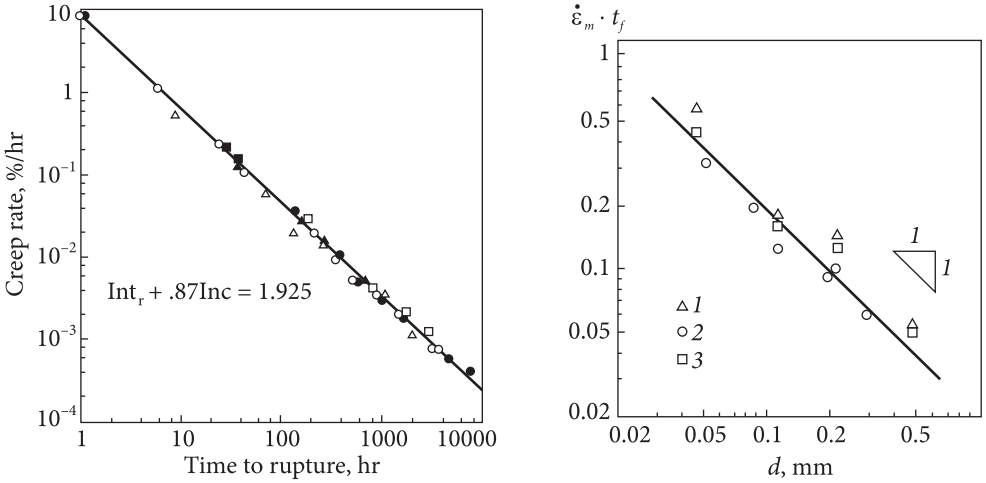

Fig. 8.2. Relation between minimum creep rate ($\dot{\varepsilon}$) and time to rupture (t_r) in the temperature range of 783-893 K for different metal alloy systems [211]

Fig. 8.3. Dependence of $\dot{\varepsilon}_m \cdot \tau_f$ on grain size for different Al—2÷5.2Mg alloys (*1, 2, 3*) by Otsuka M. and Horiuchi P., Japan, 1985-1993 [213]

GBs fracture, then one should expect better creep properties after the transition to nanostructures (with C_2 = 20 μm for Al—5.2Mg alloy).

The results of original theoretical and experimental researches in a field of strength physics, micro and nanoyield kinetics, and mechanisms of the delayed fracture and impurity embrittlement of light metals (hcp Mg, hcp Be, hcp Ti and fcc Al) are generalized in our works [214-216]. Some of them are concerned with scientific legacy of outstanding physicists-academicians V.N. Gridnev, V.I. Trefilov and A.A. Smirnov. It is deduced that existing traditional approaches to the problem of low-temperature brittleness of metals and their brittle strength based on power (athermal) criteria of the fracture nucleation do not provide valuable information for the understanding of the origin of the temperature dependences of true fracture stress to be observed in the temperature range of quasi-brittle transition in hcp and bcc metals, their solid solutions and eutectic metal alloy systems. On the basis of the thermally-activated analysis of microyield, which as a precursor accompanies the fracture propagation, another approach is proposed to estimate the athermal and thermally-activated contributions at a subcritical stage of the microcrack growth as well as interaction of structural defects with a goal of improving the strength characteristics of these metal alloy systems.

In our works, the restrictions were lifted for the first time in the development of a more general theory of quasi-brittle (thermally activated) fracture [215, 216] based on the activation of a hard to activate stage of defect growth. A new schematic diagram of the quasi-brittle transition of metals and alloys is constructed, in which the well-known Ioffe-Davidenkov scheme becomes a particular case of this approach

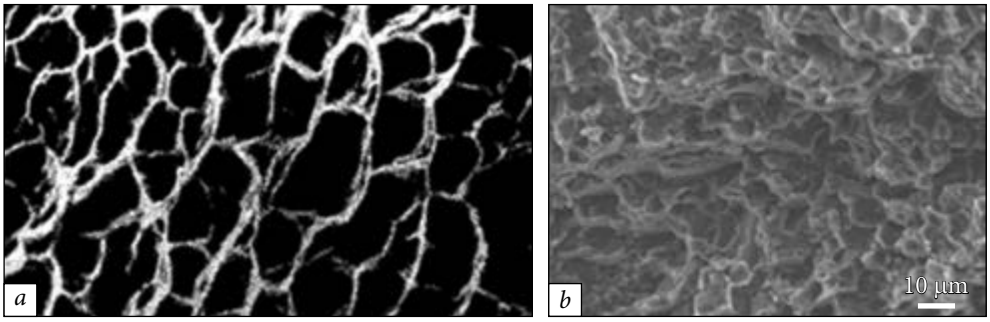

Fig. 8.4. Microstructure (*a*) and fracture surface (*b*) of Al—2Mg alloy after creep testing at 523 K and 98 MPa (d = 0.3 mm) [213]

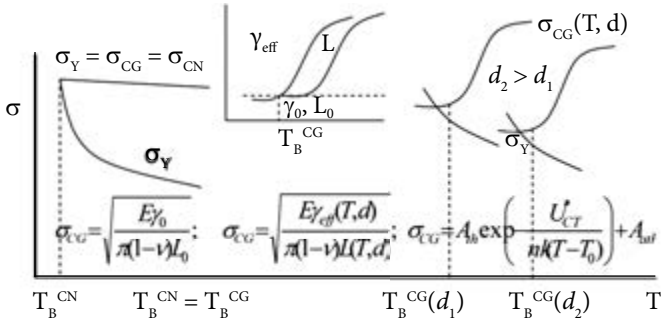

Fig. 8.5. Schematic diagram of principle for describing quasi-brittle transition of metals and alloys. Here: σ_Y is the yield stress; σ_{CG} — stress for microcrack growth; σ_{CN} — stress for microcrack nucleation; γ_{eff} — fracture energy; L — microcrack length; L_0 — i nitial microcrack length; γ_0 — surface energy; T_B^{CN} — brittleness temperature for fracture nucleation; T_B^{CG} — brittleness temperature at the microcrack growth stage

(Fig. 8.5). The proposed physical (dislocation) theory of the ductile-brittle transition describes the thermally activated resistance to subcritical fracture at the difficultly activated stage of microcrack subcritical growth.

Stroch's physical theory [208] of brittle fracture which describes in the theoretical coordinates $1/T_B$ — lnd the nucleation of submicrocrack in dislocation pile-ups is not consistent with experimental data obtained for bcc Cr—0.8La and hcp Be.

The results of T_B calculation for low-alloy Cr—La and Cr—Y systems processed in the Stroch coordinates are deviated from the straight-line dependence adopted for embryonic submicrocracks, especially in the region of coarse-grained states.

The validity of new approach is confirmed by studying the structural sensitivity of T_B for chromium and beryllium processing of these data in new coordinates (Figs. 8.6 and 8.7) reveals a high convergence of theory and experiment. The proposed analytical solutions make it possible to perform a complete comprehensive analysis of the gradual brittle transition of partially covalent metal crystals with a bcc and hcp structure using all the Hall-Petch and Mott-Stroch structural parameters reflecting

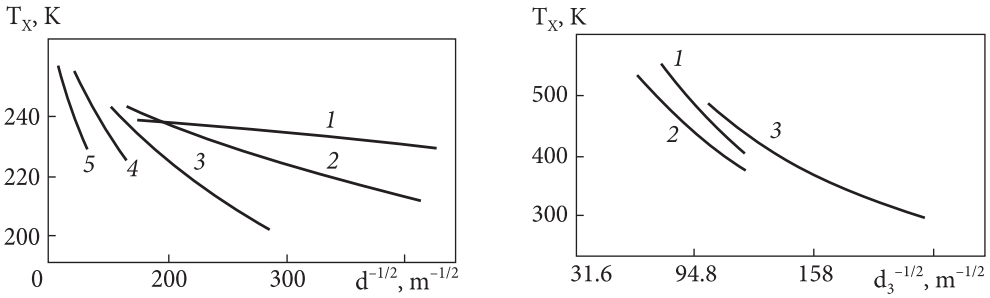

Fig. 8.6. Structural response of brittleness temperature T_B for bcc Cr-0.8La alloy with different grain sizes: *1* — 10^{-5}; *2* — $2 \cdot 10^{-5}$; *3* — $5 \cdot 10^{-5}$; *4* — 10^{-4}; *5* — $2.5 \cdot 10^{-4}$ m

Fig. 8.7. Structural response of brittleness temperature for hcp Be (99.9%); *1* — experimental data; *2* — theory (for basal submicrocrack nucleation); *3* — theory (for stable microcrack growth)

the interaction of the matrix and boundaries at the stage of plastic deformation and dynamic fracture of polycrystals. This approach predicts improvement in the physical and mechanical properties and opens up new prospects for the creation of technological alloys with a low brittleness temperature.

Theory of delayed thermally activated (subcritical) fracture [214, 216] describes the stable (subcritical) growth of microcracks in terms of the athermal and thermally activated contributions to the fracture energy:

$$T_B^{CG} = \frac{U_{CG}}{nk}\left[\ln\frac{(AEvb)^{1/n}}{\sqrt{\pi L\sigma_\gamma - \rho_m^{ST} Gb/\sqrt{2\pi R_0}}}\right]^{-1} + \tilde{T}_0, \qquad (8.2)$$

where ρ_m is the density of mobile screening dislocation in the microcrack tips; U_{CG} is the apparent a.e.; n is a parameter, controlling the value and shape of the potential barriers for the activation of growing microcrack; R_0 is the radius of plastic zone in the crack tip at τ_{cr} = const; ρ_m^{ST} is the density of screening dislocations in crack tip; A and T_0 are constants for a given crystalline material.

The newly developed physical (dislocation) theory of temperature dependence of the true fracture stress appears to be valid for bcc and hcp metals (Table 8.1). In contrast to the generally accepted Ioffe-Davidenkov scheme, operating at a constant

Table. 8.1. **Evaluation of the activation parameters for different metal crystals**

Me	Mg	Zn	Be	Cr-0.8%La	Mo
a.e., $U_{CG} \cdot 10^{19}$ J	—	0.15	0.1-0.2	0.5	0.3
a.v., V_{CG} / b^3 m	50	—	70-400	80	30-50

breaking stress, σ_{fp}^{br} = const, independent of the rate $\dot{\varepsilon}$ and deformation temperature T, and being considered as a special case of a new, more general approach, the new schematic diagram of a quasi-brittle transition is modelled by the temperature dependence of the true breaking stress σ_{fp}^{A} [216]. The presence $\sigma_{fp}^{br}(T, \dot{\varepsilon})$ manifests itself as contribution of thermally activated (short-range) processes at the stage of subcritical fracture resistance under the influence of a thermal component (with degradation of mechanical properties). On an offset circuit of equal stresses, the a.e. for motion resistance of free dislocations equates to the a.e. for motion resistance of screening dislocations at the early stages of dislocation microyield, preceding and accompanying a fracture. The proposed theory of the barrier structure of alloys, based on the physical principles of the formation of the temperature dependence of the true fracture stress, predicts the possibility of transferring subcritical microcracks into harmless, dislocation relaxed or equilibrium configurations that no longer satisfy the Griffiths criterion for brittle fracture.

8.1.1. Dislocation Nature of Fracture Resistance Mechanism

The fracture resistance may be considered in terms of the Griffith-Orowan equation for fracture of a semiductile material [217]

$$\sigma_f \infty \sqrt{\frac{E(\gamma_s + \gamma_p)}{C}} = \sqrt{\frac{E \cdot G_c}{C}}, \tag{8.3}$$

where σ_f is the fracture stress, E is Young's modulus, C is the half flaw length, γ_s is the energy per unit area required to form a new fracture surface, and γ_p is the energy expended in plastic deformation per unit area of fracture, G_c is the critical value of the crack extension energy and contains both the plastic and the surface energy terms.

The solute segregation may change both γ_s and γ_p. If the fracture happens at GB, then the GB is destroyed following a relation

$$\gamma_s = \gamma - \gamma_{GB} / 2. \tag{8.4}$$

If solute segregation at the GB has occurred, then γ_{GB} reduces causing an increase in γ_s; however, since the solute atoms are found on the fracture surface the surface energy is also reduced. In brittle metals γ_p will control fracture stress σ_f. Segregation may lower or raise γ_p depending upon change of local plasticity. Localized changes in bonding leading to a brittle region or a localized reduction in ductility due to intense solid solution hardening are possible explanations for the decrease of γ_p. It thus seems likely that the major effect in reduction of σ_f by solute segregation is the effect on γ_p of the chemistry change in the surface, although the driving force for the segregation is reduction in the surface energy.

A fracture theory has been developed which is an analogue of the Griffith one for a deformable crystalline solid [218]. In this theory the processes of bond breaking

and dislocation emission at the crack tip are treated as concomitant so that the local plastic work at fracture and the cohesive energy are established. This gives criteria for unstable microcrack extension in terms of the relevant plastic properties of the crystals and the cohesive energy.

It is well-known that bcc transition metals undergo a transition to brittleness at low temperatures. Normally, this manifests itself by the intervention of transcrystalline cleavage before extensive plastic deformation occurs. It seems to be the direct result of the decrease in dislocation mobility with decreasing thermal activation. Segregation of certain solute elements, mostly from Groups IVB to VIB, emerges at GBs reducing their cohesive strength. It follows that a phenomenon of brittleness should be considered as state of a solid, i.e., an inherently ductile polycrystalline material can become brittle due to at the segregation of the harmful solute impurities on the GBs. The definitions of brittle and ductile microcrack growth are derived from the nature of failure at their tips. The former involves a cleavage process with little or no plastic deformation while the latter displays pervasive plasticity through local ductile whole growth and link up. The ductile crack growth is a fracture toughness which is observed at low strain rates. Continuum measure of fracture dissipation is determined by the parameters such as fracture toughness, surface tension flow stress or viscosity.

In search for correlation between the dislocation microyielding prior to the macroscopic yield point on the stage preceding with fracture (precursory of fracture) and the dislocation microyielding accompanying the initial fracture, in the crack tips, on their delayed (subcritical) growth, a series of experiments has been carried out using the techniques of stress relaxation, internal friction, and tensile tests [219]. Bcc metals of VIA group have been shown to undergo a transition from ductile to quasibrittle behavior with decreasing temperature. Besides, low temperature brittleness is accompanied by a rapid rise in yield stress (Fig. 8.8) as a result of influence temperature on the resistance to plastic flow. There is, however, certain evidence (Fig. 8.8) which suggests that in some metals the transition is closely related to a rapid decrease in true fracture stress as a result of influence of decreasing temperature on the fracture resistance caused by plastic (dislocation) deformation at microcrack tips. Unlike the bcc transition metals hav-

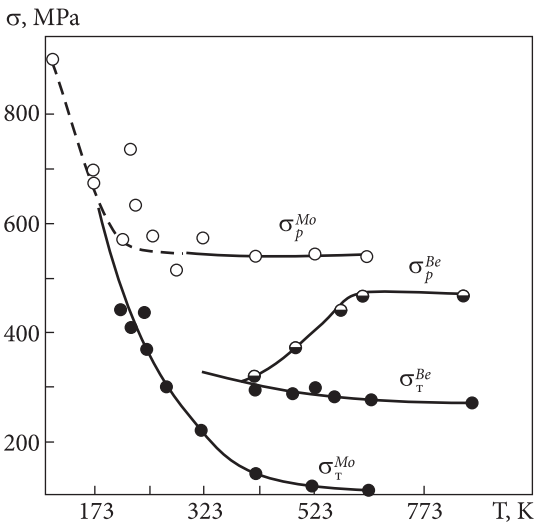

Fig. 8.8. Determination of the brittleness temperature (T_B) using the experimental temperature curves σ_Y (T) and σ_f (T) for bcc Mo and hcp Be

ing the strong temperature dependence of yield stress (Fig. 8.8), the ductile-brittleness transition in hcp metals of II A group (Mg, Be, etc.) is characterized by a week temperature dependence of yield stress, but by the strong dependence of fracture stress. It is a matter of principle, the more so in previous works there is considerable speculation discrepancy as to the treatment of the observed effects.

In our works it has been deduced that the activation of fracture inhibition mechanism is a rate-controlling process providing the delayed fracture of metals to suppress their embrittlement. In this case, for example, creep strain rate is taken proportional to growth crack rate.

A quasi-brittle dynamic fracture theory has been developed for metallic crystals on the base of new concept considering the self-organization in dislocation ensembles at the crack tip plastic zone and formation of spatial dissipative structures at the stage of microcracks subcritical growth before their spontaneous failure. A model of crack tip-screening dislocations dynamic system has been suggested for describing the evolution of the dissipative structures taking into account the short-range and long-range contributions of mobile dislocations and specific mechanisms of their energy dissipation. This makes it possible to explain the dislocation mechanism of gradual quasi-brittle transition in terms of temperature dependence of true breaking stress.

Thus, from the standpoint of dislocation physics of fracture, these is a fundamental possibility of stabilizing fracture resistance and preventing brittle fracture by thermal obstacles and stronger barriers of various nature and efficiency. This makes it possible to formulate methods of low-temperature hardening and increasing the plasticity of the most brittle metals such as bcc Cr and hcp Be, based on the structural and temperature dependence of the true breaking stress. The presence of a temperature dependence of fracture resistance means in fact the existence and the possibility of activation of thermally activated (short-range) mechanisms responsible for more efficient plastic relaxation and rapid hardening of metal alloys based on a stable equilibrium of defects in the field of local overstresses (dislocation accumulation of pile-ups and dislocation submicrocracks).

8.2. Time Delayed Fracture

The relationship between plastic deformation and fracture is universal and manifests itself at various stages and structural-energy levels. Martensite-hardened carbon steel has an increased tendency to delayed fracture, which includes: (a) easily activated initiation of submicrocracks in the presence of residual stresses arising from matrensite transformations; (b) slow growth of microcracks (along the boundaries of austenite grains); (c) brittle fracture in non-carbon complex-alloyed maraging steels (after aging at 723 K) [220]. The phenomenon of subcritical fracture is observed only at relatively low temperatures. In this case, the subcritical growth of microcracks in samples with artificially introduced defects is recorded on tensile oscillographs. The idea of controlling interface chemistry to control properties has been

used successfully to prevent the GBs embrittlement of metals and their alloys including low alloy steels where undesirable trace elements, i.e., potential segregates are either avoided or, if present, are kept in solid solutions by appropriate heat treatment. The same applies to sufficiently disoriented cells, the walls of which serve as grain boundaries. The RE such as Y binds the inevitable impurity, first of all, nitrogen into non-hazardous and harmless compounds, reducing their concentration at the grain boundaries and cell walls.

Nevertheless, the factors affecting the ductile fracturing of pure metals and their alloys with harmful impurities have not been clearly established or separated. Under the data [221], the effect of decreasing brittleness temperature, $T_{B,}$ in pure α-Fe is attributed to decreasing dislocation pinning, as interstitial carbon segregates to GBs, and to the strengthening of subgrain boundaries by carbon segregation. When carbon is allowed to segregate to GBs it could act to break up the Fe—O complexes by preferentially bound with the oxygen. Nevertheless this behavior might be caused by either the interaction between carbon and residual grain boundary oxygen or the binding effect due to the carbon itself, and possibly by both. Locking of dislocations by foreign solute atoms, especially by undesirable interstitials, would be expected to be unimportant at high temperature because the diffusion rate of interstitials is extremely high.

Diffusion-dependent fracture and time-delayed failure of polycrystals under stress was analyzed in experiments by Wilcox, Smith (Fig. 8.9) and Charles and Hayes [222, 223].

Temperature dependence of the delay time to fracture for hydrogenated nickel prestrained by 15% at 1073 K and $\dot{\varepsilon} \sim 3.3 \times 10^{-4}$ sec^{-1} with the estimated a.e. for H diffusion in Ni is shown in Fig. 8.9. The stress during delayed fracturing does not exceed 0.95 σ.

The delayed fracture mechanism consists in nucleation of nanovoids, their growth and coalescence at the GBs to form GB dimpled facets, which then are connected by shearing (Figs. 8.10-8.15). The mechanism observed conforms with that suggested for GB fracture (Figs. 8.13-8.15).The interfaces appear as preferential fracture paths at any temperature studied. However, a little has been done to clarify the nature of delayed creep fracture in slow strain conditions under constant creep stress and constant creep temperature. Further strengthening concept development should concentrate on the formation of crack-absorbing matrices, e.g., in eutectic alloys and metal matrix composites (MMCs) with a new developed structure which provides significant strengthening and, as a consequence, thermally activated (delayed) fracture. The crack -absorbing matrix permits subcritical crack growth in a wide range of stresses and cycling loads without immediate failure.

Our research suggests that the low ductility is most likely associated with the deformation behavior in alloys. The extent of strain localization appears to be much worse in hcp alloys than in other age-hardenable alloys. This may be due to very low interfacial energies and lack of coherency strains of the precipitates. TEMs taken during in situ deformation studies show strain localization in deformed precipitate free zone (PFZ) as well.

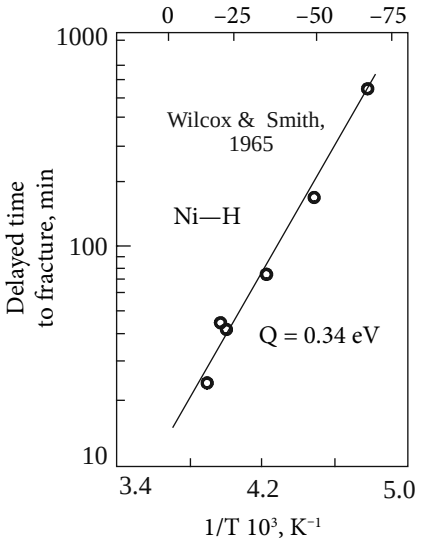

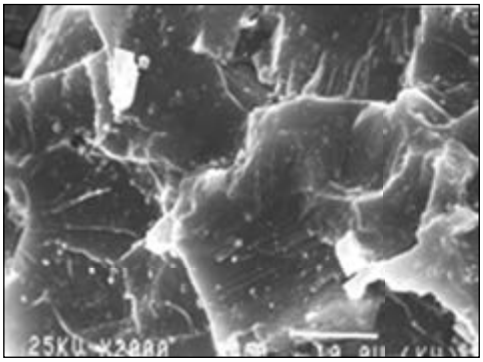

Fig. 8.10. Fracture surface formed by the stepwise displacements of slip lines during matrix sliding

◀ ***Fig. 8.9.*** Diffusion-dependent and controlled delayed fracture of Ni—H alloy [222]

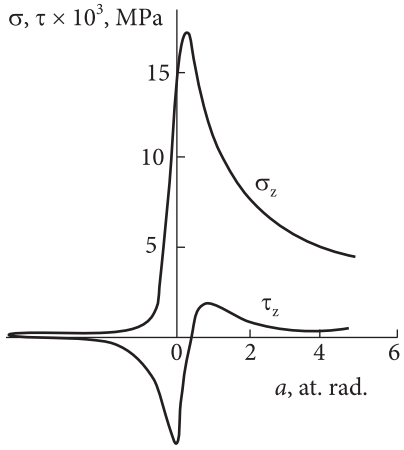

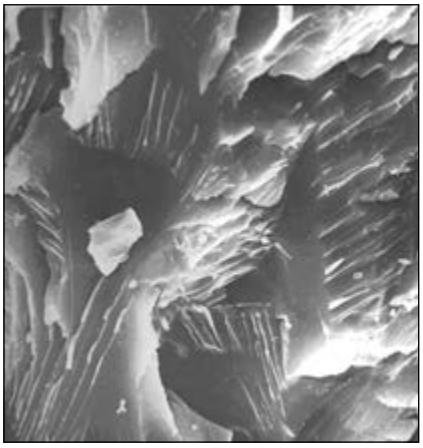

Fig. 8.11. Crack tip distribution of the normal (σ_z) and shear (τ_z) stresses caused by the rupture of interatomic bonds (Elliot approximation)

Fig. 8.12. Transcrystalline cleavage of the deformed Be—1.5Co alloy after tensile testing at 293 K (×600)

The observed decrease in macroscopic ductility can be explained qualitatively by the corresponding increased tendency for planarity and inhomogeneity of slip. The intense slip bands produce stress concentrations at grain boundaries [4] and in many cases, can shear the boundaries producing grain boundary offsets (ledges). When a small amount of sliding occurs along the grain boundary due to restricted slip and grain rotation, cracks form at the ledges. Once the crack has nucleated, it concentrates the stress, and more intensive localized deformation occurs in the vicinity [224]. The crack then expands transgranularly along the in-

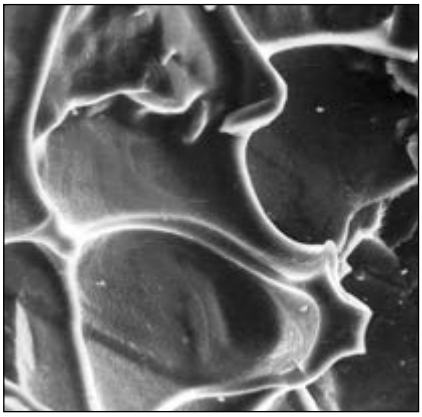

Fig. 8.13. Coalescence of microcracks relaxing on viscous grain boundaries for recrystallized hcp Be—0.5Co alloy during tensile testing at 293 K

Fig. 8.14. Localization of fracture on the grain boundaries for recrystallized alloy Be—1.5Co at 293 K (extraction replica) (×600)

tense slip bands or intergranularly along the grain boundaries. The PFZs which form in the late stages of aging are related to the age-hardened matrix, and plastic deformation can be localized in these regions [225]. High-voltage electron microscopy in situ deformation studies on lithium-containing aluminum alloys illustrates this point [226]. All of the materials have planer slip and a tendency toward strain localization for the aging conditions studied. The slip bands impinge upon grain boundaries and cause stress concentrations across the boundaries the magnitude of which depends on the slip length [226, 227]. There is a high probability that the stress concentrations will not be easily relieved by the transfer of plasticity to adjacent grain (Fig. 8.11).

The fracture surface is formed as a result of stepwise displacements caused by shifts within the grains and the emergence of slip lines (bands) on the intergranular surface (intercritical fracture). The effect was first described by Utevsky and Orlov in 1961 when studying the temper brittleness of steel [228] and is considered as a characteristic of polycrystals with low cohesive strength of boundaries under stresses at the level of the yield point. The steps caused by matrix sliding form the surface of a viscous grain boundary cleavage.

However, the activation of viscous sliding in the area of GB, cell boundaries is an effective means of reducing the temperature of the ductile-brittle transition. The presence of shear processes at the boundaries is confirmed by studies of grain-boundary and cell-boundary relaxation (Fig. 3.8) caused by the boundary dislocation motion. Localization of shear deformation at the boundaries can lead to the formation of ductile fracture along the boundaries. Lueders stripes create regions of rapid local deformation, which is responsible for the rapid hardening of polycrystals. The lack of active slip systems provides conditions for local deformation around grain boundaries.

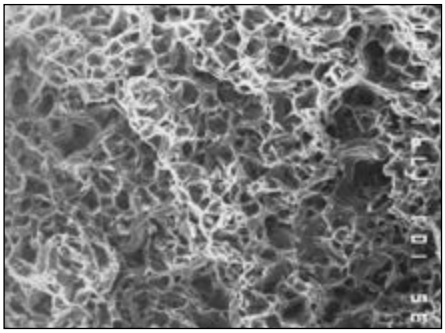

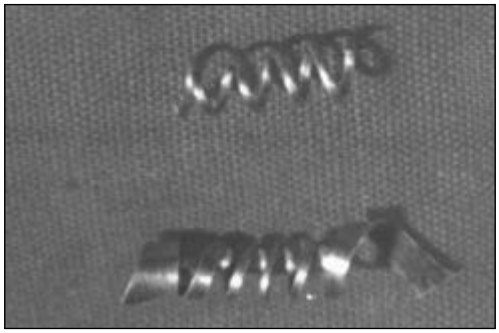

Fig. 8.15. Viscous fracture of the recrystallized Be—1.5Co after tensile testing at 1000K (×600)

Fig. 8.16. A spiral of rolled 40 μm thick strip made of Cr—0.8Y alloy with a cellular structure produced by the method of gradual decreasing rolling temperature up to r.t.

Great care should be taken in assessing the long-term operation of units and structures based on the results of short-term tests, since, with a decrease in the creep rate, their fracture can occur at any time due to the appearance of micro-flow of GBs and interphase surfaces. Further developments in physics of short-term strength enlarge the scope of the power law for creep to cover the grain boundary fracture (Figs. 8.13 and 8.14). As can be seen from the photograph, the dimple pattern which is observed on the fracture surface shows that fracture occurs by the Tetelman-Robertson mechanism [229]. The analysis of blunted fracture indicates a dimpled surface of ductile fracture.

This product (Fig. 8.16) has outstanding characteristics namely

- plastic state is up to 77 K;
- cell size does not exceed 100-150 nm;
- ultimate tensile strength reaches 1500 MPa at 293 K.

The room temperature brittleness of the polycrystalline refractory metals of the VIA group is a result of their high ductile-brittle transition temperatures T_B which can be attributed principally to the influence of grain boundaries on plastic flow and fracture [230, 231]. The segregation of impurities to grain boundaries is assumed to be the most important mechanism controlling the ductile-brittle behavior of these metals.

The same applies to sufficiently disoriented cells, the walls of which serve as grain boundaries. The RE such as Y binds the inevitable impurity, first of all, nitrogen into non-hazardous and harmless compounds, reducing their concentration at the GBs and cell walls.

8.3. Mechanism of Hydrogen Embrittlement

The Griffith condition for existing crack is never satisfied in plastic and quasibrittle solids. As could be expected, hydrogen-induced cracking, e.g., of commercial high-strength steels is developed as intergranular. When an impurity-segregation effect is sufficiently weakened, hydrogen-induced cracking occurs by a

transgranular (brittle) mode. The results of experimental study of the mechanism of hydrogen embrittlement are therefore generalized on the base of a theory of thermally activated (quasi-brittle) fracture. The notions about the nature of continuous quasi-brittle transition of Me—H solid solutions are made more precise. It is found that the evolution of hydrogen brittleness for polycrystals appears to be controlled at low (cryogenic) temperature by sliding screening dislocations overcoming segregated H atoms at the microcrack tips with activation energy of 0.05-0.1 eV typical for the critical (difficult-to-activate) stage of fracture propagation. If the concentration of excess (hydrogen- and deformation-induced) vacancies exceeds that of thermally equilibrium vacancies by 2-3 orders of magnitude, clustering the structure of Me—H solid solutions is observed within thermally activated area of dynamic deformational aging. In such a case, the formation of strong "H atom-excess vacancy" pair defects with higher binding energy (up to 0.6 eV) prevents the hydrogen segregation at the structural defects. The methods for elimination of hydrogen brittleness, repair of plasticity and strength properties of Me—H systems are suggested in terms of the formation of the new barriers for propagating microcracks in well disoriented cellular structures in clusterized hard solutions with large number of active sliding systems for screening dislocations (Ti—H, Zr—H, Al—H) or supersmall cellular structures in superplastic and plastic states of clusterized substitutional alloys with a lack of active sliding systems for screening dislocations (Mg—Ba—H, Be—Co—H).

The most precise structure-sensitive methods (electron-positron annihilation, electric resistivity and internal friction measurements) yield in the first experimental evidence for existence of hydrogen-induced lattice vacancies and hydrogen-stimulated diffusion in hcp and fcc Me-H systems which is accompanied by forming pair defects "H atom-excess (non-intrinsic) vacancy" (Chapter 2). The new method for analyzing high-temperature dependence of Me-H systems electric resistivity is developed in terms of the model for clustering a structure in solid solutions Me-H oversaturated with excess vacancies. It should be pointed out that partial thermally activated dissociation (decay) of pair defects with low binding energy (0.2 eV) appears to be a rate-controlling mechanism for hydrogen-stimulated diffusion in hydride-forming systems (Ti—H, Zr—H) (Fig. 2.3). Thermally activated association of pair defects with high binding energy (0.5-0.6 eV) is found to be a rate-controlling mechanism for hydrogen-stimulated diffusion in non-hydride-forming systems (Al—H) (Fig. 2.3). Clusterization of excess defects simplifies formation of hydrides at significantly lower temperature.

In search for a generalized approach, the results of investigation of the structural transformations in decaying hydrogenated solid solutions on the base of hcp Mg, Mg-Ba, fcc Al, and Al—Li are summarized and analysed in terms of hydrogen-induced diffusion concept and of clustering a structure model with the estimates of the relaxation rate and the activation parameters of diffusion in the temperature range of 293-900 K by means of structure-sensitive methods of measurements. It is found that observed accelerated (short-range) diffusion is realized in interstitial and substitutional solid solutions with cluster-forming structure responsible for the high rate of decay and for the

transience of the hydride nucleation at low (room) temperatures. In accordance with this, mixed (excess hydrogen vacancy-solutes) diffusion attributed by participation of the mobile diffusive cluster is considered to be one of the most probable and rate-controlling mechanism which causes the anomalous deviation of hydrogen diffusivity from classic (Arrhenius) behavior at low (room) temperatures.

The activation parameters of solutes diffusive mobility, inelasticity, microyielding, and plastic deformation of hydrogenated, interstitial, and substitutional solid solutions have been measured for metals with low (fcc Al), average (hcp Mg), and high (bcc Mo) barriers of Pierls, hydrogen-free, H-like doped, and hydrogenated alloys (Mg—Ba, Al—Li, Mo—C,H) using exact structure-sensitive methods of internal friction and mechanical hysteresis loops in the temperature range of 293-800 K (Figs. 3.3, 3.7 and 3.8). It is deduced that short-range diffusion accelerated by activation of hydrogen vacancy-solute clusters is one of the most probable rate-controlling mechanism of the decay for hydrogenated hcp metals and alloys with cluster-forming structure.

8.4. Suppression of Hydrogen Embrittlement with Recovery of Strength and Ductility

The significant improvement in ductility is associated with a change in fracture mode from the predominately intergranular rupture observed in polycrystals to transgranular dimpled rupture (Figs 8.10 and 8.15). It is clear that stress concentrations at the grain boundaries, resulted from the planar deformation, are relieved in the highly textured material by shear in neighboring grain. The low degree of disorientation between the neighboring grains reduces the effectiveness of GB as a slip barrier and guarantees nearly parallel slip systems.

A recently observed grain size dependent fracture mode transition triggered by GB sliding is thought to be related to many of the improvements in mechanical properties of IIA, IV, and VIA group metals [232]. GB sliding is especially extensive in hexagonal metals, and it has been observed at as low temperature as 78 K in high purity magnesium [233]. In very grained and pure (oxide free) beryllium GB sliding alone without the operation of other slip systems could produce extensive permanent deformation without fracture at r.t. [192, 234]. At elevated temperatures GB sliding has been revealed to produce over 90% ε of the total deformation. The presence of fracture mode transition indicates the activation of another mechanism.

Hydrogen in the hcp Ti-H system has been implicated in slow strain embrittlement during tensile testing [37, 235]. The following factors have been found to affect ductility in the presence of hydrogen: (a) hydrogen concentration; (b) strain rate, $\dot{\varepsilon}$, (c) α-Ti grain size; (d) types of alloying elements and β-stabilizers. It has been found that a fine equiaxed microstructure possesses a high resistance against crack initiation. Nevertheless, no evidence of hydride precipitation was found and thus apparently the observed effects were due to dissolved hydrogen.

In many cases the intergranular fracture and associated low ductility of alloys was attributed to embrittling tramp elements such as hydrogen segregated at grain boundaries. Measurements of internal friction in the low frequency range were carried out on deformed specimens of nominally pure α- and α-Mg containing inevitable interstitial impurity concentrations (O, N, H, C). The pinning of dislocations by the interstitials is likely to be responsible for solid solution impurity (hydrogen) embrittlement observed in hcp metals at low temperatures.

Phenomenon of thermal depinning of dislocation is attributed to reducing apparent concentration of thermally activated barriers to the dislocation movement to act by short-range mechanism. The author suggests that H is pick-up by structural defects such as dislocations and strain-produced excess vacancies. To reinforce the hypothesis, discrete temperature spectrum of hcp Mg was measured and analyzed. No peaks were positively identified after quenching as being to H-substitutional atom pairs or their pileups. H is likely to be more strongly bound to another type of lattice defects such as excess vacancies in the primary H-V_e cluster [236]. Hydrogen is assumed to be distributed between normal interstitial sites and sites adjacent to dislocation.

Two structure-sensitive (barrier) Hall-Petch (for macroscopic yield stress) and Mott-Stroch (for fracture stress) basic for "athermal" theories of short-term strength can be united into the convertible (dislocation) criterion of stable microcrack growth (Fig. 8.18). The criterion includes the contributions of dynamic fracture dragging or the serrated growth of microcrack by the Tetelman-Robertson mechanism. The formation of diffusion traps in the α-Ti—H system is associated with (i) the primary capture of hydrogen atoms by excess vacancies with the binding energy, E_b, of about 0.6 eV/atom; (ii) the release of screening dislocations (in the crack tips) from hydrogen atoms ($E_b \sim 0.2$ eV); and (iii) structural preparation of a subcritical (belayed) fracture. The change of observed fracture mechanism (Figs. 8.19-8.21) is attributed to the formation of a cell structure with the plastic relaxation of walls free of hydrogen segregation and to the increase in resistance to mobile dislocation. At elevated temperatures GB sliding has been revealed to produce over 90% ε of the total deformation.

The zone of stable regrowth of microcracks develops in microshocks as a result of $\Delta\sigma$ fluctuations of the critical Griffiths stress of $\sigma > \sigma_{kr}$ (Fig. 8.18), which is necessary for microcleavage of the plastically deformed crystal volume. The fracture surface resembles the "grooves" that occur during fatigue. The process is described by the well-known Bilby-Cottrell-Swinden model [237] concerning regeneration of suspended relaxed plastic microcracks as brittle objects or Tetelman's concept of repeated re-nucleation of viscous defects [238]. In this case (Fig. 8.18), surface energy, $\gamma_{0,}$ becomes reversible due to the ruptures of interatomic bonds (Fig. 8.11) in the absence of energy scattering.

In the theory of Bilby, Cottrell and Swinden (BCS) the plastic yielding at the crack tip was modelled by a continuous distribution of dislocations along the crack plane. The plastic zone was described by a linear pile up of dislocations. The theory

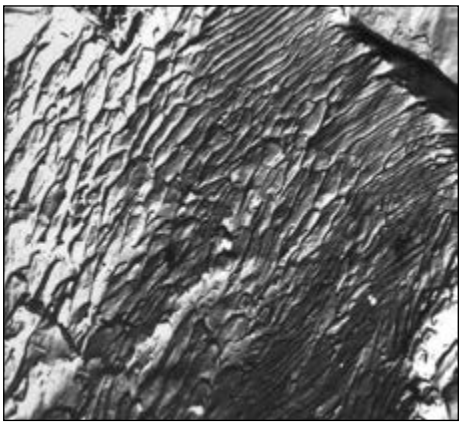

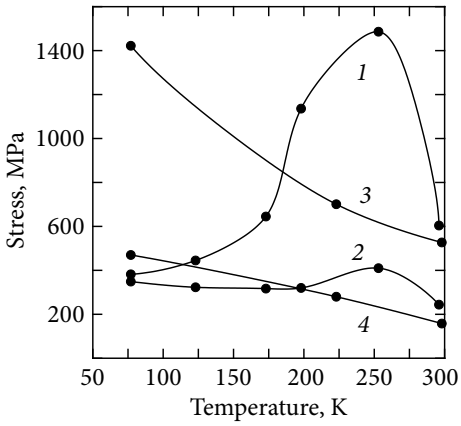

Fig. 8.18. Zone of stable regrowth of microcracks by a Tetelman-Robertson mechanism (×600) [229]

Fig. 8.19. Effect of testing temperature on the true fracture stress (*1, 3*) and on the flow stress (*2, 4*) for α-Ti—H alloy after low temperature and high temperature annealing treatment at 923 (*1, 2*) and at 1073 K (*3, 4*)

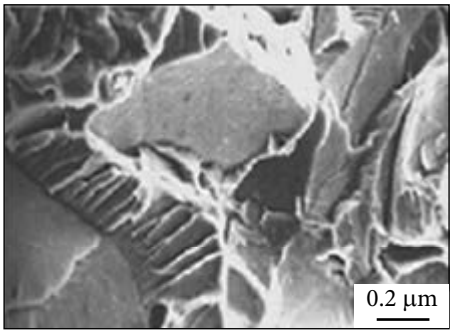

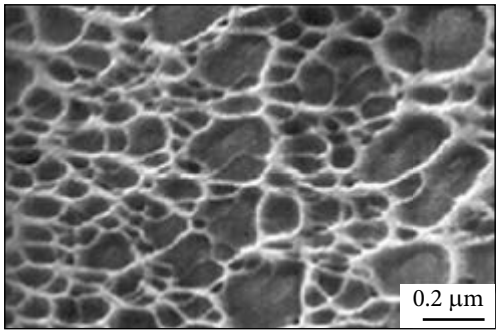

Fig. 8.20. Typical microstructural mechanism of brittle transcrystalline fracture at 77 K for Ti—H microalloy: SEM electron micrograph of the Ti—H sample fracture surface after annealing for 1 hr at 923 K

Fig. 8.21. The microstructural mechanism of viscous fracture at the relaxing cell boundaries acting as strong barriers to crack growth at 77 K: SEM electron micrograph of the Ti—H sample fracture surface after annealing for 2 hr at 1073 K

has since been widely applied to various aspects of elastic-plastic fracture. The direct observations have been made of the distribution of dislocations in the elastic zone during in situ tensile deformation in the electron microscope [239]. These observations were generally in good agreement with the BCS theory, but as more careful examination was made of the region immediately in front of the crack tip it was found that this region was often a tree of dislocations. The dislocations were observed to emit from the crack, pass through the dislocation-free zone (DFZ) and accumulate in the plastic zone.

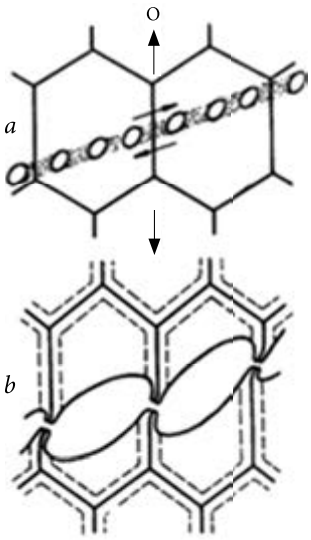

Fig. 8.22. Viscous (transcrystaline) fracture (*a*) and fracture followed by plastic relaxation of mobile microcracks on viscous cell boundaries (modification of J.C.M. Li scheme for tensile testing). (*b*)?

It is noted that the DFZ is formed when the dislocation emission mechanism is stopped after a certain number of dislocations have accumulated in the plastic zone. In order to form a DFZ, a material must be capable of generating dislocations at the crack tip before the crack propagates. The mechanism by which the cracks grow into the DFZ is not well understood at present. The brittle versus ductile fracture for the present mode can be related to the theory of Rice and Thomson [240] who proposed a criterion for the generation of dislocations at the crack tip.

The time dependent thermally activated growth or sub-critical crack growth at stresses below the Griffith value is of very considerable technological interest. There can exist a certain range of crack length in which purely thermally assisted (slow) crack growth can occur in the form of a lattice trapping around the point of fracture instability [241]. Although sub-critical crack growth at stresses below the Griffith value violates the second law of thermodynamics, but that considerable thermally activated crack growth is possible at the Griffith stress level in cases of lattice trapping of a crack where the change of surface free energy is not a smooth function of the increasing crack length [242].

The large difference in ductility can be explained in terms of the crack nucleation and fracture. Research results indicate the fracture mechanism change (Figs. 8.19-8.21). The presence of fracture mode transition is certain to testify to the activation of another mechanism (Fig. 8.22). The GB dislocation sources trigger GB sliding and as consequence GB fracture mode mechanism based on the correlations between strain rate, $\dot{\varepsilon}_{GB}$ and time to rapture, τ_f as well as between cells and grains, d and $\dot{\varepsilon} \sim d^{-1}$ [230]. Transmission electron micrographs obtained by Thompson [231] show apparent dislocation sources in cell wall of nickel. The cells decrease susceptibility of titanium to the hydrogen embrittlement (Fig. 8.19) giving rise to load fracture toughness (Fig. 8.21).

Such a process in the form of the conventional viscous (transcrystalline) structure and the GB fracture is shown in Fig. 8.22. The latter follows the microplastic relaxation of the growing microcracks interacting with the viscous (relaxing) cell boundaries by James C.M.Li modified scheme. It is valid for solid solutions with well disoriented cell structure being formed during tensile test.

8.4.1. Complex Hydride-Forming Systems for Hydrogen Storage

There has been considerable scientific interest in chemically active metal-hydrogen systems motivated by technological problems such as hydrogen storage and hydrogen embrittlement [243, 244]. The reasons for this research activity are to a large extent visible in the engineering consequences of the presence of hydrogen, which is a promising medium for both energy transmission and energy storage.

Among metal hydrides studied as possible solid-state hydrogen storage materials, magnesium hydride is one of the most promising candidates for hydrogen storage due to its high hydrogen storage capacity (7.6% in MgH_2), low cost and abundance. However, its practical application for hydrogen storage is hampered by its high thermodynamic stability and sluggish hydrating-dehydating kinetics. A great deal of research has shown that the hydrogen storage performance of MgH_2 could be improved by adding other hydrogen storage materials and doping with appropriate catalysts by ball-milling, such as transition metals, transition metal oxides and transition metal fluorides [245].

The disadvantages of the known reversible metal hydrides ($LaNi_5H_6$, $TiFeH_2$ etc.) are the high costs for intermetallics and alloys applicable for hydrogen storage which combine with their 4-5 times lower storage capacities (1.5...1.8 mass% H) with respect to MgH_2 (7.6 mass% H). At the same time, the relatively inexpensive metal hydride storing such large quantities of hydrogen has slow Mg-H reaction kinetics and is too stable for most practical applications. These two major obstacles prevent its widespread usage [244, 246]. From this point of view proposed alkali metal aluminum hydrides ($NaAlH_4$, Na_3AlH_6) with higher storage capacities (2.1...4.2 mass% H) should consider as potential novel reversible hydrogen storage materials based on complex hydrides of light metals (Al, Na, Li). However, the unsatisfactory rates of the Ti-catalyzed dehydrogenation-rehydrogenation at relatively high temperatures (> 423 K) and hydrogen pressures (60-150 bar) as well as cyclic instability eliminate them from storage application.

Further improvement of the systems can be expected by variations of the hydride composition and the catalysts responsible for catalytic acceleration of reactions in both directions (hydrogen dissociation and chemisorption). A better understanding of surface processes, such as segregation, contamination, chemisorption etc., using analytical advantages of UV- and X-ray photoelectron as well as Auger electron spectroscopies results in developing more efficient hydrogen storage materials. They include the appearance of lower temperature reversible hydrogen storage materials based on complex hydrides of light alkaline earths (Mg, Ba, etc.) with cluster-forming microstructure, which promote the increase in reaction rates and hydrogen capacity.

The presence of bimetallic magnesium clusters alloyed with barium and titanium may be of major importance in dealing with catalytic properties at the segregated

GBs in eutectic alloys. In cast alloys passing through a pre-precipitate stage, the segregated Ba atoms, indeed, produce cluster-type trapping centers with a new electron structure (excess valence electron density at the Fermi surface) retaining their isolable properties in solid solutions and controlling hydrogen dissociation. They should be regarded as complex hydride-like separations, i.e. pre-nanophases embedded in the α-Mg matrix near the GBs as well as at the dislocations, with saturated chemical compositions close to corresponding chemical compounds.

Criteria are formulated under which metallic systems including eutectic alloys (Mg—Ba, Mg—Ti, Mg—Cr) with positive mixing enthalpies can be used for these purposes. Synthesis of the novel complex hydrides with a nanocomposite structure by mechanical alloying is considered as one of the most effective approach to producing complex magnesium hydrides.

8.4.2. Structural and Phase Transformations in Alloys of the Mg—Y—Ni—H System

Magnesium-based alloys have attracted increasing interest as structural metallic materials due to their high specific strength. Nevertheless, corrosion resistance is an important attribute of a number of magnesium-based alloy systems, and the mechanisms that control their behavior in hostile environments must be understood for design of novel alloys. In this study we aim to carry out comparative analysis of structural and phase transformations in as-cast $Mg_{80}Y_5Ni_{15}$ alloy, liquid quenched as well as their hydrogenated states.

The microstructure of a ribbon obtained by TEM is presented in Fig. 8.23. It can be seen that it manifests crystalline domains (from 25 up to 500 nm in size) in amount not exceeding 5-8% in a single amorphous phase. This is evidenced by analysis of the electron-diffraction pattern and dark-field images obtained in ring reflections of point and diffusive character.

XRD research was carried out on a diffractometer DRON-UM1 in monochromatic CuK_α radiation. A graphite single crystal as a monochromator was established against the diffracted beam. For high-temperature XRD researches, an add-on device UVD-2000 was installed to operate in a helium atmosphere. Processing diffractometer data was carried out with use of Powder Cell 2.4 programs for analysis of XRD spectra from a mix of polycrystalline phase components.

Amorphous halo and weak maximum peaks of some crystal phases, in particular magnesium oxide MgO (Fig. 8.24), are fixed on the initial material XRD patterns. Saturation by hydrogen results in shift of the amorphous halo toward small diffraction angles. XRD 'in-situ' examination no changes in diffraction patterns of amorphous and hydrogenated specimens revealed up to temperature 423 K.

The first maximums of crystal phases are registered with increasing temperature up to 473 K. The analysis of XRD patterns shows that they belong to the Mg_2Ni and Mg phases. There is a broad peak of yttrium hydride YH_2 with the cubic lattice pa-

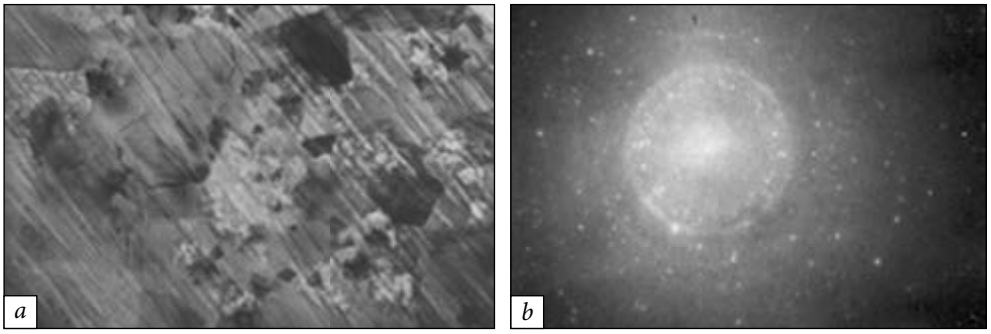

Fig. 8.23. A bright field electron micrograph showing ribbon microstructure of the $Mg_{80}Y_5Ni_{15}$ alloy produced by single roller melt spinning (*a*) and electron-diffraction pattern from this region (*b*)

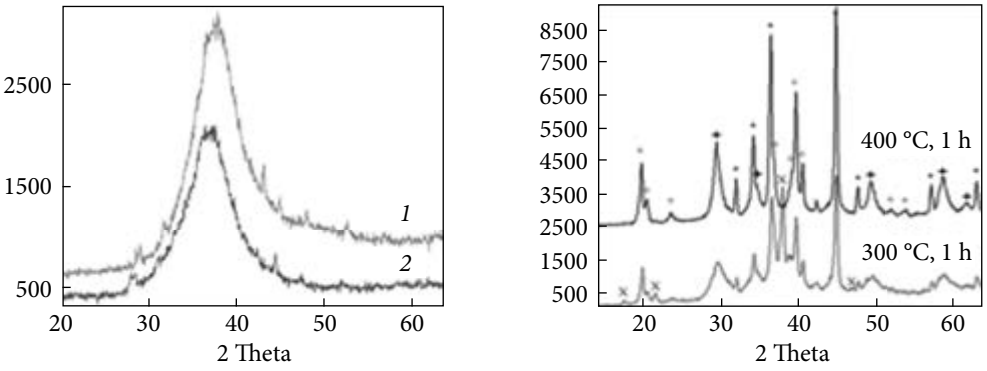

Fig. 8.24. XRD patterns for initial $Mg_{80}Y_5Ni_{15}$ after liquid quenching (*1*) and after hydrogenating (*2*)

Fig. 8.25. XRD 'in-situ' patterns of $Mg_{90}Y_5Ni_{15}$ alloy after hydrogenating and annealing. Designations of maximums: * — Mg; o — Mg_2NiH; + — YH_2; x — additional peaks

rameter a = 0.5178 nm in the hydrogenated alloy. The temperature increasing up to 573-673 K results in increasing of the intensity and narrowing of peaks from crystalline phases (Fig. 8.25). It should be noted that in both samples up to temperature 573 K a number of additional weak peaks are fixed which do not belong to any of known crystal phases. As a first approximation these peaks can be described within the framework of a tetragonal cell with the periods a = 0.7103 nm, c = 1.0050 nm.

Investigations of temperature dependence of electric resistance of as-cast and hydrogenated alloy states (Fig. 8.26) are confirmed by results of the XRD analysis. The occurrence of a maximum around 573 K on curve 3 is accounted for the decay of hydride phases, probably Mg_2NiH or an unknown phase, the reflections of which also disappear after 2 hr annealing at this temperature. The electric resistance jump at 783 K is connected to the decay of conducting phase Mg_2Ni and observed in both cases.

The electrochemical behavior of alloy $Mg_{80}Y_5Ni_{15}$ in as-cast and amorphous states was investigated in alkaline and neutral chlorine-containing electrolytes. Ano-

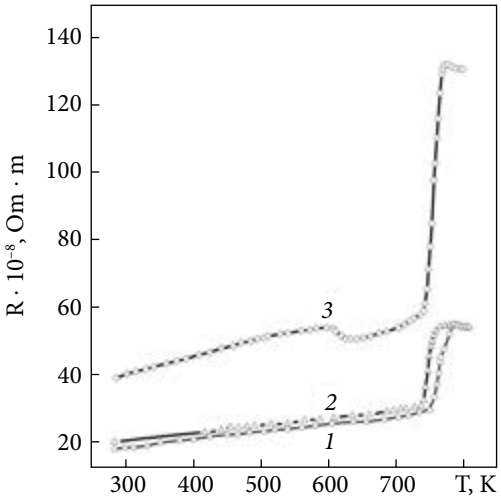

Fig. 8.26. Temperature dependences of electric resistivity of as-cast alloy $Mg_{80}Y_5Ni_{15}$ for heating (*1*), cooling (*2*) and after saturation by hydrogen (*3*)

dic and cathodic voltage-current curves ($\partial E/\partial\tau$ = 1 mV/s) are obtained in a standard three-electrode cell. As electrodes of comparison, we used mercury oxide in an alkaline medium, and in a neutral medium (sated chlorine-silver) — an auxiliary platinum electrode.

The obtained dependences testify to full identity of cathodic behavior of cast and amorphous alloys in alkaline electrolytes of both concentrations. Cathodic emission of hydrogen proceeds with a high overvoltage; the linear section slope lgi-E is equal to 0.13-0.16 V. Activation of amorphous alloy surface by cathodic reduction at five-multiple cycling potential 1.2 V in changing cathodic process parameters. The cathodic curves obtained on electrodes after activation of surface in a solution 0.5 M H_2SO_4 are characterized by essential decrease in overvoltage of hydrogen emission (by 0.3 V) and the slope of linear section 0.12 V.

Analyzing the data, it is possible to draw a conclusion that the cast alloy owing to higher structural heterogeneity and presence of grain boundaries possesses lower corrosion resistance in chloride solutions and is declined to formation of less perfect passive film in alkaline electrolytes.

Thus, according to the temperature dependence of electric resistivity and XRD researches, the effect of hydrogen on the amorphous alloy structure has been established. The analysis of phase transformations has shown the presence of an unknown phase, it is probably hydric phases which delays at 573 K. The results strongly suggest the conclusion [1] that amorphous magnesium-based alloys exhibit higher corrosion resistance than crystalline ones. The alloys of the Mg—Y—Ni system can be used in various application fields where high strength along with light weight and corrosion resistance are required.

Concluding Remarks

The physical interpretation of the criterion for the nucleation of critical (atomic-sharp) Stroch submicrocracks in the field of dislocation clusters (pile-ups) and their self-propagation according to the Griffiths mechanism becomes more obvious if we consider this athermal process from the standpoint of dislocation physics of hard-to-activate slip. However, Stroch's dislocation theory, based on the

physical principles of hard-to-activate slip, essentially considers only truly brittle fracture as a result of spontaneous propagation of nucleation defects. In this case, an incipient submicrocrack, critical to its grain, is not critical to the entire polycrystalline aggregate as a whole. Therefore, the experimental data processed in the coordinates of the Stroch T_B-lnd deviate from the linear law for the structural sensitivity of the cold brittleness temperature.

With an increase in temperature, the nucleation of microcracks in metal polycrystals turns out to be an easily activated stage of fracture, which develops according to the thermofluctuation (Orlov-Vladimirov) mechanism, and the subcritical growth of these defects precedes the macroscopical final destruction.

Developed by us together with V.I. Trefilov and I.N. Maksymchuk in the 90s, the dislocation theory of the temperature dependence of the true breaking stress describes a new schematic diagram of the quasi-brittle transition, in which the well-known scheme of the truly brittle Ioffe-Davidenkov transition is a special case.

In the first approximation, a unified activation law was established for the development of microplastic deformation at the stages preceding and accompanying fracture, i.e. equality of the activation energies of microyielding at the tips of dislocation clusters (with the e.a. for motion of primary dislocations) and at the tips of relaxing microcracks (with the e.a. for motion of screening dislocations). The theoretical results are confirmed by the activation analysis of the fracture processes in bcc and hcp metal crystals.

From the standpoint of the dislocation physics of fracture dragging, the concept of two critical difficult-to-activate fracture stages is introduced. Subcritical (hard-to-activate) growth of microcracks occurs at stress intensities that are as low as 60% of the intensity of Griffith's critical stresses. The universal nature of the relationship between plastic deformation and fracture has been substantiated at the stages (at the hard-to-activate stage) of these processes. The dislocation nature of thermally activated subcritical fracture is also emphasized.

In recent years, the theoretical and cognitive situation has changed, according to which long-term characteristics (creep, fatigue, stress relaxation), based on the control of the resistance to microyielding and associated with the problem of heat resistance, acquire paramount importance. In particular, magnesium ranks first among structural metals in terms of fatigue characteristics. A physical model of dislocation creep resistance is proposed to describe a new concept of useful long-term strength preventing the premature fracture of metal crystals.

Experiments indicate an important role of the state of boundaries in the mechanism of formation of mechanical properties of metal crystals; however, the physical nature of grain-boundary mechanisms that control the strength and fracture of materials has not yet been established or insufficiently justified. According to Armstrong and Lames Li, who estimated the density of dislocation sources at the boundaries, slip transfer may arise more likely as a result of the generation of dislocations by grain boundaries than from the action of Read-Frank dislocation sources at some distanc-

es from pile-ups. The observed types and patterns of fracture are based on the physical models of shear fracture. In this case the final fracture is a stage that is difficult-to-activate, including the subcritical propagation of stable microcracks with thermal relaxation, in particular, at viscous (relaxing) boundaries.

Finally, bcc transition metals, hcp metal crystals, and even ferritic steels undergo brittleness at low temperatures. The physical basis of embrittlement is discussed using input from other field of solid state research. We have shown that it is possible to analyze its physical nature and fracture behavior in terms of the different concepts of brittle and quasi-brittle fracture in metals and their alloys.

A theoretical treatment of the brittle fracturing is associated with the hypothesis concerning the breaking of bonds and the emission of screening dislocations in crack tips. Susceptibility to embrittlement by hydrogen may be additionally reduced when forming strong metallic bonds across the GBs and increasing electronegativity of the non-metallic elements.

Chapter

9 PHYSICAL CONCEPT OF USEFUL LONG-TERM STRENGTH

9.1. Physical Premises

Today and even more so in the future, microyield/creep in shear appears to be one of the fundamental material properties (Fig. 9.1) and key factors limiting service conditions for a new generation of metal alloys [247-250]. The increasing dynamical application of solution-hardened alloys as cost-effective structural materials stimulates extensive research to reveal the rate-controlling mechanisms responsible for improving their pre-yield (creep) resistance and long-term strength below macroscopic yield stress [250-252].

These areas of research acquire special meaning if we take into account that the characteristics of long-term strength and creep resistance make it possible to calculate the time of safe operation (resource) and outline the main tasks for solving the problem of reducing the weight of structural elements.

Nevertheless, over the years, research works under review [253-255] have been mainly performed to study the macroscopic variations in strain for a better understanding of the serrated yielding as a macroscopic phenomenon arising from the dislocation-solute interaction by a long-range diffusion-controlled mechanism. This type of discontinuous and repeated yielding commonly referred to as the Portevin-Le Chatelier (PLC) effect is attributed to dynamic strain aging (DSA), in which the isolated solute atoms interact with mobile dislocations during straining. However, up to now, there has been no evidence of a relationship between PLC banding and shear banding [255, 256]. According to Cottrell's concept [257], the DSA effect has first been associated with the dragging stress caused by the formation of dense solute atmospheres around moving edge dislocations at the same velocity of alloy constituents. DSA in solid solutions is described as the diffusion of solutes to mobile dislocations temporarily arrested at obstacles [254]. It was suggested that a PLC effect expected from solute atmosphere

dragging [258] arises from the dynamically unstable region with the jerky flow and serrated yielding subsequent to its formation. Following Cottrell's concept of jerky flow, the thermally activated process of serrated yielding should occur with the activation energy (a.e.) for solute migration towards dislocations by a diffusion-controlled mechanism. In contrast, the a.e. of the PLC effect which controls the appearance of the serrations is comparable to vacancy migration energy, while the a.e. which governs the disappearance of the phenomenon is similar to self-diffusion energy [253].

There have been several attempts [259-261] to modify the Cottrell concept and to ascertain a DSA effect and jerky flow origin but neither of them can explain quantitatively the rapidity of the hardening in metals with decreasing temperature. Besides, much of on-going theoretical models describe the related PLC and DSA effects at long-term loads close to or above macroscopic yield without respect to the observed short-range interaction of point defects [261-264]. Much as these works have contributed to the elucidation of this problem but our knowledge of it is still far from being complete. At last, there is a long-standing argument that macroscopic changes in strain are accompanied by the multiplication of dislocations so that the thermoactivation (numerical) analysis is certain to become impossible by reason of the fine structural variations. It has been until very recently that the basic assumptions of the Cottrell theory [257] have been seriously called in question [265, 266]. The disloca-

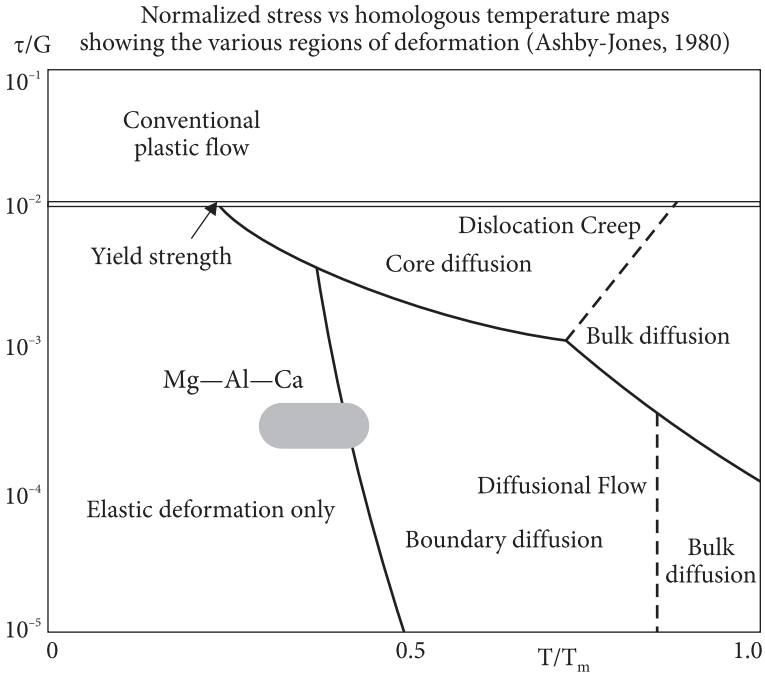

Fig. 9.1. General stress–temperature maps of microyielding mechanisms in the field of passive strain below macroscopic yield stress for metal alloy system [248]

tion atmospheres forming and the bound dislocations dragging are considered to occur during microyield at stresses $d\tau/d\upsilon D > 0$ while the PLC effect arises during plastic instability at $d\tau/d\upsilon D < 0$ [263, 267], i.e., achievement of critical dislocation rate υ_{cr} at their density appears to be critical condition for the appearance of the effect associated with discontinuous pinning of dislocations [253]. This is a starting advance as compared to the classical concept which was current two or three decades ago. Nevertheless, nearly all previous studies on the interaction between dislocations and solutes have been limited to investigations of the long-term diffusion-controlled mechanisms. With this provision, despite considerable research efforts in the past the main source of the rapid increase in solid solution strengthening is still a matter of controversy. In any case, current theories do not appear to account for the observed dislocation microyield/creep resistance leading to an increase in long-term strength. The rate of rapid solid solution strengthening in hcp metal crystals, e.g., α-Ti at elevated temperatures [268], is associated with short-range mechanism rate-controlling the thermally activated overcoming of solute interstitials by dislocations (on the first-order prism planes). The activation process of the short-range mechanism is thought to occur in the dislocation stress field at less than atomic spacings (~0.1 nm) without long-range diffusion and to enable the elastic energy of a system to be reduced. Thus, there are many questions that remain unanswered in the known approaches to dislocation dynamics problems where other mechanisms will clearly need considering.

There is a correlation between the activation energies calculated by amplitude-dependent internal friction (ADIF) and that for creep, i.e., there is an experimental correlation between metallurgical effects and physical mechanisms by which the effects are generated. First of all, there has been revealed a correlation between activation energies for creep, stress-rupture and self-diffusion for the most metallic systems [269]. This argument implies, as earlier proposed, that all the processes are correlated phenomena. Moreover, the dislocation creep and the ADIF are different aspects of the same phenomenon — microyielding, which is attributed to dislocations [270]. Al last, a.e. for climb of dislocations by self-diffusion mechanism is calculated or derived using either high-temperature background growth of internal friction or dislocation creep approach [271, 272].

Abnormal temperature dependence of shear stress (Fig. 9.2) is observed in alloys with a strong strengthening of their solid solutions due to the thermally activated dragging of mobile dislocations by interstitial/substitutional solutes (Fig. 9.3). With this provision, a serrated (repeated) yielding occurs in solid solutions in the form of the Portevin-Le Chatelier effect, caused by the appearance of dynamic instability of plastic deformation by reason of the dislocation dragging by atmospheres. This effect is confirmed by a decrease in the shear stress with increasing strain rate (insert in Fig. 9.2).

According to the model concepts [273, 274], at the peak temperature T_p (region BC? in Fig. 9.2), the dissolved substitutional atoms are carried away by mobile dislocations in the form of Cottrell atmospheres, exerting a restraining influence on their

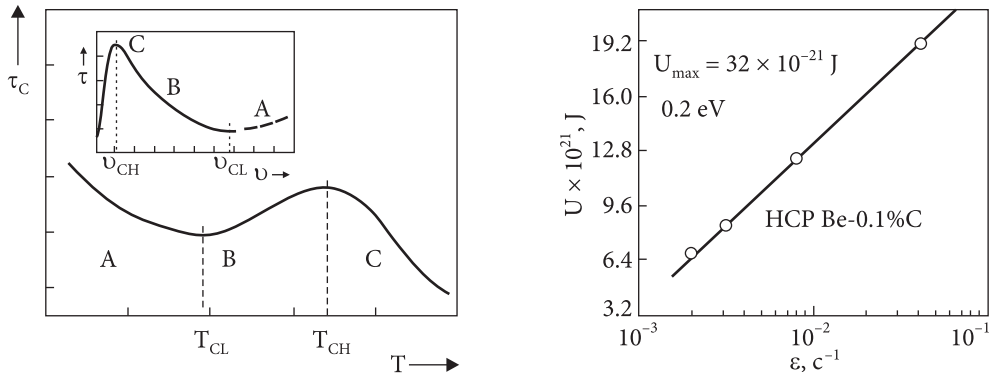

Fig. 9.2. Temperature dependence of the critical resolved shear stress, τ_C for alloys with strong effect of solid solution strengthening [258]. Insert: Dragging stress, τ by the Cottrell dislocation atmosphere as a function of the dislocation velocity, $\bar{\upsilon}_D$

Fig. 9.3. Dynamic dragging of basal dislocations by carbon Cottrell atmospheres

mobility and activity providing the maximum resistance force of this constant dislocation velocity.

Here start stress σ is determined by the Friedel law from the equation

$$U_{max} = U_B - (\sigma - \sigma_i)V^{\star}, \tag{9.1}$$

where binding energy $U_B \approx 0.20\ldots0.34$ eV; V^* is the apparent activation volume.

At temperatures $T < T_{CL}$ and $T > T_{CH}$ (Fig. 9.2), the dislocation velocities are different, but there is no retardation effect. In addition, in region B, the drop in yield (a sharp decrease in the load) is accompanied by a jump-like motion of dislocations by a short-range mechanism. However, after unblocking and releasing from the atmosphere, the dislocations go through a stage of hardening and obey the Cotrell-Bilby law $\tau^{2/3}$ for long-range diffusion of dissolved atoms [275]. Such ideas about the activation of the mechanisms of interaction between defects are contradictory, especially since a mobile dislocation in a stable state, according to the authors of [276], is always surrounded by an atmosphere of dissolved atoms. Under these data, the drag stress of dislocations increases with increasing dislocation velocity, which depends on the internal stresses of other dislocations and grain boundaries. Moreover, the slowest of them can be completely immobilized by dense atmospheres [270, 275]. Thus, the microyielding is carried out by fast dislocations, and the effect of slowing down of mobile dislocations is accompanied by the Portevin-Le Chatelier effect, i.e. repeated flow in a plastically unstable region ($d\tau/d\upsilon_D < 0$) at comparable values of the rates of diffusion and mobile dislocations. As known, the deformation of substitutional alloys is accompanied by an increase in the concentration of vacancies. The measurable effect of discontinuous flow is determined by the amplitude of the stress oscillations, i.e. the regulated serrations on smooth σ–ε curves at a constant stress rate, and thus indicates a limited activity of dislocations due to their pinning by the Cottrell mechanism with the formation of dislocation atmospheres.

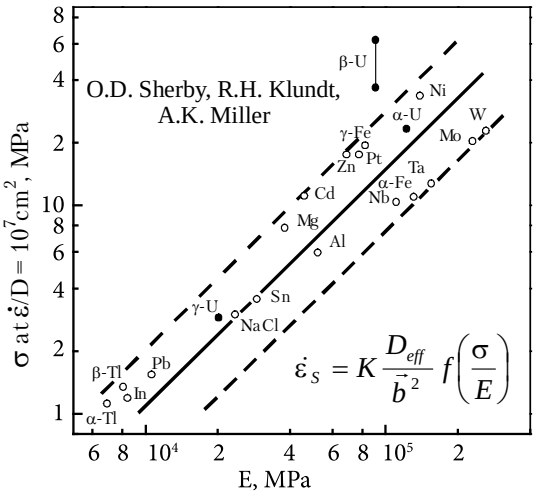

Fig. 9.4. Steady-state flow stress creep strength at a given value of $\dot{\varepsilon}_s / D_{eff}$ as a function of corresponding elastic modulus eliminating atomic mobility and creep strain rate $\dot{\varepsilon}$ as variables. (D_L is the lattice diffusion coefficient at a temperature when atom mobility is the same). Small scatter is attributed to subgrain formation in magnesium and the like [264]

According to the data of [277], alloys with solid solution hardening can be classified into two groups depending on the velocity of dislocations that control the rate of microyielding. In one of them, slip is controlled by the dragging of dislocations by solutes with the force law of the interaction of defects (n = 3) and e.a. for their including. As for either group, the creep rate is determined by the climb of dislocations at n = 5 with e.a. equal to e.a. for self-diffusion. In conditions of ascent, the dislocations cannot preserve their atmospheres. In this case, the slip of dislocations is controlled by diffusion and does not contribute to the processes of defect dragging and strengthening.

The Portevin-Le Chatelier effect is characterized by a sharp decrease in creep strain (ε), a negative creep rate (έ), and a positive temperature dependence of the flow stress [278]. On this basis, it is logical to expect that a significant increase in the resistance to microyielding (creep) and long-term strength is determined by the dynamic (stress-induced) dragging of dislocations by nonequilibrium solute atmospheres, in full accordance with the physicochemical principle of Le Chatelier-Braun's mobile equilibrium [279].

The flow stress at a given strain rate is shown to be primarily a function of the corresponding elastic modulus when comparison is made at a temperature when atom mobility is the same (Fig. 9.4). The small scatter shown is primarily attributed to other factors such as subgrain size and stacking fault energy. Following Sherby et al. [264], an equation to calculate steady state creep in the power law region ($\dot{\varepsilon} \sim \alpha \times \times \sigma^n$) can be written as

$$\dot{\varepsilon}_S = K\frac{D_{eff}}{b^2} f\left(\frac{\sigma}{E}\right), \qquad (9.2)$$

where D_{eff} is the effective diffusion coefficient, K is a material constant; b is the Burgers vector; f (σ/E) is a yet unspecified function of the modulus-compensated stress. The impressive correlation, i.e. a linear relation (on log-log scale) is observed between high temperature creep strength and corresponding elastic modulus when comparisons are made where atom mobility is the same (Fig. 9.4). Elastic modulus

influencing creep is important because the rate of dislocation slide and climb are strongly influenced by the elastic stress fields of dislocations obstructing the path of moving dislocations. A twofold increase in modulus E will increase the creep strength by a factor of two. Alloy design efforts to develop new creep resistance materials should take into consideration a method of changing elastic constant as a means of improving the creep properties in terms of the diffusion-compensated strain rate and modulus-compensated stress.

Atom mobility (diffusion coefficient) and elastic modulus are the two principal factors influencing the creep rate (at a given stress) of polycrystalline metal above 0.4 T_m. The creep rate is proportional to the effective lattice and dislocation pipe diffusion coefficient. The diffusion rate can be reduced by (a) decreasing the test temperature; (b) increasing the melting temperature using alloying; (c) forming the more resistant to diffusion (close packed) structures; (d) increasing the valence state (by solute additions). At low values of σ / E and high temperature T, the a.e. for creep it is around the a.e. for lattice self-diffusion (1.4 eV) while at high values of σ / E and low T it is around a.e. for dislocation pipe diffusion (1.05 eV) [264]. These data suggest that the concept of an effective diffusion coefficient controlling creep is valid. However, power law region is found at low values σ/E while power law breakdown is revealed at high stresses. Besides, f(σ / E) is a still unspecified function.

Diagnostics of the material condition is considered to be one of the priority avenues for the improvement of reliability and in-service life extension of structural elements and constructions. For some time past specialists of our country and abroad in their predictions of physical materials science and modern metallurgy advancement put forward the change in fracture resistance as one of the basic criteria of evaluating the quality of new promising experimental alloys and commercial materials [247, 249]. It should be noted that existing approaches to be justifiable for technical diagnostics methods and techniques are realized in terms of harmful defects (such as microcracks, etc.) which should be detected or eliminated. The tendency still persists. With that according to modern notions, the sustained (time-dependent) loading can result in macroscopic final fracture of real crystals at critical stresses that are much smaller than the macroscopic yield stress [250, 251]. The general picture which has emerged is the result of the joint effort by a large number of research groups [252, 256, 258]. In well-known theoretical approaches based on classical (Arrhenius) behavior of metal crystals there have been considered the active and fresh dislocations as well as dislocations with fixed nodes of pinning [254, 255]. Incidentally results of theoretical investigations are compared with experimental data for the short-term tests to register the tensile curves at constant speed of loading $\dot{\varepsilon}_t$. However the level of macroscopic (short-term) mechanical properties (σ_Y, σ_f, K_{1C}, etc.) produced by an active deformation under continuous tensile condition hardly could be a sufficient criterion for assessment of materials quality and proper construction modules working under long-term service conditions below the macroscopic yield stress σ_Y, when the high specific stiffness E / ρ, low moment of inertia and resistance of time-depend-

ent microplastic strain or microyield become controlling factors [252]. Therefore, in accordance with the decisions of the International Conferences (Magnesium-2003 and Euromat-2005) higher demands were announced towards structural alloys to allow for a great influence of relaxed time-dependent elastic modulus, microyield, and long-term fracture resistance. Some tentative ideas were put forward to explain the observed effects. Over the past several years, applied physics, successfully advanced in terms of dislocation theory on the whole, the new theoretical-cognitive situation has shaped, which requires development of more accurate (quantitative) criteria of improving mechanical properties. Following the situation, it is much appropriate to develop a diagnostic approach to provide for opportunity of predicting and preventing harmful and dangerous defects for safe long-term performance of machinery. Since metallurgical effects and physical mechanisms are correlated phenomena, the use of promising metal alloys in industrial applications requires a basic understanding of their properties. With that despite the well-documented evidence of validity for empirical relations, the physical nature of dislocation dragging needed to provide microyield resistance during mechanical relaxation and to increase long-term strength is still unclear especially for higher temperatures of thermal microstructure resistance. On the basis of such approach, investigations of the dislocation (quantitative) criteria of long-term strength suitable for assessment of long-term service becomes a physical promise for further search in the field theory. Following the data [247, 250, 258, 259] the increasing dynamical application of light metal alloys as cost-efficient structural materials has stimulated extensive research to reveal the rate-controlling mechanisms responsible for improving their creep resistance and long-term strength.

For the last twenty years and so in dislocation strength physics the current models concern largely the structural sensitivity and structure-related (power-law creep) properties which are controlled by long-range athermal barriers on the distances no less 30-40 nm. In these cases, such a structural analysis and suitable empirical treatment ignore the necessity of allowing for the short-range interactions between defects which assist the microyield to operate at interatomic distances of about 0.1 nm and to contribute to a long-term strength. In spite of a great deal of research effort expending in the past decade to understand the physical aspects of long-term strength, no information is available yet about the contribution of short-range dislocation-solute interaction to time-dependent strain effects including the localized microyield (creep) resistance. Furthermore, none of the researchers has been able, as yet, to develop analytical theory based on models and quantitative criteria permitting numerical thermoactivation analysis to quantify the activation parameters of long-term testing in terms of lattice-defect physics.

The present work was undertaken to advance the physical knowledge of the dislocation dynamics and defect kinetics in metal crystals under long-term stresses below the macroscopic yield stress. The main purpose of the present study is to develop a physical theory for useful, preventing the premature fracture, long-term strength

based on a dislocation model of microyield resistance and to give the idea of physical origin of microyield resistance and useful long-term strength (ULTS).

9.2. Processing of Experimental Data

Describing steady-state creep strain rate relates to the well known experimental equation

$$\dot{\varepsilon} \cong \sigma^n \exp\left(\frac{U^* - \tau^* \cdot V^*}{kT}\right), \tag{9.3}$$

where n is the apparent stress exponent, i.e., $n = d\ln\dot{\varepsilon}/d\ln\sigma$. The exponent n is approximately constant over several orders of magnitude in strain rate [272, 277]. The power law $\dot{\varepsilon} \cong \sigma^n$ by its nature characterizes the athermal contribution of the force unactivated interaction of dislocations and the stage of deformation (dislocation) strengthening at long-range distances (around 300 interatomic distances). It is accepted that the strain hardening coefficient $n \sim 1$ for diffusion mechanism; $n \sim 3$ for mechanism of non-basal sliding; $n \sim 5$ for dislocation climb mechanism.

A typical creep curve is presented in Fig. 9.5. Kinetic curve-isotherm of dislocation creep is one of the characteristics of the long-term strength of metal crystals.

Constant structure steady-state creep tests are normally performed to evaluate the activation energy (a.e.) and stress exponent (n or m*) for creep rate and time to rupture (Figs. 9.5 and 9.6). When an alloy is subjected to an applied stress which is lower than that required for immediate fracture ($\sigma \sim 0.7\sigma_f$) (Fig. 9.7), it gradually deforms plastically over time to give an allowable creep deformation. The creep deformation rapidly reaches a steady-state (secondary) condition I, the creep strain rate of which, $\dot{\varepsilon}$, remains constant over time (Fig. 9.6).

In tests for long-term (time-dependent) strength of heat-resistant alloys, the deformation capacity of material or true plasticity (uniform deformation) is assessed by the relation $D = \ln[1 / (1 - \psi)]$ with the relative transverse constriction ψ.

Unfortunately, due to necking, the main ductility is formed by concentrated deformation under conditions where the ultimate strength slightly exceeds the yield strength.

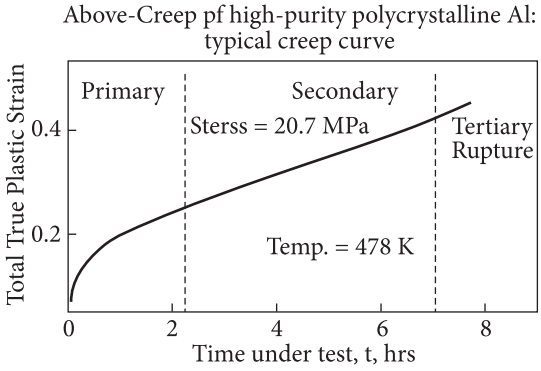

Fig. 9.5. Creep curve at 478 K for high-purity polycrystalline Al [280]: *1* — initial creep; *2* — steady-state creep; *3* — tertiary creep

9.3. Theoretical Background of Novel Approach

A possibility for solute atoms to interact with dislocations if the time is too short to activate the long-range diffusion-controlled mechanism was first suggested by Snoek [281] and analyzed by Schoeck [282]. The most striking advance in the understanding of the rapid interaction of individual solute atoms with individual mobile dislocations was achieved by Fleisher [283]. Nevertheless, despite considerable research efforts in the past, in any event, current theories fail to explain with the present evidence the observed rapid kinetics of hardening in solid solutions as well as the deviation of the fundamental equation for short-range order strengthening from experimental data. Some good work is underway along these lines, but original diffusion rate equations can lead to serious discrepancies since the kinetic parameters are no longer consistent with the values taken from the diffusion data. The correctness of such an interpretation is based on several grounds. Firstly, a dragging effect is related to the direct solute-dislocation interaction with binding energy E_b rather than to the mobility D / kT by the Einstein relation, i.e. diffusion drift velocity [263]. Unlike the theoretical aspects of macroscopic changes in diffusivity D describing in the form of diffusion drift macroscopic flows of substance, the binding energy E_b gives a result of short-range interaction at atomic distances. Secondly, since the diffusion is not necessary constituent or integral part of high-temperature creep [284], it is difficult yet to calculate the diffusion process numerically due to the vacancy mechanism which needs clarifying many yet unknown quantities. Only a few theoretical approaches to this problem have been advanced in the literature. To illustrate, according to Sherby with co-workers [264], the atom mobility and elastic modulus-compensated stress σ / E are believed to be two principal factors influencing the creep strain rate $\dot{\varepsilon}$ at a given stress. Nevertheless, although at the same diffusion mobility of solutes, an excellent correlation between $\dot{\varepsilon}$ and σ/E has been observed

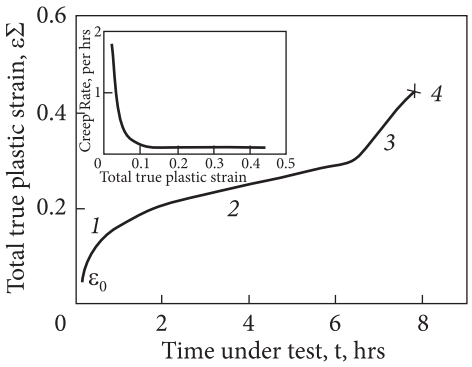

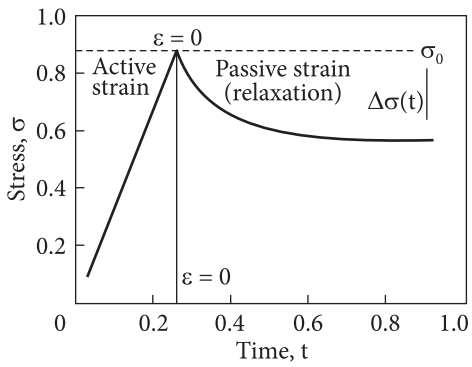

Fig. 9.6. Change in strain rate during creep for high-purity polycrystalline Al [280]

Fig. 9.7. Dislocation relaxation of elastic stresses during microyielding below macroscopic yield stress for solid solution of metal crystals (typical curve) [279]

in many metal alloy systems, in the suggested rate-equations [264], the relevant to this problem term $f(\sigma / E)$ is yet an unspecified function.

Unlike the Cottrell atmosphere, the ordered Snoek atmosphere is formed in the effective stress field of dislocations by a short-range ordering mechanism [282, 285], which causes the dragging force for dislocations moving against the energy gradient depending upon their velocity. Since Snoek short-range ordering precedes the Cottrell mechanism of the solute atmosphere formation, the subcritical value of dislocation velocity υ_D is attained for high-purity α-Fe crystals at $\dot{\varepsilon}$ of 10^{-8} s^{-1} even at r.t. [282]. This result is in reasonable agreement with the calculated values of υ_D for high-purity magnesium alloy crystals under examination at the same dislocation density [252]. The Snoek-type dislocation atmosphere is believed to be formed as a complex consisting of an excess vacancy and a solute element. The idea for a local loss of the crystalline lattice stability near linear defects was first advanced by Clapp [284] for vacancy clusters and complexes of point defects having elastic distortions around them. With that, the achievement of critical parameters for the store internal energy, e.g., the local critical density of dislocations during time-dependent strain is thought to be caused by deformation instability, first of all, by reason of loss of shear stability of a dislocated crystalline lattice and localized shear below the macroscopic yield stress. These effects are accompanied by decreasing microyield/creep resistance and long-term strength.

The process of dislocation sliding at the early stages of plastic deformation has a fundamental significance for further deformation behavior of metal alloy polycrystals at higher strains (beyond the yield stress) as it often determines the subsequent microstructural evolution and, as a result, the mechanical properties of polycrystals during strengthening (Fig. 9.8). It has been agreed that elastic fields of internal stresses attributed by dimension or modulus misfit, interaction with dislocation cores as well as by local ordering a structure, contribute to processes of dragging the mobile dislocations and result in solid solution strengthening [259, 260].

The results of thermoactivated analysis presented in Table 9.1 are mainly based on the experimental data obtained in the course of tensile (short-term) tests.

Table 9.1. **The special features of current thermoactivation analysis**

Current theoretical approaches	Creep testing	Rate-controlling equations	References and notes
Short-range properties (active deformations, free dislocations) of pure metals	Continuous tension, $\sigma \neq$ const	$\dot{\varepsilon} = NAb\upsilon_0 \exp\left(-\frac{\Delta G - \tau_f \cdot V}{k_b T}\right)$	Arrhenius type equation [286]
Dislocations with fixed pinning nodes of the network		$\dot{\varepsilon} = 2\upsilon \exp\left(-\frac{\Delta G}{kT}\right) \cdot sh\left(\frac{\sigma_f \cdot V}{kT}\right)$	[287, 288]
Long-term strength	Kinetic time-dependent isotherms, σ = const	$\dot{\varepsilon} = \sigma^n \cdot \exp(U / kT)$	Current approach (Brown-Ashby type empirical equation) [248]

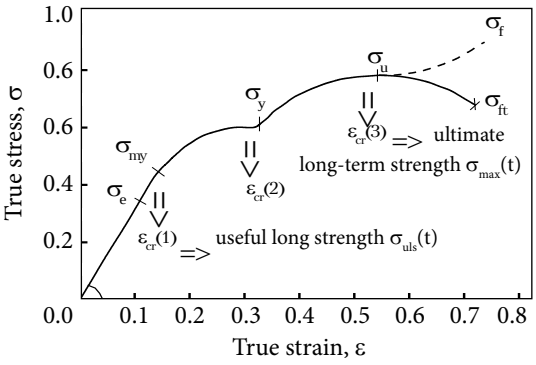

Fig. 9.8. Schematic representation for defining the critical points (bifurcations) on the stress-strain curve with different structural-energetic levels of active deformation

The scheme in Fig. 9.8 unites the short-term and long-term (time-dependent) characteristics of metal crystals including: (i) ε_{cr} (*1*) is the ultimate transition (below the macroscopic yield stress) from uniform to localized (concentrated) strain during time-dependent microyielding in the pre-yield region; (ii) ε_{cr} (*2*) is the ultimate transition from upper macroscopic yield stress to multiplying of dislocations strengthening on set; (iii) ε_{cr} (*3*) is the ultimate transition from axial to combined (triaxial) tension before fracture.

Plastic deformation is a simple method of introducing dislocations and point defects. Their concentration is larger than that required for thermodynamical equilibrium. In the absence of impurities, temperature dependence of macroscopic yield point is associated with high rate of work hardening in the microstrain range, i.e., between inelastic limit and macroscopic yield point.

Fundamental effect of interstitial solutes such as, e.g., hydrogen on the macroscopic softening and possible embrittlement relates to the increment of dislocation mobility considered in terms of hydrogen-enhanced localized plasticity mechanism [255]. Owing to these calculations, hydrogen enhances dislocation mobility (softening) due to the reduction of energy barrier or due to shielding effect associated with the reduction of the interaction between edge dislocations. Nevertheless, shear localization and concentrated sliding may lead to premature fracture when internal shear energy is quite enough to nucleate atomically a sharp submicrocrack providing its spontaneous propagation by a cleavage mechanism. Thus, the susceptibility of the polycrystalline materials to shear strain localization can be a main factor which limits their tensile ductility, long-term strength and fatigue resistance [247, 249, 260]. Furthermore, it should be considered as a criterion for assessment of useful, preventing fracture and long-term strength. Luders slip bands propagate through crystal and cause a yield phenomenon due to geometric softening of crystals in certain orientations [261]. The submicroscopic regions in which the active glide planes are concentrated should be considered as glide zones or a glide bands when the zones intersect the crystal surface. This means that between two adjusted zones the crystal is deformed elastically (for one set of active glide planes).

For sufficient low rates of loading, plastic strain produced by nanoindentation of amorphous metal becomes completely discretized, i.e., localized in a series of isolated events of yielding [262]. A transition from discrete to continuous yielding is observed with increasing the loading rate. The suitable transition from localized to homogene-

ous plasticity seems to associate with the existence of self-organized narrow shear bands which individually undergo local shear transformations.

Plastic deformation is localized in definite soft regions resulting in high stress concentration, for example, in grain boundary triple points [263]. Strain localization observed at the age hardening conditions is associated with formation of a two-phase field as a result of structural decomposition of a supersaturated solid solution due to the continuous precipitation of dispersoids coherent with the matrix and the appearance of GB zones free of precipitates (PFZs). In this case many of age hardenable metal alloys suffer problems associated with low ductility as well as inadequate fracture toughness caused by strain localization. In order to overcome this problem, alloy development efforts should be concentrated on the addition of dispersoids to refine the grain size and to minimize strain location. In particular, in the USA the attempts are being undertaken to develop the Al—Li—Mn and Al—Cu—Li alloys with fine scale-grained structure and minimal strain localization.

As well known, a continuous theory describes well only long-range elastic strain of a dislocation for length scale beyond a few lattice spacings because of problems with singularity near the dislocation cores, whereas in strength physics the long-range interactions responsible for structure-sensitive properties are independent of strain rate $\dot{\varepsilon}(T, \tau^*)$. Consequently, they represent the long-range internal stress field at any given structure and relate to the assessment of athermal stress τ_G proportional to the shear modulus G(T) resulting from crystal lattice resistance. There has been a great deal of interest in describing accurately the short-range interactions between dislocations and the structural defects, density of which exceeds that of thermally equilibrium by several orders of magnitude [258]. Seeing that thermally activated processes of dislocation microyield/creep and the dislocation relaxation are controlled the same mechanism responsible for the strain rate $\dot{\varepsilon}$, dislocation relaxation should be considered as a creep at variable stress. This allows one to unite activation (numerical) analysis of available data for testing a validity of the existing and proposed models.

9.3.1. Thermal Activation of Short-Range Mechanisms

A thermally activated process in terms of the temperature dependence of the reaction rate constant should obey the well known Arrhenius Equation:

$$\dot{\varepsilon} = A \exp(-Q/RT), \tag{9.4}$$

where A is the frequency factor, assumed to be a constant; Q is the a.e.; T is the absolute temperature, R is the gas constant.

It is now generally accepted in many cases that deformation of metals is governed thermally activated processes. For single controlling mechanism for deformation, according to [290] the strain rate is given by

$$\dot{\varepsilon} = A \exp(-G / kT) = A\exp(S / R) \exp(-H / RT), \tag{9.5}$$

where A is effectively the product of the rate at which attempts to overcome the barrier are made and the strain produced by a successful fluctuation is obtained; G = = H-TS is the Gibbs free energy of activation; H is the enthalpy of activation commonly termed as "activation energy"; S is the entropy of activation. A, G, H and S generally depend upon stress, temperature and structure. H can be derived from experimental data only if certain simplifying assumptions are made.

Eq. (9.5) describes low temperature deformation, and consequently the a.e. is a function of the effective stress $\tau^* = \sigma = \sigma - \sigma_G$, where σ_G is the long-range internal stress at any given structure and is proportional to the shear modulus G. Besides, the a.e. H (T, τ^*) may also be a direct function of temperature.

In discussing results of previous measurements of the steady-state creep rate [291], it is suggested that they *were* interpretable in terms of the hypothesis relating the creep rate of solid solutions to the coefficient of lattice self-diffusion, e.g., in magnesium (~135 kJ · mol^{-1}) and diffusion of Al solute atoms in Mg (~143 kJ · mol^{-1}). A question arises whether their applied (shear) stress can be identified with the macroscopic yield stress responsible for the multiplication of dislocations. It is anticipated that there will be a breakdown in power law behavior at high stress levels. It cannot be answered from available data. There is no good agreement among reported values for other hcp metals where the stress is considered as a parameter characteristic of the material. The temperature dependence is also uncertain. Only thermally activated processes are considered in our study. The basic equation used in the literature for a quantitative estimation of the reversible change in flow stress reduces to the following form [292]:

$$\dot{\varepsilon} = \dot{\varepsilon}_0 \exp\left[-U(\tau^*) / kT\right], \tag{9.6}$$

where $\dot{\varepsilon}$ is the strain rate; $\dot{\varepsilon}_0$ is the rate constant equal to $\rho Ab\nu$; ρ is the density of points of activation per cm^3; A is the area covered by the dislocation loop in one activated jump; b is the strength of the dislocation; v is the dislocation jump frequency; U is the a.e. of the process which is dependent only on the effective applied shear stress τ^* at the obstacle, i.e.,

$$\tau^* = \tau - \tau_i \tag{9.7}$$

and

$$U(\tau^*) = U_0 - \tau^* \cdot V. \tag{9.8}$$

In this case, the work done by the effective stress τ^* on the dislocation loop decreases the a.e. U_0 linearly. Besides, the activation volume (a.v.) V is assumed to be a function of the stress. If the thermal obstacle depends on thermal component τ^* of applied stress, the a.v. should be determined

$$V = -dU / d\tau^* \cong \text{const}. \tag{9.9}$$

For small τ^* the stress dependence is described by the following assumption

$$V = V_0 (1 - \alpha\tau^*), \tag{9.10}$$

where V_o is the a.v. in the unstressed state.

The τ^* contribution disappears at temperatures above T_0. The forest dislocations do not provide the necessary obstacles to dislocation movement. The two remaining

possibilities are: (a) jogs in screw dislocations; (b) impurity atoms or their clusters. According to Hahn-Rosenfield approximation [293],

$$\tau^{\star} = 1/2\ (\sigma - \sigma_0) \approx 1/2\ \mathrm{K}d^{-1/2}, \tag{9.11}$$

where σ is the applied stress; σ_0 is the stress required to move dislocations. The maximum value of $\tau^{\star} = 1/2\ (\sigma_Y - \sigma_0)$ where σ_Y is the yield stress; $\mathrm{K}d^{-1/2}$ is the interstitial depinning parameter; d is the average grain diameter. However, this treatment is now open to question.

Irregular (serrated) curves σ-ε caused by the impurity interstitials diffusion towards mobile dislocations appear in changing macroscopic strain rate $\dot{\varepsilon}$. Besides, it is accepted that the critical $\dot{\varepsilon}_{cr}$ is proportional to the rate of lattice diffusion available for interstitials by a long-range Cottrell-Bilby mechanism:

$$\dot{\varepsilon}_{cr} = \mathrm{C} \cdot \mathrm{D} / kT, \tag{9.12}$$

where C is the constant depending on the dislocation density and physical properties of crystalline lattice; D is the diffusion coefficient.

9.4. Physical Theory of Useful Long-Term Strength

Since there is little information in the literature on the theoretical dislocation long-term strength of solution-hardened alloys below the macroscopic yield stresses (Table 9.1), it therefore seems appropriate to indicate the possibility for continued work along these lines. The main purpose of the present study is to develop a physical theory for useful long-term strength excluding the premature fracturing of solution-hardened alloys below the macroscopic yield stress. The work is nicely motivated by first considering the theoretical microyield/creep resistance. The research aims at a better understanding of the basic principles of dislocation creep resistance responsible for the increase in the long-term strength of metal crystals. To provide further in-depth insight into the physical origin of dragging effects, the on-going study focuses on the theoretical analysis of the dislocation calculations based on physical modeling and activation of the most probable (short-range) mechanisms in order to identify them in the so-called multi-level solute defect structure enriched with substitutional solutes and strain-produced excess vacancies. Besides, such an approach evaluates the current understanding of relationships between microstructural parameters, dislocation pre-yield resistance and long-term properties of some promising metal alloy systems. From this view, it would be appropriate to clarify the subject of the pinning effects in rapid-hardening alloys and to reveal short-range rate-controlling mechanisms acting in the selected metal alloy systems. This is likewise the intention of the study to subject the measurements to a complete analysis.

In this study, a new physical theory of useful long-term strength (ULTS) based on a dislocation model of microyield/creep resistance adequately describes two rate-

controlling dragging mechanisms responsible for the rapid (short-range) dislocation pinning by solute/vacancy-containing atmospheres with the a.e. equal to that for excess vacancy migration at $\tau^* \cdot V^* > kT$ and the serrated (repeated) dislocation pinning at $\tau^* \cdot V^* << kT$ with the thermal a.e. for the excess vacancy/solute complexes migration reduced to a double binding energy. Besides, the theory enables the full-scale (numerical) thermoactivation analysis of theoretical parameters in the kinetic rate equations. The present approach is found to be adequate for the representation of the stress relaxation including large values of time. The ULTS theory has been advanced to formulate the quantitative (numerical) criterion of ULTS preventing a premature fracture in a wide range of temperatures and stresses.

Our strength design relates to the edge dislocation theory for microyielding where the dislocation sources operate prior to macroscopic yield stress. There has been a great deal of interest in accurately describing the short-range interactions between dislocations and excess vacancies, the density of which exceeds that of thermally equilibrium ones by several orders of magnitude [285]. Since thermally activated processes of dislocation microyield/creep and dislocation relaxation are controlled by the same mechanism responsible for the strain rate, the dislocation relaxation will be considered as a creep at variable stress. A numerical thermoactivation analysis permits the rate-controlling mechanisms to be revealed and allows a decision to be made concerning the thermal (short-range) obstacles. In this regard, the thermal stability of structure is a main condition for the current determination of the a.v. V^* and consequently for clearing up the rate-controlling mechanism. This enables the numerical termoactivation analysis of available data to be carried out using an unchanged dislocation structure for modeling and testing as well as permits a single activation process to be extracted from a more complicated pattern. Based on these simulations, analytical rate-equations can be derived in order to reveal the rate-controlling dragging mechanisms responsible for the increase in dislocation creep resistance and long-term strength. Constant structure steady-state creep tests are performed to evaluate the a.e. and activation volume (a.v.) for selected solution-hardened alloys in the most promising hcp Mg—Al—Ca system and to compare them with those in the fcc Fe—Ni—C system under the loading conditions of interest in this study.

A forefront of research activity in material science is the continued effort to recognize and develop materials that can supply creep resistance and long-term strength as well as specific stiffness at as high as possible temperatures. To be useful, the potential of high-temperature material must satisfy certain physical and chemical criteria many of them are highly sensitive to resulting internal structure. This will require overcoming a set of difficult problems related to dislocation dynamics and kinetics of structural defects during straining.

Alloying was quite successful in the past in developing magnesium alloys for high temperature service aerospace applications. This is evident in comparing the "maximum usefulness temperature" of various metals. A measure of maximum usefulness temperature is arbitrarily defined as the temperature at which the alloy can

withstand a stress of ~69 MPa (or 10.00 psi) for 100 hr without fracturing [247, 294]. Table 9.2 lists some of the metals (best possible alloys) with respect to this criterion. It may be used to evaluate the effectiveness of an alloying element for pure metals. For magnesium, it should be pointed out that the best alloys (mainly RE containing and, in the past, thorium containing) can compete very well with aluminum alloys.

The Reed-Hill criterion is believed to destine for the qualitative assessment of alloying effectiveness.

9.4.1. Dislocation Model of Microyield/Creep Resistance

For an ideal (defect-free) structure, the condition for the transition to elastic instability of the crystal lattice follows from the relation

$$\Delta\tau^{\star} = U_e / \dot{\varepsilon}, \tag{9.13}$$

where U_e is the limiting elastic energy.

For the so-called defect structure, this ratio is converted to the form [295]

$$\Delta\tau^{\star} \cdot t^{\star} \cong E_D \cdot \rho_D / \dot{\varepsilon}. \tag{9.14}$$

For isothermal time-dependent strain $t^{\star} \cdot \dot{\varepsilon} \equiv$ const, and, hence, for so called defect structure eq. (9.13) is converted to the form [295].

The elastic energy of crystal lattice distortions corresponds in hcp Mg to 0.03 eV and 0.003 eV in dilute substitutional solid solutions (Cu—Si).

The classical Pieirls model assumes that the formation of double kinks controls the mobility of dislocations. In accordance with the model of plastic deformation proposed by Seeger [296], the rate of plastic shear deformation is controlled by the intersection mechanism of forest dislocations and is characterized by a simple linear dependence of the activation energy on the effective stress at dislocations

$$\dot{\gamma} = N\Delta F b \nu_o \exp\left(-\frac{U_0 - \nu\tau^{*}}{kT}\right). \tag{9.15}$$

Here N is the number of obstacles for sliding dislocations (per 1 cm^3); ΔF is the area swept after activation, ν_0 is the attempt frequency for a dislocation; U_0 is the a.e.

Table 9.2. **Maximum usefulness temperatures of the metals for potential alloys [294]**

Base metal	Melting point, K	Maximum usefulness temperature, K	Absolute melting point, %
Mg	923	606	67
Al	933	581	60
Ti	1977	922	46
Fe (martensitic)	1811	1005	56
Fe (austenitic)	1811	1144	63
Ni	1728	1244	78

for intersections (forest dislocations); a.v. V = *bdl*; shear stress $\tau = \tau^* + \tau_G$; τ_S is the effective stress on dislocations; τ_G is the internal stress field. The predominantly exponential function $\dot{\gamma}(\tau^*)$ dominates over any other dependence.

Following Seeger [296], sliding dislocations (on the slip plane) overcome internal long-range stress fields τ_G (from other dislocations and their clusters), as well as short-range (localized) thermally activated obstacles at lattice distances (τ^*).

We have to admit that the models based on recombination and splitting of screw dislocations by Pieirls, Dorn-Rajnak and Seeger are not suitable for explaining the results obtained. Our results are in the best agreement with models based on the mobility of dislocations controlled by the thermally activated interaction of dislocations with dissolved atoms.

The most aspect of dislocation dynamics is the velocity-stress relation. In the model of plastic deformation proposed by Johnston and Gilman [297] the dependence of dislocation velocity $\bar{\upsilon}_D$ is given by

$$\bar{\upsilon}_D = \frac{\tau^* \cdot b}{B} \tag{9.16}$$

and

$$\bar{\upsilon}_D = B(\tau^*)^{m^*}. \tag{9.17}$$

Then

$$\dot{\gamma} = \rho_{mD}\, b\bar{\upsilon} = \rho_n b(\nu l) \exp\left(-\frac{\Delta G(\tau^*)}{kT}\right), \tag{9.18}$$

where $\dot{\gamma} = 0.73\,\dot{\varepsilon} \Rightarrow \dot{\varepsilon} \cong 1.4\,\dot{\gamma}$

Under the data [288], $\bar{\upsilon}_D$ can be calculated from expression

$$\bar{\upsilon}_D = 2\rho_D \cdot \nu \exp\left(-\frac{U}{kT}\right) \sinh\left[\frac{\tau^* \cdot V^*}{kT}\right] \tag{9.19}$$

The logarithm of $\bar{\upsilon}_D$ is used for convenience. In this case, the partial derivative is given by

$$\frac{\partial \ln \bar{\upsilon}_D}{\partial \tau^*}\Big|_T = \frac{m^*}{\tau^*}, \tag{9.20}$$

where stress exponent m* is equal to m at zero plastic strain. Then for macroscopic deformation the equation is given in [26]

$$m = \frac{\partial(\ln \dot{\varepsilon})}{\partial(\ln \sigma)} = m^* - \frac{\partial(\ln \rho_D)}{\partial(\ln \sigma)}. \tag{9.21}$$

According to the Taylor-Orowan equation, the dislocation velocity is proportional to the strain rate

$$\dot{\varepsilon} = \alpha b \rho_m \bar{\upsilon}_D, \tag{9.22}$$

where α is a geometric factor; ρ_m is the density of mobile dislocations; $\bar{\upsilon}_D$ is the average velocity of the mobile dislocations; b is the Burgers vector.

In the context, the present method is suitable to calculate the breaking process of a dislocation from its atmosphere when the dislocation velocity υ_D is accelerated. The dragging stress τ_d effects on the dislocation by its solute atmosphere. There is a critical value of υ_{cr} at which τ_d increases with increasing υ_D. Below υ_{cr} it decreases contrarily for $\upsilon_D > \upsilon_{cr}$. Under the data by Schoeck [282], critical value of υ_D is attained in a high-purity α-Fe at strain rate $\dot{\varepsilon}$ of 10^{-8} s^{-1} even at r.t. These experimental data are in agreement with the calculated values of $\dot{\varepsilon}$ and υ_D for high-purity magnesium alloy crystals with a dislocation density of $10^8/cm^2$ [298]. To attain higher values of strain rate (10^{-10} … 10^{-12} s^{-1}), it is necessary to expand the range of uniform strain.

The kinetic rate equations give rise to reveal the most probable drag mechanisms responsible for increase in microyield/creep resistance to improve the dislocation long-term strength of multi-level defect structure in solution hardened alloys, e.g. in the hcp Mg—Al—Ca and Mg—Al—Ca—Ti systems. The model proposed was tested on selected hcp and fcc metal alloys in the Mg—Al—Ca and Fe—Ni—C systems, respectively. The quaternary hcp Mg—Al—Ca—Ti system is the most promising of the investigated systems for application in automobile industry. Theoretical considerations related to jerky flow and serrated yielding are consistent with experimental data as well.

The reliability/validity of the model is confirmed by reliable experimental data. In contrast to the models of Dotsenko and Sherby with colleagues [262, 279], which cannot be verified by numerical methods and compared with experiment, our approach makes it possible to perform a full-scale (numerical) thermoactivation analysis using four activation parameters that are critical for the selection of control mechanisms.

It is widely accepted that strengthening mechanisms in physics of crystals remain controversial. The proposed dislocation theory based on the model of microyield resistance provides a means for accurate prediction of the time for uniform plastic strain preventing a fracture by localized shear. Such an alternative approach is therefore believed to be based on the resistance to dislocations motion rather than straining in the pre-yield region. The theoretical expressions derived are found to be in good agreement with the experimental results. Unlike the theory of serrated yielding by McCormick [261] connecting the distinction between the temporal and spatial instability, i.e. a loss of homogeneity of strain with the effect periodic oscillation of the stress relaxation, we consider the onset of the process at the earliest stage of jump-like movement of dislocations. Therefore, the thermal stability of structure is the main condition for correct determination of the thermal activation energy and effective activation volume, and consequently for clearing up rate-controlling mechanisms.

Unlike the Cottrell concept of solute atmosphere, our model, like the new model by Jingli and Sia-Nemat-Nasser [299] has been proposed to be used for describing interaction between moving dislocations and mobile point defects at the earliest stage of formation of core dislocation atmospheres.

The extent of smooth plastic strain preceding (by short-range mechanism) jerky flow has been evaluated in the $\ln\dot{\varepsilon}$ – 1/T coordinates by Wilson and Russel [300]. Besides, measured effect of serrated yielding is defined by stress oscillation amplitude, i.e., the height

of regulated serrations on the smooth σ-ε curves at $\dot{\varepsilon}$ = const. In the case, the jump-like movement of dislocations is sure to occur by a short-range mechanism as well.

The alternative approach is based on the existence of a dislocation microyield / creep resistance at stresses below the macroscopic yield stress. It seems to be a powerful framework to describe dislocation dynamics in metal systems with interacting structural defects and to account for short-range deviations from classical (Arrhenius) behavior in alloys with destroyed long-range order. The dislocation model of microyield/ creep resistance leads to the rate equations which can be applied best to metal alloy crystals containing paired defects in solid solutions over saturated by excess vacancies.

A constitutive model has been proposed to describe the mechanisms based on various types of material transport including lattice/GBs diffusion and dislocation plastic flow occurring during microyield/creep resistance below the macroscopic yield stress [298]. Shear localization may lead to the premature sliding when internal energy of shear is quite enough to nucleate an atomically sharp submicrocrack (see Chapter 8). From this point of view, the model of dislocation creep resistance considers the conditions that prevent a premature fracturing. They are as follows: a) dislocation structure is believed to remain invariable microyielding below the macroscopic yield stress. In this case, multiplication of dislocations is thus excluded from consideration; b) a transition to dislocation climb at higher stresses when dislocations break the way from their solute atmospheres is not considered either. As the relaxation can only be the result of plastic deformation it seems evident that even at stresses well below temperature of quasibrittleness some dislocation movement takes place and does proceed.

9.4.2. Newly Developed Analytical Rate Equations

A rate-controlling model for the resistance to microyield/creep strain permits the short-range dragging effects to be recognized. The higher probability $W_{1,2}$ of the successful thermally activated jump for a dislocation in the force direction during passive dislocation relaxation or dislocation creep resistance can be calculated from the relation

$$\bar{\upsilon}_D = \alpha \bar{\lambda} (W_1 - W_2) = \alpha \cdot \bar{\lambda} \cdot \nu, \tag{9.23}$$

where $\bar{\upsilon}_D$ is the average dislocation velocity during dragging; α is the proportional coefficient dependent on the obstacle nature and dislocation parameters; ν is the attempt frequency of the successful dislocation jumps ($\upsilon = 10^{10}$ s^{-1}); $\bar{\lambda}$ is the activation distance between short-range obstacles where a dislocation is delayed during the waiting time $t_e \cong \nu^{-1} \exp (U^* / kT)$. Here the settled lifetime for an atom in the field of minimal potential energy is given by

$$\tau = \tau_0 \exp (U^* / kT), \tag{9.24}$$

where τ_0 is a frequency factor dependent on lowering the potential barrier; U^* is the energy of thermal activation needed for overcoming a thermally activated obstacle by a short-range mechanism.

The relation (9.26) for an atom in the field of dislocation is different from well-known relation (2) by the amount of the binding energy E_b

$$\tau = \tau_0 \exp (U^* + E_b / kT), \tag{9.25}$$

where E_b is the binding energy of a solute atom (a pair defect or an associate) with a dislocation.

Some manipulation of equations (9.23) and (9.26) yields a dragging effect, if a single activation process controls the microyield/creep resistance and the number of places where the strain per successful fluctuation can take place. The rigorous description of the stress-induced dragging effect in terms of dislocation physics leads to two types of differential kinetic rate equations which represent related phenomena such as dislocation dragging during incipient pre-yielding and pre-yield (dislocation) relaxation.

In the $\tau^* \cdot V^* > kT$ pre-yield range there is no breaking off dislocations from the atmosphere due to strong binding energy E_b between them. By reason of enough pinning of dislocations, the height of potential barrier U^* increases by the value of E_b, i.e., becomes $U^* + E_b$ with a fraction of line defects proportional to exp (E_b / kT). Then for describing thermally activated dynamical dragging by the dislocation atmospheres, the equation for the shear microstrain rate can be reduced to the following form

$$\dot{\varepsilon}_m = 2\bar{\rho}_D (b\bar{\lambda}\nu) \exp \left(-\frac{U^* + E_b - \tau^* \cdot V^*}{kT} \right), \tag{9.26}$$

where $\dot{\varepsilon}_0$ is equated to $2\bar{\rho}_D (b\bar{\lambda}\nu)$; $\bar{\rho}_D$ is the average mobile dislocation atmosphere density; b is the Burgers vector; $\bar{\upsilon}_D = \bar{\lambda} \cdot \nu$ is the velocity of dislocation atmosphere dragging; $V^* = L_C b^2$ is the dislocation activation nanovolume; L_C is the activation length of mobile dislocation nanosegment between mobile nodes of pinning; $\tau^*(\dot{\varepsilon}, T)$ is the thermal component of applied stress.

At higher stresses and elevated temperatures ($\tau^* \cdot V^* > kT$), the dislocation creep resistance for a given magnesium alloy in the Mg—Al—Ca system is found to be essentially governed by a rate-controlling mechanism operating with an a.e. of 0.80 ± ± 0.02 eV or 1.28×10^{-19}J for excess vacancy migration in the stress field of dislocation atmospheres (Fig. 9.9). In addition, the value is in agreement with those estimated for some alloy crystals [301-303] and constitutes roughly one-third of that for self-diffusion ($2.08 \ldots 2.24 \times 10^{-19}$J). Snoek's locking [281] is believed to be a stress-induced ordering mechanism operating in these alloys with a high rapidity due to the migration of excess vacancies to form solutes atmosphere around moving dislocations. Strong pinning of dislocations should be expected when locally bound matrix atoms find themselves part of a passing dislocation [304]. Aging is as caused by the vacancy movement around immobile solutes and, as a sequence, by the rotation of solute-excess vacancy pairs to form segregations around moving dislocations [258]. The rate equation (9.7) confirms the rapid nature of short-range interaction between dislocations and solutes in solid solutions enriched with excess vacancies. According to the analyti-

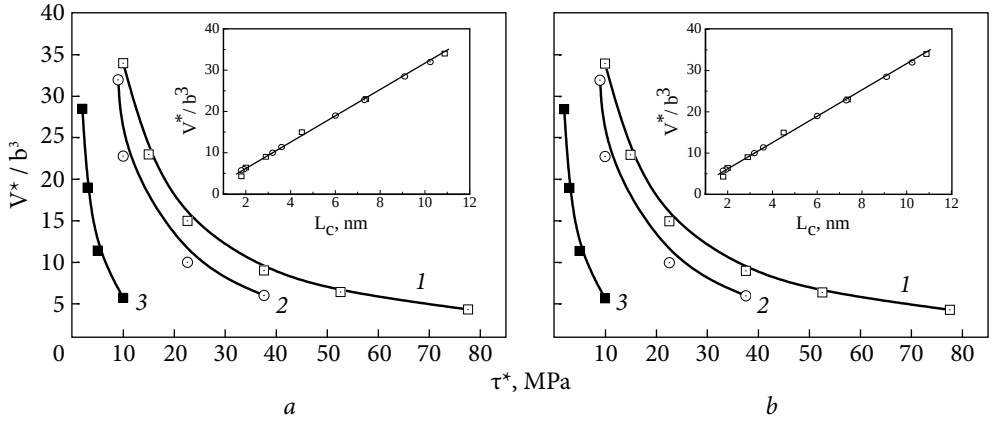

Fig. 9.9. Activation volume V* as a function of applied stress thermal component τ* (*a*) for a dislocated solid solution in hcp Mg—12.5Al—1.3Ca system (*1*, *2*) compared with that of the fcc Fe–32Ni—0.1C system (*3*): *1* — dynamical dragging of mobile dislocations by solute–excess vacancy atmospheres with the a.e. of 0.8 eV at 423 K evaluated by Eq. (9.26); *2* — discontinuous (repeated) pinning of dislocations in early stage of jerky flow conditions with the a.e. of 0.5 eV at 523K evaluated by Eq. (9.27); *3* — dynamical dragging of dislocation by solute atmospheres under jerky flow for Fe—32Ni—0.12C alloy [23]. Insert: variations of activation volume V* with the activation length of mobile dislocation nanosegment L_C (*b*). Here $\upsilon \cong 10^{10}$ Hz; $b = 3.2 \times 10^{-10}$ m; $E_b \cong 0.3$ eV $kT = 0.036$ eV at 423 K and 0.045 eV at 523 K; $\dot{\varepsilon} = 10.24\ s^{-1}$; $\overline{\rho}_D \cong 10^{11}$ / m². $L_C \cong 6.0$ nm (for $V^* = 20\ b^3$), $L_C = 10.8$ nm (for $V^* = 36\ b^3$)

cal estimations of rapid kinetics in the $\tau^* \cdot V^* > kT$ range, the dislocation atmospheres are certain to generate strain-produced excess vacancies in magnesium alloys.

In the temperature range corresponding to the manifestation of the Portevin-Le Chatelier effect, i.e. under the conditions $\tau^* \cdot V^* << kT$, dislocations jerkily interact with the Cottrell atmosphere causing their jump-like motion with limiting the mobility in solid solutions and abrupt flow of microyield/creep.

In this case, studies of the dislocation-impurity interaction, incl. the formation of atmospheres from dissolved atoms (alloying elements) around mobile dislocations, as well as the Portevin-Le Chatelier effect caused by the inhibition of dislocations by atmospheres at the stage of dynamic strain aging are of great interest for improving the long-term strength of heat-resistant alloys.

In the $\tau^* \cdot V^* < kT$ pre-yield range, i.e., at lower stresses and higher temperatures, in crystals containing solute atoms of low pinning strength [301], the binding energy E_b makes possible the jump-like movement of dislocation typical for the onset of jerky flow by strain to the first jerk. Therefore, the energylevel of ground state for the potential barrier U might be split up into two energy level substates with the increased a.e. of $U^* + E_b > U$ and a fraction proportional to $\exp(E_b / kT)$ for the dislocations to be pinned as well as with the decreased a.e. of $(U^* - E_b) < U$ and a fraction proportional to $\exp(-E_b / kT)$ for the mobile dislocations to be depinned. In other words, the height of potential barrier U changes by the magnitude of E_b, i.e., fluctu-

ates within ± E_b. Hence, exp (E_b / kT) reproduces the attractive part of potential energy, while exp (–E_b / kT) does its repulsive part, e.g. detachment of dislocation from isolated atoms, paired defects or their complexes.

The motion of dislocation in its slip plane is, in general, a discontinuous process [254], so that there are reasons to believe that the short-range dislocation dragging in the onset of jerky flow is expected to be consistent with the well-known Le Chatelier — Braun physical-chemical principle of mobile equilibrium shifting. Then the dynamical dragging by the repeated pinning of dislocations will satisfy the equation for microstrain rate where kT is the thermal energy of a solvent lattice. The original idea for dislocation analysis is that $\tau^* \cdot V^* < kT$ at the thermally activated energetic level is split into two sublevels of the short-range potential obstacle due to the discontinuous (repeated, positive and negative) increment of internal stress $\pm\Delta\tau^*$. The latter arises out due to the two dragging forces needed for the thermally activated depinning and repeated thermally activated pinning of dislocations [305] to satisfy Eq. 9.27 and the Le Chatelier–Braun principle.

$$\dot{\varepsilon}_m = 2\bar{\rho}_D (b\bar{\lambda}\nu) \exp\left\{\left(-\frac{U^* - \tau^* \cdot V^*}{kT}\right) \cdot \sinh\left(\frac{E_b}{kT}\right)\right\} \tag{9.27}$$

From the physical point of view, over the $\tau^* \cdot V^* < kT$ range splitting of the energetic potential means its growth $U^* + E_b$ at $\bar{\upsilon}_D < \bar{\upsilon}_{cr}$ and its decrease $U^* - E_b$ at $\bar{\upsilon}_D < \bar{\upsilon}_{cr}$ [258, 267]. At $\tau^* \cdot v^* << kT$ the dislocation movement in the stress field is additionally dragged by $\dot{\varepsilon}_0 \cdot \sinh (E_b / kT)$ term which is not dependent on τ^* and t. Thus, the binding energy E_b is one of the important parameters controlling dislocation creep resistance in the solid solution systems with a mobile defect structure.

At lower stresses and higher temperatures ($\tau^* \cdot V^* << kT$) the dislocation creep resistance is assumed to be controlled by a dragging mechanism operating with a.e. of 0.50 ± 0.02 eV or 0.85×10^{-19}J for migration of excess vacancy/solute paired complexes in the stress field around mobile dislocations (Fig. 9.10). Its reliable value yielded by the solution of Eq. (9.27) is significantly lower than that for self-diffusion (1.35 eV) and that for isolated vacancy formation (0.8 eV) and diffusion of any alloying element, i.e. another most probable dislocation mechanism is rate-controlling.

The relaxation spectra of internal friction in hcp magnesium alloy indicates that solute atoms are expected to be paired with excess (strain-produced) vacancies, which strongly attract them producing large (tetragonal) lattice distortions [252]. With this provision, the vacancies remain in the solution being associated with the solutes. The solute-excess vacancy complexes are actually elastic dipoles with different binding energy. Published data and experimental evidence reported in the periodic literature [303, 305] strongly support our identification of the dragging mechanisms proposed. For example, under the data by Rose and Glever [301], the a.e. has been estimated as the a.e. for vacancy migration (approximately 0.9 eV in the fcc Fe—Ni—C system). However, the theoretical values of the a.e. for the vacancy migration (0.65 eV for FCC Al) are essentially higher than those obtained from experimental data in the Al—Mg

system (0.45 eV) due to the formation of a vacancy/solute complexes with binding energy $E_b \sim 0.2$ eV [303].

As soon as an atmosphere consisting of the complexes is formed around a dislocation, the activation short-range ordering mechanism in the stress field of dislocations enables dragging effect to be enhanced much more compared to single solute atoms. Taking into account that the delocking of pinned dislocations and the motion of depinned dislocations are controlled by the same thermally activated mechanism [281, 282], the thermally activated slip dragging by the excess vacancy/-solute complexes having a high rapidity of the short-range pinning is believed to be the most likely rate-controlling dragging mechanism responsible for the pre-yield resistance.

According to the kinetics of DSA [301], the observed rapid jerky flow on the serrated stress-strain curves can be explained on the basis of the stress-induced short-range ordering mechanism [281, 282] rather than Cottrell elastic approximation or Suzuki chemical dislocation pinning mechanism. The rate equation (9.27) for repeated pinning of dislocations evaluates the extent of smoothening curves of plastic strain at the initial stage upon occurring the first plastic deformation jerks in preceding jerky flow. As a matter of fact, jump-like (discontinuous, repeated) pinning of moving dislocations is likely to facilitate rather than to cause the proceeding of jerky flow or DSA. By reason of its general sense, the magnitude of initial jerks in the form of stress drag increment and abrupt fall in load can be regarded as indicative of the stress differential between the breakdown stress at which dislocations escape from their atmospheres and the stress at which they move easily through the lattice before being pinned again [262]. It is reasonable to assume that in the $\tau^* \cdot V^* << kT$ range the dragging effects under examination are typical for the onset of jerky flow by strain to the first deformation jerk the jerkiness effect relates to mesoscopic phenomena occurring below the macroscopic yield stress, our system of newly developed rate equations can be expected to give a good result for describing the onset of jerky flow. Unlike the Cottrell concept for the solute atmospheres to activate beyond dislocation cores, a new model by Jingli Cheng and Sia Nemat—Nasser [299] has been developed for describing interaction between moving dislocations and mobile point defects with the formation of dislocation core atmospheres.

9.4.3. Numerical Analysis of Stress (Dislocation) Relaxation

Stress relaxation is determined by the following relation [279]:

$$\frac{d\tau^*}{dt} = -K_M \dot{\varepsilon}_0, \tag{9.28}$$

where t is the relaxation time for applied stress; K_M is the elastic rigidity in tension, constant at any test conditions. For the thermally activated dislocation mechanisms of dragging by solute atmospheres at $\tau^* \cdot V^* > kT$, the parameters of relaxation can be

determined as follows. By combining Eqs. (9.23), (9.26), and (9.28), one can obtain the differential relaxation equation (9.29) of the form

$$-\frac{d\tau^*}{dt} = K_M \dot{\varepsilon}_0 \exp\left(-\frac{U^* + E_b - \tau^* \cdot V^*}{kT}\right), \tag{9.29}$$

We omit here some intermediate computations involving the mathematical treatment of Eq. (9.29) by combined operations of separating the variables and setting up a relevant integral equation to meet conditions $\tau^*(t) = \tau^*_{max}$ at t = 0 and $\tau^*(t) = \tau_G$ (final time of relaxation). Then this relaxation equation was integrated and the logarithm was found. After some manipulation, the expression obtained was re-arranged into the equation of dislocation relaxation which can be described by the expression

$$\Delta\tau^* \cdot V^* = (U^* + E_b) - kT \ln(\beta \cdot t), \tag{9.30}$$

where $\beta = \frac{K_M \dot{\varepsilon}_0 V^*}{kT}$; $\dot{\varepsilon}_0 = 2\bar{\rho}_D \cdot b\bar{\lambda}\nu$; $V^* = L_C b^2$; $L_C = 2r/C_0 \cdot \exp(-E_b / kT)$; L_C is the length of dislocation nanosegment between mobile nodes of pinning; r is the radius of curvature for a dislocation ($r = Gb / \tau^*$); C_0 is the initial concentration of solutes.

Taking the antilogarithm of Eq. (9.30), we get the modified equation for the relaxation time

$$t = \frac{1}{\beta}\exp\left(\frac{U^* + E_b - \Delta\tau^* \cdot V^*}{kT}\right). \tag{9.31}$$

In going from thermal to athermal component τ_G (at $\tau^* \cong 0$), Eq. (9.30) of stress relaxation reduces to the second-kind equation of relaxation

$$U^* + E_b = kT \cdot \ln(\beta t_G). \tag{9.32}$$

By analogy with the above-mentioned procedure, the stress relaxation equations can also be deduced for the discontinuous (repeated) pinning of dislocations in the $\tau^* \cdot V^* << kT$ range. For the case, the course of calculations is almost the same as that used for $\tau^* \cdot V^* > kT$. Then the dynamic dragging of mobile dislocations is described by the relation

$$\Delta\tau^* V^* = U^* - kT \ln(\beta t) - \ln\left(\dot{\varepsilon}_0 \frac{E_b}{kT}\right). \tag{9.33}$$

The present stress relaxation analysis is found to fit generally semi-logarithmic relationships obtained previously by Dotsenko [279] and Sargent [298]. Nevertheless, numerical analysis of the equations in the early models of relaxation [279, 298, 299] is absent which makes it difficult to examine their reliability and justification in their analytical solutions. At the same time, all the terms in our newly developed equations of stress (dislocation) relaxation have physical meaning.

A pronounced solid solution strengthening effect is attributed to the large long-range stress fields due to the athermal stresses τ_G, while the relative strength of the short-range obstacles produced by solutes is not so obvious. The energy of dislocation, when unaided, is insufficient to get over a tetragonal (paired) defect as

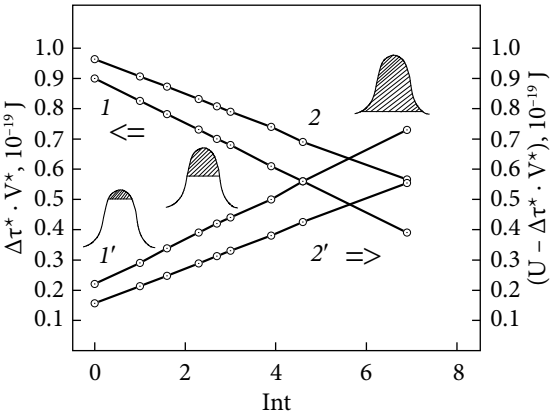

Fig. 9.10. Numerical analysis of the dislocation relaxation for hcp Mg—12.5Al—1.3Ca—0.1Ti alloy with separating the time-dependent contributions of the power $\Delta\tau^* \cdot V^*$, (*1* and *2*) and thermal $U - \Delta\tau^* \cdot V^*$, (*1′* and *2′*) components to the net activation energy for overcoming a short-range potential obstacle by a dislocation at 523 K (*1* and *1′*) using Eq. (9.33) and 423 K (*2* and *2′*) using Eq. (9.30) in nanovolumes $36b^3$ and $20b^3$, respectively. Here U is the full free (available) energy for thermally activated overcoming the short-range obstacle; $K_M = 4 \times 10^6$ J / m^2; G ≅ 17 GPa; μ = 0.35

a short-range barrier. The extra energy to overcome it must be supplied by thermal fluctuations. The present theory enables the net a.e. needed for overcoming the height of short-range barrier potential to be resolved into two time-dependent constituents associated with the partial a.e. for power (elastic) interaction between alloy ingredients, and the partial a.e. for long-term thermal vibrations of a lattice (Fig. 9.10). The observed logarithmic plot of stress (dislocation) relaxation at each temperature is certain to consist of the two linear segments separating the data into thermal and power (elastic) energetic contributions. The two energy-sharing components acting at atomic distances (~0.1 nm) may be exemplified by two energy terms: (i) the first term $\Delta\tau^* \cdot V^*$ is due to the work done by the drag stress component τ^* and (ii) the second term $U - \Delta\tau^* \cdot V^*$ in Eqs. (9.26) and (9.27) should be considered as energy of thermal vibrations for a crystal lattice. Thermal energy as a driving force equal to the shaded area on the diagram will move dislocation at a short-range distance by the energy of atomic thermal fluctuations linked to the crystal lattice vibrations. The idea of separating the time-dependent contributions concerning the thermal and mechanical breaking of dislocations is consistent with the concept of thermally activated dislocation depinning by Saul and Bauer [305]. Numerical analysis of the dislocation relaxation following Eqs. (9.30) and (9.33) shows that the power component τ^* decreases linearly with loading time and tries to be as high as the athermal component τ_G (at $\tau^* \Rightarrow 0$), while the energy when supplied to the short-range obstacle by long-term thermal fluctuations, on the contrary, increases linearly with time up to the value of resistance to the dislocation motion. The ordering forces exerted by a stress field around dislocation are opposed by the disordering forces of lattice thermal vibrations [301], the thermal energy of which tends to randomize a solute distribution. The growing contribution of thermal activation energy (Fig. 9.10) signifies the increase in the time-dependent strain produced by efficient thermal fluctuations. This theoretical calculation is a good test for the physical sense of the model proposed.

9.4.4. Dislocation (Quantitative) Criterion of ULTS

Unlike the usefulness temperature criterion introduced by Reed-Hill [294] for best possible alloys, we set forward a new (dislocation) quantitative criterion to evaluate the effectiveness of alloying elements (AE) for pure metals. The novel resulting microstructure formed dynamically during creep without fracturing leads to useful long-term creep strength and thus the both microcrack nucleation and propagation are eliminated. Accordingly, a measure of maximum useful long-term (creep) strength is arbitrary defined as the stress at which a metal alloy system can provide critical time with the requirement that time-dependent (creep) strain under uniaxial tension occurs without necking to eliminate metastable structural and phase transformations development.

Principles of effective alloying have been quite successful in the past in developing alloys for high-temperature aerospace applications. Following the concept [247, 294], a measure of "maximum usefulness temperature" during straining is arbitrarily defined as the temperature at which the alloy can withstand the stress of about 69 MPa for 100 hr without fracturing. This qualitative criterion allows evaluating the alloy-efficiency for pure metals. Over the past several years, in applied physics successfully advanced in terms of preceding dislocation theory, on the whole, a new theoretical-cognitive situation has shaped which requires the development of more accurate (quantitative) criteria for further improving physicomechanical properties of metal crystals below the macroscopic yield stress [249, 256, 265, 307]. Following the situation, it is much appropriate to develop a diagnostic approach that provides for the opportunity of predicting and preventing harmful and dangerous defects in solution-hardened metal alloys for their safe long-term performance in machinery. Some manipulation yields energy balance for the steady-state of dislocation creep $\varepsilon_s = \dot{\varepsilon} \cdot t$ and for the characteristic time t^* to achieve a measured quantity of useful (uniform) strain before a localized shear, i.e. $(\Delta\tau^* \cdot t^* = E_D \bar{\rho}_D / \dot{\varepsilon}_s)$, and $t^* = E_D / \Delta\tau^* b \bar{\upsilon}_D$. This makes it possible to combine the equations for the linear energy of dislocation $E_D = [Gb^2 \ln(r / r_0)] / [4\pi (1 - \mu)]$ and Eq. (9.23) for $\bar{\upsilon}_D$ with Eq. (9.26) for strain rate $\dot{\varepsilon}_m$ at $\tau^* \cdot V^* > kT$. For the case, the general ultimate transition to the elastic instability should be replaced with a newly developed dislocation criterion of instability for a defect structure as

$$\Delta\tau^* t^* < \left[\frac{\alpha G b \ell n(r/b)}{8\pi(1-\mu)\upsilon_{cr}}\right] \exp\left(\frac{U^* + E_b - V^*\tau^*}{kT}\right); \tag{9.34}$$

$$\Delta\tau^* t^* < \left[\frac{\alpha G b^2 \ell n(r/b)\bar{\rho}_{cr}}{8\pi(1-\mu)\dot{\varepsilon}_{cr}}\right] \exp\left(\frac{U^* + E_b - V^*\tau^*}{kT}\right). \tag{9.35}$$

With this provision, at $T \to T_s^*$ and $\tau^* \to 0$

$$\Delta\tau^* \cdot t^* < \frac{\alpha G b \ell n(r/b)}{8\pi(1-\mu)\cdot \upsilon_{cr}} \cdot \exp\frac{U + E_b}{kT_s}. \qquad (9.36)$$

Here $\Delta\tau^*$ is the threshold dragging stress, under which transition from uniform strain to localized shear is the most likely to occur at $\overline{\upsilon}_D(\tau^*, T) > \overline{\upsilon}_{cr}$; α — Schmidt factor; μ — Poisson's ratio; Gb — the elastic shear stability (rigidity) of crystalline lattice; $\alpha Gb^2 = f(\tau^*, T)$ — the linear tension (excess energy) of a dislocation with an a.e. of about 0.2 Gb^3; $\upsilon_{cr}(T, \tau^*) = \lambda \cdot \nu$ — the threshold dislocation velocity corresponding to the measured strain rate $\dot{\varepsilon}$; ρ_{cr} — the density of dislocations; $\dot{\varepsilon}_{cr}$ — the threshold strain rate; T_{us} — the useful temperature by Read-Hill et al. [247]; T_s — the entropic temperature, under which thermal fluctuation are capable to overcome a short-range potential obstacle without stress ($\tau^* = 0$).

According to the criterion, the threshold stress of dragging is related directly to the elastic shear stability of crystal lattice, strain rate, density, excess energy and velocity of dislocations as well as to strength of interatomic bonds (through E/G modulus). Interconnection of the subcritical parameters ($\dot{\varepsilon}$, $\overline{\upsilon}_D$, $\overline{\rho}_D$) with various rigidity, i.e. the shear stability of crystal lattice (αG) and linear tension (excess energy) of dislocations (αGb^2) enables one to predict the attainment of the dislocation strength at short-range distances. The analytical equations with the same structure furnish a consistent criterion of the useful long-term strength connecting the threshold stress $\Delta\tau^*$ with properties of the crystalline lattice, elastic fields of mobile dislocations as well as with the activation parameters that reveal the nature of the most probable rate-controlling mechanism. Besides, the energy (dislocation, quantitative) criterion describes a subcritical transition from the uniform elongation through a uniformly dense dislocation distribution to the concentrated slipping and localized shear responsible for the loss of the shear elastic stability for crystal lattice and, as a sequence, microplastic (dislocation) instability.

At low strain rates, dragging stress in steady-state increases almost linearly with the dislocation velocity $\overline{\upsilon}_D$ only at the early stage of the solute atmosphere formation. According to the inequality (9.34) at $d\tau^* / d\overline{\upsilon}_D < 0$ the dragging stress is expected to increase with decreasing the dislocation velocity $\overline{\upsilon}_D$, when it exceeds the critical value υ_{cr} by a Cottrell solute diffusion-controlled (long-term) mechanism [258, 306]. The delay time is inversely proportional to the dislocation velocity ($\sim 1 / \upsilon_D$) and has a maximum at a critical dislocation velocity υ_D and hence for strain rate $\dot{\varepsilon}_0$ according to Eqs. (9.34) and (9.35). In this case, after passing a maximum at υ_{cr} and $\overline{\rho}_D$ = const due to a partial unlocking of rapid dislocations, the system in the stable state turns into dynamically unstable plasticity state in the region with rapid dislocation sliding. The theoretical results obtained for dislocation velocities by inequality (9.34) fitting a measured strain rate $\dot{\varepsilon} < \varepsilon_{cr}$ by inequality (9.35) are in good agreement with modeling study and theoretical calculation of the critical dragging maximum observed by Yoshinaga and Morozumi [258].

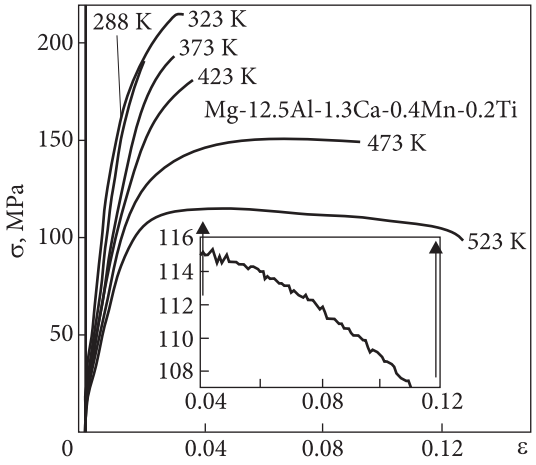

Fig. 9.11. Serrated yielding in magnesium alloys of the Mg-Al-Ca, Ti system. Insert: an example of enlarged serrations on the stress — strain curve

By assuming that the density of mobile dislocations remains unchanged invariable during creep tests, the rate equation for rapid-hardening crystals thermally activated at $\tau^* \cdot V^* > kT$ by a short-range mechanism can be expected to be given by

$$\dot{\gamma} \cong \left(\frac{\tau - \tau_b}{G} \right)^{m^*} \cdot \dot{\gamma}_0 \cdot \exp\left[\frac{U^*(\tau^*) + E_b - \tau^* \cdot V^*}{kT} \right], \tag{9.37}$$

where $\dot{\gamma}$ is the shear strain rate; τ^* is the effective shear stress; $m^* = \frac{\partial \ln \dot{\gamma}}{\partial \ln \tau^*}$; τ_b is the back stress in $\tau^* = \tau - \tau_b$; E_b is the binding energy; U^* is the effective energy of thermal activation; V^* is the activation (dislocation) volume.

For heat-resistant alloys (at $\tau^* \cdot V^* << kT$), the rate equation (9.36) should be modified to the following form

$$\dot{\gamma} \cong \left(\frac{\tau - \tau_b}{G} \right)^{m^*} \cdot \dot{\gamma}_0 \left[\frac{U^*(\tau^*) - \tau^* \cdot V^*}{} \cdot sh \frac{E_b}{kT} \right]. \tag{9.38}$$

For macroplastic deformation, the rate equation (at $\tau^* \cdot V^* > kT$) is given by

$$\dot{\varepsilon} = \left(\frac{\sigma}{E} \right)^m \cdot \dot{\varepsilon}_0 \exp\left[\frac{U^* + E_b - \tau^* \cdot V^*}{kT} \right] \tag{9.39}$$

where σ is a constant; $m = \frac{\partial \ln \dot{\varepsilon}}{\partial \ln \sigma} = f(\dot{\varepsilon})$; σ_G is the athermal component of applied stress:

$$m = \frac{\sigma}{\sigma^*} \cdot m^* \quad \text{or} \quad \frac{m}{\sigma} = \frac{m^*}{\sigma^*} \tag{9.40}$$

$$\sigma_G = \sigma - \sigma^* = \sigma(m - m^*)/m \tag{9.41}$$

9.5. Evaluation of Results

Specimens for creep testing were machined from ingots of as-cast crystalline materials. Before testing the specimens of 25.4 mm gauge length and 3 mm in diameter were annealed at different temperatures. Then they were tested at a

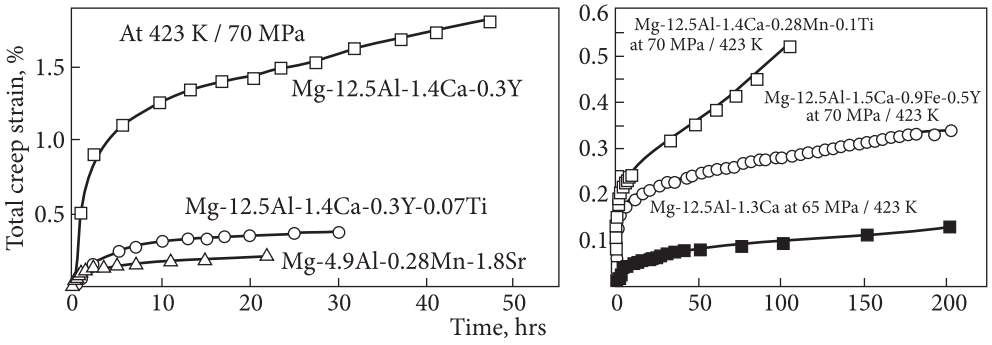

Fig. 9.12. Creep strength of magnesium alloys in the Mg—Al—Ca, X systems at higher temperatures and stresses

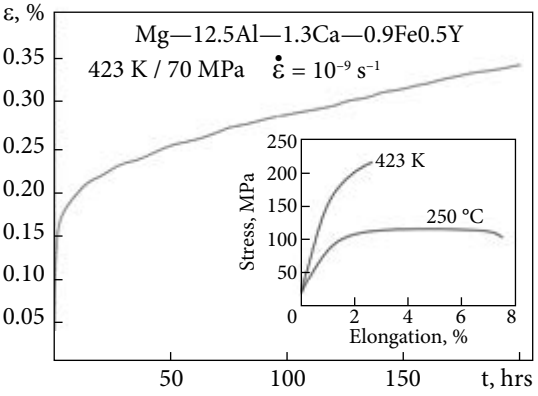

Fig. 9.13. Tensile creep curve of the model magnesium alloy, containing Fe and Y and satisfying technical assignment. Insert: short-range properties of the alloy

constant loading rate in a machine type NICIMP until the load-elongation curve σ-ε was reached in the pre-yield region. The serrated (irregular) curve σ-ε manifests the instability of plastic deformation occurring at higher temperatures and low strain rates έ with a.e. equal to the a.e. for interstitials diffusion while regular (smooth)

Table. 9.3. **Micromechanical properties of conventional and newly developed experimental magnesium alloys at 423 K**

Alloy systems	σ_Y, MPa at r.t.	Critical creep parameters				Creep strain rate $\dot{\varepsilon}_m$, s^{-1}
		Creep strength, MPa	Load timing t*, hr		Allowable creep strain ε_Σ, %	
			Exp.	Theory		
Mg—9Al—1Zn	170	35	200	185	1.93-2.50	≥10^{-7}
AZ91D (Dow Chemical Corp., USA)		64	50-100		Fracture	
AZ91D—1.3Ca	220	64	50	70	0.1	10^{-8}
Mg—12.5Al—1.3Ca	157	65	160-180	220	0.17-0.24	≥10^{-8}
Mg—12.5Al—1.3Ca—0.1Ti	180	70-80	150-200	277	0.2-0.4	≥10^{-9}

Table abbreviations: r.t. (room temperature); hr (hours); Exp. (experiment).

Table. 9.4. **Dislocation creep resistance and long-term strength of several RE-bearing magnesium alloys at 423 K**

Alloy composition, mass%	Creep strain rate, $\dot{\varepsilon}_s$, s^{-1}	Creep strength, MPa	t, hr	Required creep strain, ε, %
AZ91D (Dow Chemical Corp., USA)	10^{-7}	35 64	200 100*	2.50 Fracture*
Mg—12.5Al—1.3Ca	10^{-8}	64	200	0.35
Mg—12.5Al—1.4Ca-0.3Y	10^{-8}	70	48	0.40
Mg—12.5Al—1.3Ca—0.5Y—0.9Fe	4×10^{-9}	70	200	0.24
Mg—12.5Al—1.3Ca—0.3Y—0.5Fe	1×10^{-9}	70		0.21
Mg—12.5Al—1.3Ca—0.3Y—0.2Gd	1×10^{-9}	70	200	0.40

curve indicates its stabilization at higher $\dot{\varepsilon}$ to operate over the temperature range considered (Fig. 9.11).

The validity of the present dislocation criterion was experimentally verified using a strain-rate change test which has been described in detail elsewhere [302, 305]. The creep rates $\dot{\varepsilon}$ calculated with Eqs. (9.26) and (9.27) and compared with experimental data are summarized in Tables 9.3 and 9.4. It is noteworthy that the contribution of the short-range thermally activated mechanisms to the dislocation microyield/creep resistance is thought to be enhanced with slowing strain rate (dislocation velocity). The newly developed magnesium alloy in the hcp Mg—Al—Ca system is found to have the best combination of short-term and long-term properties compared with commercial alloy AZ91D.

The best result of improving creep resistance and useful long-term strength (without fracture) for magnesium alloys of Mg—Al—Ca, Ti system: $\dot{\varepsilon} \sim 10^{-9}$-$10^{-10}$ s^{-1} at $\boldsymbol{\varepsilon}_{\Sigma} = 0.2\ldots0.4\%$ and 70-80 MPa for 170-200 hr.

Concluding Remarks

A new first-order physical theory of useful long-term strength (ULTS) based on a dislocation model creep resistance and analytical rate equations has been advanced for describing dynamic (time-dependent) microyield/creep resistance responsible for a potentially useful uniform strain preventing a premature fracturing in rapid-hardening crystals. The concept of ULTS relates to the rapid strengthening in terms of the short-range dislocation mechanisms with the thermal activation that provides overcoming thermal obstacles such as solutes and their clusters at lattice distances. Such a diagnostic approach enables the short-range rate-controlling mechanisms to be identified for stressed crystals in terms of the thermoactivation numerical analysis of rapid strengthening using constant structure steady-state creep tests and dislocation relaxation techniques. A more accurate (dislocation) criterion of useful long-term strength is formulated for solution-hardened alloys. The criterion

could be used for the quantitative assessment of the short-range dragging effects preventing a transition from the structurally uniform sliding to the localized shear strain which governs a premature fracture of metal crystals.

The basic conclusions can be drawn from the results obtained and be stated as follows:

• A physical theory of useful long-term strength based on mathematical modeling of the thermally activated (short-range) resistance to dislocation movement and on the Le Chatelier-Braun's physical-chemical principle of shifting the mobile equilibrium has been evolved for adequate describing solid solutions enriched with excess vacancies and their rapid-hardened alloys with hcp and fcc structure. The theory furnishes an explanation of the above dragging effects at the early stage of their formation including the onset of atom ordering and describes the direct interaction between defects and solutes involving the jump-like movement of dislocations with increasing temperature. This makes it possible to separate the time-dependent contributions of power and thermal components to the net activation energy needed for overcoming the short-range obstacles. It is shown that in case of the examined mechanism, the thermal component of stress tends to the athermal component over relaxation time, and energy, applied to the obstacles by the thermofluctuation mechanism, increases linearly up to the potential barrier for dislocation motion.

• Judging the results obtained, at least two underlying types of the dislocation dragging mechanisms were identified by using new model-based analytical rate equations when evaluating the activation energies intrinsic to creep-resistant alloys in the hcp Mg—Al—Ca, Ti and fcc Fe—Ni—C systems. At higher stresses and elevated temperatures ($\tau^* \cdot V^* > kT$), the movement of glide dislocations is most likely to occur jointly with their solute atmospheres so that for the case, the dynamic dragging of microyielding is provided by the resistance of mobile dislocation atmospheres with the a.e. for vacancy migration. At lower stresses and higher temperatures ($\tau^* \cdot V^* << << kT$) the dynamical dragging of creep strain is believed to be due to the constant (discontinuous, repeated) interactions between mobile free dislocations and solutes by a jump-like mechanism. For the case, of a peculiar interest is an enhanced effect of dragging at the early stage of the jerky flow. It may be appropriate for improving the long-term strength of high-temperature alloys.

• Over the time-dependent microyield/creep range, theoretical simulations and experimental evidence predict a potentially useful measure of long-term strength formed in the stress fields of mobile dislocations. The quantitative (dislocation) criterion of useful long-term strength is proposed for quantitative assessment of the alloying effectiveness as to the best possible metal alloy crystals with minimum strain location. The criterion describes material conditions that prevent a transition from uniform strain to localized shear leading to the elastic and microplastic instability of a dislocated crystal lattice. The present theory suggests that the transition state might be considered as being a physical restriction in dislocation long-term strength. In the context, a threshold dragging stress as a function of uniform strain resistance is di-

rectly related to elastic (shear) stability of a dislocated crystalline lattice, line tension (excess energy), velocity and density of sliding dislocations.

• The findings obtained are in reasonable agreement with strain rate change and stress relaxation measurements, test findings and isothermal observations, which are suggestive of the cluster-like complexes. In summary, therefore, the present theoretical study will hopefully stimulate further experimental investigations which could lend a better understanding of the mechanisms responsible for the formation of dislocation creep resistance and long-term strength in metal crystals. The present newly developed diagnostic approach is believed to provide a physical basis not only for a proper understanding of dragging effects but also for alloy development. The proposed method can be expected to be appropriate in describing the creep behavior of metal alloy systems as a starting point for further development of the rapid-hardening and creep-resistant alloys with a minimum of localized shear effects.

Within the framework of mesoscopic (structure-energetic) concept of localized shear, a first-order physical theory of useful long-term strength (ULTS) based on an analytical dislocation model of time-dependent microyield resistance has been advanced for so called excess point defect-solute structures with different physical kinetics of mobile defects below the macroscopic yield stress. In the pre-yield region theory predicts a potentially useful measure of long-term strength preventing a premature fracture. The quantitative (dislocation) criterion of ULTS is formulated to describe a subcritical transition from structurally uniform sliding to localized shear strain. It connects a threshold drag stress as a function of strain rate with elastic (shear) stability of a crystalline lattice, excess energy, velocity and density of sliding dislocations as well as their linear tension in the stress field. The theoretical calculations of dislocation strength influenced by elastic fields of dislocations produced by mobile pair defects with excess vacancies are in a reasonable agreement with the original and published experimental data. The approach proposed is the most valid for precise measurements when tested under the conditions of constant structure and changing strain rate as well as for stress relaxation tests and constant load creep testing. The analytical tractable solutions could be expanded to promising metal alloy systems as a starting point for further development of the newly developed alloys with minimum localized shear effects. Such an approach indicates decisive role of a localized shear in the structural preparation of the premature fracture.

Chapter

10 DESIGN AND MICROSTRUCTURAL ANALYSIS OF LIGHT ALLOYS FOR DYNAMICAL APPLICATIONS

10.1. Premises. Progress beyond the State-of-the-Art Research

Analysis of ongoing magnesium alloy development activities throughout the world indicates current efforts in the development of die casting alloys with improved elevated-temperature properties and with acceptable cost to the automobile industry. Nevertheless, the current commercial magnesium alloys of the Mg—Al and Mg—Al—Zn systems making up the bulk of those used in automotive industry do not exhibit creep resistance while maintaining die castability and room temperature strength.

Two groups of structural magnesium alloys are being developed in industrial use to meet requirements for further development of technical progress [306, 307]: (i) high temperature-strength magnesium-based alloys containing Y, Sc and RE as alloying elements for high-loaded parts in aircrafts, helicopters, automobile engines, etc.; (ii) high creep-resistant, light and low cost magnesium alloys for automobile, radio engineering and other dynamic applications.

Expensive RE-Containing Magnesium Alloys

The first group of these alloys of the Mg—Al—RE and Mg—Al—Si systems offer borderline improvement in creep resistance but the cost and poor die castability are their main disadvantages. Besides the Mg—Al—Ca and Mg—Zn—Al—Ca systems, other patented experimental alloys also contain expensive RE additions [308]. In order to expand magnesium application into crankcase and engine block operating at temperatures as high as 443-473 K, the additional alloy age by RE could be required. An alloy designated MEZ and containing typically 2.5% RE, 0.35% Zn and 0.3% Mn was developed by Magnesium Electron Ltd. This alloy exhibits creep re-

sistance significantly better than that of AE42 alloy at temperatures in the range of 423-448K under loads of 45-60 MPa. However, it has very low ductility and maximum strength at room temperature, which can restrict its application. Nevertheless, MEZ alloy is still being evaluated by some users [306, 309]. Another example is related to alloy ACM522 based on AM50 alloy added with 2.5% Ce-based mish-metal and 2% Ca. This alloy was developed by Honda R&D Co and is already in industrial use for production of oil pans for Honda's 1-liter engines for "Insight" hybrid cars with fuel consumption of 35 km per liter. It was demonstrated that this alloy exhibits creep strength in the range of 423-473 K similar to that of aluminum alloy A384. However, in addition to rather high cost, it has very low ductility (2-3%) and impact strength (4-5 J), which can restrict its application. Moreover, the presence of 2% Ca in this alloy can lead to hot cracking problems in components with variable wall thickness and more complicated shape than in specially designed oil pans with wall thickness in the range of 2.5-3 mm [307, 309].

A relatively high contents of Y (up to 4 mass%) and Zn (up to 1 mass%) cause the splitting of dislocations into partials where this mechanism is rate-controlling to decrease stacking fault energy in α-Mg matrix considerably. Stacking faults and partial dislocations accommodate thermal stresses arising during cooling down of the squeeze cast $MgY_4Zn1Mn1$ alloy.

Low Cost RE-free magnesium alloys

Taking into consideration seller's prices for REs, which restrict their adoption in a mass production, aerospace-, acoustician- and car-designers are interested in development of the second group of lower cost, high creep-resistant, and light structural materials not containing RE in order to use them in dynamic applications where a low moment of inertia, good static stiffness and high resistance to deformation at elevated temperatures are essential.

For creep-resistance forming magnesium, a suitable element is calcium, which has shown to have an excellent strengthening effect in the binary Mg—Al alloys depending on the Ca/Al mass ratio. The Ca addition, as a cheaper and lighter alternative to RE, also contributes to high temperature properties. When this ratio is more than ~0.8, the GBs precipitates in both Mg_2Ca and Al_2Ca result in considerable increase in hardness. Moreover, increasing the calcium to above 2% improves castability by partial eliminating hot-tearing. At the Ca/Al mass ratio less than 0.8 the creep resistance in Mg—Al—Ca alloys can be improved by suppressing the formation of the β-$Mg_{17}Al_{12}$ phase [310]. The Al_2Ca compound stable at high temperatures is responsible for creep resistance and beneficial effect of Ca in AX alloys (similar to AE 42 alloy with good corrosion resistance) when 2-6 mass% Al and 0.6-1.0 mass% Ca are added to magnesium [310, 311] According to this invention [311], the creep-resistant magnesium alloy has a creep extension of about 0.5% at 423K. Up to now, none of these experimental magnesium alloys with Ca addition has yet led to a commercially efficient

alloy. More work with the Mg—Al—Ca system is needed to optimize the composition of magnesium alloys containing Ca for die-casting. The Mg—Al—Ca system should be further investigated for optimum castability. However, in the range of investigated compositions and usual casting conditions Ca leads to an excessive hot-cracking and die-soldering especially in the Mg—Al—Ca alloys containing small addition of Al and above 1 mass% Ca. Subsequent addition of 8 mass% Zn causes improving the die castability but the creep properties were found to vary over a wide range [312].

The less expensive Mg-2…6% Al-0.25…5.5% Ca alloy with composition to give Al_2Ca precipitation [313] has had die castability problems including hot-tearing when prototyping an automatic transmission case. A subsequent version of the alloy, Mg-Zn-Al-Ca has had promise in eliminating die cast problems [314] but the alloy seems to work only in an extremely narrow composition range and to exhibit variations in properties as well.

Innovative Brand — Technology

The new cast alloys of the Mg—Al, Zn, Mn group such as commercially available AZ91 D for high-pressure die casting with corrosion resistance improved by the reduction in trace heavy metal impurities (Fe, Ni, Cu) have generated a significant interest for aerospace and particularly the US automotive sector. However, these alloys have numerous drawbacks: poor mechanical properties above 393K, variant with section thickness out cropping microporosity, lack of pressure tightness. Expensive RE-containing magnesium alloys, in particular, high strength Mg—Y alloys are now available with usable long term properties to 523 K.

It is however recognized that the demands for improved power/drive system performance and overall efficiency are ever increasing. To meet them, Magnesium Electron Ltd (MEL) has developed a new family of alloys based on the Mg—Y—Nd—RE system. Due to the proper combination of superior temperature stability, inherent corrosion resistance, and excellent mechanical properties, the alloy considered most suitable for aerospace applications is WE 43 (4% Y, 2.25% Nd, 1% HRE*, 0.6% Zn). The envelope of long-term temperature capabilities has been increased to 523K. WE 43A-T6 competes directly with commonly used aerospace aluminum-based alloys such as A355-T6, A3566, A201-T7 and A203 and can prove even better at elevated temperatures, with a dramatic potential weight saving of around 30%. Exposures for up to 10,000 hours at various temperatures up to 523 K have shown no significant reduction in r.t. tensile properties, while tensile properties of A201 and C355 fall quite drastically after long-term exposure.

In spite of the fact that magnesium has the lowest density and the best machinability of all the engineering metals, it has only found restricted applications as an engineering material due to limitations to the mechanical properties and corrosion

* Heavy Rare Earths, principally ytterbium, erbium, dysprosium and gadolinium.

resistance. It is reported that the main factor affecting the mechanical properties of more reactive magnesium alloys is the grain size. Novel material processes such as enhanced directional as well as rapid solidification technology (RST) including Free Jet Melt Spinning (MS) and Planar Flow Casting (PFC) expand the application of wrought (extrusion) reactive magnesium alloys with enhanced properties provided by structured refinement and solid solution extension. The strong correlation between the grain size and the tensile yield strength is indicated by the Hall-Petch relation.

Rapid solidification processes (RSP) like Free Get Melt Spinning and PFC result in a substantial microstructure refinement giving a considerable increase in the mechanical strength of the alloys. Rapidly solidified and then extruded AZ91 with additions of RE and silicon is characterized by week texture and a fine grain size of 0.3-1.0 μm and particles size of 0.2-0.7 μm ($Mg_{17}Al_{12}$) and 30-70 nm (Mg-RE) dependent on processing parameters like casting and consolidation conditions [315]. Rapid solidification technology is looked upon as a way of avoiding the limitations of traditional metallurgy in metals and extensive research into aluminum alloys has resulted in promising improvement of the properties.

The Research Center (France) and PECHINEY NORSK HYDRO (Norway) have started a joint program with objectives to develop new magnesium alloys with high strength and improved corrosion resistance using the RSP. Outstanding improvements in strength at 473-623 K, equal compressive and tensile strength and excellent corrosion resistance have been reported, in particular for new magnesium alloys of Mg—Al, Zn, Zr, RE systems produced from raw materials like PFC tapes of 100 μm thick and 12-15 mm wide and MS ribbons of 40 μm thick and 5 mm wide using extrusion conditions for RSP materials (ratio 40 : 1 and 20 : 1; speed of 0.14...2.40 m/min). Nevertheless, these alloys have no potential for creep improving although addition of Si, for instance, keeps the grain boundary pinning effect up to 573 K.

Continued development has produced new products such as rapidly solidified magnesium alloys of the Mg—Al—Zn—Nd system (EA 55) with tensile strengths up to 550 MPa in the as-extrusion conditions. Rather low fracture toughness is improved by a heat treatment which dissolves the precipitated $Mg_{17}Al_{12}$ in the structure. Another important benefit appears to be enhanced is corrosion resistance, offering the prospect of producing alloys of the system with equivalent corrosion resistance but higher specific strength than aluminum alloys.

In the periodic literature [316] it is reported that the same level of creep resistance is observed in the RE-free Mg—Al 5-Ca1 alloys (AX51) at much lower cost due to formation of new strengthening phase Al_2Ca. It should be pointed out that the temperature interval of solidification is substantially wider for the Ca-containing alloy AX51 than for the RE-containing alloy AE42.

The intensive research program initiated by Volkswagen AG and DSM (MRI) with the aim to develop low cost magnesium alloys led to the development of new alloys designated as MRI 15X. They have a great advantage in creep resistance compared to conventional alloys. In particular, they exhibit higher a.e. for creep than that

of AS21 alloy (~1.72 eV against 1.63 eV) and creep resistance at 408 K under stresses of 90-110 MPa superior to that of a commercial AZ91D and AS21. Moreover, the newly developed alloys of MRI 15X series exhibit die castability, corrosion resistance (of rate 0.09 against 0.11 mg/cm^2/day for AZ91D) and elevated temperature strength similar or better than that of AZ91D, AE42 and AS21. Finally, MRI 151 and 153 alloys exhibit at 408 K under 85 MPa minimum (steady-state) creep rate $\dot{\varepsilon} \sim 10^{-8}\ s^{-1}$ which is lower than that of commercial alloy AZ91D ($\dot{\varepsilon} \sim 10^{-7}\ s^{-1}$) by an order of magnitude. Nevertheless, all the above-mentioned developments seem to be suitable for gearbox applications in the temperature range of 408-423 K.

Besides the Mg—Al—Ca and Mg—Zn—Al—Ca systems, other systems also contain the expensive rare earth additions [317, 318]. The less expensive Mg—2...6Al—0.25...5.5Ca with composition to give Al_2Ca precipitation [317] had die castability problems including hot tearing when prototyping an automatic transmission case. A subsequent version of the alloy, Mg—Zn—Al—Ca has had promise in eliminating die cast problems but the alloy seems to work only in an extremely narrow composition range and to exhibit variation in properties as well. Thus, more data have to be generated on the present and newly developed types of alloys to confirm that magnesium product is a serious candidate for the desired applications (running gear, engine blocks, etc.).

10.2. Newly Developed Magnesium Alloys

10.2.1. Background

The material selection for automobile design and mass production is one of the most critical problems connected with competition for abundant inexpensive raw materials supply. Research on die-casting technology has reached a status where in design studies the basic requirements for highly loaded materials have been identified. The requirements for the affordable cost and good die castability of new experimental magnesium alloys reduce possible options to alloying systems which are coating Al and Zn as major elements and Mn, Si, Ca, Sr, RE as relatively small additions [306]. Much progress has been made [306, 307] but, nevertheless, any attempts to design magnesium alloy systems consisting of inexpensive alloying elements face some problems that concern definition of secondary processing issues such as limited plasticity at r.t., decreased corrosion resistance, soldering with a mold in a die-casting technology, welding and joining (enhanced diffusion binding) of parts/products/panels constructed of them.

The new magnesium-based alloys of the Mg—Al—Ca, X system which have been developed in recent years for use as functional and structural materials in engineering can perform well in engine and transmission cases [306-310]. They have attracted attention due to their desirable engineering properties such as creep resistance and long-term strength at elevated temperatures during long-term usage as well as due to their greater potential for weight savings, for example, in automobile indus-

try. No insurmountable problems have arisen so far. Nevertheless, up to now none of these experimental magnesium alloys with additions of Ca has yet led to a commercially successful alloy. More work with the Mg—Al—Ca system is needed to optimize of the magnesium alloys composition containing Ca for die-casting. The Mg—Al—Ca system should be further investigated for optimum castability. Furthermore, in the range of investigated compositions and usual casting, addition of Ca leads to an excessive hot-cracking and die-soldering especially in Mg—Al—Ca alloys containing small addition of Al and above 1 mass% Ca [308]. Subsequent addition of 8 mass% Zn causes improving the die castability but the creep properties were found to vary over a wide range [312].

At the present time there is no commercial application of the new experimental magnesium alloys although many components have been fabricated from them and have performed quite satisfactorily in testing. Moreover, the commercial production of the sound castings capable of being processed into uniform homogeneous microstructures is difficult in the case of a high degree of alloying. Thus, it is evident that most of the future applications, for instance, in automobile industry are not realistic with the currently available die casting magnesium alloys. Hence, additional fundamental and applicable research is required in all areas of magnesium production on the basis of the synergistic effect of magnesium processing and alloy development in order to substantially increase the use and application of magnesium alloys.

Unfortunately, no existing die casting alloy is well suitable for producing drive train components operating at temperature higher than 403-423 K under 70-80 MPa. Castability, creep resistance and stress relaxation are critical parameters. Besides, in the case of high-pressure die casting/high volume production technique, the alloy cost represents a significant proportion of the component cost and so becomes a major restriction in the alloy development. It means indeed that the newly developed alloys should be cost-efficient and cost-competitive with existing ones.

The main purpose of the present study is to develop new experimental die casting magnesium alloys of Mg—Al—Ca, X system with higher castability, considerable creep resistance and higher long-term creep strength at elevated temperatures by carrying out their full-scale research, observation and testing standards driven to low-cost application and mass production. With this provision, the alloys with superior strength are expected to have superior strength in order to operate under a given set of conditions namely at larger stresses and higher temperatures (70 MPa and 423 K). To identify the rate-controlling creep mechanisms responsible for the power law and thermally activated (Arrhenius) behavior, the alloys will be investigated in a wide temperature range up to 523 K suitable for automotive power train, oil pump and other advanced commercial applications.

Development of creep- and corrosion-resistant casting Mg—Al—Ca, X alloys (referred to as "the developed alloy" hereafter) which must satisfy all of the following requirements: (1) the yield strength of the developed alloy should be larger than 150 MPa at r.t. and 130 MPa at 423 K; (2) the total creep elongation of the developed alloy

should be less than 0.4% after exposure at 70 MPa and 423K for 200 hr; (3) the corrosion rate of the developed alloy with an appropriate protection should be less than 0.1 mg/cm^2/day in salt-spray test; (4) a higher castability of the developed alloys, which means combination of good fluidity and die-filling property of the melt and sound microstructure without any solidification defect such as porosity, die sticking and hot cracking, etc., should be much the same as for AZ91D; (5) development of creep and corrosion-resistant casting Mg—Al—Ca, X alloys should involve compositions not containing expensive alloying elements such as RE, etc., with nanophase microstructures as well as, if needed, containing very small amount (about 0.1-0.3%) of one of additions such as Y, Gd, Sr, etc.; (6) identification of rate-controlling creep mechanisms responsible for the power law and thermally activated (Arrhenius) behavior of the alloys to be investigated in a wide temperature range up to 523 K for automotive power train, oil pump and other advanced commercial applications.

The work is a continuation of the cooperative effort of the ICEMS, Ukraine and the KIMS, Republic of Korea for the purpose of evaluating and comparing the creep properties of newly developed magnesium alloys and of verificating their processing-composition-microstructure-property relationships. To better understand solidification structures and attain the stated final result, both research groups of Ukraine and Korea aim to identify rate-controlling creep mechanisms responsible for the power law and thermally activated (Arrhenius) behavior of the alloys in a wide temperature range of 293-523 K to be used in automotive power trains, oil pumps and other advanced commercial applications.

10.2.2. Principles of Alloying

The main reason of slow introduction of magnesium alloys into the automobile market is insufficient castability, high cost and insufficient reproducibility of their properties. From the viewpoint of the Dead See Magnesium Ltd; and Volkswagen A.G. joint research group, requirement of low cost along with castability problems reduces possible options to alloy systems containing Al or Zn as principal alloying elements, with using Mn, Si, Ca, and Sr as relatively small additions as well as Ce or La-based mish-metal [306, 307]. We believe that there are at least three approaches to strengthening the phase (eutectic) component in the structure of α-Mg matrix: (i) to change the nature of binary chemical compound, for example, high-temperature strength Al_2Ca instead of unusable soft $Mg_{17}Al_{12}$ which softens at higher temperatures; (ii) to eliminate the formation of $Mg_{17}Al_{l2}$ in the Mg—Al—Ca system (Fig. 10.1); (iii) to substitute one of the elements in soft $Mg_{17}Al_{l2}$ lattice with higher melting temperature element and this way to strengthen the GBs by ternary magnesium-bearing phase.

The isothermal section of the Al—Ca—Mg system at 573 K was calculated using published data [74]. Replacing the expensive alloying elements such as RE with Ca in promising creep resistant and long-term strength magnesium alloys could lower their cost, without impairing their mechanical properties.

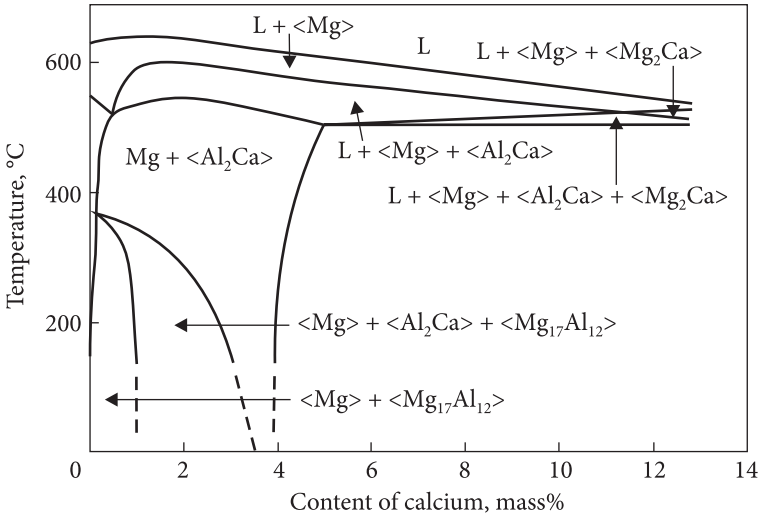

Fig.10.1. The equilibrium phase diagram: polythermal cross-sections of the Mg—Al—Ca system at constant 4.5 mass% Al content [319]

In this work, a new approach will be made with Ca as an alloying element in the Mg—Al—Ca system. To overcome the abovementioned disadvantage of the system, the now-how Ca/Al ratio has to be changed (with simultaneous increasing the Al and Ca contents) as well as additional alloying components have to be chosen, fulfilling the conditions for optimizing the novel compositions. Ca is selected as the second alloying element, use of which for our approach is desirable as shown by thermodynamics, raw materials situation and our extensive work in the field. As a new addition to the creep-resistant and high-strength magnesium alloys of Mg—Al, Ca, X system, Ca provides an excellent combination of creep performance and castability due to enhancing the contribution of eutectics with negligible mutual solubility of components.

A sufficient amount of Al in the magnesium alloy melt is considered to provide its good die-castability properties. At the same time formation of eutectic corrosion-resistant $Mg_{17}Al_{12}$ intermetallic results in decreasing the creep resistance. As well-known, replacing RE with Ca for magnesium alloys in Mg—Al system could lower their cost without impairing the mechanical properties. The same level of creep resistance for AX 51 alloy in the Mg—Al—Ca system containing the strengthening phase Al_2Ca is produced at much lower cost than for AE 42 alloy containing RE (Ce) [310].

It has been found that the addition of Ca induces a noticeable strengthening effect substantially modifying the microstructure after homogenizing treatments and reducing the solubility of Al through pinning of GBs by dispersoids of the ternary phase $Mg_{17}Al_{12-x}Ca_x$. The resulting microstructure of magnesium matrix nanophase particulate-reinforced composite is able to optimize uncorrelated (thermal, electrical and strength) parameters and cost efficiency. Optimum microstructural engineering in new experimental magnesium-based alloys of Mg—Al, Ca, X systems of eutectic origin

(with larger ratio of Al/Ca) and their MMCs reinforced by SiC-nanoparticles as well as methods of its control in rapidly and directionally solidified ingots are summarized and analyzed using electron microscopy characterization of magnesium alloys [320].

Upon small-scale alloying magnesium alloys of Mg-Ti system exhibit large positive values of enthalpy of mixing (16...30 kJ / mole [321]), a tendency to clustering the structure of α-Mg solid solution and effective solubility on dislocations in the nonequilibrium conditions of crystallization thereby overcoming a barrier of their solubility.

Novelty of the approach consists in developing physical principles of precision (on atomic-energy level) alloying of Mg—Al—Ca matrix with promising additions having a large positive enthalpy of mixing using processing technique of rapid solidification. They are based on high sensitivity of the selected alloying elements such as Ti, Gd, and Sr to the solidification/cooling rates. This makes it possible to overcome a potential barrier of solubility in the nonequilibrium conditions and facilitates introducing in the melt of additions insoluble in equilibrium conditions (Table 10.1).

Any die-casting process is succeeded by rapid solidification of a magnesium melt, the rate of which varies within the limit of 313...333...373 K per sec. The relevant dislocation structure formed in as-cast condition can be expected to interact only with the fast-acting alloying elements which are able to trap dislocations in the nonequilibrium conditions of crystallization. Original idea is to select those of them which will be able to inhibit the initiation of critical dislocation density responsible for deterioration of creep properties at higher temperatures and thereby to enhance contribution of the refractory metal diffusion responsible for increase in heat resistance. It is these alloying elements such as Ti, Gd and Sr that can do this having negligible or low lattice solubility in hcp magnesium at elevated temperatures. Since AEs exhibit high sensitivity to the high-speed treatment, they can be expected to increase effective solubility (on structural defects) thereby extending limit of their solubility. This effect is succeeded by essential pinning of moving dislocations with solute atmospheres by Cottrell's hardening mechanism [275]. Its activation in the stress field should minimize solute effects to increase creep resistance and long-term strength up to 70 MPa at 423 K for 200 hr with slow creep rate at 10^{-9} s^{-1}.

There are two bimetallic magnesium-based systems of different kind with negative and positive enthalpy of mixing. The vast majority of them are formed in the systems with negative heat and enthalpy of mixing (e.g., Mg—

Table 10.1. **EDXS analysis of elementary composition of the fracture surface at 293 K for the tensile stressed Mg—12.5Al—1.3Ca—0.3Mn—0.1Ti alloy**

Element	Mass%	At. %
Mg	18.68	25.69
Al	39.36	48.76
Ti	0.28	0.19
Cr	0.36	0.23
Mn	40.02	24.35
Fe	1.30	0.80
Total	100.00	100.00

Zn, — 4 kJ/mole; Mg—Si, –26 kJ/mole; etc.) due to the reduction of Gibbs free energy upon mixing to form solid solution or intermetallic compound [321]. A large negative heat of mixing in the liquid characterizes a high glass-forming ability for metallic alloys. At the same time the Mg—Ti system relates to positive heat-of-mixing metallic systems which do not have a thermodynamic driving force and is characterized by a large positive heat of mixing (16 kJ/mole) in both the liquid and solid states according to the Miedema model [322].

As known, systems with a positive heat of formation (enthalpy of transformation to standard elements) tend to favor "de-mixing" as well as to local ordering. For reasons given, their formation requires very high cooling rates: local structure evolves rapidly requiring mostly short-range diffusion and arrangements. However, rapid kinetics of Ti (Gd, Sr) microsegregation under a high-rate treatment is at variance with the slow kinetics of the thermal and stress-induced decomposition. By doing so, the mobile fluctuations of chemical composition promote the dislocation pinning. Unfortunately, in the study of the systems to date, convincing evidence is generally lacking in establishing the exact extent of alloying of the atomic-level homogeneity. Multicomponent additions may change the value or even sign of the heat of mixing so that their incorporation should be carried out on the segregation-level scale due to the rapid solidification-induced dislocation structure. In order to alloy a pair of constituent "immiscible" elements revealing little or no mutual solubility even in liquid state up to very high temperatures, it is necessary to employ highly nonequilibrium processing that overcomes a solubility barrier, for example, through a rapid quenching route. In order to solve the problem in the multicomponent Mg—12.5Al—1.3Ca containing 0.1-0.2 mass% Ti, the authors have used for the first time a processing technique of rapid quench from solid phase rather than mechanical alloying which is unsuitable for die-casting technology. Rapid solidification rate in the experiments closely resembles that to be expected from die-casting procedure (up to 373 K/s). Moreover, the approach provides the extent of atomic-level alloying with Ti, Sr, Gd, etc. due to as-cast dislocation structure having binder and accommodation capacity at the atomic segregation-level.

The Mg—X systems (where X—Gd, Sr) should be likened to those bimetallic systems with particular thermodynamic properties seeing that the same causes produce the same effects. As one should expect, this approach is in agreement with the well-known Le Chatelier-Braun principle of mobile equilibrium which is useful in the linear thermodynamics of nonequilibrium processes [323]. According to [321], Ti possesses the largest positive enthalpy of mixing (making up 16…30 kJ/mole for bimetallic system Mg—Ti) and therefore is considered as insoluble alloying element relative to hcp Mg. Nevertheless, we revealed 0.28 mass% (0.19 at%) Ti in magnesium alloy using rapid solidification method (Table 10.1).

10.2.3. Experimental Procedure

The newly developed alloys were melted in graphite crucibles using an electrical resistance heating furnace and a special impeller designed in our laboratory to provide continuous stirring. The molten alloys were held at 1013 K and then poured into a permanent copper mold.

The Mg—30Ca and Al—10 Sr master alloys were used as a ligature to different cast alloys of the Mg—Al—Ca, X system. Mg—Al—Ca based alloys were prepared by melting stoichiometric amounts of the constituent elements in an induction melting furnace (ligature) and then in an electric resistance furnace under flux (ingot casting) in an argon atmosphere as well as CO_2 with 0.5 % SF_6 to protect the melt from oxidation. The actual chemical compositions were measured quantitatively by ICP atomic spectroscopy and investigated with transparent electron microscopy (TEM), scanning electron microscopy/energy dispersive spectroscopy (SEM/EDS) analysis, quantitative electron probe microanalysis (EPMA), X-ray diffraction (XRD) techniques to identify the phases in the Mg—Al—Ca, X system and to determine their compositions.

Thermal analysis was carried out in real time using measurement of the phase changes involved in these systems under the rapid solidification (up to 100 deg. s^{-1}). The temperature range for the phase transformations and types of reactions to form compounds were determined (Figs. 10.1 and 10.2, Table 10.1).

Our previous investigations of phase equilibria in the ternary Mg—Al—Ca system studied by the DTA, EPMA and XRD methods have been resulted in constructing the isothermal section at 423 K and polythermal sections at 4.5 and 8.5 mass% Al. Additions of Al and Ca were established to decrease the liquidus temperature of the magnesium alloys from 923 to 711 K. It was shown that the three-phase region <Mg> + + <Al_2Ca> + <$Mg_{17}Al_{12}$> exists at 423 K with the corresponding two-phase fields and temperature dependence of the homogeneity range of the α-Mg solid solution as well as temperatures of the phase transformations which occur in the investigated system (Figs. 10.1 and 10.2).

As reported in Ref. [324], creep rate decreases and long-term strength increases with increasing rate of crystallization of the eutectics by a dispersion hardening mechanism. Therefore, magnesium alloys were synthesized and produced under nonequilibrium conditions of crystallization at a cooling rate of about 333 K. sec^{-1}. Used as additions to cast different magnesium alloys based on Mg—Al—Ca—X system of eutectic origin were Mg—30Ca, Al—10Ti and Al—10Sr master materials. The new experimental alloys were prepared by melting stoichiometric amounts of the constituent elements in an induction melting furnace (additional alloys) and then in an electrical resistance furnace under flux (ingot casting) using argon as well as CO_2 with 0.5% SF_6 to protect the melt from oxidation. They were melted in graphite crucibles; the molten alloys were held at 1013 K and then poured into the permanent copper mold ø 20 × 60-70 (mm).

Measurements of castability for magnesium alloys were carried out using an original installation (on the basis of induction vacuum furnace), which is encapsulated,

pumped and filled with inert gas (99.998% Ar). During melting of an alloy of 50 g in mass, the excess pressure of argon makes up about 0.2–0.4 atm gage. After melting the liquid alloy is maintained during 10 min under the excess pressure, controlled with an accuracy of 0.01 atm by precision manometer. The sample length is measured (in mm) after its cooling to r.t. When comparing data obtained in the vacuum section, casting temperatures should be in excess of 323 K (over liquidus curves) for all the magnesium alloys under investigation [307, 314]. The results obtained are much the same as compared with the result produced by using a complex U-shaped sample in well-known Nekhendzi–Kuptsov's method under the stabilized experimental conditions: about 63 mm for AZ91D industrial alloy and 90 mm for Mg—12.5Al—1.3Ca—0.28Mn—0.2 Ti alloy at the pouring temperature of 873 K.

The dislocation structures in as-cast magnesium alloys produced were characterized by using well-known techniques [325-329] such as SEM. TEM, SEM/EDS analyses, quantitative EPMA, as well as XRD techniques to identify the phases in the Mg—Al—Ca, X system and to determine their compositions.

The standard XRD analysis of the new experimental alloys was performed using a diffractometer DRON-UM1 with monochromatic CuK_a-radiation and monocrystal of graphite as a monochromator located in the place of secondary beam. Stepwise X-ray registration with angle step of 0.05° was employed for determination of lattice parameters. Approximation of diffraction profiles was carried out through the pseudo-Foght function by means of LS-variation of their K-component angle position, integral intensity, half-width and asymmetry. CIB programs package was employed for more precise lattice parameters calculation. The correction of X-ray penetration into the sample depth was taken into account. A peak-breadth analysis has allowed X-ray evidence of the volume-weighted crystalline size and microstrain averaged all over the coherence length perpendicular to the diffracting planes [326].

The precise XRD studies were carried out using a continuous drive diffractometer to characterize the dislocation densities of a magnesium alloy before and after small creep strain (up to 0.5%) for better understanding the rate-controlling creep mechanism. In combination with a graphite monochromator as a filter providing the divergence and width of beam to be up to standard 50 angular seconds and no more than 0.15 mm, respectively, XRD measurement parameters (angle interval, step length, etc.) as well as XRD peak-broadening analysis were employed to single out lattice distortions. This is well-known advanced technique and its main features have been reviewed in the textbooks [327, 328]. All data were collected by using CuK_a radiation and by operating the X-ray diffractometer equipment in a step scan mode with 0.01° in 2Θ per step. Under this provision, the peak width could be measured with the accuracy of ±0.01° in 2Θ. XRD patterns were taken from solidified ingots in order to obtain all the diffraction peaks given by the indices of certain phase. Volume ratio of phase compositions was estimated from the integrated intensities of the peaks.

Torsional experiments were performed on samples having a gauge length of 70 mm and of 1 mm in diameter. The variation of internal friction, $Q^{-1}(T)$, in magnesium al-

loys as a function of temperature was studied in the range of 293-800 K by the free-decay method as developed by Ke [330]. Discrete temperature spectra of internal friction for magnesium and its alloys were recorded by using a relaxometer such as inverted-torsion pendulum operating in the low frequency range (at 1 Hz) with constant strain amplitude of 1×10^{-5} in the mode of free-damping torsional vibrations.

As known, $Q^{-1}(T)$ background displaces an exponent, which is dependent on properties of mobile dislocations in the bulk solid solution so that high temperature internal friction is independent of strain amplitude and appears to follow a law of the type:

$$Q^{-1}(T) = A\exp(-U / kT). \tag{10.1}$$

The apparent activation energy (a.e.) of the internal friction is obtained by plotting ln Q^{-1} vs. 1/T, which gives a straight line, if Eq. 10.1 is obeyed due to some thermally activated dislocation relaxation or diffusion-controlled dislocation relaxation which are responsible for the energy dissipation. At wt = 1 the temperature dependence of internal friction is described closely by the equation

$$Q^{-1} = \Delta M\{\tau\omega / (1 + \tau^2\omega^2)\} \tag{10.2}$$

in which

$$\tau = \tau_0 \exp(\Delta H / RT), \tag{10.3}$$

where ΔM is the magnitude of relaxation strength, ($\Delta M \cong 2\ Q^{-1}_{max}$); ω is the angular frequency of the torsional pendulum when measured at 1 Hz and τ is the relaxation time, $\tau_0 = h / k\ T_{max}$, where T_{max} is the maximum temperature of an internal peak Q^{-1}_{max}; h is the Planck's constant.

According to the Maxwell-Boltzmann concept, the relaxation time can be described by the relation

$$\tau = (Az\upsilon)^{-1}\exp(Q_m / RT), \tag{10.4}$$

where υ is the frequency of atomic vibrations ($\cong 10^{13}\ s^{-1}$); A is the entropy of activation ($\cong 1$); z is the coordination number of the lattice; Q_m is the a.e.

In this case, dislocation velocity is determined as

$$\upsilon_D \sim \exp(-U / kT), \tag{10.5}$$

where U is the a.e. for movement of a free lattice dislocation.

Eq. (10.3) gives τ in terms of the a.e. ΔH and another constant of the material τ_0. According to Eq. (10.2), the adjustable parameter ΔM is fixed to give agreement with the experimental points for a single relaxation time. The a.e. is obtained by the well-known method of measuring the peak shift position due to temperature change.

Amplitude-dependent damping attributed to dislocations [331] was measured with increasing strain amplitude γ up to $5 \cdot 10^{-4}$. The binding energy E_b for dislocation-solute interaction was calculated from experimental data on amplitude-dependent internal friction via the conventional form of the linear relationship between ln tg*a* and 1/T, in which tg*a* is the slope coefficient for straight line. These results were

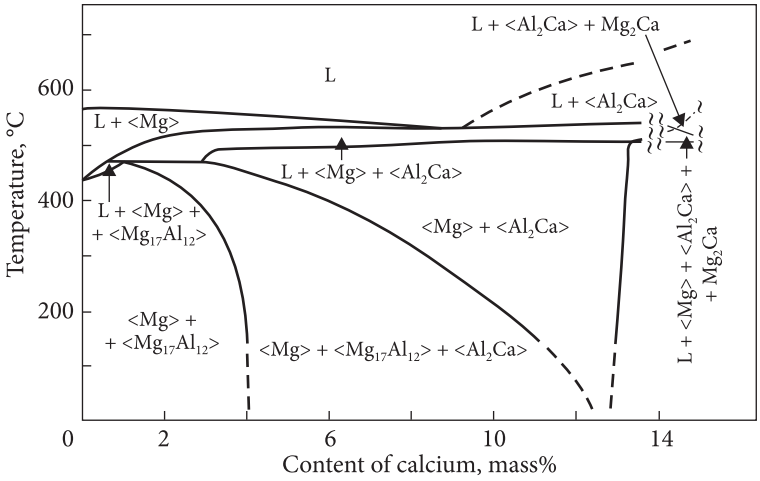

Fig. 10.2. Polythermal cross-sections of the Mg—Al—Ca system at constant 16.0 mass% Al content [319]

checked on using relaxation time τ for depinning the lattice dislocations which is associated with temperature by the relation

$$\tau = 1/\upsilon \times \exp(E_b/kT), \tag{10.6}$$

where E_b is the binding energy of a dislocation with a solute or a vacancy; $\tau \cong 10^{-8}$ s; $\omega\tau = 1$; $\omega < 10^5$ s^{-1}. Dislocation damping measurements were performed on as-cast magnesium alloys in order to determine the binding energy between solute atoms and pre-existing dislocations at temperatures ranging from 293 to 733 K.

Short-range tensile tests were performed at a constant cross-head speed giving an initial strain rate of 10^{-3} s^{-1} at temperature of interest. Creep tests were carried out in tension using a constant lever arm tester and a temperature averaging extensometer, which employs a super linear variable capacitor to measure the strain. Cylindrical tensile samples 3 mm in diameter and 25.4 mm gage length were machined from as-cast material. The apparent a.e. for creep Q_c was determined experimentally from an Arrhenius relationship where the logarithm of the long-term creep strain rate is plotted against the reciprocal temperature [332]:

$$\dot{\varepsilon}_C = A\sigma^n \exp(-Q_c / RT). \tag{10.7}$$

The values of Q_c and stress exponent n are necessary to identify thermally activated (rate-controlling) mechanism in particular temperature and stress rate ranges.

The fracture surfaces of the test specimens were observed using a Hitachi S-2700 scanning electron microscope equipped with the Link-4 energy-dispersive X-ray system to analyze the tensile fracture features. Microstructural observations were carried out using optical microscopy, SEM and TEM techniques.

To ascertain whether Ti used as the basic promising addition is an appropriate element or not, three compositions were produced with the nominal Ti contents of 0.07, 0.1 and 0.2 mass% (Table 10.2). The Mg—Ti equilibrium is such that a classical solutionising and ageing treatments are not appropriate. Specimens to examine by electron microscopy were prepared using a satisfactory technique developed by Roberts. TEM/SEM observations were used to reveal the resultant (amorphous, cluster-forming nanophased, and nanocrystalline) structure using a JEOL JXA-8200 for EPMA.

Particles formed by aging may be detected by observation changes in the direction of their moiré fringes [327] to obtain a dense distribution of nanoparticles stabilizing the grain boundaries and the matrix of polycrystals. Nanoparticles as small as 20 nm in size may be identified by proper electron microscopic techniques. To determine the nature of nm dispersoids, selected area electron diffraction analyses were made. Interplanar spacings were determined from SAD patterns.

Based on previous studies [60] and the results shown in Table 10.1, Figs. 10.1 and 10.2, the compositions of magnesium-based alloys were sorted for further evaluation and temperatures were selected as the most desirable temperatures to compare with operating temperatures in service. The procedure was applicable whether the product was pure or contaminated. Chemical compositions of magnesium alloys were selected as being the best for producing any likely nanoparticles. All alloy compositions are defined in mass percents, unless otherwise stated.

The activation energies (a.e.) for dislocation creep resistance were determined on the basis of previous experience with the present available method and by standard procedure.

Modeling calculations of the strain rate variations for dragging stress were examined theoretically to compare results obtained with pre-existing observations in hcp metal alloy systems.

To check the strain-rate sensitivity in question, special experiments and measurements were performed on hcp zirconium alloy of the Zr—Sn—Nb system with evaluation of the nanoparticles effect by a dispersion strengthening mechanism. Their crystal structures were characterized by TEM, SEM, and XRD analyses. These resolvable pre-placement techniques were combined with the results produced by electron-microprobe and X-ray analyses, Auger-electron, UV and X-ray photoelectron spectroscopy techniques to carry out additional structural investigations, to evaluate the alloying effectiveness in the resultant structure and to assess chemical bond strength.

Selection-area diffraction patterns taken from the matrix and individual precipitates were photographed and measured. Thermal investigation was performed using a Setaram Setsys DSC-1200 instrument. The DSC measurements were carried out with heating and cooling rates of 2 and 10 °C/min from r.t. to 700 °C. More details of the DSC experiments and their interpretation were reported in Ref. [340].

All samples with high creep properties at 70 MPa / 423 K, for example Noranda Ltd. Co Magnesium Creep Resistant Die-casting Alloy (ε_{Σ} = 0.29% for 200 hr, Mg—

5Al—1.8…2.2Sr; and ε_{Σ} = 0.44% for 200 hr, Mg—5Al—1.2...1.7Sr), were manufactured using cold-chamber die-cast or ingot casting technique.

In accordance with "Metals Creep Test Method" adopted by the Ukraine legal system as a standard, the instantaneous plasticity or "athermal jump of plastic" component of elongation under initial loading ($\tau \to o$) was excluded from consideration. Subject of research /by contract/ was creep resistance and hence creep strain rather than athermal jumps of initial deformation (for tens of seconds) which do not describe the time dependent creep deformation during τ up to 200 hr. We should accept the fact. Unlike the ingot casting creep testing samples, no jumps can be expected after die casting creep testing.

The fracture surfaces of the test specimens were observed using a Hitachi S-2700 scanning electron microscope equipped with a Link-4 energy-dispersive X-ray system to analyze the tensile fracture features. Microstructural observations were carried out using optical microscopy, SEM and TEM techniques.

XRD patterns were taken from solidified ingots in order to obtain all the diffraction peaks given by the indices of the certain phase. Volume ratio of phase compositions was estimated from the integrated intensities of the peaks.

10.2.4. Results and Discussion

Microstructural Analysis

We believe that there are at least three approaches to strengthening the phase (eutectic) component in the structure of α-Mg matrix: (i) to change the nature of binary chemical compound, for example, high-temperature-strength Al_2Ca instead of unusable soft $Mg_{17}Al_{12}$ which softens at higher temperatures; (ii) to eliminate the lattice with a higher melting temperature element and this way to strengthen the GBs by ternary (magnesium-bearing) phase (due to the formation of $Mg_{17}Al_{l2}$ in the system of Mg—Al—Ca system; (iii) to substitute one of the elements in soft $Mg_{17}Al_{l2}$ lattice with a higher melting temperature element and this way to strengthen the GBs by ternary (magnesium-bearing) phase. In the present research the main attention is given to magnesium alloys of the Mg—Al, Ca, X system of eutectic origin as well as to discontinuous SiC (Al_2O_3) particle-reinforced Mg-matrix composites to be produced via different routes of advanced processing. The evaluated temperature creep and specific strength properties appear to be significantly better (at the creep limit of 65 MPa and 423 K) than that of the commercially available MgAZ91D alloy with divorced eutectics (Dow Chemical Corp., USA).

Thermal analysis indicates that temperatures of phase transformations depend on the chemical composition of new experimental magnesium alloys containing low-cost AEs. The kinetics of their decomposition and bulk cooling under solidification by crystallization is accessed at 333 K/s [250, 333]. By reason of the rapid solidification during pressure die casting, the Mg—Al alloys such as AM50, AM60 as well as AZ91D are affected by supersaturation of α-Mg solid solution in as-cast condition.

Moreover, due to the divorced nature of binary eutectics, they are laminated to form regions of highly supersaturated α-Mg adjacent to the GBs. This leads to an unstable microstructure and extensive precipitation which continues for many hundreds of hours. The slow kinetics of the thermal decomposition gives rise to keeping metastable α-Mg matrix solid solution and to decreasing creep resistance of commercial Mg—Al alloys [334]. Addition of Ca under know-how ratio of Al to Ca [335] results in stabilization of α-Mg solid solution in the Mg—Al—Ca alloy system. At the same time, fast kinetics of segregation/desegregation restricts long-term strength at 423 K for 200 h to the creep strength of 64 MPa. Nevertheless, alloying of magnesium with a greater quantity of aluminum (up to 12.5 mass%) leads to an increase in its castability (up to 30%). This allows using the family of magnesium alloys for manufacturing the parts that are very difficult to cast. Besides, increasing the Al content (nearer to eutectic point) leads to doubling the volume fraction of dispersed eutectic structural component b-$Mg_{17}Al_{12}$ to be strengthened by third solute AE (Table 10.2).

The practical interest in microstructures of eutectic origin arises from the chemical equilibrium of two phases, e.g. α-Mg and β-$Mg_{17}Al_{12}$, which are unaffected by chemical decay [316, 336, 337]. Moreover, they have interfacial phase bonding capable of effectively transferring the loading from phase to phase and to call effect of natural eutectic strengthening. The microstructure of eutectic origin compares favorably with their thermal stability due to formation during solidification of low energy phase-to-phase states, which makes them good for creep resistance. SEM observations (Fig. 10.3) exhibit different contrasts clearly visible in the micrographs. It follows that the commercially available AZ91D alloy of the Mg—Al, Zn, Mn system should be specified by divorced eutectic and laminated Mg—Al solids solution (Fig. 10.3, *a*), and, as consequence, low creep strength at higher temperatures.

The addition of Ca to some magnesium alloys can lead to the precipitation of metastable or stable hcp thin (nano-scale) plates parallel to the basal planes of hcp α-Mg matrix. They are likely to be very effective obstacles to cross-slipping basal dislocations at elevated temperatures up to 548 K [74]. They were identified in Mg—Ca—Zn system both in as-cast and annealed conditions after solution treatment and after creep at 423 K and 51 MPa (Fig. 10.3) as well as in rapidly solidified Mg—1Ca after isochronal annealing up to 413 K.

Magnesium alloys of the Mg—Al, Mn system are known to undergo a solid-state α-β transformation to produce continuous and discontinuous (disperse) precipitation of the β-$Mg_{17}Al_{12}$ phase from α-Mg matrix. In our case, the soft, having low melting temperature (~367 K) β-$Mg_{17}Al_{12}$ is strengthened by refractory additions such as Ca, Ti, Sr, etc. The presence of these AE-filled inclusions seems to have little effect on the short-term (tensile) properties. Although the particles are not Orowan obstacles for moving dislocations (at creep strain rates of 10^{-9} s^{-1}), they promote and can affect stabilization of phase composition ($Mg_{17}Al_{12-x}Ca_x$). Moreover, the second phase particles appear to be fracture resistant and are not preferential fracture paths.

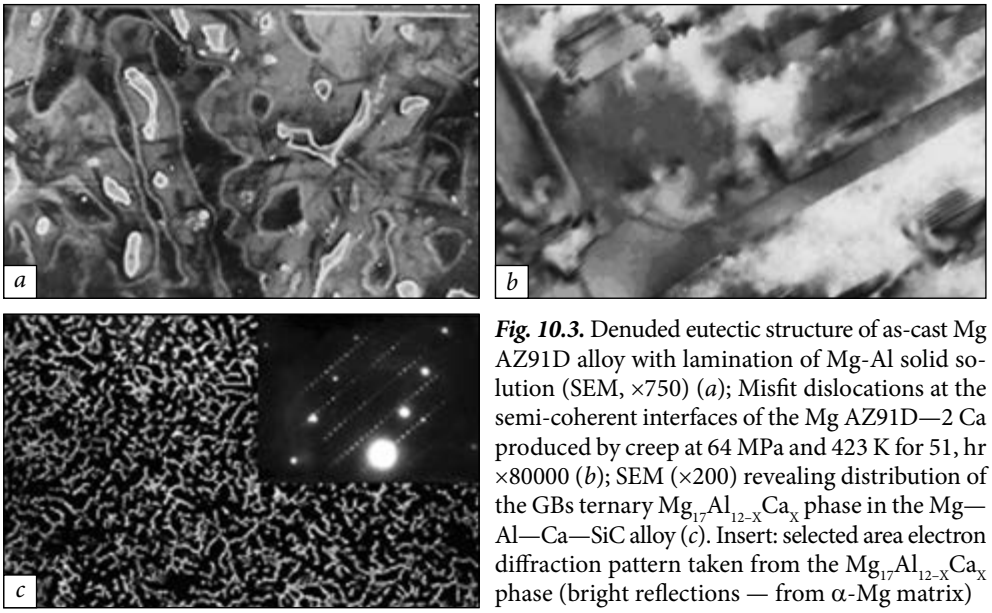

Fig. 10.3. Denuded eutectic structure of as-cast Mg AZ91D alloy with lamination of Mg-Al solid solution (SEM, ×750) (*a*); Misfit dislocations at the semi-coherent interfaces of the Mg AZ91D—2 Ca produced by creep at 64 MPa and 423 K for 51, hr ×80000 (*b*); SEM (×200) revealing distribution of the GBs ternary $Mg_{17}Al_{12-X}Ca_X$ phase in the Mg—Al—Ca—SiC alloy (*c*). Insert: selected area electron diffraction pattern taken from the $Mg_{17}Al_{12-X}Ca_X$ phase (bright reflections — from α-Mg matrix)

Commercial AZ91D alloy of the Mg—Al, Zn, Mn system is characterized with divorced eutectic and laminated Mg—Al solid solution (Fig. 10.3, *a*) and as consequence low creep strength at higher temperatures relative to Mg—Al—Ca alloys with a larger volume fraction of second component of eutectic (Fig. 10.3, *c*). Surface (misfit) dislocations surrounding the precipitates, although poorly resolved, are indicative of the partial coherency (Fig. 10.3, *b*). Replacement of the coherent interface of the metastable (ordered) phase by a partially coherent interface of the stable phase is expected to give rise to change in the mechanism of dislocation interaction, namely,

Table 10.2. **Lattice parameters of α-Mg and β-$Mg_{17}Al_{12}$ phases in magnesium alloys of eutectic origin**

Metal alloy system	α-Mg solid solution		β-$Mg_{17}Al_{12}$		Standards for verification
	a, nm	c, nm	a, nm	Volume fraction, vol%	
Mg—12.5Al	0.31650	0.51454	1.05463	25.5	hcp Mg: sp. gr. $P6_{3/mm}$
Mg—12.5Al—1.3Ca	0.31730	0.51574	1.05883	11.2	a = 0.32093 nm
Mg—12.5Al—1.4 Ca—0.3Mn–0.1Ti	0.31724	0.51546	1.05883	14.2	c = 0.52112 nm c/a = 1.62375 c/a = 1.633 (ideal value) [20, 21]
Mg—12.5Al—11.7 Sr—0.3Mn—0.1Ti	0.31735	0.51540	1.05633	11	$Mg_{17}Al_{12}$ (sp.gr. I–43m) with bcc lattice of α-Mn type:
Mg—12.5Al—1.3 Ca—0.3Y—0.1Gd	0.31715	0.51528	1.05892	18.75	a = 1.05438 nm [21, 22]

Distortion of the $Mg_{17}Al_{12}$ lattice parameters makes of about 1.1%.

from a cutting to by-pass (Orowan) mechanism. It can be seen that the advanced microstructure is characterized by a more uniform distribution of the $Mg_{17}Al_{12-X}Ca_X$ phase components with respect to conventional approach. Magnesium alloys of Mg—Al—Zn and Mg—Al—Mn systems are characterized by divorced eutectics. Increase in the strengthened β—$Mg_{17}Al_{12}$ volume fraction in magnesium alloys of the Mg—Al—Ca system (up to 18.8 vol%) seems to cause an additional (natural) eutectic strengthening (Table 10.3 and Fig. 10.3). It is noteworthy that the experimental magnesium alloys especially those containing small additions of Y and Gd are phase-stable at least up to 430 K (volume fraction of 18.8% at 293 K against 18% at 430 K for Mg—12.5Al—1.3Ca—0.3Y—0.1Gd alloy). It is not at all essential to examine in detail the observed dislocation structure in as-cast magnesium alloys following TEM observations methods of internal friction with mechanical spectroscopy and amplitude dependent damping involved.

General microstructural characterization of new experimental as-cast alloys X-ray measurements of lattice parameters presented in Table 10.3 indicate the presence of solid solutions in terms of α-Mg and β-$Mg_{17}Al_{12}$ structural components, as claimed by Massalski [338]. The data obtained are in a good agreement with the refined lattice parameters for hcp Mg and its alloys in systems Mg—Al and Mg—Al—Zn [339]. It is obvious that their lattice distortions are composition-dependent. It is very difficult to elucidate the physical nature of the solid solutions because of complexity of determining factors that contribute to mutual solubility of solute and solvent atoms without attracting the concepts concerning electron structure and relative valency rule. Nevertheless, there is a tendency to contraction of the distorted lattices for the both structural components (Table 10.3) thereby testifying to some interaction between solute and solvent atoms. In any case, the relative valency and chemical affinity seem to be important factors upon alloying magnesium with additions under investigation, as previously indicated [338]. Standard XRD analysis has revealed only two-phase structure of eutectic origin consisting of decaying α-Mg solid solution enriched with soluble AE as well as much more refractory β-$Mg_{17}Al_{12}$ strengthened by the same AE. Volume fraction of β-$Mg_{17}Al_{12}$ in new experimental magnesium alloys based on the Mg—12.5Al—1.3Ca matrix ranges 11.2-18.8 vol %, if amount of the additional AE such as Ti, Gd and Y does not exceed 0.1-0.3 mass% (Table 10.3).

Internal friction measurements

The internal friction of magnesium alloys under investigation was measured as a function of their chemical compositions based on the Mg—Al—Ca matrix. The results of the measurements are presented in Figs. 10.4-10.6.

Structural studies by mechanical spectroscopy (Fig. 10.4) yield a discrete temperature spectrum of internal friction with a broad inelastic maximum of relaxation origin, which may be decomposed into two main components produced by grain boundary (GB) relaxation [60, 116]. The first peak at 460 K is associated with GB

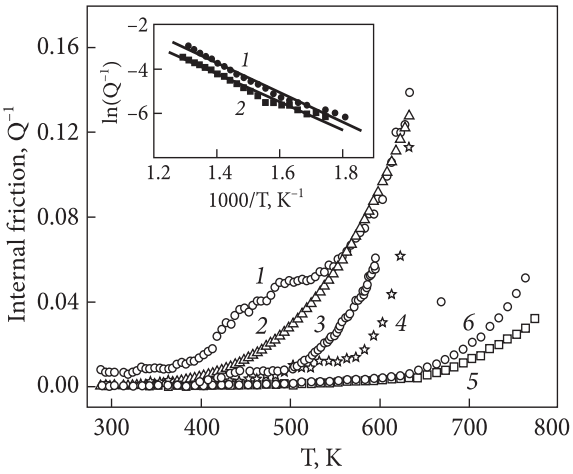

Fig. 10.4. Discrete temperature damping spectra of as-cast magnesium (99.96%) and its alloys investigated at low frequency vibrations of about *1* — Hz (1 cps): *1* — magnesium, *2* — Mg—2Ca, *3* — Mg—12.5Al, *4* — Mg—12.5Al—1.3Ca, 5 — Mg—4.9Al—0.28Mn—1.8 Sr, *6* — Mg—12.5Al—1.4Ca—0.28 Mn—0.1Ti. Insert: processing of the background-produced experimental data to evaluate the apparent a.e. U_a of the rate-controlling mechanism at higher temperatures: *1* — Mg—12.5Al—1.4Ca—0.28Mn—0.1Ti testified by U_a = 0.57 eV, *2* — Mg—4.9Al—0.28 Mn—1.8Sr testified by U_a = 0.54 eV

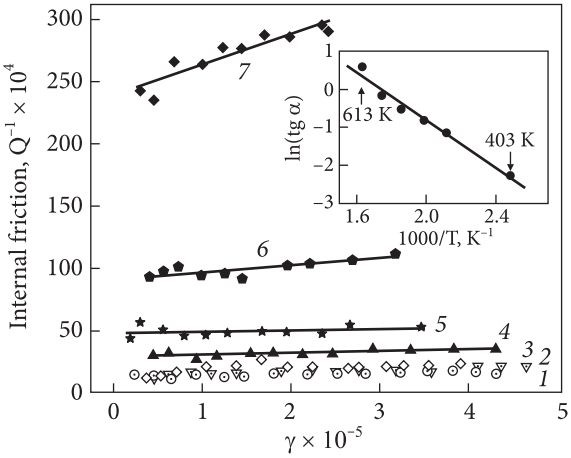

Fig. 10.5. Variation of internal friction with strain amplitude at different temperatures for Mg—12.5Al—1.4 Ca—0.28Mn—0.1Ti alloy: *1* — 293, *2* — 363, *3* — 403, *4* — 448, *5* — 503, *6* — 563, *7* — 633 K. Insert: linear relationship between the slope of ln(tg α) and reciprocal temperature for determining the dislocation-solute binding energy testified by E_b equal to 0.27 eV

dislocation-induced relaxation while the second one at 480 K is attributed to GB solute segregation-induced relaxation. The experimental profile and experimental points (around 460 K) of the broad maximum indicate that the same GB peak with a.e. of about 1.3 eV appeared as those already found at 458 K and 483 K for doubly sublimated hcp Mg of high purity and for conventional hcp Mg, respectively [339, 340].

The width of the GB maximum of $Q^{-1}(T)$ in the as-cast magnesium essentially exceeds its theoretical value by reason of the existence of inevitable impurities in hcp

Table 10.3. **Apparent background energy U_a as a function of alloy composition**

Alloy composition	Mg (99.96%)	Mg—1.5Ca	Mg—12.5 Al—1.3Ca	Mg—12.5Al—1.4 Ca—0.28Mn—0.1Ti	Mg—4.9Al—0.28 Mn—1.8Sr
U_a, eV	0.30	0.47	0.66	0.57	0.54

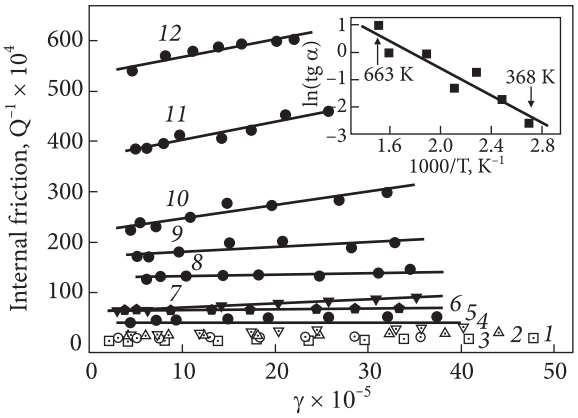

Fig. 10.6. Variation of internal friction with strain amplitude at different temperatures for Mg—4.9Al—0.28 Mn—1.8Sr alloy: *1* — 293, *2* — 368, *3* — 403, *4* — 438, *5* — 473, *6* — 503, *7* — 533, *8* — 583, *9* — 628, *10* — 663, *11* — 703, *12* — 733 K. Insert: linear relationship between the slope of ln(tg α) and reciprocal temperature for determining the dislocation-solute binding energy testified by E_b equal to 0.21 eV

Mg. We have noticed that their segregation at the GBs seems to cause additional GB segregation-induced relaxation at higher temperatures [161]. Therefore, the higher temperature 483 K-peak within the maximum of $Q^{-1}(T)$ seems to be a consequence of the influence of inevitable impurities such as solute hydrogen and oxygen [60, 116].

The effect of the GB segregation-induced inelastic relaxation to some extent masks the original GB dislocation-induced relaxation peak. Moreover, the existence of relaxation time spectrum and grain-size distribution, which are typical for any as-cast metal alloy system also changes intensity of the both original GB dislocation-induced relaxation and GB solute segregation-induced relaxation.

Detailed structure consisting of GBs dislocations is vitally important in understanding GB sliding and creep properties of the magnesium alloys studied. Some localized strain is apparent near the interface between the α-Mg and β-$Mg_{17}Al_{12}$ phases (Fig. 10.3, *b*). The evidence for GB sliding is derived principally from damping measurements (Fig. 10.4) according to the model of viscous sliding in analogy to the GB sliding suggested for polycrystalline fcc Al [341] intensity of GB dislocation-induced relaxation determined by density of GB dislocations [161, 341]. Introduction of calcium is succeeded by effective suppression of the both types of GB relaxation in magnesium alloys of the Mg—Ca and Mg—Al—Ca systems (Fig. 10.4, curves *1, 2, 3* and Table 10.3). The process is completed by blocking GB dislocations and GB strengthening because of thermal and stress-induced segregation of calcium on GBs.

It is significant that additions of Ti and Sr with negligible and limited solubility in hcp Mg, respectively, shift their transition points to the high-temperature background

Table 10.4. **Binding energy E_b as a function of alloy composition**

Alloy composition	Mg (99.96%)	Mg—12.5 Al—1.2Ca	Mg—12.5 Al—1.3Ca	Mg—12.5Al—1.4Ca—0.28Mn—0.1Ti	Mg—4.9Al—0.28 Mn—1.8Sr
E_b, eV	0.21	0.32	0.50	0.27	0.21

of internal friction (Fig. 10.4, curves *5* and *6*) demonstrating essential increase in thermal resistance (approximately by 393-433 K). Thus, their segregation on dislocations extends temperature ranges of existence of thermally stable microstructure.

The approach gives rise to elucidation of the physical nature of titanium beneficial effect, which is attributed to the occurrence of limited-mobility dislocations in the high-stress regime. These notions are supported by experimental observations including the ADIF measurements (Figs. 10.5 and 10.6), discrete temperature spectra change (Fig. 10.4), XRD analysis (Figs. 10.8-10.10) and repeated (serrated) yielding (Fig. 9.11).

Following the ADIF data (Figs. 10.4 and 10.5) for magnesium alloys containing 0.1% Ti and 1.8% Sr, the procedure reveals temperature of the Cottrell's atmosphere condensation on dislocations (T_0 ~ 453-473 K), which divides regions of the thermally activated pinning (at lower temperatures) and the thermally activated depinning of dislocations from the solute atmosphere (at higher temperatures). It is evident that pre-existing dislocations typical for as-cast structure have already been pinned upon rapid crystallization seeing that tgα ~ const at lower temperatures $T < T_0$ (Figs. 10.5, curves *1-4* and 10.6, curves *1-6*). In the lower temperature range where dislocation relaxation is the dominant rate-controlling mechanism, and time-dependent microdeformation is controlled by dislocation creep, microstructural changes in as-cast microstructure are succeeded by thermal stabilization of α-Mg solid solution upon additional alloying with Ti and Sr. It follows that Ti and other similar atoms (Table 10.4) interact preferentially with pre-existing dislocations with binding energy E_b which is large enough to maintain the dislocation atmospheres at temperatures lower than certain of the dense atmosphere condensation, T_0, different for various magnesium alloys.

This should be considered as indication of some limited dislocation activity due to pinning the dislocations by Cottrell's mechanism with formation of dislocation atmospheres. Jerky flow in Ti-containing magnesium is observed during tensile tests. With this provision, regular serrations are certain to occur in the temperatures range of 403-523 K. Microsegregation of the AE such as Ti and Sr occurs during rapid solidification and continues under cooling and even subsequent heat treatment by analogy with other nonequilibrium metal alloy systems with well-defined short-range order.

Thermally activated dislocation depinning is certain to occur with increasing temperature $T > T_0$ (Figs. 10.5, curves *5-7* and 10.6, curves *7-12*). The statement is supported by the increase in tga with increasing temperature. At higher temperatures $T > T_0$ the atmospheres begin to decompose by the depinning dislocation mechanism. In any case, for as-cast microstructure with decaying α–Mg solid solution, the apparent a.e. calculated from high-temperature Q^{-1} background data (Fig. 10.4, insert and Table 10.3) are in good agreement with the a.e. obtained for β-$Mg_{17}Al_{12}$ precipitation reaction at elevated temperatures [342, 343].

The principal part of the discussion is therefore concerned with the Q^{-1} (T) changes which occur during successive alloying with the additions under investigation. Detailed structure consisting of GB dislocations is vitally important in under-

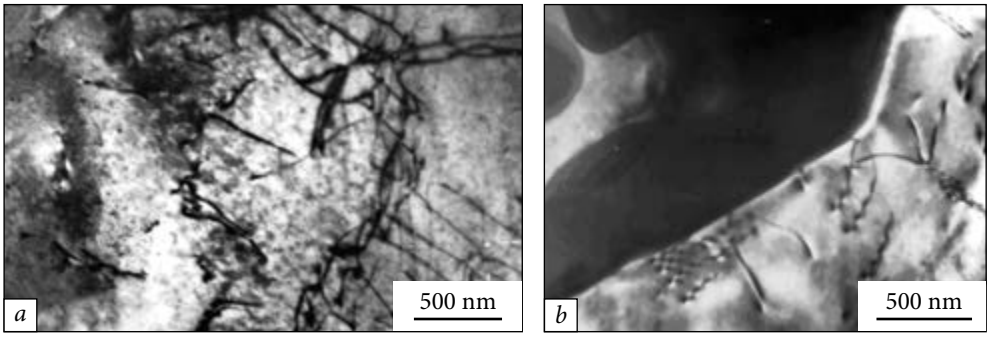

Fig. 10.7. Typical dislocation structures formed in the bulk α-Mg grain (*a*) and near the interface of the $Mg_{17}Al_6Ca_6$ phase (*b*) of as-cast alloy of Mg—Al—Ca system produced by rapid solidification technique

standing GB sliding and creep properties of the magnesium alloys studied. Some localized strain is apparent at the interface (Fig. 10.7, *b*). The evidence for GB sliding is derived principally from damping measurements (Fig. 10.4).

The experimental profile and experimental points (around 458 K) of the maximum in hcp Mg (Fig. 10.4, curve 1) seem to follow GB inelastic relaxation, which is very similar to that already found for the GB peak in doubly sublimated hcp Mg of high purity at 1 Hz [339]. The height of the GB Q^{-1} maximum is approximately proportional to the GB dislocation density. This maximum is thermally activated and characterized by the a.e. of 1.3 eV. GB contribution of the dislocations to GB sliding is totally suppressed in Mg—Ca alloy.

In the periodic literature [339, 340, 344, 345] discussion is essentially based on correlation between the GB relaxation and the intrinsic GB sliding. It has been previously shown that GB internal friction in hcp Zn resolved in two components is associated with diffusive motion of GB dislocations. A similar interpretation was used to explain the features of GB dislocation-induced relaxation and GB solute segregation-induced relaxation in hcp Mg (Fig. 10.4). Detailed considerations of the two mechanisms of damping are reported in other papers [340, 345]. The mechanism of extrinsic GB sliding discussed so far is consistent with the analysis of the GB relaxation phenomenon occurring along GBs and with the real origin of the new kind of GB relaxation observed (Fig. 10.4). It should be pointed out that the first broad Q^{1-} (T) maximum is overlapped by some small peaks of the dislocation origin, answering the description of Fig. 10.4 (curve 1) in internal friction measurements.

Following the data of mechanical spectroscopy [344], two GB peaks are found to be present in the temperature-dependent damping spectrum of the Mg-3%Ni alloy. First of them is ascribed to thermally activated dislocation relaxation, while second Q^{-1}(T) peak seems to be attributed to the GB solute relaxation.

Softening effect of grain boundary sliding in hcp Mg polycrystals arises in the stress-temperature ranges of interest for automotive applications. Furthermore,

precipitation from the saturated α-Mg solid solution is succeeded by deterioration of their properties during creep. These two main effects are the most likely to decrease creep resistance and long-term strength of magnesium alloys in the Mg—Al—Mn and Mg—Al—Zn systems. It is considered that in order to design for good creep resistance, the recovery and softening effects should be minimized. Poor creep resistance of hcp Mg is enhanced by increase in macroscopic sliding due to the existence of relaxing GB dislocations in Mg polycrystal. The apparent complexity of the grain boundary internal frictional maximum for hcp Mg (Fig. 10.4) seems to preclude a detailed description of the dissipation mechanism. Nonequilibrium grain boundaries provide a large number of excess dislocations for slip [346, 347]. GB dislocations and back stress were used to account for large stress-exponent n ≈ 2…5. Following the calculated data, the solutes in the GBs effectively retard the GB dislocation-induced relaxation (Fig. 10.4) thus significantly decreasing both the minimum creep rate and creep strain, as one should be expected.

Microchemistry-microstructure-property relationships

Before proceeding to presentation of the approach it should be pointed out that XRD data considered here are limited to the analytic potentiality of the XRD method, as is clearly shown in Figs. 10.8-10.10. In particular, some lines (for example, line of Ti at 38°, etc.) on the XRD patterns have disappeared (Figs. 10.9 and 10.10). In addition, the traces of another phase are observed as four lines with reflecting angles 30.6°; 34.8°; 37.7°; 38.3°. In some samples the 34.8° peak is imposed on the

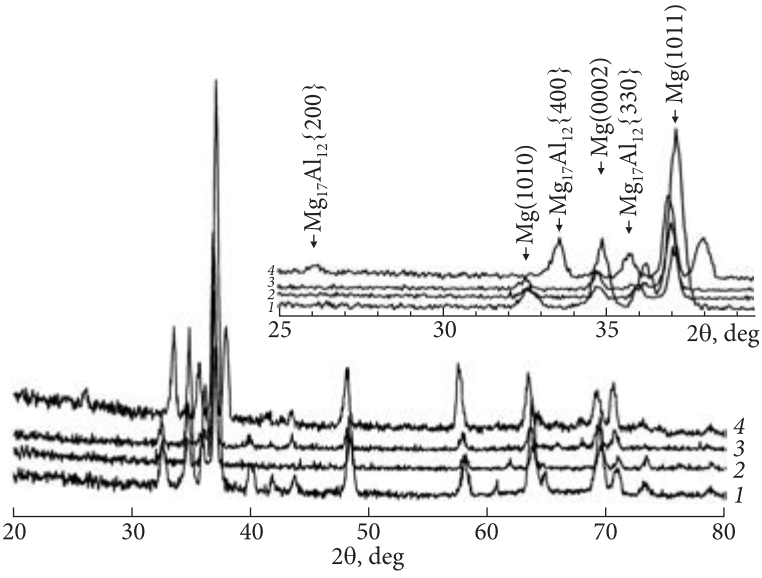

Fig. 10.8. XRD patterns in the relative intensity, % — 2Θ, deg coordinates for the Mg—12.5Al—1.4Ca—0.3Y alloy: (*1*) as-cast state (deformation-free head) and (*2, 3, 4*) after total creep strain 0.3% (*2* generatrix) 0.5% (*3* generatrix), and 0.5% (*4* neck) under tensile stress 70 MPa at 423 K

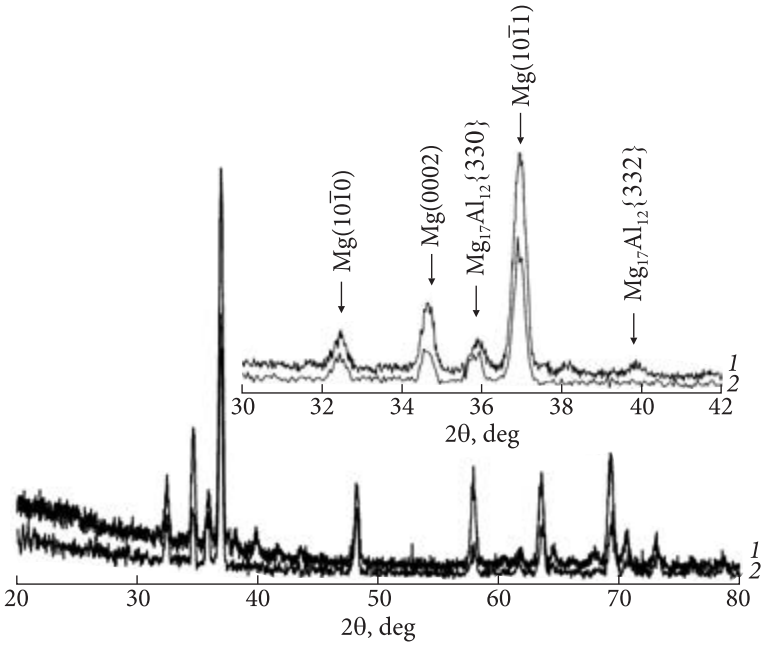

Fig. 10.9. XRD patterns of the Mg—12.5Al—1.4Ca—0.28Mn—0.1Ti alloy: (*1*) as-cast state (deformation-free head), (*2*) after total creep strain 0.37% under tensile stress 70 MPa at 423 K

(002) peak of hcp Mg lattice. These additional lines may be identified within the framework of hexagonal cell with a = 0.2770 nm and c = 1.6454 nm or of orthorombic cell with a = 0.2770 nm; b = 0.2921 nm; c = 1.4100 nm. In such a case, it is very difficult to carry out a thorough XRD analysis and to obtain exact structural determinations regarding the behavior of almost insoluble Ti in hcp Mg by analyzing XRD evidence only. In a word, we cannot detect decomposition of α-Mg solid solution at its early stages and to analyze behavior of small additions by reason of limited accuracy of XRD analysis. At the same time Q^{-1} experimental technique is capable of improvement in accuracy. In fact, the damping measurement (Figs. 10.4-10.8; Tables 10.3 and 10.4) is a true reflection of the observed behavior of magnesium alloys in the Mg—Al—Ca system containing small additions of Ti and Sr.

Using the precise XRD, the authors succeeded in obtaining the data on microstructure changes and progressive phase transformations arising during small creep strain at 423 K under tensile stress of 70 MPa for magnesium alloys in the Mg—Al—Ca—Y system. The idea of stress-induced strengthening is supported by XRD analysis of a microstructure after creep strain (Figs. 10.8-10.10). The observed Θ–2Θ XRD patterns of the Mg—12.5Al—1.4Ca alloy with addition of 0.3Y taken in the angle range $18° < 2\Theta < 80°$ from specimen in as-cast (unstrained) condition (*1*), after creep strain of 0.3% (*2*), in the region excluding necking as much as 0.5% (*3*), and in the neck after

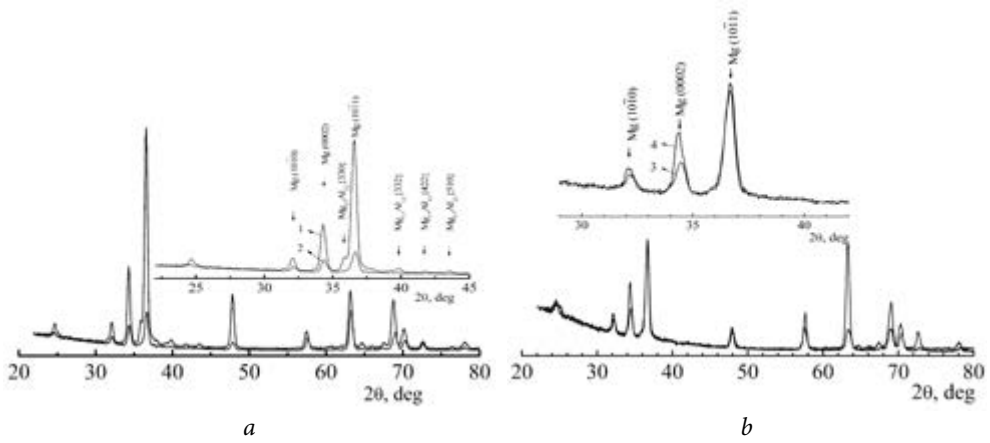

a *b*

Fig. 10.10. XRD patterns of the Mg—12.5Al—1.4Ca—0.28Mn—0.1Ti alloy: (*1*) as cast state (deformation-free head), (*2, 3*) after total creep strain accumulated during long-term test for 200 hr under tensile stress 70 MPa at 423 K (3 generatrix and 4 cross-section)

creep strain of 0.5% (4) are illustrated in Fig. 10.8. As seen from this figure (curves *1-3*), in case the creep strain does not exceed 0.4%, no change in its phase constitution and lattice distortion (dislocation) density appears to occur.

As a matter of fact, the authors observe actual coincidence of the diffraction angles for most reflections, slight redistribution of their observed intensity and insignificant change of their half-width as a measure of the physical state upon deformation. Undoubtedly, the stable behavior of the Mg—Al—Ca—Y alloy before its necking is supported by strong resemblance of X-ray lines for specimens in unstrained and creep strained conditions. By contrast, in case the necking occurs, the existent XRD peak positions are displaced and broadened and the new XRD pattern appears in the neck region (curve *4*, see arrows). Shifting of the diffraction lines ($1 \geq 2 \geq 3$) characterizes continuity of the stress-induced solid solution disintegration succeeded by phase transformation in critical point (*4*). This implies that the constant stress-induced creep at such a small isothermal strain (0.4% ε up to 200 hr) is controlled by saturation of dislocation density because of the preferential contribution of lattice distortions (stored energy). Its critical value is a criterion of plastic instability at 0.5% ε. According to the findings and notions, the widening of existent reflections testifies to dislocation density growth and stresses level increase while the displacement and appearance of new reflections testify to phase transformations [327, 328]. It is obvious that peak-broadening of all the lines and their shifts in XRD pattern (*4*) relative to ones (*1-3*) seems to interconnect not only with solid state phase transformation (essential change of phase composition), but also with increase in dislocation density during creep strain up to 0.5%. It can be seen that ever-increasing amount of stored energy because of lattice distortion broadening is accumulated upon deformation while no essential change in crystalline size broadening appears to occur at such a small creep strain. Hence, peak broadening is entirely due to lattice distortions.

Development of creep strain at 423 K and 70 MPa is succeeded by saturation of critical lattice distortion (dislocation density) under tensile loading and, as consequence, dynamically unstable decomposition of α-Mg solid solution to initiate the tensile-stressed disperse phase transformations. Especially it is very clearly seen in the neck region that the plastic instability arises from creep strain of 0.5% (Fig. 10.8, curve *4*). Thus, useful long-term strength is controlled by the critical time before building-up the neck under combined (three-axial) tension, which is responsible for starting of the accelerating stage of creep. In such a case, the stable microstructure of the magnesium alloy based on Mg—Al—Ca—Y system is destroyed because of creep strain which is localized due to the necking in plastic instability condition. Reflections of unknown phase under 2Θ–36° (curves *1, 2, 3* Fig. 10.8) and 2Θ–38° (curve *2,* Fig. 10.9) angles corresponding to the lattice spacings 0.247 and 0.237 nm, respectively, are observed. They fit neither α-Mg nor β-$Mg_{17}Al_{12}$ phase (Figs. 10.9-10.13).

The Mg—Al—Ca—Y and Mg—Al—Ca—Ti alloys exhibit significantly different behavior upon being creep strained. It is appropriate to compare the plot in Fig. 10.8 with ones shown in Figs. 10.9 and 10.10. XRD pattern of Mg—12.5Al—1.4Ca—0.28 Mn—0.1% Ti in as-cast state demonstrates the presence of many X-ray lines of small intensity, which may be connected to some insoluble quantities of second phase particles that are not observed after creep strain. It follows that the over-alloyable titanium atoms seem to be solved in α-Mg on the structural defects, namely dislocations, which could be chemically bound with solute atmospheres by Cottrell's hardening mechanism. In Fig. 10.9 XRD pattern shows additional X-ray lines (0002) and $(10\bar{1}\bar{1})$ near the reflection angles 2Θ-38° and 40°, respectively. They are likely to be caused by the presence of an additional phase as a result of over-alloying. It should be underlined that after strain the lines (0002) and $(10\bar{1}\bar{1})$ disappear by reason of the phase dissolution with increasing the strain-induced dislocation density. The results obtained are in a good agreement with the amplitude-dependent internal friction data (Fig. 10.5), which is in favor of pinning the dislocation structure with binding energy of about 0.3 eV (Table 3). Low dislocation mobility requires a higher driving stress for

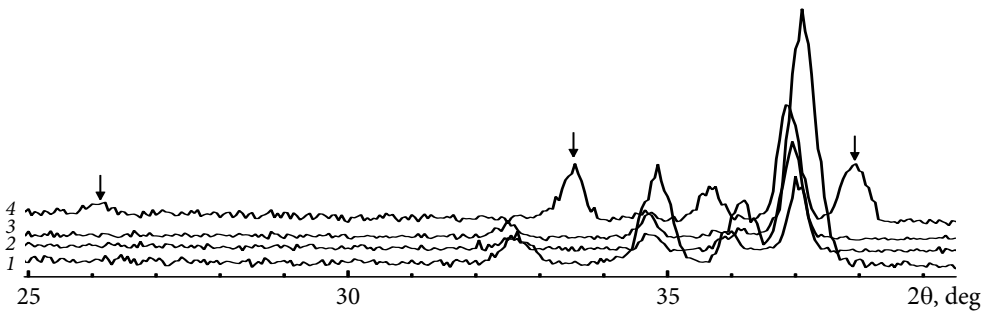

Fig. 10.11. XRD patterns in the relative intensity, % — 2θ, deg coordinates for the Mg—12.5Al—1.4 Ca—0.3Y alloy: (*1*) as cast state (deformation-free head) and (*2, 3, 4*) after total creep strain 0.3% (*2*, generatrix), 0.5 % (*3*, generatrix) and 0.5 % (*4*, neck) under tensile stress 70 MPa at 423 K

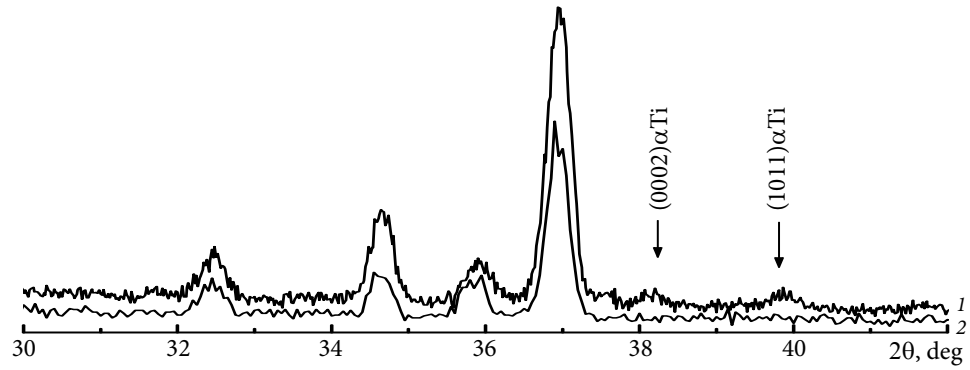

Fig. 10.12. XRD patterns of the Mg—12.5Al—1.4Ca—0.28Mn—0.1Ti alloy: *1* — as-cast state (deformation — free head); *2* — after total creep strain 0.37 % under stress 70 MPa at tensile 423 K

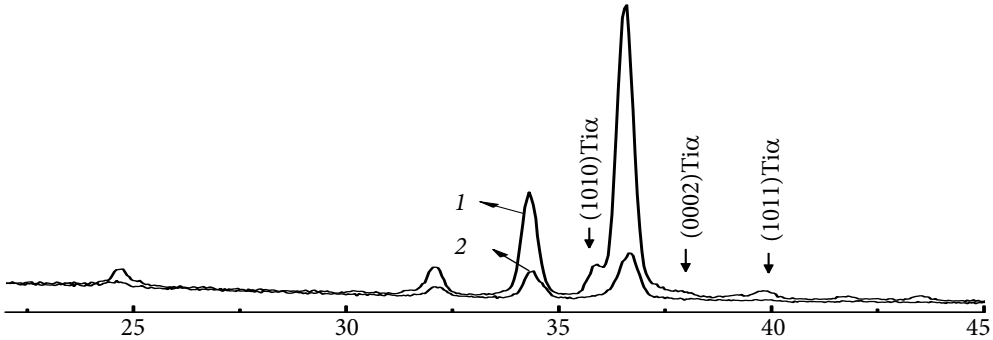

Fig. 10.13. XRD patterns of the Mg—12.5Al—1.4Ca—0.28Mn—0.1Ti alloy: *1* — as cast state (deformation-free head); *2, 3* — after total creep strain accumulated during long-term test for 200 hr under tensile stress 70 MPa at 423 K (*3*, generatrix and *4*, cross-section)

creep strain to occur without any phase transformations. Promising alloying elements such as titanium which possesses effective solubility on structural defects in α-Mg (Fig. 10.4, curves *6* and *3*) are capable of binding moving dislocations and thereby to play the role of traps delaying the formation of critical dislocation density during creep deformation as long as 200 hr. There is an evidence that jerky flow (Fig. 9.11) and other yield point phenomena trigger activation of the rate-controlling mechanism [348, 333]. In the course of tensile tests, serrations typical for the Portevin-Le Chatelier effect are observed in magnesium alloys containing Ti, Sr, and Gd additions at a stress rate of about 10^{-3} s^{-1}. The a.e. of the phenomenon which controls the appearance of the serrations is comparable to the vacancy migration energy (~0.8 eV), while the disappearance of serrations is similar to the self-diffusion energy (~1.35 eV).

It is noteworthy that jerky flow (the Portevin-Le Chatelier effect) occurs while introducing AE such as Ti and the like with large positive heat (enthalpy) of mixing, ΔH_m. For the Mg—Ti system ΔHm makes up 16 kJ/mole [349]. The measurable effect of jerky flow is determined by the serrations on the smooth curve $\sigma - \varepsilon$ at $\dot{\varepsilon}$ = const (Fig. 9.11).

Power creep law relation and thermally activated behavior

As well-known, temperature-dependent (Arrhenius) (Figs. 10.14 and 10.16) and stress-dependent (power law) steady state creep rate, $\dot{\varepsilon}_s$, is described by the following relationship:

$$\dot{\varepsilon}_s = A\sigma^n \exp(-Q_c / RT), \quad (10.8)$$

where Q_c is the a.e. for creep; n is the stress exponent; *A* is a constant. The parameters, *n* and Q_c, are related to the dominant (rate-controlling) mechanism of creep deformation, which depends on applied stress and temperature. Therefore, abrupt changes in Q_c and n may be found when changing the dominant creep mechanism. The experimental results of tests at 423 K for all stresses (up to 90 MPa) show a reasonable fit to a straight line with different stress exponents in the appropriate stress ranges (Fig. 10.14). According to [350], n is equal to 1...2 if diffusion creep is rate-controlling mechanism, n ~ 3 for some solid solutions and n ~ 4...5 for many other alloys and pure metals. It is thought that microdeformation mode below the macroscopic yield is controlled by dislocation creep [351]. Alloys of Mg—Al—Zn, Mg—Al—Ca and Mg—Al—Ca—Y exhibit a pronoun power law creep regime with no stress threshold to demonstrate solid solution strengthening for AZ91D ($\sigma \approx$ 20-60 MPa) and Mg—12.5 Al—1.4Ca alloy ($\sigma \approx$ 30-60 MPa) (Fig. 10.14, curves *1* and *2*). For Mg—12.5Al—1.5Ca—0.3Y alloy $\dot{\varepsilon}_s$ obeys the power low, $\dot{\varepsilon}_s \infty \sigma^n$, where n ≈ 6 (Fig. 10.14, curve *3*). Such values of the stress exponent are typical for high temperature dislocation creep mechanism accommodated most likely by solute diffusion of Y to the dislocations. Indeed, dislocations at the interface control creep resistance following the power law at higher temperatures [350].

Temperature dependence of the creep rate is shown by the Arrhenius plots in Fig. 10.14, curve *4*. The slope of the straight line relationship multiplied by K (gas constant) gives the apparent activation energy for creep, a.e. Q_c, to be equal of about 0.8 eV for the magnesium-based alloy of the Mg—Al—Ca system at 64 MPa. Unlike

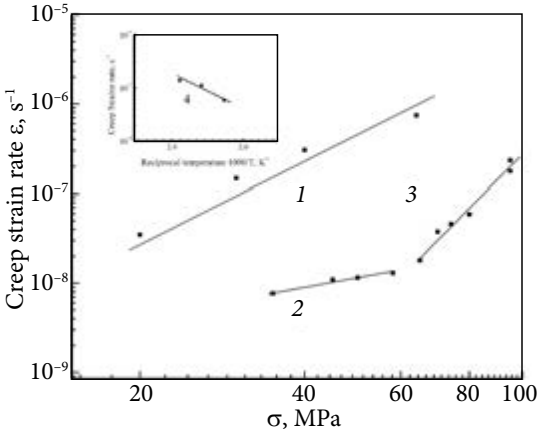

Fig. 10.14. Dependence of measured steady state creep strain rate on the applied stresses at 423 K (power law) for different magnesium-based alloys: AZ91D (Dow Chemical Corp., USA) (n ~ 3) (*1*), Mg—12.5 Al—1.4Ca (n ~ 2) (*2*), Mg—12.5Al—1.4 Ca—0.3Y (n ~ 6) (*3*). Insert: Arrhenius plots in the power low creep regime for Mg—12.5 Al—1.4Ca alloy with a.e. of 0.8 eV

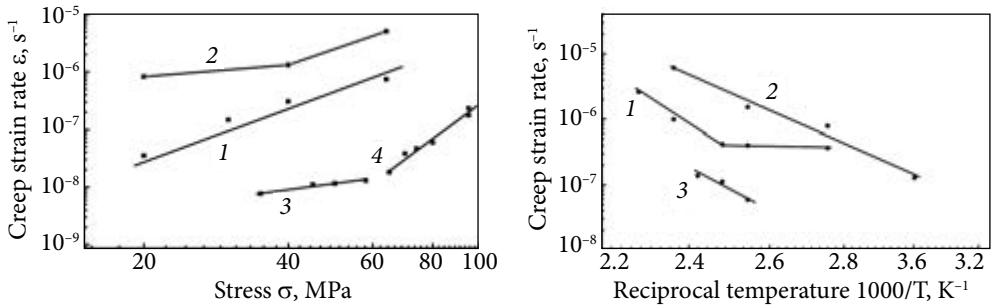

Fig. 10.15. Dependence of measured (steady state) creep strain rate on the applied stresses at 423 K (power law) for different magnesium-based alloys: AZ91D (Dow Chemical Corp., USA) (n ~ 3) (*1*); Mg—7% Ba model alloy (n_1 ~ 1 and n_2 ~ 3.2) (*2*); Mg—12.5Al—1.4Ca (n ~ 2) (*3*); *4* — Mg—12.5 Al—1.4Ca—0.3Y (n ~ 6) (*4*)

Fig. 10.16. Arrhenius plots in the power low creep regime for AZ91D alloy (*1*), Mg—7% Ba alloy model with the averaged a.e. 0.48 eV (*2*) and Mg—12.5Al—1.4Ca alloy with a.e. 0.7 eV (*3*)

Al, Mn and Zn, alloying with Ca as a slower-diffusing substitution element enhances contribution of the accommodated mechanism of GB-diffusion in segregated alloy (Fig. 10.14, curve *2*), thus increasing a.e. of diffusion from 0.3 to 0.4 eV (GB-self diffusion in hcp Mg) to 0.7-0.9 eV upon additional alloying with Ca. It is important that the value coincides with a.e. required for migration of vacancies. At larger stresses (60-90 MPa) (Fig. 10.14, curve *3*) creep strain rate for magnesium alloy of Mg—Al—Ca—Y system is the most likely to be controlled by bulk (lattice) dislocation climb (n = = 3-6). For reasons given, corrections to the chemical composition in the Mg—Al—Ca system was carried out to improve the solid solution strengthening and creep resistance of the magnesium alloys in terms of new ratio of Al to Ca [335] and additional alloying with promising elements such as Ti, Sr and Gd.

Creep resistance and long-term strength

Up to now, none of these experimental magnesium alloys with Ca addition has yet led to a commercially successful alloy. More work with the Mg—Al—Ca system is needed to optimize composition of the magnesium alloys containing Ca for die-casting. The Mg—Al—Ca system must be further investigated for optimum castability. However, in the range of investigated compositions and usual casting conditions Ca leads to an excessive hot-cracking and die-soldering especially in Mg—Al—Ca alloys containing small addition of Al and above 1 mass% Ca. Subsequent addition of 8 mass% Zn causes improving the die castability but the creep properties were found to vary over a wide range.

Unlike an AZ series of magnesium alloys with divorced eutectics (AZ91D etc.) (Figs. 10.15 and 10.16), alloys of the Mg—Al, Ca system with pre-precipitate (cluster-forming) structure near GBs and stable/hard precipitates of nanoparticles $Mg_{17}Al_{12-x}Ca_x$ at

GBs are expected to provide high creep resistance (at 423 K) and excellent creep fracture strength (50-70 MPa) (Fig. 10.17).

The great advantages of new experimental alloys were revealed during creep tests. As can be seen from Table 10.5 and Fig. 10.18, at 423 K under stress of 70 MPa they exhibit creep strain which grows significantly less than that of AZ91D and AE 42 magnesium alloys. Furthermore, their creep rate ($\acute{\varepsilon} \sim 10^{-9}$ s^{-1}) makes up the value which is by two order of magnitude less than that of AZ91D alloy ($\acute{\varepsilon} \sim 10^{-7}$ s^{-1}) at a much less value of creep stress, 35 MPa. It is considered that in order to design for good creep resistance, the recovery and softening effects should be minimized [352]. Shape of curves after tensile tests at r.t. and 423 K is found to be comparable with shape of creep curve at 423 K (Fig. 10.18). This indicates that creep strain in the new developed magnesium alloys based on the ternary Mg—Al—Ca system is accumulated exhibiting deformation strengthening without recovery.

The significantly higher creep properties of magnesium alloy containing inexpensive additions of Sr (1.8%), Gd (0.2%) and very small addition of Ti (0.1-0.2%) (Fig. 10.19; Tables 10.5 and 10.6) differ favorably from AE42 alloy containing expensive additions of 2-3% RE that provides $\varepsilon_{\Sigma} \sim 0.84\%$ for 200 h at 423 K / 70 MPa. Stress-

Table 10.5. **Creep strain rate at 423 K as a function of chemical composition**

Alloy composition (destination)	Creep strain rate $\acute{\varepsilon}_s$, s^{-1}	Creep strength, MPa	t, hr	Creep strain, ε, %
AZ91D (Dow Chemical Corp., USA)	10^{-7}	35 64	200 100	2.50 Fracture
Mg—12.5Al—1.3Ca	10^{-8}	64	200	0.35
Mg—12.5Al—1.3Ca—0.3Y	10^{-8}	70	48	0.40
Mg—12.5Al—1.3Ca—0.3Y—0.2Gd	1×10^{-9}	70	200	0.40
Mg—12.5Al—1.3Ca—0.3Mn—0.1Ti	1×10^{-9}	70	200	0.55
Mg—12.5Al—1.3Ca—0.3Mn—0.2Ti	1×10^{-9}	70	200	0.28

Table. 10.6. **Dislocation creep resistance and long-term strength of several RE-bearing magnesium alloys**

Alloy composition, mass%	Creep strain rate $\dot{\varepsilon}_s$, s^{-1}	Creep strength ε, MPa	*t*, hr	Required creep strain, ε, %
AZ91D (Dow Chemical Corp., USA)	10^{-7}	35 64	200 100	2.50 Fracture
Mg—12.5Al—1.3Ca	10^{-8}	64	200	0.35
Mg—12.5Al—1.4Ca—0.3Y	10^{-8}	70	48	0.40
Mg—12.5Al—1.3Ca—0.5Y—0.9Fe	4×10^{-9}	70	200	0.24
Mg—12.5Al—1.3Ca—0.3Y—0.5Fe	1×10^{-9}	70		0.21
Mg—12.5Al—1.3Ca—0.3Y—0.2Gd	1×10^{-9}	70	200	0.40

induced effective solubility of α-Ti atoms on dislocations causes effect of self-strengthening for the inexpensive Mg—12.5Al—1.4Ca—0.3Mn—0.1Ti alloy thereby improving its useful long-term strength during creep strain at 423 K. Under such conditions creep limit amounts to 70 MPa at creep strain no more than 0.5% and $\dot{\varepsilon}_s$ of about 10^{-9} s^{-1} during up to 200 h.

It is important to emphasize that long-term features exhibit some correlation between creep strain rate $\dot{\boldsymbol{\varepsilon}}_s$ and time to a given creep strain (Table 10.5, Figs. 10.14 and 10.18) for all alloys under investigation. Somehow or other $\dot{\varepsilon}_s$ level indicates their survival probability. We abandon the idea that one should not carry out all the cycle of creep testing (up to 200 hr) to save time and resources provided single rate-controlling mechanism to operate. The proximate analysis unambiguously displays source data as creep strain rate rather that time interval. It might therefore be expected that solute-induced dragging is the most probable rate-controlling mechanism responsible for delaying the dislocation activity at the 10^{-9} s^{-1} level. This assumption is supported by the appearance of regular serrations on the smooth curve during tensile test of magnesium alloy containing T_i addition (Fig. 9.11 and Table 10.5) as well as by dislocation damping investigations (Figs. 10.5 and 10.6).

10.2.5. Comparable Data Analysis

It is considered that the attractive magnesium alloy compositions containing cheap elements with negligible mutual solubility with respect to α-Mg cannot be produced using conventional ingot metallurgy due to excessive alloying element segregations and the formation of coarse equilibrium constituent particles which degrade mechanical properties. A further problem in the casting process is the structural and chemical inhomogeneity of the engineering material which limits its use as a dimensional stability product. Preliminary studies indicate that novel magnesium alloys should be synthesized with unique combinations of microstructure and properties using rapid solidification rate up to 373 $K \cdot s^{-1}$.

Conventional alloys, for example, of Mg—Al, Zn, Mn (trademark AZ91D, etc.) derive their high strength at r.t. from the solid solution or the precipitation mode of

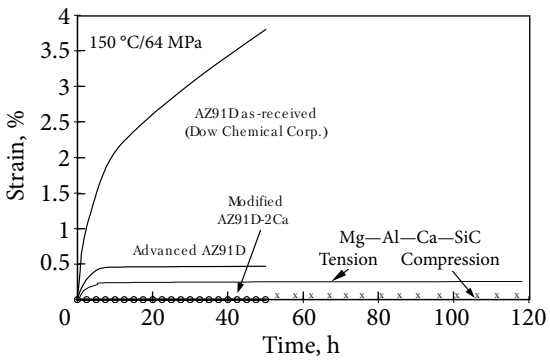

Fig. 10.17. Summarized creep data for as-cast Mg AZ91D alloy and magnesium matrix composite material of the Mg—Al—Ca—SiC casting system at constant creep temperature and constant creep strength

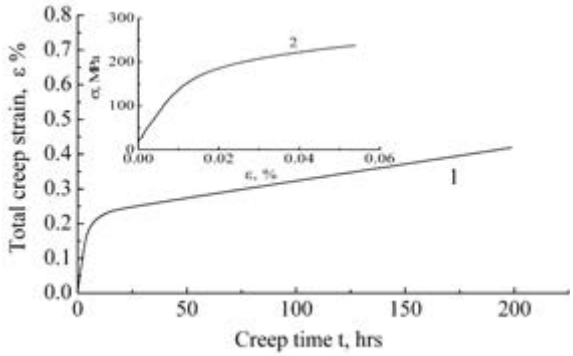

Fig. 10.18. Short-range and long-term properties of the newly developed magnesium-based alloy Mg—12.5Al—1.4Ca—0.3Y—0.2Gd: creep curve at 423 K / 70 MPa for 200 hr (*1*), typical tensile strain-stress curve at 293 K (*2*)

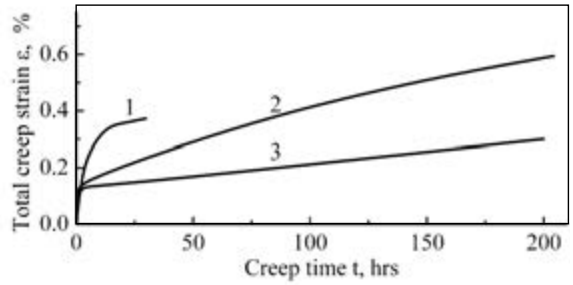

Fig. 10.19. Creep curves for magnesium alloys containing titanium: Mg—12.5Al—1.4Ca—0.3Y—0.07Ti (*1*), Mg—12.5Al—1.4Ca—0.28Mn—0.1Ti (*2*), and Mg-12.5Al—1 .3Ca—0.4Mn—0.2Ti (*3*)

dispersion strengthening, however lose much of their long-term strength and creep resistance when exposed to temperatures above 393 K. Moreover, conventional melting and casting techniques are unsuitable for making dispersion-strengthened materials because the disparity in density between matrix metal and dispersoid leads to segregation in the melt.

One of the problems associated with using precipitation/dispersion strengthening by Orowan loop and bypass-mechanism results from the difficulty in producing a dispersion of small, hard, closely-spaced incoherent particles on the base of employing normal ingot casting procedure. The inherently slow ingot solidification rates enhance the precipitation of coarse particles which lower ductility and fracture toughness with increasing particle size when the volume fraction is constant. Another problem is embrittlement which accompanies this strengthening method.

It stands to reason that additional alloying of the commercially available Mg—Al, Zn, Mn system by strengthening additions of calcium in combination with clustering a structure whose strengthening clusterization of the structure of the extended near GB solid solution by the assembly mechanism demonstrates further increase in the creep resistance for the commercial grade Mg AZ91D produced by the rapid solidification technique.

Superimposing of electronic field improves the macro- and microstructure of well-known magnesium alloys differing in lamination of solid solutions, liquation, and other compositional or structural defects [353]. Its modifying effect is due to the increase in the centers of forced crystallization and impediment of linear rate of crystallization. This results in essential refinement and enhancement of homogeneity of the solidified structure with a lower level of anisotropic properties.

Considerable experimental effort over the world is being expended on developing long-term strength structural magnesium alloys containing, as a rule, light ele-

ments to operate in the transport (automobile, powertrain) industry at higher useful temperature and larger stresses. By using computer modeling, TEM, SEM, XRD, Auger-electron and mechanical spectroscopy as well as all-the-round creep tests, structural and thermoactivation analyses were carried out to account for the fundamental characteristics of creep-resistant materials and to analyze the rate-controlling mechanisms responsible for temperature dependence of their pre-yielding and strengthening. To compensate the useful RE-effect in expensive prototypes, a family of cheaper magnesium alloys in the Mg—Al—Ca, X system were developed for higher temperature dynamical applications. Of the main interest in magnesium for the automotive and aeronautic industries is its low density compared with aluminum and steel, which can reduce vehicle weight and fuel consumption. Mg—Al based alloys (AZ or AM alloys) have been used widely as die casting alloys and have been considered as wrought magnesium alloys. They exhibit good castability and have reasonable room temperature mechanical properties and corrosion resistance in many environments. However Mg—Al based alloys have poor high temperature creep resistance, which is believed to be associated with the GB (discontinuous) precipitation of the β-phase ($Mg_{17}Al_{12}$). To overcome and minimize the deterioration of high temperature physical properties, Mg-Sn based alloy systems have been actively investigated in order to develop new magnesium alloys which have stable microstructure and good mechanical properties such as high creep and corrosion resistance at high temperatures. In addition, Sn is a reasonably cheap alloying element compared with other alloying elements like RE. Although magnesium-based materials have a long history of important commercial applications, including automotive industry, there remains much to be learned about the basic properties of the metal and its alloys. With the recent renewed interest in light wrought materials, including both sheet and tube applications, there has been an increased focus on developing a better understanding of novel magnesium alloys, including those that incorporate additions of Mn and Al. These alloy systems, along with other potential candidates, are being actively pursued as possible routes to develop magnesium materials with improved ductility, or even practical room temperature formability [354]. The properties of cast or wrought material depend first and foremost on the phases and microstructural constituents (eutectics, precipitates, solid solutions, etc.) which are present. In an alloy with several alloying elements, the phase relationships are very complex.

Metallographic structure of the cast Mg AZ91D consists of α-magnesium grain columns surrounded by a continuous GB network of Al, Zn-enriched phase. The furnace cooling also results in a coarse distribution of continuous GB film, which is expected to be predominantly $Mg_{17}Al_{12}$ phase, with average interparticle spacing to be 100 μm.

Difference in phase morphology results from the different cooling rates during melting and heat treatment of cast ingots. Optical micrographs show changes in phase size and its distribution in quenched and heat-treated materials. As expected, a very rapid cooling from the solution temperature produced a very finely dispersed phase distribution with average particle spacing to 1-3 μm. The effect of the heat

treatment on creep behavior of the cast Mg AZ91D with coarse structure was studied in specimens which were cooled from solution treatment at 673 K, 1 hr by water-quenching and then were aged at 443 K, 12 hr. It was found that quenching produces grain refinement (from 100 μm to 20 μm) and changes the particles size and their morphology. Besides, heat treatment of the cast Mg AZ91D destroys the GB phase continuity, as could be expected from the theory of enhanced diffusion through GBs for the diffusion-controlled precipitation. Indeed, there is an experimental evidence suggesting that significant phase refinement and redistribution occur in Mg AZ91D alloy following such a thermal treatment.

The metallographic structure of the cast Mg AZ91D consists of α-magnesium grain columns surrounded by a continuous GB network of Al, Zn-enriched phase (Figs. 4, *a* and 5, *a*). The furnace cooling also results in a coarse distribution of continuous GB film, which is expected to be predominantly $Mg_{17}Al_{12}$ phase, with an average interparticle spacing of 100 μm (Fig. 5, *a*).

The industrial and commercially available AZ91D alloy has sufficient strength at ambient temperature and corrosion resistance to be employed for some components of cars. However, its use is restricted to conditions less than 400 K because of low creep resistance. Therefore, searching for a combination of additional alloying elements of the modified magnesium alloy systems is needed to provide sufficient creep resistance in the 473-573 K range and to use the potential materials for applications such as engine blocks and other areas of high service load conditions. One approach is to add calcium and thereby to increase the creep resistance. The second approach is to carry out remelting using pulsed treatment for better corrosion resistance. There is a pronounced effect of the electromagnetic oscillations on the melt interfaces to exceed the rate of chemical reactions for additional attaining higher creep resistance and long-term strength which depend on the cluster-forming composition and solidification conditions [353].

High magnification TEM examination of the phase reveals that there is noticeable change in its structure after quenching at 673 K, 1hr. The smooth interface becomes cusped and irregular. The heat treatment leads to gradual breaking up of the Al, Zn-enriched phase with a distinctive separation into fine rounded grains.

The activity of non-based slip systems plays an important role in the deformation behavior of magnesium alloys and their MMCs [355]. Different reactions between ā based dislocations and (c + a) pyramidal dislocations appear to be responsible for the increase in density of forest dislocations.

Choice of chemical compositions and melting parameters should be considered in the context of physical metallurgy dividing design of alloys and melting technology. It is the compositions that predetermine the melting technology which involves the cooling rate, constitutional supercooling, temperature gradient, etc. Much effort has been undertaken to lower the production cost of structural parts fabricated from magnesium alloys having intricate shapes, especially for high-performance applications (e.g., aircraf**t).** The saving of magnesium materials as well as machining cost is

believed to reduce the total cost of the magnesium parts significantly provided of sufficient quantities to be produced.

In purified crystals of magnesium, the strong GB sliding is observed at higher temperatures, while deformation twinning at lower temperatures. The multicomponent Mg—Al—Ca—Ti/Gd system is one of the most thoroughly studied systems in our laboratory to compare it with theoretical calculations. Its suitable composition is just chosen to suppress GB sliding and deformation twinning and thereby to maximize the excess vacancy concentration in the hcp crystalline lattice.

Using the principles of rapid solidification technique, a family of new experimental magnesium alloys of the ternary Mg—Al—Ca system has been developed which meets the technical assignments of the contract (creep strain ≤0.4% at 423 K, 70 MPa for 200 hr), first of all, due to know-how ratio of Al to Ca and excellent castability. The research has shown that the creep-resistant and long-term strength magnesium alloys with know-how addition of Ti and Sr are among the most promising ones of the family not only due to their potential as good heat-resistant systems but also due to their α-Mg matrix strengthened by the GB tertiaries of $Mg_{17}Al_6Ca_6$ and large volume fraction of eutectic compound β-$Mg_{17}Al_{12}$ enriched with more refractory alloying elements (Ca, Ti, Sr, etc.).

The best of them were subjected to rough examination and relevant processing technique via tensile and creep testing to evaluate their potential for high temperature applications in automobile industry. The effect of additional alloying with Ti, Sr and Gd on the effective diffusivity of the Mg—Al—Ca matrix is thought to be the cause for the improvement of creep resistance and long-term strength of the magnesium-based alloys under investigations. The dominant (rate-controlling) mechanisms of creep deformation operative in the stress-temperature regime tested were determined using stress and temperature dependences of the measured creep strain rates. The stress transition from dominant power law creep to dominant diffusional creep was found to occur in the range dividing processes of pinning and depinning dislocation network. The a.e. for the power law regime was close to that of GBs precipitation of disperse (nanosized) particles of binary compound $Mg_{17}Al_{12}$ and tertiary compound $Mg_{17}Al_6Ca_6$. At the same time, a.e. for the diffusion (Coble) creep regime was close to that of GBs self-diffusion in α-Mg. A detail characterization of their fine microstructure was conducted by using TEM, SEM/EDS and APMA analytical approaches, XRD and other up-to-date techniques. Under the data of mechanical spectroscopy, it was found that magnesium alloys containing additions of Ti and Sr appear to be the most thermally stable systems (up to 473-523 K).

TEM/SEM observations as well as XRD analysis of the microstructure before and after creep testing revealed the main features of the best alloys which are attributed to the favorable changes in the GB microstructure with desirable engineering properties for structural applications. A physics-based constitutive model of dislocation creep retardation is suggested on the basis of the structural-energy efficiency concept of useful long-term strength valid for metal alloy systems. It takes account of physical defect ki-

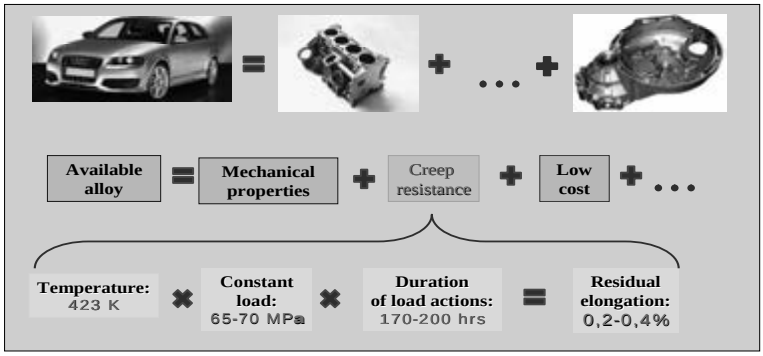

Fig. 10.20. Up-to-date requirements for magnesium alloys destined for mass production in automobile industry

netics, i.e., rate change and dislocation dragging by solute atmospheres consisting of slower diffusing refractory AE with special thermodynamic properties. The approach gives rise to elucidation of the physical nature of titanium beneficial effect, which is attributed to the occurrence of limited-mobility dislocations in the high-stress regime. These notions are supported by experimental observations including the ADIF measurements (Figs. 10.5 and 10.6), discrete temperature spectrum change (Fig. 10.4), XRD evidence analysis (Figs. 10.8-10.13) and repeated (serrated) yielding (Fig. 5.7).

Any die-casting process is succeeded by rapid solidification of magnesium melt, the rate of which varies within the limit of 313…333…373 $K \cdot s^{-1}$. The relevant dislocation structure to be formed in as-cast condition can be expected to interact only with the fast-acting alloying elements which are able to trap the dislocations in the nonequilibrium conditions of crystallization. An original idea is to select those of them which will be able to inhibit the initiation of critical dislocation density responsible for deterioration of creep properties at higher temperatures and thereby to enhance the contribution of the refractory metal diffusion responsible for increase in heat resistance. It is those alloying elements such as Ti, Gd and Sr that can do this having negligible or low lattice solubility in hcp magnesium (a-Mg) at elevated temperatures. As the AEs exhibit high sensitivity to high-rate treatment, they can be expected to increase effective solubility (on structural defects) thereby extending limit of their solubility. This effect is succeeded by essential pinning of moving dislocations with solute atmospheres by the Cottrell hardening mechanism [348]. Its activation in the stress field should minimize solute effects on increase in creep resistance and long-term strength up to 70 MPa at 423 K for 200 hr with slow creep rate 10^{-9} s^{-1}. It is considered [352] that magnesium alloys of Mg—Al—Ca system suffer from creep caused by both dissolution-diffusion change and thermal decomposition. However, new information provided for multicomponent (quaternary) Mg—Al—Ca—Ti and Mg—Al—Ca—Sr systems forms a strong basis for magnesium alloy design concept based on preferential contribution of stress-induced decomposition and stress-in-

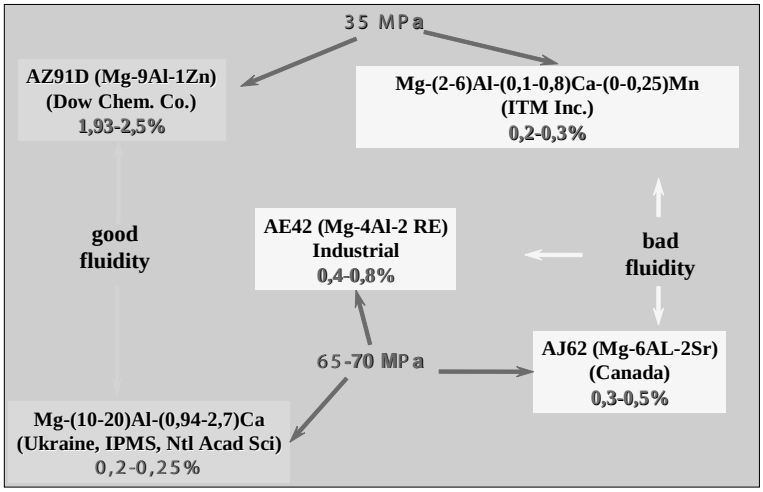

Fig.10.21. Comparative characteristics of magnesium alloys at 423 K for 200 hr

duced diffusion-controlled reactions to occur during long-term creep testing (Figs. 10.4, 10.8-10.10, 10.16-10.19). In this case, AE dissolution occurs on the structural defects such as dislocations. As such, solute atmosphere dragging becomes a rate-controlling mechanism responsible for improvement of creep properties and heat resistance (Figs. 10.4, 10.15-10.19) based on Cottrell hardening (Figs. 10.5, 10.6, 9.11). The idea of self-strengthening is supported by XRD analysis of the microstructure after creep strain at 423 K/70 MPa (Figs. 10.8-10.10).

To summarize the above the main advantages of the newly developed experimental magnesium alloys are reduced to the following:

1. *Castability* is considered to be the main critical property of any die-casting alloy. Higher castability (up to 30%) and good melt handling of the newly developed Al-rich magnesium alloys compared to the commercial alloys AZ91D, AE42 and AS21 is insured by new ratio of Al/Ca which has been patented. Due to Al-rich compositions, the magnesium alloys studied are intended to parts which are very difficult to cast.

2. *Higher creep resistance and long-term strength.* The newly developed magnesium alloys of Mg—Al—Ca—Ti and Mg—Al—Sr—Ca—Ti and Mg—Al—Ca—Y—Gd systems are found to have the best combination of room and creep temperature properties revealed by successful short-range and long-term range tensile testing at 64...70 MPa and 423-448 K. Their appropriate compositions covered by patent pending due to basic matrix Mg—Al—Ca patented in Ukraine. The creep properties at 403-423 K under stress of 50-70 MPa are significantly better than those of the commercial alloys AZ91D, AE42 and AS21 (Figs. 10.20 and 10.21). Unlike the AZ series of magnesium alloys with divorced eutectics (AZ91D, etc.), the new experimental magnesium-based alloys containing cheaper additions exhibit higher creep and heat resistance as well as better long-term strength compared to magnesium alloys AS21

(Mg—2Al—1.5Si), and AE42 (Mg—4Al—2.5RE) containing expensive additions, in the temperature and stress ranges of interest for automobile applications.

3. *Longer life creep strength* of Mg—12.5Al—1.3Ca basic matrix is found to be 64 MPa. The creep strength is increased up to 70 MPa upon its alloying with small additions of Ti et al. The new family of creep-resistant and long-term strength materials presents a cost-efficient system capable to operate at 70 MPa / 423 K for 150-200 hr with allowance of total creep strain 0.2...0.6%.

Concluding Remarks

A microanalytical characterization of cast magnesium alloys of eutectic origin based on the Mg–Al–Ca ternary matrix system has been carried out in order to investigate the influence of alloying elements on their microstructure as well as microchemistry-processing-microstructural relations using structure-sensitive techniques of electron microscopy, mechanical spectroscopy (internal friction), XRD and advanced microanalytical methods including the electron probe compositional analysis. Following the data obtained, there has been established a direct correlation of microstructure with creep properties of the new experimental magnesium alloys. The creep and heat-induced properties of the multicomponent magnesium alloys containing low range of inexpensive additions of titanium (0.07-0.2%) or strontium (of about 1.8%) are defined by resulting structure dynamically formed during creep strain (up to 200 hr). It is noteworthy that Ti as a novel alloying element competes for creep resistance and cost with Sr and attracts as-cast desirable properties minimizing solute effects at ambient temperatures due to the pinning of slowly moving dislocations with the binding energy no more than 0.3 eV as well as due to stress-induced strengthening. The Ti and Sr solute atmosphere dragging is believed to be the rate-controlling mechanism responsible for radical improvement of creep resistance and long-term strength in the newly developed magnesium alloys at elevated temperatures. The new alloys are superior to commercial alloys AZ91D, AE42 and AS21 following their creep resistance, long-term strength, heat resistance, and castability because of their novel microstructure having desirable engineering properties for structural applications (creep strain e_c below 0.3-0.4% at 423 K and 70 MPa for 200 hr; $\dot{\varepsilon}_s \sim 10^{-9}$ s^{-1}). The newly developed magnesium alloys with improved castability may be used in die-casting technology and automobile (powertrain) industry for manufacturing components which are difficult to cast with desirable microstructure.

The basic conclusions to be drawn from the results obtained may be stated as follows:

• following the data of internal friction measurements, the introduction of Ca is found to suppress GB relaxation and to promote the GB strengthening of magnesium alloys in the ternary Mg—Al—Ca system. Increasing the Al content to 12.5 mass% and to fractional increase of Ca content leads to doubling the volume fraction of second eutectic component β-$Mg_{17}Al_{12}$ to be strengthened. Lattice distortions in the

both α-Mg solid solution and β-$Mg_{17}Al_{12}$ are composition-dependent. Such a structure enhances contribution of natural eutectic strengthening;

• XRD studies reveal the structural and phase transformations that arise during long-term creep testing in the neck of a specimen; the critical residual micro-strain is found to be responsible for the localized necking which should be regarded as physical limitation of useful long-term strength of magnesium alloys in the Mg—Al—Ca—Y system;

• introduction of small additions of Ti (about 0.1-0.2%) and large amount of Sr (up to 1.8%) into the basic melt causes significant solid solution strengthening due to pinning of slowly moving dislocations by the solute atmosphere mechanism with binding energy of about 0.2-0.3 eV. Titanium having a large positive enthalpy of mixing is introduced in the matrix for the first time using processing technique of rapid quench (up to 373 K/s) from high-temperature solid phase;

• following the internal friction measurements, the alloying of the Mg—Al—Ca basic matrix with more refractory additions, such as Ti and Sr, extends the temperature range of their interaction with pre-existing dislocations increasing high-temperature strength of the Mg—12.5Al—1.3Ca—0.3Mn—0.1Ti and Mg—4.9Al—0.3Mn—1.8Sr alloys by 393-533 K due to the formation of phase and thermally stable structure;

• it is deduced that resulting dynamic structure formed during creep straining appears to be responsible for improvement of the observed creep resistance and long-term strength due to thermally activated dislocation relaxation accommodated by diffusion of alloying elements (Al, Ca, Ti, Gd, Sr in their best combination);

• an excellent increase in creep resistance and long-term strength at higher temperatures and larger stresses (70 MPa at 423 K) is provided by solute-induced dynamic dragging (retardation) of dislocations moving at $\dot{\varepsilon}_s \sim 10^{-9}$ s^{-1}. The finding is in agreement with the Le Chatelier-Braun principle of mobile equilibrium;

• the physicochemical principles of precision (at segregation-energy level) alloying are suggested for so-called immiscible systems with a large positive heat of mixing and high sensitivity of the selected refractory alloying elements (Ti, Gd, Sr) to high-rate treatment to get their effective solubility on structural defects such as dislocations. From this point of view, three of the most promising alloys designated as UKOR-C1 (Mg—12.5Al—1.3Ca—0.3Mn—0.1Ti), UKOR-C2 (Mg—12.5Al—1.7Sr—0.3Mn—0.1Ti), and Mg—12.5Al—1.4Ca—0.3Y—0.2Gd (UKOR-C3) having excellent short-range mechanical properties (157-174 TYS, MPa; 239-268 UTS, MPa at r.t. and 153-206 MPa at 423 K; true fracture stress 240-265…292 MPa at r.t. and 229 at 423 K; 4.8 elong., % and 6.7 Red. A. at F., %) can be selected for upscale production and further investigation to subject them to detail examination for the die-castability, fluidity (die filling), sticking in die, susceptibility to hot cracking and porosity formation. Titanium as a know-how alloying element is competitively capable to strontium and provides desirable properties changing solid-solution effects at ambient temperatures and increasing heat resistance.

Chapter

11 NANOPHASE STRENGTHENING OF HEXAGONAL METAL ALLOY CRYSTALS

11.1. Premises

Elevated-temperature magnesium, aluminum, titanium and zirconium-based alloys have received considerable interest with regard to the beneficial properties and major advantages, which are very attractive for wider and more reliable applications of them as structural materials in the industry [356-359]. In recent years, much progress has been made in the alloy development programs which produce their best-elevated temperature properties [356, 360, 361] for different dynamic applications in construction modules and high-speed rotating systems where excellent creep resistance to time-dependent deformation, long-term strength, high stiffness, low moment of inertia and dimensional stability are essential and still required. Much efforts of international scale are being expended to lower costs in the technologically much demanded aircraft, automobile and nuclear industries. Traditionally, the strengthened states of high-temperature alloys are achieved by the formation of a structure preventing the motion of dislocations by the precipitation or age-hardening mechanism. With this provision, their strength behavior may be essentially improved due to the nucleation and uniform distribution of the desired quantity of coherent nanoparticles. However, the suitable alloys produced by conventional metallurgy approach cause a series of problems associated with the deterioration of their properties with increasing temperature. To illustrate, harmful precipitate free zones adjacent to GBs of polycrystals contribute to the stain localization effects and premature fracture of their inhomogeneous structure. The upper operating temperature of conventional creep-resistant alloys strengthened by a known precipitation hardening mechanism is sure to be restricted to the limiting temperature above which they no longer exhibit useful long-term strength due to dissolving or coarsening nanoparticles in the matrix. For example, their use for automotive applications is limited by the rapid shear failure due to the localization of macro-

scopic plastic flow and shear band formation. Besides, the obtainable results in the case are often limited by the dissolution capacity of matrices for alloying elements. Furthermore, up to now, it is basically difficult or practically impossible to introduce non-metallic dispersoids in substantial amounts by alloyage and heat treatment typical for the above systems. Finally, this is of particular concern for so-called immiscible metal alloy systems.

Nanophase alloys and nanocomposites made of them represent a brood class of materials in which the matrix is reinforced by certain volume fraction of incoherent nanoparticles. Dispersion or nanophase strengthening has great potential for increasing the temperature capabilities, e.g., of Al-based alloys containing dispersoids such as nm Al_2O_3 and nm Al_4C_3 with extremely high stress sensitivity ($n \approx 200$) at elevated temperatures. It is also related to superalloys strengthened by nm Y_2O_3 dispersoids, which combine dispersion and precipitation hardening. They are most promising metallic high temperature materials with negligible GB sliding due to highly elongated coarse grain structure [362]. The development of advanced nanophase materials based on alloys in the metallic systems has become increasingly attractive in recent years. However, the effectiveness of high-temperature strengthening increment by a conventional age-hardening mechanism is lost at temperatures approaching the solvus temperature. Alternatively, the nanophase strengthening has emerged as a means to overcome some shortcomings inherent to the age-hardening technique. Metal matrix nanocomposites is a promising class of structural materials, first of all, for aerospace and automobile industries, and nanophase strengthening is one of the most effective and productive avenues for achieving an optimal combination of properties that can be utilized at much higher temperatures than those presently available by conventional precipitation hardening [363].

Nevertheless, there are many difficult problems that limit the widespread use of many newly developed nanophase reinforced alloys in industrial applications, in particular, because of their low thermal stability, poor creep resistance, weak or inadequate long-term strength. Furthermore, high sensitivity of extremely reactive hcp metal crystals such as magnesium, zirconium and titanium to oxygen and hydrogen also restrains their use as structural materials. The deficits are being overcome by further alloying and/or process development. A recent approach to alloy design is based on fundamental concepts of their strengthening associated with drag of mobile dislocations by certain components of microstructure solutes, precipitates and dispersoids [364, 365]. With that, despite research and commercial developments on these systems over the last two decades [366, 367], the nanophase-strengthened polycrystalline materials based on them have failed to reach high commercial potential. Unlike thermally activated obstacles such as solute atoms, precipitates, grain/subgrain boundaries and nanoparticles as strong athermal barriers are much more effective for the retention of energetically favorable high-temperature properties of hcp metal crystals to be necessary for the increase in their dislocation long-term strength and stress-rupture life. To optimize the nanoparticle-dislocation interaction in a

microstructure, one should check structural and strain-rate sensitivity of metal crystals in question. In order to overcome this problem, alloy development efforts are focused on addition of dispersoids to refine the grain size and to minimize strain location. In particular, the attempts have been undertaken to develop the Al—Li—Mg and Al—Cu—Li alloys with fine-grained structure and minimal strain localization [368]. In the context, there is a great need for development of metal alloys having long-term strength at increasingly higher temperatures and stresses. Due to the limited resources in metals and the high demand for new materials with unique properties, the development and use of energy-saving materials such as metal matrix nanocomposites has recently been of great interest for the aerospace and automobile industries all over the world. Dispersion strengthened alloys, especially the oxide-dispersion-strengthened metal alloys represent an exceptionally promising class of structural materials with a homogeneous distribution of nanoparticles which can provide useful long-term strength theoretically up to the operating temperatures approaching the eutectic point of the nanocomposite [365]. The nanocomposites advantages over their conventional counterparts are due to the uniform distribution of thermally stable and non-coursing nanoparticles acting as barriers to dislocation motion in the matrix (crystal lattice).

It, therefore, seems appropriate to indicate the possibilities for continued work along these lines, since nanophase-reinforced alloys could be utilized at much higher temperatures than those presently available. The main purpose of the on-going study is to explore the design potential of the structural alloys with the aim of improving their microyield/creep resistance and long-term strength below the macroscopic yield stress and of making the best of the potential in obtaining a better combination of properties in selected hcp magnesium and hcp zirconium alloys for different applications. In the context, it is expedient to analyze their composition — processing — microstructure — property relations, in particular, with respect to the impurity interstitials.

11.2. Background of the Approach

Strengthening Effects due to Ordered $L1_2$ Structure

The main purpose of the development of discontinuously reinforced intermetallic matrix composites is an increase in fracture toughness at low temperatures and plastic deformation (creep) resistance at elevated temperatures [364]. In particular, the Ni_3 (Al, Ti) intermetallic compound has a favorable effect on the hardening, ductility and fracture toughness of a nickel alloy with chromium additives. The hardening effect in this case is explained by the unique properties of the alloy, including the interface coherence with the ordered structure of $L1_2$, stability (up to 1253 K) as well as an increase in strength with increasing temperature and ductility at low temperatures. The observed beneficial effects are explained by the passage of dislocations through the lattice of the ordered Ni_3 (Al, Ti) phase. Inside the

particles, the order is violated by the dislocations that have passed through the lattice. In this case, ordering is restored as a result of diffusion at low stresses and temperatures. In other words, the contribution to hardening from the ordered structure is determined by the state of the antiphase boundaries. The greatest strengthening effect is observed in titanium alloys Ti—48Al—2V—2Mn based on the ordered intermetallic Ti_3Al ($L1_1$) with the introduction of up to 7 vol % TiB_2 (σ_Y up to 573 MPa; σ up to 704 MPa; E from 159 to 180 GPa).

Many intermetallic compounds show high yield strength, good stability and creep resistance up to relatively high temperatures. An interesting example is Ni_3Al, a material for which an increase in yield strength occurs with increasing temperature [365]. The major difficulty with intermetallic compounds, however, is their tendency to show brittle fracture or decreased ductility in the polycrystalline form. The reasons for the mechanical behavior of intermetallics have to be found in the chemical order, which reduces atomic mobility and is also responsible for the presence of less mobile superdislocations [366].

The research into nanostructured metals and its success in improving the ductility of ceramics [367, 368] has motivated the development of nanostructured intermetallic compounds [368]. It is expected that the deformation behavior of nanostructured materials is a GB diffusion-controlled mechanism, which does not involve movement of dislocations. This means that materials which are brittle as coarse grained polycrystals because of an insufficient number of independent dislocation slip systems, can exhibit ductility in the nanocrystalline form owing to a diffusion-controlled mechanism.

Intermetallic compounds that become amorphous under irradiation are those which in equilibrium conditions remain ordered up to the temperature at which they either melt or decompose into other crystalline phases.

For this reason, it has been suggested that radiation-induced disordering is a factor that promotes the destabilization of the crystalline structure [369]. An inspection of experimental results shows that electron-irradiated alloys generally undergo a loss of long-range order before becoming amorphous [370]. Nevertheless, there are cases where disordering takes place but of may or may not be followed by amorphization. Examples of such behavior are two aluminides Ni_3Al and Zr_3Al, both with the $L1_2$ crystalline structure. It is apparent from these examples that although chemical disordering plays an important role in the crystalline-to-amorphous state transition, the other factors affecting all the aspects of microstructural evolution under irradiation such as point defect behavior must also be involved. There is no observable microstructural evolution in alloys that will be rendered amorphous under irradiation. This is indication that there is point defect accumulation and, with it, a considerable increase in the system free energy. But in some intermetallic compounds (Zr_3Al), microstructural evolution in the form of point defect clusters has been observed during the disordering of Zr_3Al under both electron and ion bombardment [369, 371].

The presence of other point defect sinks provides an alternative way to accommodate point defects. Besides, the defect accumulation is coupled to the loss of long-

range order. The experimental observations have led us to conclude that the driving force for the amorphization of intermetallic compounds is not chemical disorder alone but essentially the free energy excess due to defect accumulation. What chemical disorder provides is the condition for a viable mechanism of defect formation.

In age-hardening alloys, there are two types of phase precipitates which can be identified as (i) metastable (ordered) precipitates coherent with disordered matrix, and (ii) stable precipitates partially coherent with disordered matrix due to misfit dislocations. Following the Clark concept [372], the age-hardening of magnesium alloys in the hcp Mg—Al system can be explained by the occurrence of coherent precipitates oriented properly to prevent a basal slip as well as by adequate interprecipitate spacing not so small to cause a precipitation hardening effect. However, the decomposition of a solid solution is most likely to occur by different mechanisms depending on the degree of oversaturation. The strong oversaturation is specified by the homogeneous distribution of nanoprecipitates. Alternatively, at weak oversaturation, the preferential nucleation of nanoprecipitates occurs on the existing dislocations rather than on the GBs or interfaces. According to [373], replacement of the coherent interface of the metastable phase by a partially coherent interface of the stable phase is expected to give rise to changing the mechanism of dislocation-particle interaction. Unfortunately, the operative dislocation cutting mechanism is certain to result in the inhomogeneous slip in the form of strong dislocation pile-ups. Besides, the observed transition from the cutting mechanism to bypass one can occur only on dislocations and GBs with the age-hardening response of the system at higher annealing temperatures. Furthermore, low creep resistance of magnesium is attributed, first of all, to the GBs sliding that might be revealed even at 77 K as well as to local stresses concentrated in triple joints of grains. Since sliding GBs can be the sites of preferential microdeformation and localized shear, hcp metal alloys should have their GBs pinned. The dispersoids lock the GBs making the alloys less sensitive for exposure to elevated temperatures in all the strain rate range [374].

The rate-controlling mechanisms provide important information for understanding the strengthening as a phenomenon. An original atomistic approach was proposed on the basis of the kinetics of edge dislocation-cluster interactions being simulated at any strain rate within 10^{-7} to 10^{7} s^{-1} for hcp Zr [28]. Under the data of simulations, the dislocation climb mechanism is expected to operate in terms of the coupled thermal and stress activation effects. Proceeding from this, the coupling of strain rate and thermal activation is considered as a fundamental physical principle of an edge dislocation pinning by clusters of self-interstitial atoms. Atomistic simulations by Yue Fan et al. [375] are consistent with a climbing mechanism modeled by Arzt et al. [376, 377].

Following the theoretical concept [375, 376], the dispersoids introduced through technological cycle (high-speed treatment, precipitation from the liquid, etc.) form with matrix incoherent boundaries which attract glide dislocations with increasing temperature. The relaxation of their stress field should be considered as a source of

local microyielding [378] with some density of mobile dislocations which delay the strain localization. Thermally activated dislocation detachment from the particle is assumed to be the rate-controlling mechanism of dislocation creep. With that, the concept of nanophase strengthening should be experimentally verified in addition. The pair defects (associates) are expected to be relatively stable due to the opposite strains and electronic charges imposed by the excess vacancies and additions on the crystal lattice to provide their lowest energy positions within a certain distance from a dislocation in the stress field. The second stage is believed to be the formation of cluster compounds A_mB_n converted from vacancy-type paired defects. In such a manner, the precipitate nucleation is assumed to occur by a cluster-forming mechanism. Since dislocations are weakly pinned by solute atoms on the basal planes [379], the major efforts in the present study were focused on magnesium alloys having more stable and strong barriers to dislocation movement compared to the thermal obstacles. Furthermore, the presence of a high density of the GB nanoparticles is evidenced to be a more stable phase than the matrix strengthening phase [380]. The susceptibility of polycrystalline materials to shear strain localization can be the main factor that limits their tensile ductility, long-term strength and fatigue resistance [357, 381, 382]. When slip is likely to be relatively easy, the plastic deformation is localized and accumulated in soft regions resulting in high-stress concentration, for example, GB triple points. The ductility and toughness deficiencies in a variety of metal alloy systems are caused by strain localization and weakened precipitate free zones (PFZs) [368]. It has been analytically proved [381] that dislocation long-term strength controls the amount of uniform microyield including creep for slow dislocations which results in the successful advancing of a product. With that, under the data [383] a critical value of dislocation velocity for high-purity crystals is attained at a strain rate of 10^{-8} s^{-1} and dislocation density ~10^6 / cm^2 even at 293 K. These results are in agreement with the values calculated for high-purity magnesium alloy crystals with reference to the criterion of useful long-term strength. To attain lower values of strain rate (10^{-10}…10^{-12} s^{-1}), it is necessary to extend the range of uniform dislocation strain. Upon treatment of developed alloys and useful materials made of them, the new special measures should be taken to prevent a premature localization of shear (time-dependent) strain and thereby to improve their creep resistance and long-term strength.

Further essential support for our concept comes from XRD analysis of the diffraction patterns before and after creep tests of magnesium alloys [384]. The patterns indicate that the constant dislocation density is only is retained up to 0.4 % ε. At relative strain ε > 0.5 %, the shear localization is certain to occur with increasing dislocation density. This effect is accompanied by the ultimate transition to the plastic instability and necking due to the disintegration of the primary solid solution and local softening its defect structure.

Unlike precipitation hardening, the nanoparticle strengthening of metal matrix composites increases the effectiveness of the uniform strain evolution due to the alignment of slip systems in hcp metal alloys and hence extends the useful long-term

to higher temperatures. Since the relaxation of the incoherent particle stress field is a source of local microyielding [364], some density of mobile dislocations should be generated to prevent undesirable localized shear. Further, one can observe an additional increase in the dislocation creep resistance of a given alloy by a nanophase strengthening mechanism. If nanoparticles decorate GBs, this microstructure proved to be very stable at elevated temperatures. The nanophase strengthening is an avenue for achieving an optimum combination of properties and effective method to prevent early crack nucleation due to strain localization. The approach offers important advantages compared to conventional decisions for strengthening particles incorporated in the micrometer range. Metal alloy properties can be additionally improved by equalizing the deformation behavior of structural components on the whole material in terms of: a) incorporation of nanoparticles like nm Al_3Zr in hcp Mg and nm ZrO_2 in hcp Zr provides aligning local creep properties of both structural components for the advanced metal alloy systems due to uniform distribution of the dispersoids and, as consequence, additional dispersion strengthening; b) equal-channel angular pressing, i.e. a widely-known method of severe plastic deformation in which shear occurs through keeping up the uniform disperse structure using the reusable cycles of the treatment to improve their strength according to the Hall-Petch relation [385]. Nevertheless, although the strength increases through the dislocation pile-ups at the GBs by Hall-Petch effect, the pinning of GBs by nanoparticles is sure to be more effective due to the stronger interfacial bonding between the nanoparticles and the matrix.

The presence of various kinds of impurity elements cannot be taken into full consideration when plotting ternary and quaternary equilibrium alloy phase diagrams. The sensitivity of extremely reactive matrix materials with hcp structure such as zirconium, titanium and magnesium to oxygen, nitrogen and hydrogen interstitials produces a problem that has frequently been tackled in alloys prone to impurity interstitial segregations around mobile dislocations. In particular, the rate of solid solution strengthening, e.g., with α-Ti, at elevated temperatures is controlled by mechanism responsible for the thermally activated overcoming of solute interstitials by the first-order prismatic dislocations with an a.e. of 1.25 eV [386]. Moreover, under the data of amplitude-dependent internal friction in pure hcp Zr containing free dislocations, the activation parameters are consistent with those determined for thermally activated deformation mechanism attributed to interstitial solute atoms of oxygen [387]. Following Cottrell-Bilby's concept, the solute atoms can diffuse fast enough to allow dynamic interaction with dislocation during deformation, meanwhile, in substitutional alloys, the strain-produced vacancies are likely to enhance the diffusion of substitution solutes. However, a new situation arises in substitutional alloys when inevitable impurity interstitials form their dense oxygen-containing Cottrell atmospheres which are able to immobilize any sliding system due to large lattice distortion and to give rise to the strain localization. The detrimental interstitial solute segregations are more likely to lock the sliding dislocations by the Cottrell hardening mechanism.

Strain rate sensitivity of pure hcp metal alloy crystals is normally described by the quantitative (dislocation) criterion of useful long-term strength [381]. However, results obtained are in a good agreement with the evaluations to be expected from the postulated mechanism only for nanophase-reinforced magnesium alloy polycrystals of high purity. For commercially available and technical grades of hcp zirconium alloys, larger long-term strength is sure to be kept only after interaction with fast dislocations (at strain rates 10^{-3}–10^{-5} s^{-1}). Unusual strain rate response to nm ZrO_2 content is associated with the competitive interaction of mobile dislocations with the interstitial impurity solutes by thermally activated interstitial site mechanism and the substitutional solutes by vacancy (diffusion-controlled) mechanism. For cross-slip or dislocation climb mechanism, impurity interstitials such as oxygen are more deleterious than excess (strain-produced) vacancies. The diffusion of interstitials causes the effect of shielding by the Cottrell locking mechanism for dislocation-nanoparticle interaction. Unfortunately, thermal stability of dislocation structure in α-Zr matrix is associated with the formation of oxygen atmosphere having very strong binding energy of about 2 eV due to the effective pinning. For this reason, it is believed that the shielding effect [388] resulting from Cottrell-Bilby interstitial solute blocking could be caused by short-range ordering of solute interstitials in the stress field of mobile dislocations, as predicted by Snoek-Schoeck's dragging concept [383]. The possibility of interference of another mechanism cannot be discarded. At low strain rates the poor correlation between the dragging stress and its strain rate sensitivity is most likely to be associated with the preferential oxygen segregations on slow dislocations by long-range (diffusion) mechanism to lock their sliding towards nanoZrO_2 athermal barriers. Therefore, a decrease in the dislocation mobility in alloys with impurity interstitials is controlled by the formation of dense Cottrell (oxygen-containing) atmospheres, which suppress the interaction of slow dislocations with ZrO_2 nanoparticles.

Incoherent particles in dispersion hardened alloys (DHA) exert an attractive interaction with mobile dislocations [376, 377]. Their detachment with a.e. of about E_d is assumed to be rate-controlling mechanism. The idea is supported by TEM observations and theoretical studies [377]. The creep rate equation based on the particle–dislocation bypass mechanism at higher temperature can be expressed as an Arrhenius type equation.

$$\dot{\varepsilon} = \dot{\varepsilon}_0 \, (-E_d / kT), \tag{11.1}$$

where E_d is the a.e. of detachment.

The Eq. (11.1) is connected with detachment frequency ν by

$$\dot{\varepsilon} = \bar{\rho}_D \cdot 2\lambda \cdot \nu \cdot b \tag{11.2}$$

Combining Eqs. (11.1) and (11.2) gives the resulting expression

$$\dot{\varepsilon} = \frac{6D_v \cdot \lambda\rho}{b} \cdot \exp\left(- \frac{Gb^3 \cdot r[(1-k)(1-\sigma/\sigma_d)]^{3/2}}{kT} \right), \tag{11.3}$$

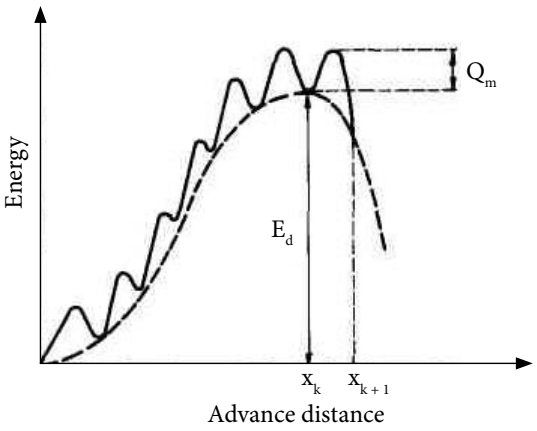

Fig. 11.1. Schematic energy barrier for detachment of a climbing dislocation from the attraction [377].

where $\dot{\varepsilon} = 6D_v \cdot \lambda \cdot \bar{\rho}_D / b$; $\nu = \nu_0 \exp(-E_d / kT)$; $\nu_0 = n/2 \cdot \nu^*_0 \exp(-Q_n / kT) \exp(-Q_m / kT)$; n is the number of near-neighbors; Q_n is the a.e. for vacancy nucleation; Q_m is the a.e. for vacancy migration; ν^* is the frequency of dislocation successful jumps; $\nu^* \sim \exp(Q_m/kT)$ and $\nu^* = 3D_v/b^2 \exp(-E_b/kT)$; σ_d is the athermal engineering stress; $\sigma_d = M\tau_d$; M is the appropriate Taylor factor or reciprocal of the Schmid factor for single crystals; λ is the mean free path between the obstacles; r is the radius of particle; K is the relaxation parameter ($K < 0.9$ in alloys with highly attractive dispersoids); $D_v = 1/6\, nb^2 \nu_0 \exp[-(Q_n + Q_m)/kT]$; $\nu^* \cong \nu_0 \exp(-E_d/kT)$; ν_0 is the frequency of vacancy absorption; k is the Boltzmann constant; E_b is the binding energy; b is the Burgers vector.

It is obvious that Eq. (11.3) does not contain a "true" threshold stress. Moreover, it seems to be applicable at very low stresses.

Dislocation reaches the critical configuration in point x_0 (Fig. 11.1) via climb with the probability which is given by the experimental term (11.1). Climbing dislocation detaches from the particle with frequency ν and moves under absorption of a vacancy.

From the Orowan type approximation (11.4), particle size dependence results to $d\ell n\sigma / d\ell nr \approx -1$ at stresses near the threshold stress, i.e., the creep strength is predicted to double when the particle size is halved. A priory estimate of the bowing Orowan stress is made from the simple expression:

$$\sigma_0 = 0.84\, M \cdot G\, b / 2\lambda \qquad (11.4)$$

where $\lambda = (\pi/6f_v)^{1/2} \cdot r$; f_v is the volume fraction of particles; $\dot{\varepsilon} \cong \bar{\rho}_D \cdot 2\lambda \cdot \nu \cdot b$; $r^* \sim 0.78\, r$ is the average radius for non-spherical particle.

At the same time thermal activation of the Orowan process fails to give the correct temperature dependence of creep strength in dispersion hardened materials. The activation of the detachment process, by contrast, is associated with such low activation energies that consideration of thermal activation does become important.

Physically, E_d (r) comes about because (i) the probability of thermally activated detachment is raised at small dispersoids, and (ii) large particles are associated, at fixed volume fraction, with a lower Orowan stress and hence a smaller athermal detachment stress σ_d. As for detachment by Rosler and Arzt [377], their equations (11.5-11.7) lead to a weaker particle size dependence of the creep strain rate, $\dot{\varepsilon}$ bears the optimum (Fig. 11.1).

Analytically, the optimum particle size is given by

$$\left(\frac{r}{b}\right)_{opt} = \left[\frac{5}{3(1-k)}\right]^{3/2} \left[\frac{\ell n\left(\dot{\varepsilon}_0/\dot{\varepsilon}\right)\cdot kT}{Gb^3}\right]; \tag{11.5}$$

$$\frac{d\ell n\sigma}{d\ell nr} = \frac{2}{3}\cdot\frac{B}{(r/b)^{2/3}-B} - 1 \tag{11.6}$$

with

$$B = [(\ell n\dot{\varepsilon}_0 / \dot{\varepsilon})\, kT \cdot Gb^3]^{2/3} / (1 - k). \tag{11.7}$$

According to the Rosler-Arzt model, very small particles should therefore be insufficient barriers to the motion of dislocations at high temperatures, and detachment will no longer be the rate-controlling mechanism. Besides, dislocations do not adhere to dispersoids smaller than a critical size. It is predicted to increase with rising temperature (at fixed $\dot{\varepsilon} / \dot{\varepsilon}_0$) and, less sensitively, with decreasing strain rate. The creep strength maximum in the detachment model leads to a reduced sensitivity of the creep rate to particle coarsening. However, theoretical studies by Srolovitz et al. [389] have shown that an attractive interaction between dislocations and incoherent particles is in fact expected at high temperatures because the incoherent interface can relax parts of the dislocation stress field by slipping and rapid diffusion. The particle-matrix interface is stressed in the presence of a dislocation. Diffusion in the interface leads to a viscous-like relaxation of the shear tractions resulting in a sliding interface. As a result of the diffusional relaxation, a dislocation on any glide plane that intersects the particle is always attracted towards the particle. These results differ from the diffusional interaction, where attraction occurs only when the shear modulus of the matrix exceeds that of the particle. Attractive interaction between dislocations and hard spherical particles is modeled during the process of dislocation bypass by local climb [376].

Thus, dislocation climb alone appears to be insufficient to control the creep behavior of dispersion strengthened materials at high temperatures [364]. In general, it appears that precipitation hardened alloys behave like materials without particle-attractive dislocation interaction whereas dispersion strengthened alloys behave like materials with a strong attractive particle-dislocation interaction.

An important difference between the two particle types is that precipitates, unlike dispersoids, have to overcome a nuclear barrier and thus are forced to form low energy, i.e., strongly bound phase boundaries. Weakly bound interfaces are however needed to allow for the relaxation of the dislocation stress field by atomic rearrangement and fast diffusion along the interface. This may be the reason why small precipitates appear to be less capable of relaxing the line energy than small dispersoids. Although detailed understanding of the particle-dislocation interactions at high tem-

peratures is certainly not far advanced, it thus appears that on the basis of a varying degree of interfacial bond strength and of particle coherency across the interface, the creep behavior of particle-strengthened alloys may be consistently understood.

The ability of interface to attract dislocations at high temperatures may be related to poor interfacial binding. Its weakening might be possible due to segregation alloying or by pre-treatment of dispersoid material [390].

In conclusion, at high $\dot{\varepsilon}$ the creep mechanism approaches that of dispersoid free matrix and is no longer directly determined by the particle dispersoid. The rapid degradation of the creep strength at the lowest $\dot{\varepsilon}$ and highest T may be caused by an increasing contribution of GBs. This implies that the contribution can give rise to the abnormally high a.e. There are two principal differences in the approach from the Orowan concept: (i) the particle radius r is introduced instead of the particle spacing λ by Orowan; (ii) the high temperature strength imparted by any particle dispersion cannot exceed about 60% of the Orowan stress.

In developing new experimental alloys, particular attention should be paid to the properties of the particle-matrix interface. It stands to reason that a high degree of dislocation relaxation can be achieved at an incoherent interface with a high specific energy. An alternative approach is proposed by Nardone and Tien, Schroder and Arzt [391]. It is based on the existence of an attractive particle-dislocation interaction, as suggested by TEM studies of dislocation structure in crept specimens.

11.3. Experimental Procedure

The chemical compositions for alloys in the ternary and quaternary hcp Mg—Al—Ca, X and hcp Zr—Nb—Sn, X systems were selected so as to examine the effects of nanoprecipitation hardening and nanodispersion strengthening as well as to evaluate their short-term and long-term strength. The choice of the base materials is strongly limited by the favorable compatibility and wetting ability of nano dispersoids such as nm Al_3Zr and nm ZrO_2 for hcp magnesium and hcp zirconium matrices, respectively. One of the problems is associated with the difficulty in producing a dispersion of hard, closely-spaced and incoherent nanoparticles using normal ingot casting. Chemical compositions were proposed to obtain castable alloys with higher heat- resistance and long-term strength of the alloys under investigation.

It is recently that work has been done to explore and develop new magnesium alloys, primarily because of the well-known engineering problems concerning their melting and suitable fabrication free of contamination. On the basis of previous experience [361, 384] with the model magnesium crystals in the Mg—Al system, it was selected as being the best for our hypothesis testing in terms of the kinetic (dislocation) criterion of useful long-term strength [298]. The magnesium alloys nanophase-reinforced by Al_3Zr were prepared from high-purity starting materials (with mass content of 99.98 % magnesium and 99.999 % aluminum), processed and produced on the basis of our experience. The known alloying method was chosen to introduce the nanoparticles into

the melt by using an initial pulsed treatment of melt followed by its rapid solidification (up to 373 K per sec). A priority method of incorporating nanoparticles under the pulse treatment prior to casting makes it possible to expand the solubility limits for so-called immiscible systems with alloying elements having the positive heats of formation, e.g., titanium. This is effectively done in the calcium and aluminum containing magnesium alloys additionally strengthened by the stable natural nanoparticles which have been identified by an electron diffraction technique as nm $Mg_{17}Al_6Ca_6$ phase natural nanoparticles with an average size of 40 nm and strong bonding with the crystal lattice.

The maximum strengthening increment from oxides (up to 4 vol.%) was obtained in Ni and Cu-based matrices without unacceptable loss of ductility. One of the oxide species ZrO_2 was used in commercially available zirconium alloys. ZrO_2 oxide was selected as a thermally stable and non-coarse compound with the negative free energy of formation. Several refractory commercially available zirconium alloys nano-reinforced with nm ZrO_2 particles were manufactured to analyze the creep resistance of the technical grades in the presence of oxygen. Dispersion strengthening behavior of zirconium-based alloys of the Zr—Sn—Nb system containing strong and infusible ZrO_2 nanoparticles (down to 10 nm) as well as incidental impurities of oxygen (up to 0.15 % O_2) were studied after electric arc melting in the as-cast condition with strain rate change-related experiments and creep testing at 673 K. The principal nanoparticles were identified in as-cast materials by proper electron diffraction technique [392], EPMA, and XRD analysis as nm Al_3Zr in magnesium alloys and nm ZrO_2 in zirconium alloys under examination.

Analytical XRD method for the mean crystallize size and lattice distortions was also used to calculate the relative values of nanoparticles [384, 393]. A peak-breadth analysis was also performed to estimate the volume-weighted crystallite size and a microstrain averaged all over the coherence length perpendicular to the diffracting planes [394]. Tensile creep tests by standard procedure (at constant and variable stresses [395]) were commenced after a minimum of 3 hr at the creep-testing temperature to allow for good temperature stabilization. Other details of the testing have been previously reported elsewhere [384]. The Cottrell-Bilby time law testing was performed on selected hcp metal crystals to verify a model for solid solutions with different solutes and excess vacancies by experimental data of dislocation damping (amplitude-independent internal friction), Δ and mechanical spectrometry, Q^{-1} (T). Primary kinetic curves-isotherms of amplitude-independent internal friction $Q^{-1}(t)$ were measured for various aging temperatures after solute solution treatment and quenching of specimens prepared from hcp metal crystals.

11.4. New Look at Interaction between Dislocations and Incoherent Nanoparticles

Advanced nanostructured and nanophase materials are receiving increasing interest in both science and applied research [395]. They are unique due to the significant contribution of surface atoms and the dimensions of their nm-struc-

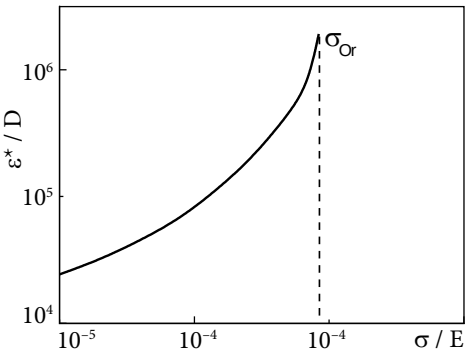

Fig. 11.2. Parameter ε* / D as a function of normalized stress [376]

ture being smaller than the interaction length scale of various phenomena. In the case, they demonstrate novel properties unattainable for the conventional materials. However, only some of the synthesis methods are promising for the nanocrystalline materials at production scales.

Undeformed dispersoids generate a large number of geometrically necessary dislocations [248], which contribute to the yield strength. If the particles are bypassed, the strengthening is independent of their properties, and the yield strength can be described by the modified Orowan relations:

$$\sigma_Y = \sigma_0 + 0.8 \cdot G \cdot b / L \tag{11.8}$$

If the particles are sheared, strengthening depends of their intrinsic properties, i.e.

$$\sigma_Y = c \cdot f^m \cdot r^p \tag{11.9}$$

where c, m and p are constants; f is the volume fraction.

In the case, strengthening effects are reduced due to a local decrease in resistance to further dislocation motion. An additional work is required to resolve the problem of theory which otherwise appears to be useful in understanding the complex nature of sieving and screening.

The shearable particles affect the strength, deformation behavior, and ductility and increase the elastic modulus, yield strength, tensile strength along with a concomitant reduction in strain to fracture.

Screw dislocations of the (c + a) type can move to parallel planes by double cross slip, i.e. by the local climb mechanism with subsequent annihilation. The decrease in dislocation density recovers the matrix decreasing in the working hardening rate.

It should be emphasized that Cottrell's theory predicts the existence of uniform deformation prior to serrated yielding. However, non-uniform microyield (creep) deformation is enhanced with increasing temperature, but progressively more localized deformation and hence plastic instability is believed to occur as applied stress approaches to the Orowan stress (Fig. 11.2).

It is generally accepted that unpenetrable particles, such as carbides or nitrides, can be passed over by dislocations which leave loops behind by the Orowan mechanism at stresses above the Orowan bowing stress. During straining, the particles are overcome by local cross slip mechanism, stored dislocations being also obstacles for moving dislocations.

Selected magnesium and zirconium-based alloys reinforced by nanoprecipitation hardening and nanodispersion strengthening mechanisms were examined in the

power law regime using long-term testing, strain-rate change measurements and constant structure steady-state creep tests to analyze the deformation and kinetic behavior of hcp Mg—Al—Ca — nm Al_3Zr and hcp Zr—Sn—Nb — nm ZrO_2 alloys at 423 K and 673 K, respectively [396]. The microstructures generated in these hardened alloys were assessed by analytical electron microscopy aiming at controlling and understanding the composition modification in the nanophase-reinforced and nanophase-free hcp magnesium and hcp zirconium alloys. The experimental studies were employed to optimize the composition — processing — microstructure — strength properties of the nanoparticle-reinforced composite materials with extended uniform strain. Kinetic hardening of alloys in the hcp Mg—Ba and hcp Be—Fe, C systems carried out isothermally indicate the deviations from the Cottrell-Bilby time law due to the non-isothermal kinetics of nanoparticulate nucleation by a pre-precipitate (cluster-forming) mechanism [122]. Such an approach has emerged as a means to suppress the strain localization effects responsible for the degradation in dislocation creep resistance and long-term strength in hcp metal alloy crystals.

11.5. Strength of Age-Hardened Alloys

The decomposition of a supersaturated solid solution during subsequent heat treatment leads to the formation of metastable phases or precipitation of equilibrium phases due to the low diffusion coefficient and small equilibrium solubility of alloying elements (AE). Effective solid solution strengthening requires AEs with a high solid solubility providing a large lattice distortion, which limits solubility and restricts solid solution strengthening in most commercial alloys. It is now generally excepted that effective precipitation and dispersion strengthening depend on the size, spacing, fine distribution and degree of coherency of second phase particles which are either looped and bypassed or sheared by mobile dislocations during plastic deformation.

The strengthening of metals and alloys is associated with the dragging of mobile dislocations by certain components of structure such as thermally activated obstacles-solutes with weak dragging effect (as small as 0.2 Gb^3) and athermal strong barriers (to 2.0 Gb^3).

One should expect good creep resistance even in small grained polycrystals due to fine particles pinning GBs and impeding dislocation movements [18, 28]. The creep resistance and long-term strength of cast hcp metal crystals can be substantially improved by precipitation hardening but the obtainable results are limited by temperature dependence of dislocation capacity of their matrices for alloy atoms. Besides, for the alloy systems with limited solubility of their components, quenching from single phase into two phase region of equilibrium diagrams results in the formation of metastable precipitates.

Two quantitative dislocation theories of the strength of solid solutions of age-hardened alloys have been presented by Mott and Nabarro [397, 398] who consid-

ered the interaction between dislocations and internal stresses caused by solute atom clusters (Guinier-Preston zones) in the matrix prior to coherent precipitation as well as by Kelly and Fine [399] who estimated the stress necessary to force a dislocation through these zones, using heats of reversion as a measure of the energy. Strengthening due to the presence of Guinier-Preston zones was calculated by summing the contributions from Mott and Nabarro's coherency strengthening, Kelly and Fine's chemical strengthening and the strength of residual solid solution. It is generally accepted that the mechanism of aging in terms of structural changes is well understood and has been discussed in the literature.

11.5.1. Precipitation-Hardening Mechanism

For alloys with large volume fractions of coherent precipitates, dislocations normally shear the precipitates during deformation. Potential strengthening contributions include strain fields origin from precipitate-matrix lattice misfit and antiphase boundary hardening due to the order within the precipitates [400]. For a given microstructure, a coherency strain mechanism and order hardening mechanism predict different temperature dependences of flow stress. It is reasonable to associate precipitation hardening in these systems, at least in part with coherency strains. Assuming a strengthening increment due to coherency strain, one expects a direct dependence on the shear modulus.

Weakly bound interfaces are however needed to allow for the relaxation of the dislocation stress field by atomic rearrangement and fast diffusion along the interface. This may be the reasons why small precipitates appear to be less capable of relaxing the line energy than small dispersoids. Although the detailed understanding of the particle-dislocation interactions at high temperatures is certainly not far advanced, it thus appears that on the basis of a varying degree of interfacial bond strength and of particle coherency across the interface, the creep behavior of particle-strengthened alloys may be consistently understood.

The interface ability to attract dislocations at high temperatures may be related to poor interfacial binding. Its weakening might be due to segregation alloying or by pre-treatment of dispersoid material. For example, Ni additions weaken the interface bonding whereas Cr and Mo have the opposite effect [401]. In conclusion, at high $\dot{\varepsilon}$ the creep mechanism approaches that of dispersoid free matrix and is no longer directly determined by the particle dispersoid. The rapid degradation of the creep strength at the lowest $\dot{\varepsilon}$ and highest T may be caused by an increasing contribution of GBs. This implies that the contribution can give rise to the abnormally high a.e. There are two principal differences of the approach from the Orowan concept: (i) the particle radius r is introduced instead of the particle spacing λ by Orowan; (ii) the high temperature strength imparted by any particle dispersion cannot exceed about 60% of the Orowan stress. In developing new experimental alloys, particular attention should be paid to the properties of the particle-matrix interface. It stands to reason that a high degree of dislocation relaxation can be achieved at an incoherent interface

with a high specific energy. An alternative approach is proposed by Nardone and Tien [402]. It bases on the existence of an attractive particle-dislocation, as suggested by TEM studies of dislocation structure in crept specimens.

The concept of dislocation hardening originated with the sintered aluminium product dragging in which magnesium is additionally strengthened by the presence of nano SiC [403]. The principle of dispersion hardening has been successfully applied to other pure metals such as Cu, Bi, Al, Be, etc., in which the disperse phase is a hard inert refractory oxide (Al_2O_3, BeO, ThO_2, etc.) added mechanically. Al—Al_2O_3 alloys have shown excellent strength properties at room and elevated temperatures but the ductility is poor. In dispersion strengthened alloys prepared by powder metallurgy, the cohesion between the oxide particle and the matrix seems to be a mechanical one. Strength increases at the expense of ductility.

The alloying elements having high solubilities and high diffusion rates are normally used for precipitation hardening. At the same time dispersoids forming by elements having low solubilities and low diffusion rates can also give adequate high temperature strength reducing GBs sliding, diffusion (Nabarro-Herring) and dislocation (Ashby) contributions to stead-state creep/microyield of dispersion-hardened alloys. Unfortunately, their limited solid solubility makes it impossible to obtain a fine dispersion of closely spaced incoherent particles using conventional ingot casting procedure and technology. The inherently slow ingot solidification rates enhance and facilitate the precipitation of coarse particles which lower the ductility and fracture toughness [404]. Rapid or supercooling (less than 10^5 K/s) is currently used in advanced solidification technology, e.g., by quenching droplets of molten metal. Such a procedure enables the thermodynamic limitations to be avoided. Besides, it promotes enhanced supersaturation of solute elements and refinement of structure. Decomposition of the solid solution produces desired fine dispersion of precipitate. Although the model [402] predicts an increase in strength with decreasing interparticle spacing, and therefore with volume fraction for a constant particle size, the negative ductility factor imposes restrictions on solute concentrations. It has been shown that when the volume fraction of particles approaches some critical value, interaction effects come into play and interfacial stresses are enhanced due to overlap of the plastic zones around the particles. This results in interface separation at very low strains.

A reduction in grain size, which can be obtained under thermomechanical processing has been shown to be effective in preventing premature failure in other systems by reducing the dislocation pile-up length and therefore the high local stress concentrations which cause early crack nucleation. Nonuniform deformation including in the pre-yield region is certain to be enhanced with increasing temperature [405]. Progressively more localized deformation and hence plastic instability are believed to occur as the normalized stress σ/E approaches 10^{-3}, i.e. the threshold Orowan stress (Fig. 11.2).

The precipitates having interfacial strain may aid in shearable homogenizing deformation. Coherent precipitates occurring in the course of the precipitate hardening can be crossed by the mobile dislocations.

11.5.2. Nanoprecipitation Hardening in the Mg—Al—Ca System

Age hardened alloys suffer problems associated with low ductility and inadequate fracture toughness caused by the sites of preferential strain localization. The effect is due to the precipitation of fine, coherent with the matrix dispersoids in association with the formation of weaker solute-depleted precipitate zones adjacent to GBs [368].

Unlike the laminated Mg—Al solid solution with divorced eutectics and low creep resistance, the maximum solubility of calcium reduces with increasing the aluminum content and decreasing temperature for the equilibrium states of alloys in the Mg—Al—Ca system (Table 11.1).

At higher mass concentration of aluminum (up to 12.5 %) with the liquidity improved by 30% the volume fraction of eutectic component β-$Mg_{17}Al_{12}$ strengthened by calcium increases as much as by 15% with the simultaneous formation of $Mg_{17}Al_6Ca_6$ nanoparticles on the GBs [361] due to the saturation of primary Mg—Al solid solution with a fine-grained structure. With this provision, calcium impedes the decomposition of the Mg—Al solid solution stabilizing the nanophase composition of $Mg_{17}Al_6Ca_6$ on the GBs. The interface between the precipitate and the alloy matrix is highly irregular due to the misfit (Fig. 11.3). The surface dislocations surrounding the precipitates, although poorly resolved, are indicative of the partial coherency. With this provision, stable precipitates partially coherent with the disordered matrix are formed due to the dislocation network accommodating the misfit.

Since the hcp magnesium matrix reveals some covalency, coherent (ordered) particles may cause embrittlement by a dislocation cutting mechanism due to the inhomogeneous slip and strong dislocation pile-ups (Fig. 11.4). Replacement of the coherent interface of the metastable (ordered) phase with a partially coherent interface of the stable nm $Mg_{17}Al_6Ca_6$ seems to occur preferentially on GBs. In hypoeutectic systems, the nanophase strengthening of GBs is most likely to superpose on that contributed by so-called eutectic strengthening which extends the useful long-term strength to higher temperatures.

Table 11.2 summaries the best ternary and quaternary combinations of micromechanical properties obtained for magnesium alloys in the Mg—Al—Ca system. A

Table 11.1. **Maximum calcium solubility in magnesium and hcp Mg—Al alloys**

Alloy system	Temperature, K	Content, mass%
Mg	789	1.34
Mg—4.5Al	793	0.5
	723	0.02
Mg—8.5Al	723	0.01
Mg—12.5Al	643	None

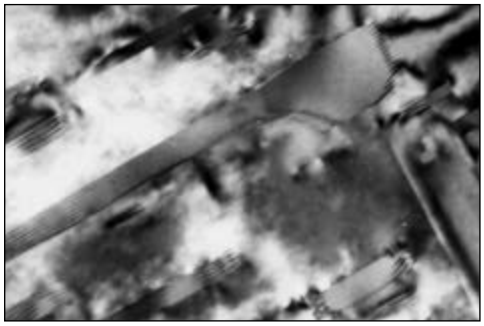

Fig. 11.3. Misfit dislocations at the interface of semi-coherent precipitates after the decomposition of α-Mg solid solution

Fig. 11.4. Dislocation pile-ups at the interface of coherent precipitates after the decomposition of α-Mg solid solution

Table 11.2. **Micromechanical properties of conventional and newly developed experimental magnesium alloys with nanoreinforced GBs at 423 K**

Alloy system	σ_γ at r.t., MPa	Critical creep parameters				Creep strain rate $\dot{\varepsilon}_s$, s^{-1}
		Creep strength, MPa	Loading time t*, hr		Allowable creep strain ε_Σ, %	
			Exp.	Theory [14]		
Mg—9Al—1Zn AZ91D (Dow Chemical Corp., USA)	170	35 64	200 50-100	185	1.93-2.50 Fracture	$\geq 10^{-7}$
AZ91D—2Ca	220	64	50	70	0.1	10^{-8}
Mg—12.5Al—1.3Ca	157	65	160-180	220	0.17-0.24	$\leq 10^{-8}$
Mg—12.5Al—1.3Ca—0.3Mn—0.1Ti	180	70	150-200	277	0.2-0.4	$\leq 10^{-9}$
Mg—12.5Al—1.3Ca—0.4Mn—0.2Ti	210	70	200	—	0.28	$\leq 10^{-9}$

purified commercially available magnesium alloys in the Mg—Al—Ca—Ti system with the extended uniform tensile creep strain retains their high creep resistance (at $\dot{\varepsilon} \sim 10^{-9}\ s^{-1}$) after 200 hr creep testing with constant applied load 70 MPa. These alloys do have potential in terms of achieving properties suitable for automobile alloys and may be successfully adopted to high and low pressure die-casting thanks to their excellent liquidity (by 30%), creep resistance and long-term strength.

The inhibition of dislocation mobility by above-mentioned mechanisms and their forced resistance provide very slow microyielding (at rates of about $10^{-9}\ s^{-1}$) making it less sensitive for exposure to higher temperatures, offering heat resistance and causing a delayed fracture. These processes postpone the achievement of the critical dislocation density for a new family of the creep-resistant and long-term strength alloys presenting a cost-efficient system capable to operate with an allow-

ance of total creep strain of up to 0.4% (Table 11.2). For a given creep strain, long-term strength of the quaternary Mg—Al—Ca, X alloys is compared favorably with AZ91D and ascertained to be 70 MPa at 423 K for 200 hr (see Table 10.7).

11.6. Nanodispersion Strengthening Mechanism in Magnesium Alloys

In order to overcome the problem of strain localization in solution-hardened alloys, the efforts are focused on the addition of dispersoids to refine the grain size and to minimize strain location. In particular, the attempts have been undertaken to develop the Al—Li—Mn and Al—Cu—Li alloys with fine-grained structure and minimal strain localization [406]. Nanoreinforced strengthening should be considered as a powerful means for aligning the micromechanical properties of structural components all over the bulk of a given alloy. Uniform distribution of the strengthening nanoparticles to much higher temperature applications and delays a premature fracture of the newly developed metal alloys. The higher thermal stability of dispersion systems is provided by low-energetic interphase structures, i.e., low values of the interfacial specific energy, solubility and diffusivity typical for metallic alloys of eutectic origin [407].

The practical interest in microstructures of eutectic origin arises from the chemical equilibrium of the two-phase alloys with constituents that are unaffected up to the chemical decay. Nevertheless, commercially available magnesium alloys such as AZ91D and the like are certain to be specified by divorced eutectic and laminated solid solution and, as a consequence, by low creep strength at higher temperatures.

Microstructural investigations based, in particular, on TEM and SEM data furnish direct evidence of the nature of the Al_3Zr ordered phase precipitated coherently, as can be seen from its spherical shape (Fig. 11.5, *a*). Indexing the selection area diffraction pattern (Fig. 11.5, *b*) produces enough information to identify the Al_3Zr nanodispersoid. Incorporation of the ordered nanophase into the hexagonal matrix is of great interest due to its wetting ability for the magnesium melt and the use of fcc Al-nm Al_3Zr as an alloying composition ligature via rapid solidification technique based on a pulsed treatment) [361].

Moreover, their phase interfacial bonding is capable of effectively transferring a load from phase to phase and to call the effect of natural composite strengthening. Strain rate change creep testing of magnesium alloys in the Mg—12.5Al and nanoreinforced Mg—12.5Al—10 nm Al_3Zr systems is presented in Fig. 11.6. Micromechanical properties of purified magnesium alloys under examination can be additionally improved by equalizing the deformation behavior of their structural components throughout the material when incorporating nanoparticles like nm Al_3Zr in the matrix.

To illustrate, the points A′ and A″ indicate the shift of the ultimate transition from uniform to concentrated plastic deformation with localized shear in the activated sliding region upon introducing nanoparticles like nm Al_3Zr in the crystalline

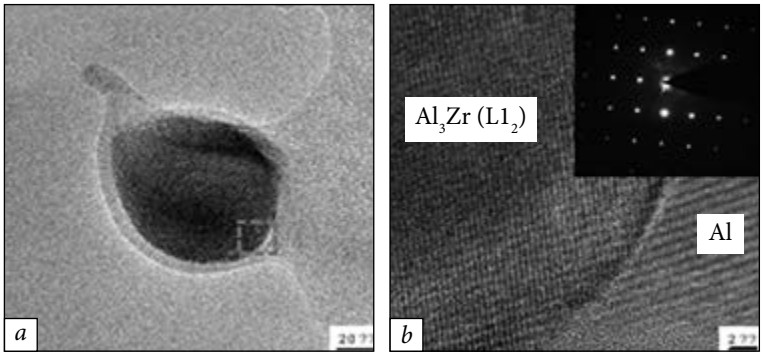

Fig. 11.5. SEM micrograph of nm intermetallic Al_3Zr with the effect of strengthening in fcc Al matrix (*a*) and a SAD pattern from the Al_3Zr nanophase with a cubic-type $L1_2$ lattice which satisfy the criteria of structural isomorphism and the high-resolution image of the selected areas (*b*)

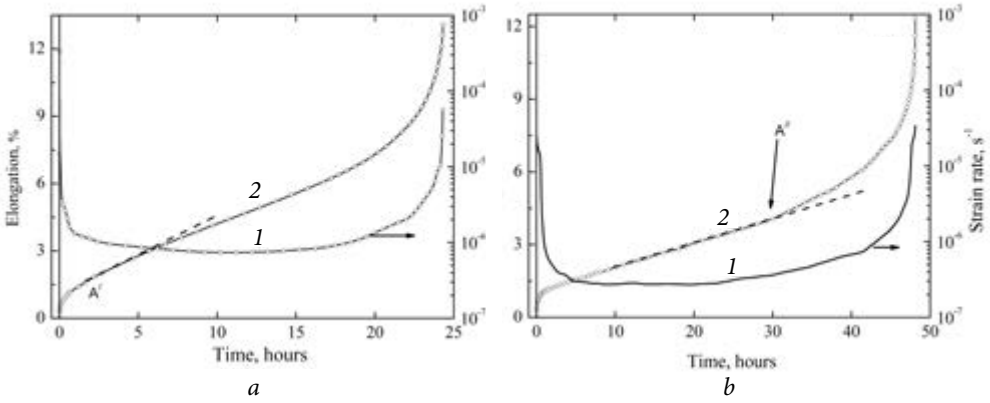

Fig. 11.6. Responses of creep resistance (*1*) and time-dependent elongation (2) at 100 MPa and 423 K for magnesium alloys in the hcp Mg—12.5Al (*a*) and hcp Mg—12.5Al—0.5 mass% nm Al_3Zr (*b*) systems; insert: typical tensile stress-strain curves for Mg—12.5Al (*3*) and Mg—12.5Al—0.3 mass% nm ZrO_2 alloys (*4*) at 423 K

matrix of the Mg—Al primary solid solution. A minute quantity of the useful uniform creep strain is seen to increase by 2% for the given nanophase reinforced alloy. The nanomodificated structure of the magnesium alloy increases creep resistance and strength as well as doubles its lifetime (from 24 to 48 h). Furthermore, the strain rate $\dot{\varepsilon}$ reduces from $7.4 \cdot 10^{-7}$ s^{-1} to $2.5 \cdot 10^{-7}$ s^{-1} at 100 MPa and 423 K. Thus, the dragging effect in purified magnesium alloys can be enhanced by a nanophase strengthening mechanism provided that the thermally stable nanoparticles pin the GBs.

REs with atomic numbers from 58 to 71 all have the same chemistry except gadolinium. The main advantage of using RE alloying elements is that their small amounts to hcp metal alloys produced by ingot metallurgy technique result in more

uniform distribution of fine incoherent nanoparticles [356]. However, in magnesium alloys (Table 9.4), under the data of chemical and XRD analyses, most of the stable RE-bearing nanodispersoids having additions of Y and Gd pin mainly GBs, and α-Mg matrix is essentially free of the dissolved RE.

The creep properties of magnesium alloys under investigation at 423 K and 70 MPa are significantly better than that of the commercial alloys AZ91D, AE42 and AS21. Unlike an AZ series of magnesium alloys with divorced eutectic (AZ91D, etc.), these experimental magnesium-based alloys containing cheaper additions compare favorably with higher creep and heat resistances as well as long-term strength against, e.g., magnesium alloy AE42 (Mg—4Al—2.5RE) containing expensive additions in the temperature and stress ranges of interest for automobile applications.

11.7. Development of High-Performance Zirconium-Based Alloys for Nuclear Energetics

The present study is concerned with nanooxide-reinforced zirconium alloys in the Zr—Nb—Sn—Fe system containing up to 1.5% nm Y_2O_3 and 1.2 % nm ZrO_2. They have been designed and examined mechanically and chemically using spectrographic, chemical and XRD analyses as well as strain-rate sensitivity tests and isothermal tensile creep testing to reveal processing-chemistry-structure relations responsible for the strengthening effects. In this study, a series of new experimental alloys based on the hcp Zr—Nb—Sn—Fe system and reinforced by nanooxides has been designed to improve their mechanical strength and dislocation creep resistance. To achieve this purpose, the effectiveness of their nanophase strengthening mechanisms was verified in as-cast, deformed and annealed conditions. An innovative method for nanooxide incorporating in the melt was developed to provide more uniform distribution of nanoparticles. Nanosized refractory oxides Y_2O_3 and ZrO_2 were identified by proper electron microscopy technique. Stress relaxation and strain rate change tests were performed to optimize the specific properties of short- and long-term strengths at 293 and 673 K.

This research also outlines a detailed study of mechanical properties of zirconium alloys in the Zr—8Al and Zr—8Al—1Nb systems using strain rate change measurements and tensile tests in a wide temperature range to optimize their specific properties such as dislocation creep resistance, high temperature strength and low temperature ductility. In this approach, a suitable combination of the innovative is melting, hot-working and annealing treatment of the Zr—8Al—1Nb alloy to produce a substantially continuous matrix of the $L1_2$ ordered intermetallic compound Zr_3Al (up to 92%). A series of mechanical tests has been carried out with the Zr_3Al-based alloys which should be considered as discontinuously reinforced composite materials by the very nature. Post thermomechanical treatment of as-cast Zr_3Al-based alloys indicates their unchangeable yield stress at 293 and within 673-973 K.

Mechanical properties of the essentially ordered Zr_3Al-based alloys are at least twice higher than those observed for solution-hardened zirconium alloys (Zircaloys). The Zr_3Al-induced structure developed by thermomechanical treatment with subsequent annealing improves the chemical and structural homogeneity of the composite material as a whole. The formation of inhibited jog-type obstacles on the screw dislocations is assumed to be the rate-controlling deformed mechanism of Zr_3Al ordered alloy strengthening which is dependent on the dislocation density. Excellent combination of short-term mechanical properties at 293 K and relaxation strength at 673-773 K revealed in the Zr_3Al-based alloys leads to their ability for high performance applications.

11.7.1 Nanooxide Strengthening of Zirconium Alloys

Historically, zirconium alloys, for example, the Zircaloys series, are still used in nuclear power engineering as shell materials [408-411]. Besides, new experimental alloys (Zirlo, M5, etc.) with additions of Nb significantly improve the creep resistance and performance of the fuel element cladding [409]. According to [410], niobium, under certain conditions, forms atmospheres of dissolved atoms around dislocations and thus slows down sliding during creep. In this case, the creep deformation is accompanied by the dislocation climb. Industrial zirconium alloys, the main alloying elements of which are niobium and tin (E-110, E-635, etc.) are widely used in the manufacture of claddings for fuel elements of thermal neutron power reactors with a water-steam coolant. In this regard, it is necessary to significantly increase the efficiency of such power nuclear reactors, in particular, to increase the coolant temperature to 673-723 K. Under these conditions, zirconium alloys E-110 and E-635 cannot be used, primarily due to insufficiently high creep resistance and long-term strength.

Usually, the hardened state of cast heat-resistant alloys is achieved by creating a structure that prevents the formation and movement of dislocations, mainly by the mechanism of precipitation hardening. However, precipitation-hardened alloys create a number of problems associated with a decrease in plasticity and inadequate premature fracture (long before neck formation) due to localization of deformation in soft regions of polycrystals with a high concentration of overstress, in particular, near-boundary Guinier-Preston's zones, free of precipitates, or at triple points (junctions) of grains. In the USA, a complex of technological developments of high-strength Al—Li—Mn and Al—Cu—Li alloys with minimal localization of microflow was carried out [368, 406]. According to [412], Al—Sc alloys hardened by the precipitation hardening mechanism have the lowest thermal stability due to accelerated coalescence caused by increased diffusion mobility of Sc and the loss of coherence by 30 nm Al_3Sc-coherence particles which create large fields of elastic distortions. Disruption of coherence in such cases occurs as a result of the formation of misfit dislocations. In addition, this alloy under the influence of atomic hydrogen becomes embrittled, for example, in space.

In the search for the most effective solutions, the systems of alloys with nanophase hardening are of particular interest, the advantages of which are associated with the possibility of artificially introducing nanodispersoids (no more than 10-50 nm in size) into the matrix at various stages of technological or industrial production and discrete modification of the structure [376]. Nanooxides ZrO_2, Y_2O_3, SiO_2, Al_2O_3, TiO_2 and La_2O_3 have selective wettability in melts, compatibility with components of complex alloyed alloys and do not actively interact with the matrix in a wide temperature range. Their introduction into liquid matrix of alloys based on copper and nickel in the range 3-4 vol. % causes the maximum increase in strength without unacceptable loss of ductility [411, 413].

Yttria is one of the oxides with the highest negative free enthalpy of formation, attesting to its thermal stability, and consequently only negligible dispersoid coarsening occurs in mechanically alloyed composite materials during exposure to temperatures lower than 1273 K for even more than 10,000 hr [367]. The average spacing between 30 nm oxide dispersoids is expected to be approximately 100 nm; the desired uniformity of the dispersoid distribution was confirmed at the level of TEM analysis. In our works [364, 365], complex alloyed zirconium alloys were studied using the Zr — Nb—Sn—nm ZrO_2 system with a discrete distribution of nanooxides up to 5 nm in size. In this case, in alloys with additions of 0.5 and 1.2% nm ZrO_2, it is possible to achieve, respectively, a twofold and threefold increase in the short-term strength. Taking into account the high results obtained, it is advisable to continue research in these areas with the verification of other no less promising nanooxides (Y_2O_3, La_2O_3, etc.), which also have good wettability with the zirconium melt. The development of cast zirconium alloys with Y_2O_3 nanooxide hardening becomes of paramount importance if we take into account that similar alloys obtained by powder metallurgy methods [411] with addition of up to 2% Y_2O_3 (200 nm in size) retain at 773 K the parameters of the creep rate and long-term strength up to the values close to the parameters for undoped zirconium.

Disperse (nanophase) hardening of alloys is characterized by increased resistance to high-temperature creep. In particular, dispersed refractory oxides, introduced during technological processing (for example, by mechanical alloying) or industrial production, form incoherent boundaries with the matrix, which, according to [376], attract dislocations at elevated temperatures.

Disperse oxide strengthening of metals (in particular, nanostructured copper) with Al_2O_3 nanoparticles increases the strength of the material by 1.5 times in tension and by an order of magnitude in creep [413]. ZrO_2 in zirconium alloys significantly increases the resistance to dislocation creep at temperatures of about 673 K [414]. Using thermomechanical treatment in the range of stability of the nanostructure, nanocomposite materials based on commercially pure titanium were obtained in terms of dispersion hardening of such a material with the precipitation of Ti_2C nanoparticles increasing its strength to a level typical for multicomponent titanium alloys ($\sigma_{0.2}$ ~ 850 MPa, σ_b ~ 1100 MPa) [415]. Therefore, in recent years,

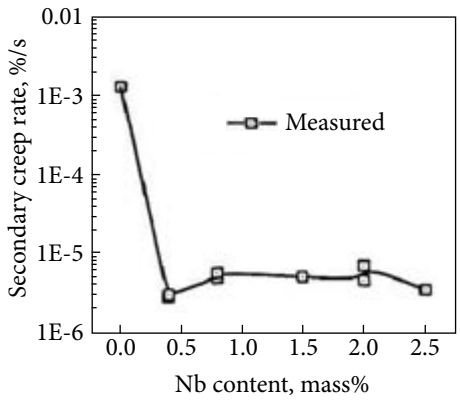

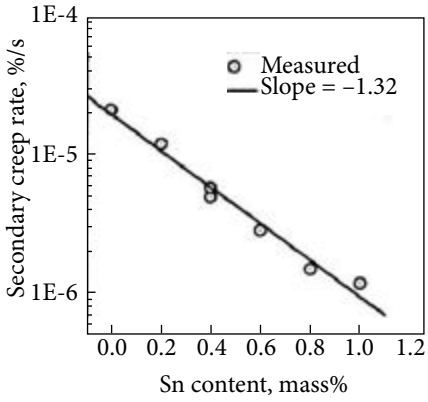

Fig. 11.7. Effect of Nb content on the steady-state creep rate of Zr-0.4Sn-xNb alloys [416]

Fig. 11.8. Effect of Sn content on the steady-state creep rate of Zr-0.8Nb-xSn alloys [416]

special attention has been paid to the nanophase hardening of the most promising alloy systems.

This research presents the results of measurements of the short-term and long-term strength parameters for complex-alloyed alloys based on the Zr—Nb—Sn, Fe systems containing nanoparticles of ZrO_2 and Y_2O_3. The data obtained were used to check the rate sensitivity of stresses and to select the most probable dislocation mechanism responsible for nanophase hardening, which provides an increase in the resistance to dislocation microflow/creep and long-term strength of these alloys with solid solution hardening.

Experimental Procedure

Zirconium alloys in the Zr—Nb—Sn—Fe system with additions of traditional solutes (Figs. 11.7 and 11.8) were chosen as a matrix of nanomodified composite materials taking into account data published in the open literature: nm ZrO_2 monoclinic modification with a size of about 4 nm in the amount of about 1.2 mass%, as well as nm Y_2O_3 cubic modification in an amount of up to 1.5 mass% of about 40 nm. Alloys based on iodide zirconium were smelted in an electric arc furnace with a non-consumable electrode in an argon atmosphere. A titanium iodide melt was used as a getter for gaseous impurities. For uniform distribution of nanooxides, a four-fold remelting was carried out in the Zr—Nb—Sn—Fe system together with the tin melt. After melting, the nanooxides were identified by TEM (JEOL JEM-100 CX P), XRD and X-ray photoelectron spectroscopy.

Research Results

According to the data of synchronous thermal analysis (STA), which combines the simultaneous measurement of mass (thermogravimetry, TG) and thermal effects (differential scanning calorimetry, DSC) (Fig. 11.9), the conclu-

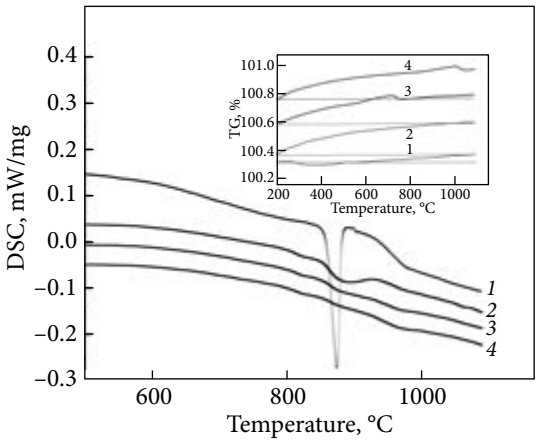

Fig. 11.9. The synchronous thermal analysis of iodide zirconium during four remelting by using DSC and TG techniques; insert: thermogravimetry as a function of temperature. The figure on a curve corresponds to the number of remelts. Gravimetric curves of the mass gain are as follows: *1* — 0.08; *2* — 0.23; *3* — 0.21; *4* — 0.21% (oxygen)

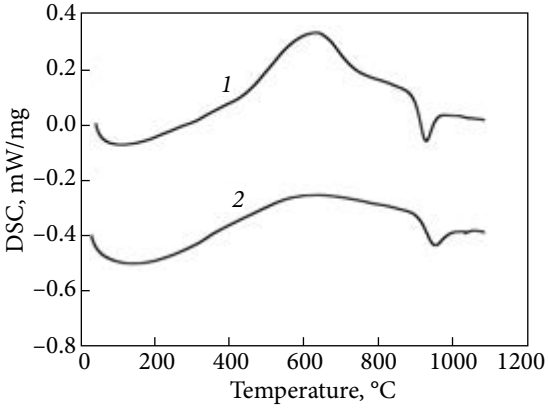

Fig. 11.10. DSC curves produced in the melting temperature range for zirconium alloys in the Zr—3Sn (*1*) and Zr—3Sn—0.5 nm ZrO_2 (*2*) systems

sion is justified that the second remelting of iodide Zr is accompanied by contamination (saturation) with oxygen, which suppresses the α-β phase transition. To fulfill the requirements for chemical homogeneity of Zr alloy ingots, at least 4 remelts are required. According to DTA/DSC data, with the introduction of Sn, the range of the α-β polymorphic transformation appears and expands. In this case, a shift in the temperature of transformation and expansion of the two-phase region are observed due to the slow kinetics of grain growth of the α-phase and the fast kinetics of grain growth of the β-phase (Fig. 11.10)

According to the XRD analysis (Table 11.3), the Zr—1Nb—1.5Sn—0.17Fe—1.5 nm Y_2O_3 alloy consists of an α-solid solution of zirconium and yttrium oxides (Fig. 11.11) shows a typical electron micrograph of the structure of the Zr—1Nb—0.6Sn—0.17Fe—0.8—nm ZrO_2 alloy, which reveals, at a higher resolution, high volume fraction (distribution density) of ZrO_2 nanooxides (Figs. 11.11 *a, b*).

The electron microdiffraction patterns of this alloy revealed two types of reflections from Zr (002) with an interplanar distance of 2.585 ± 0.001 Å and from ZrO_2

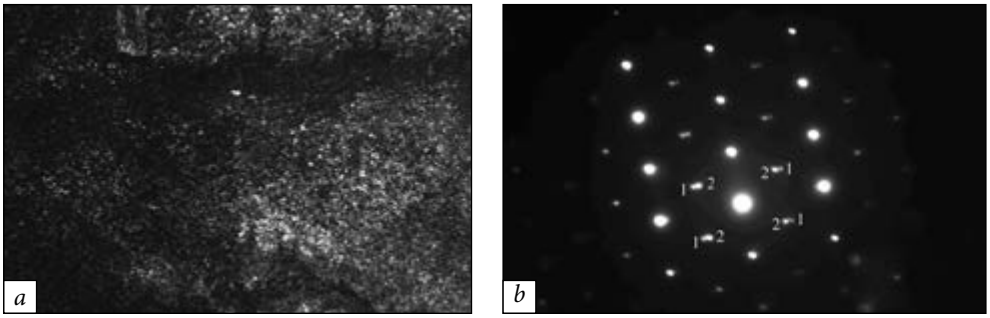

Fig. 11.11. Electron micrograph of the microstructure of the Zr—1Nb—0.6Sn—0.17Fe—0.8 nm ZrO_2 alloy after short-term tests at 673 K with the distribution of nanoparticles (dark-field image) (*a*) and electron microdiffraction pattern with reflections from the matrix and nanooxide ZrO_2 (*b*)

(111) with an interplanar distance of 2.847 ± 0.016 Å. The dark-field images with phase reflections show nanoparticles with a high distribution density. They were based on electron microdiffraction calculations, which are identified as particles of ZrO_2 nanooxide. Therefore, the chosen method of the consolidation for nanosized particles of refractory oxides in zirconium-based allows not melts only their introduction into liquid alloys, but also ensures a uniform distribution of nanooxides in the bulk of these alloys. It is important to emphasize that this technological solution ensures the formation of high hardness, heat resistance, creep resistance, and long-term strength of the investigated dispersion-strengthened zirconium alloys.

Deformation effectively affects the static and dynamic deformation aging of the studied zirconium alloys, in particular the kinetics of the decomposition of their solid solutions, and contributes to a more complete pinning of dislocations at low velocities, often corresponding to the creep rate. Thus, repeated loading of samples after intermediate holding is accompanied by an increase in stress and the appearance of the so-called yield point on stress-strain curves during unloading. In the case dislocations are pinned with the formation of Cottrell impurity atmospheres based on interstitial elements (oxygen). These experiments clearly demonstrate the participation of residual (accompanying) or technologically inevitable interstitial impurities in the formation of the resulting metallic properties of alloys in the Zr—Nb—Zn—Fe system. In this work, special short-term tests were carried out, which made it possible to reveal the interaction of the residual interstitial impurities, primarily oxygen, with the dislocation structure of remelted zirconium iodide alloys. When the deformation of the nano-hardened alloy Zr—1Nb—1.5Sn—0.17Fe—1.5nmY_2O_3 is carried out

Table 11.3. **Phase composition of the Zr—1NB—1.5Sn—0.17Fe—1.5nmY_2O_3 alloy**

Phase composition	Content, %	Lattice parameter, nm	
		a	c
αZr (hcp)	98.71	0.32446	0.51699
Y_2O_3 (cub)	1.29	1.0602	—

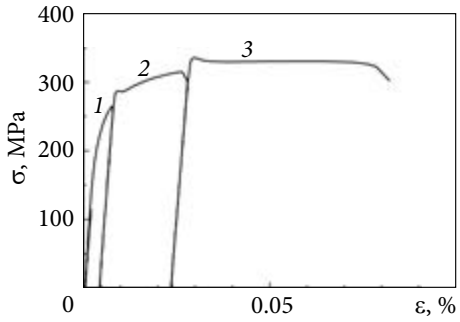

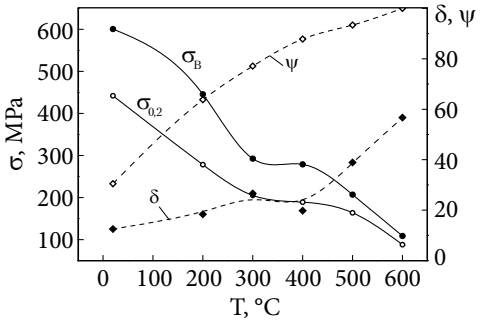

Fig. 11.12. Tensile curves at test temperatures of 878 (*1*), 778 (*2*), and 678 K (*3*) for Zr—1Nb—1.5 Sn—0.17Fe—1.5nmY_2O_3 alloy

Fig. 11.13. Temperature dependence of the mechanical properties for Zr—1Nb—0.6Sn—0.17Fe—0.8nmZrO_2 alloy subjected to deformation in the temperature range of 293-873 K

with intermediate loads from maximum to zero, its tensile curves at 773 and 673 K exhibit a yield point described in the literature by many researchers (Fig. 11.12).

In the case of continuous deformation, a yield point is absent. Its appearance on the tensile curve is associated with the activation of the Cottrell mechanism for interstitial elements [364]. In the initial stage of deformation, a sharp increase in the density (multiplication) of dislocations occurs. During the unloading of the sample in the temperature range of 293-873 K, condensation most likely of oxygen atoms occurs on immobile dislocations with the formation of Cottrell impurity atmospheres (Fig. 11.13).

Repeated loading (stretching) causes the appearance of a yield point, as predicted by Cottrell's strain aging theory. It should be noted that the oxygen concentration increases after each remelting of complex alloyed zirconium iodide alloys, which is confirmed by the data of chemical analysis and the corresponding increase in the elastic modulus. It is necessary to emphasize also other signs of the dislocation nature of strain aging. The serrations in the tensile curves are observed even at room temperature and disappear at temperatures above 873 K; i.e., in the region of severe deformation, when no Cottrell atmospheres are formed (Fig. 9.11).

The presence of the effect of dynamic strain aging on the curves of the temperature dependence of the mechanical properties of the deformed (and annealed) alloy Zr—1Nb—0.6Sn—0.17Fe—0.8nmZrO_2 (Fig. 11.13) is another confirmation of the activation of the mechanism controlling the interaction of mobile dislocations with mobile dissolved interstitial oxygen atoms, the concentration of which increases with the number of remelts (Fig. 11.9).

From a comparison of the rate sensitivity of stresses for iodide zirconium and its alloys, it follows that the alloy hardened with 40 nm $Y_2O_{3-}$with a concentration of 1.5% provides a higher resistance to dislocation microyielding than the alloy reinforced with 10 nm ZrO_2 with a concentration of up to 1.2%. Thermomechanical treatment (at 973...1073 K) enhances the effect of nanooxide hardening of the investigated

alloys (Tables 11.4 and 11.5) as a result of increasing the density (multiplication) of mobile dislocations and grinding the so-called martensitic structure of the primary α-Zr solid solution. Under these conditions, a change in thermal activation parameters is observed.

The most typical research results for the rate sensitivity of stresses in alloys of the Zr—Nb—Sn—Fe system, nano Y_2O_3-strengthened are shown in Figs. 11.14 and 11.15. On these graphs, the points correspond to the experimental data, and the lines — to the extrapolated dependences. Thermoactivation analysis of the creep rate in the steady-state stage for these alloys was carried out using the relation

$$\dot{\varepsilon} = \dot{\varepsilon}_0 (\sigma)^n \exp\left(- \frac{H_0 - \tau^* \cdot V^*}{kT} \right) \tag{11.10}$$

where $\dot{\varepsilon}_0$ is a constant; σ is the applied stress; τ* is the effective stress; V* is the apparent activation volume; n is the degree of strain hardening associated with the dependence of the density of mobile dislocations on stress; H_0 is the apparent activation energy; k is Boltzmann's constant; T is the absolute temperature. The apparent stress exponent n can be obtained by differentiation of the equation [377]:

$$n = \frac{d\ell n \dot{\varepsilon}}{d\ell n \sigma} = \frac{3}{2} \cdot \frac{Gb^2}{2kT} (1-k)^{3/2} (1 - \sigma / \sigma_d) \cdot \frac{\sigma}{\sigma_d} \tag{11.11}$$

where $0.2 \le \sigma / \sigma_d \le 0.9$.

Table 11.4. **Mechanical properties of cast zirconium alloys at 673 K**

Chemical composition, mass%	*E*, GPa	$\sigma_{0.002}$, MPa	$\sigma_{0.2}$, MPa	σ_{us}, MPa	δ, %	ψ, %
Zr—1Nb—1.5Sn	77.5	39	159	220	13.8	86.6
Zr—1Nb—1.5Sn—0.5ZrO_2	74.6	65	214	275	13.3	85.2
Zr—1Nb—1.5Sn—1.2ZrO_2	77.6	131	240	300	12.5	47.1
Zr—1Nb—0.6Sn—0.17Fe—0.8ZrO_2	70.2	84	192	260	20.0	77.8
Zr—1Nb—1.5Sn—0.17Fe—1.5Y_2O_3	79	146	245	330	7.7	17.4

Table 11.5. **Mechanical properties of deformed and annealed zirconium alloys at 673 K**

Chemical composition of alloy*, mass%	*E*, GPa	$\sigma_{0.002}$, MPa	$\sigma_{0.2}$, MPa	σ_{us}, MPa	δ, %	ψ, %
Zr—1Nb—1.5Sn—1.2ZrO_2	83.6	179	270	348	19.6	83
Zr—1Nb—0.6Sn—0.17Fe—0.8ZrO_2	65.8	—	191	285	18.8	87.8
Zr—1Nb—0.6Sn—0.17Fe—0.8ZrO_2	66.5	—	215	321	18.3	82.7

* Hot deformation from 61 to 87 % ε and treatment at 1073 K for 10 min.

The Rosler-Arzt equation is then equivalent to the usual power-law creep equation with very high value of n. For $\sigma/\sigma_d \geq 0.9$ the creep strength degrades with decreasing $\dot{\varepsilon}$ (to low n). With this provision, the attractive detachment vanishes with the detachment barriers disappearance. Climb effect exerts a back stress σ_b on moving dislocations ($\sigma^* = \sigma - \sigma_b$).

Under the preliminary data of thermoactivation analysis in the range of normalized stresses ($0.6\text{-}4.4 \times 10^{-3}$ σ/E) and the temperature range 673-873K, the rate of microplastic (creep) deformation is controlled by some thermally activated dislocation mechanisms with the apparent a.e. $H_0 \cong 4.3$ eV (~1Gb^3) and a.v. $V \cong 31.5b^3$, as well as with a.e. $H_0 \cong 3.4$ eV (~0.8 Gb^3) and a.v. $V \cong 22.5b^3$ for the cast and deformed states of the Zr-1Nb-1.5Sn-0.17Fe-1.5nmY_2O_3 alloy, respectively (Figs. 11.14 and 11.15). Decrease in a.v. for V after intense thermomechanical treatment of this alloy indicates a reduction in the activation length of a dislocation nanosegment (L_C) and a possible increase in the number of jogs at a dislocation.

Post thermomechanical treatment of as-cast zirconium alloys shows its beneficial influence on the better combination of strength and ductility of the nanoreinforced zirconium alloys (Table 11.6).

Nanodispersion strengthening discovers new possibilities for increasing the high-temperature strength of experimental zirconium alloys. In particular, at 673 K the short-term strength of alloys in the hcp Zr—3Sn-0.5—nm ZrO_2 is doubled, and increases threefold in the hcp Zr—1.5Sn—1Nb—1.2— nm ZrO_2 compared to Zr—3 Sn alloy (Fig. 11.16). Nevertheless, the steady-state creep behavior of a given zirconium alloy (Figs. 11.14 and 11.15) is similar to that obtained for magnesium alloys (Fig. 11.6, *a, b*) only at higher strain rates when the rapid thermally activated dislocations interact with athermal barriers such as SiO_2 nanoparticles. The curves were di-

Table 11.6. **Ultimate mechanical properties of deformed and annealed zirconium-based alloys upon tensile testing**

Chemical composition, mass%	Test temperature, K	YS, MPa	MPa, US	EL, %	RA, %
Zr—1.0Nb—1.5Sn—1.2nmZrO_2		751	872	13.3	38.3
Zr—1.0Nb—1.5Sn—0.17Fe—1.5nmY_2O_3	293	590	752	12.8	15.1
Zr—1.0Nb [417]		200	350	30	—
E635 [418]	293	500	590	16	—
E 110—Zr_2O [418]	293	580	—	22	—
Zr—1.0Nb—1.5Sn—0.17Fe—1.2ZrO_2	673	270	348	19.6	83
Zr—1.0Nb—1.5Sn—0.17Fe—1.5nmY_2O_3	673	245	330	7.7	17.4
Zircaloy 2 (Sandvik Co)	673	130	210	28	—
E 110: Zr—1.0Nb*	673	90	186	38	—
E 635: Zr—1.0Nb—(1.1—1.4)Sn—(0.3—0.5)Fe	673	253	288	18	—

* Typical strength of zirconium alloys at 773 K does not exceed 150 MPa.

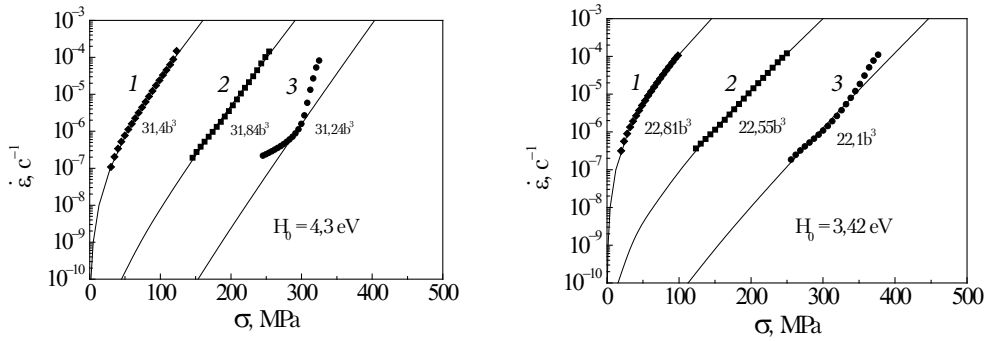

Fig. 11.14. Creep strain rate, $\dot{\varepsilon}$, as a function of stress, σ, for cast alloy Zr—1Nb—0.5Sn—0.17Fe—1.5nmY_2O_3 at test temperatures of 873 (*1*), 773 (*2*), and 673 K (*3*)

Fig. 11.15. Creep strain rate, $\dot{\varepsilon}$, as a function of stress, σ, at test temperatures of 873 (*1*), 773 (*2*), and 673 K (*3*) for Zr—1Nb—0.5Sn—0.17Fe—1.5 nm Y_2O_3 alloy subsequent to its hot deformation by 0.68 ε and annealing at 1073K, 10 min

rectly calculated by interpolating the data obtained from the mechanical tests. The observations were performed in order to describe the strain rate sensitivity of zirconium alloys in the commercially available hcp Zr—Nb—Zn system.

Modeling calculations and strength design indicate that the abrupt curves of stress increment Δσ vs the content of nano ZrO_2 obtained at higher steady-state creep strain rates gradually change into the smooth curves at lower strain rates (Fig. 11.17). The plot is expected to consist of two regions separating the entire data on high and low strain rate sensitivity. A transition to lower strain rates is accompanied by weakening of ZrO_2 nanophase strengthening. The resulting drag effect on sliding dislocations due to the ZrO_2 nanoparticles is active enough only at higher strain rates (10^{-3}-10^{-5} s^{-1}), as can be seen in Fig. 11.17.

It might appear at first glance that the nature of this variation would be rather unexpected. This finding might be well understood if properly provided for a shielding effect [24] of mobile interstitial oxygen which can inhibit the interaction between dislocations, migrating solute atoms and nm ZrO_2 particles upon slowing down strain rate. It is quite obvious that the dragging effect depends on the velocity of dislocations proportional to the strain rate in the thermally activated region. At higher strain rates the waiting time should be expected to be too short to form the dense Cottrell solute oxygen-containing atmosphere by a long-range diffusion-controlled mechanism. Thermal activation of rapid (short-range) mechanism appears to be energetically favorable for fast dislocations whereas Cottrell blocking by solute atmospheres is rate-controlling for slow dislocations. It is well-known that zirconium and its alloys are extremely strain sensitive to the presence of oxygen. The impurity interstitial solutes (0.15% O_2) affect essentially the stain rate and ability to the dislocation dragging effects in substitutional solution-hardened alloys. A striking example of this unusual behavior is given by Zr—Nb—Sn and Zr—Nb—Sn—nm ZrO_2 systems in the course

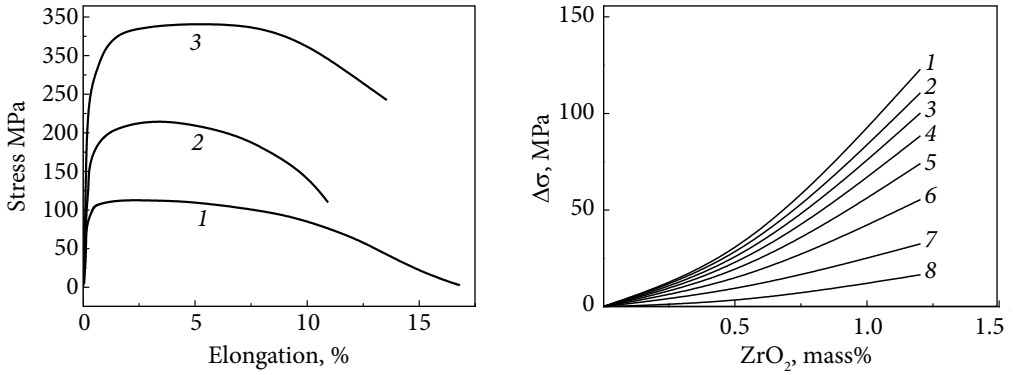

Fig. 11.16. Tensile curves at 673K for zirconium-based alloys in the systems hcp Zr—3Sn (*1*), Zr—3Sn—0.5nmZrO_2 (*2*), and Zr—1.5Sn—1Nb—1.2 mass% nm ZrO_2 (*3*)

Fig. 11.17. Stress increment as a function of 10 nm ZrO_2 content for Zr—1Nb—1.5Sn—nano ZrO_2 alloy at 673 K for different strain rates: 10^{-3} (*1*), 10^{-4} (*2*), 10^{-5} (*3*), 10^{-6} (*4*), 10^{-7} (*5*), 10^{-8} (*6*), 10^{-9} (*7*), 10^{-10} (*8*) s^{-1}

of strain-rate change tests. Oxygen is an attendant (technologically inevitable) impurity in technical grades of zirconium with an a.e. for vacancy migration of about 1.6 eV/atom and vacancy concentration on the interfacial surface ZrO_2–Zr to be 4.2×10^{20} vacancies/cm^2 [413]. Under the data on amplitude-dependent internal friction, the observed dislocation damping (Fig. 11.18) is the binding energy E_b between a dislocation and an interstitial solute-vacancy paired defect to be of about 2.0 eV associated with the presence of interstitially soluble oxygen in a parent zirconium matrix which forms the so-called paired defects consisting of an oxygen atom and an excess (strain-produced) vacancy [121].

These defects migrate in the stress field and pin the mobile dislocations by Cottrell locking with the high binding energy E_b of 2.0 eV (Fig. 11.18). With this provision, vacancy-type defects are assumed to relax the lattice strain caused by the action of oxygen atoms. In free crystalline lattice, substitutional solute atoms are much lower than interstitial ones. Therefore, at high strain rates they are too slow to cause hardening during tensile testing, while at slower strain rate they can compete with the interstitial atoms in the stress field around dislocations. Following the kinetics for a solid solution, solutes re-arrange first on the dislocation cores by Snoek stress-induced ordering mechanism or by the Schoeck-Seeger-Fisher-Fleisher short-range (rapid) mechanism and then they form solute atmospheres, for example, by the Cottrell long-term (diffusion-controlled) mechanism. The kinetic effect of Cottrell locking is thought to be negligible at high strain rates provided that time taken for the activation process of dislocation-interstitial interaction is too short to allow the formation of dense oxygen-containing Cottrell atmospheres. On the contrary, at slow strain rates, the oxygen atoms give a considerable contribution to the Cottrell atmosphere formation shielding their movement to the athermal barrier (nm ZrO_2).

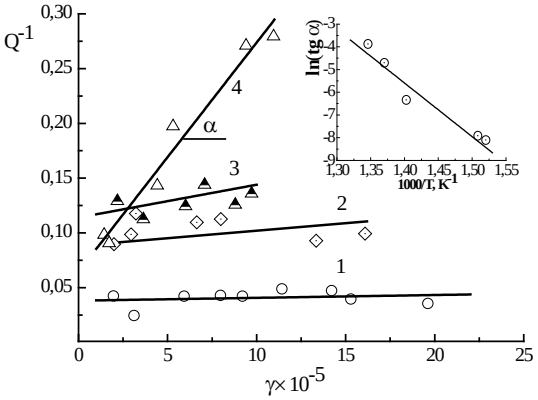

Fig. 11.18. The amplitude dependence of internal friction for hcp Zr (matrix) containing 0.15 mass% O_2 evaluated in the ln (tgα) — 1/T coordinates

Unusual strain rate response of nm ZrO_2 content is most likely to associate with the competitive interaction of mobile dislocations acting by an interstitial site mechanism with the impurity solutes and by a vacancy mechanism with the substitutional solutes. The slow kinetics of the poor strengthening indicates the preferential segregation of interstitial impurities towards the slow dislocations. The solute atmospheres provide a dragging effect on the stress fields of mobile dislocations when they pass through a lattice and cause the redistribution of solutes and excess vacancies due to their chemical affinity to oxygen. The principal idea is to neutralize the detrimental effect of foreign impurities on creep resistance and long-term strength of hcp metal alloy crystals. Since interstitial impurity atoms such as oxygen and the like impose a strain on solvent lattice restricting dislocation movement in the lattice strain field, it is necessary to remove the strain from the total lattice strain by refining or scavenging interstitial oxygen from primary solid solution using, e.g., erbium, cerium and yttrium. This approach allows the respective oxides to be formed due to their large negative free energies. With this provision, the main advantages of commercially available zirconium alloys under consideration could be kept at lower creep strain rates.

Nanodispersion Strengthening Mechanism in Zirconium Alloys

Dispersion hardening is the result of phase transformations typical, in particular, for the kinetics of the decomposition of a solid solution with the natural release of coherent nanoparticles. Nanophases are formed under conditions far from equilibrium [419, 420], including the rapid crystallization of highly supersaturated states [421]. The fcc Al — fcc Al_3Sc system is an impressive example of this kind of behavior. Sc dissolves in Al up to 0.3% at T_m. The lattice parameters of fcc Al and fcc Al_3Sc differ by only 1.3%. Therefore, nanoparticles with a diameter from 3 to 0.5 nm cause a very strong nanophase hardening effect. However, these metastable coherent nanoparticles rapidly grow larger after the coherence breakdown.

Until now, there is no simple theory that could unambiguously predict the mechanism of nanophase hardening based on the interaction of gliding dislocations with high-strength athermal barriers (up to 2.0 Gb^3). Therefore, in particular, creep and stress relaxation tests are performed for each new experimental alloy. There is no

general agreement among researchers on the dislocation mechanism that controls the rate of microplastic deformation at elevated temperatures for other reasons. According to Sastry data [414], an increase in the temperature dependence of stresses with a decrease in the test temperature is observed for deformed and annealed high-purity α-Zr and α-Zr containing impurities of interstitial elements (0.15% O_2, etc.). In this case, the controlling mechanism is associated either with the interaction of dislocations with interstitial impurity elements, or with the potential Peierls relief, which is overcome as a result of the formation of pair kinks at the dislocations. However, the actual a.e. H_0 is not a critical parameter or event to identify a control mechanism. Additional measurements or calculations of a.v. V^* are some reason for choosing a physical mechanism provided that the dislocation structure is retained. If we take into account that the activation of the transverse slip mechanism, adopted by many researches for thermal activation analysis, does not create pile ups and, therefore, does not cause the effect of strain hardening, and if we take into account that a constant structure creates thermal resistance, thermomechanical treatment followed by annealing of zirconium alloys eliminates the activation of the precipitation hardening mechanism. Usually, the power law characterizes the athermal contribution of the force interaction of dislocations and the stages of deformation (dislocation) hardening at long-range distances (~300 interatomic distances). The formation of incoherent interfaces between refractory nanooxides (Y_2O_3, ZrO_2) and a metal matrix is an important advantage of the dispersion hardening mechanism. In the periodical literature, direct evidence has been obtained for the existence of a threshold stress of dislocation creep, at which athermal depinning of dislocations trapped by dispersed particles occurs [422]. In this case, $d\sigma / \sigma\dot{\varepsilon}$ and $d(\sigma / E) / d\dot{\varepsilon}$ tend to zero at the critical value of σ. Dislocation creep of zirconium alloys is observed in the investigated temperature range 673-873 K. In this case, the threshold stress is not reached. The well-known principle of disperse hardening is based on a uniform volumetric distribution of nanoparticles (in the matrix, at GB, and at interfaces). In alloys with solution hardening, the strength of thermal obstacles, for example, dissolved substitutional alloying elements Nb, Sn in α-Zr, for gliding dislocations does not exceed 0.2 Gb^3, while the strength of athermal barriers increases by an order of magnitude (2.0 Gb^3) [364, 423]. Relaxation of stress fields around incoherent particles generates a certain local density of mobile dislocations. Since activation of this mechanism is a source of additional microplastic deformation, it limits the localization of shear in hcp crystals with a lack of active independent slip systems [396, 424].

Quite high values of a.e. H_0 (above the a.e. of bulk diffusion) and practically identical values of a.v. V^*, which does not depend on the grain size, indicate the validity of the performed thermoactivation analysis and, at the same time, the activation of a mechanism with a high barrier effect (0.8-1.2.) Gb^3. This mechanism differs from the mechanism of solid solution hardening with the strength of thermal obstacles (for example, dissolved substitutional atoms, Nb and Zn) not exceeding 0.2 Gb^3, or the conservative motion of jogs at dislocations with an energy of 0.3-0.5 Gb^3 [190,

423, 424]. These data indicate the activation of the most probable mechanism of nanooxide hardening of complex alloyed zirconium alloys. The values of the activation parameters calculated in this work correspond to a greater extent to the conditions of thermally activated bypass of nanooxides by gliding dislocations. At elevated temperatures, the interphase surfaces of nm Y_2O_3 and nm ZrO_2 become sinks for slip dislocations as a result of their attraction due to the weak chemical bond between the nanooxide and the matrix, i.e., between the phases at the interface. These observations are consistent with the models [376, 377], according to which, after attraction, the local climb of dislocations in front of a strong barrier becomes not only energetically possible, but even energetically favorable. At the first glance, it seems unexpected that the effect of nanooxide hardening caused by coarse Y_2O_3 oxides (up to 40 nm), is higher than that of 5 nm ZrO_2 hardening. However, an increase in the dragging path for nanoparticles when they are bypassed by 40 nm Y_2O_3 oxides, the energy consumption for the attraction of dislocations and the change in the radius of the dislocation bypass are not taken into account in this model. From this point of view, 40 nm Y_2O_3 can be more effective in comparison with 5 nm ZrO_2. In this context, one should expect an increase in resistance to dislocation microyielding (creep) and long-term strength.

In contrast to strain aging based on substitutional elements, in the process of dynamic strain aging, strong and fast (almost instantaneous) blocking of dislocations by interstitial elements (surfactants) occurs with the activation of the Snoek mechanism, which sharply increases the density of randomly distributed dislocations. The interaction of dislocations with tetragonal distortions caused by dissolved impurity interstitial atoms controls the rapid increase in the shear stress. This mechanism is believed to control the rate sensitivity of stresses at low strain rates corresponding to creep. Direct evidence has been obtained for the interaction of oxygen with dislocations, which causes the appearance of a yield point and a serrated yielding in Zr—1.5Nb—O alloys at temperatures up to 573 K [410]. Oxygen atoms provide dragging of mobile dislocations, hindering their transverse sliding and thereby enhancing the DSA effect. The a.e. for interstitial migration of interstitial atoms is determined by the elastic strain energy of the matrix lattice [425]. In this case, in the hcp lattice of α-Ti, N atoms with an a.e. of about 2.2 eV cause larger changes in volume than O atoms with an a.e. of about 2.0 eV. In accordance with the model concept, the relaxation energy of the fcc lattice of Al around of a hydrogen atom is 0.18 eV with a volume expansion of the unit cell in the tetrahedral position up to 12%.

The alternative Snoek-Kester model [427], which is consistent with many observations, considers the stress-induced diffusion of interstitial impurity atoms in a distorted lattice around dislocations. Snoek-Kester relaxation in bcc metals containing a high local concentration of interstitial atoms is associated with the formation of kink pairs at screw dislocations and the migration (diffusion) energy of the interstitials [428]. Due to the strong chemical affinity between titanium α-Ti and oxygen located in the octahedral interstices of the hcp lattice, a.e. of relaxation increases due to the

electronic interaction of α-Ti-O_2 [429]. In solid solution a.e. of diffusion becomes above a.e. of self-diffusion, if alloying elements increase elastic moduli (E and G), which indirectly characterize the energy of interatomic bonds in the crystal lattice.

In the temperature range corresponding mainly to the basic slip in hcp crystals, the climb of edge dislocations to different levels for the basal planes forms connecting sections, which are difficult to activate pinning points and obstacles for other basic dislocations [430]. At the same time, the activation volume caused by the non-conservative motion of jogs at dislocations cannot be lower than $100b^3$ due to their partial annihilation when interacting with vacancies and interstitial atoms [386]. In particular, in the study of cold-deformed Zr—1Nb alloys containing sulfur and oxygen additives, it was found [410] that the deformation rate is controlled by the interaction of dislocations with these atoms, which are responsible for a decrease in the activation volume from $110b^3$ to $80b^3$, taking into account the change in the activation length of the dislocation segment. Moreover, in the discrete temperature spectrum of deformed and annealed α-Zr, using low-frequency internal friction methods, at 753 K a peak was found due to thermally activated debonding of dislocations from oxygen atoms, and at 803 K — a peak caused by their tube diffusion [387]. Finally, in zirconium crystals containing simultaneously impurity interstitial (oxygen) atoms and substitutional atoms (Fe, Si, etc.), the 753 K peak of internal friction attests reorientation of pair defects in the field of cyclic stresses of pair defects, i.e., complexes consisting of substitution atoms and oxygen atoms. In this case, the relaxation time is consistent with the diffusion jumps of oxygen atoms occupying the octahedral positions closest to the substitutional atom.

Under these conditions, the interaction of dislocations with dissolved atoms during their segregation at linear defects is considered to be the most probable thermally activated mechanism that controls the deformation rate in the Zircaloys system of zirconium alloys [410]. For example, Nb atoms form Cottrell atmospheres segregate around mobile dislocations and thereby impede their sliding at moderate temperatures [426]. The strengthening of traditional Zr—Nb—O alloys is best explained by the thermally activated mechanism of interaction of dislocations with segregating atoms of dissolved elements. The effect of nanophase hardening indicates the activation of another alternative mechanism taking into account the thermal component of the resistance to dislocation motion.

Complex alloyed zirconium alloys strengthened with nanooxides have an increased resistance to dislocation creep, since they form incoherent boundaries with the matrix. Due to the weak coupling between the phases, they become sinks for dislocations and attract them at elevated temperatures. According to [367], hard and strong particles in a soft matrix cause localization of shear deformation at the particle — matrix interface. The results of these studies show good agreement with the experimental data obtained on alloys reinforced with nanooxides Y_2O_3 and Al_2O_3 in the Fe—Cr—Al [427]. According to these data, in the microstructure of an alloy containing Y_2O_3 nanooxides with a size of 24.5 nm at distances between them on average 109 nm, there is no evidence to the classical mechanism of particle bending proposed by

Orowan, i.e., $\sigma < \sigma_{or}$. On the contrary, dislocations are attracted by nanoparticles and climb over the interface between the particle and the matrix. In this case, the possibility of relaxation of the dislocation core is considered, which requires additional expenditure of the energy (work of the applied stress field).

An increase in the rate of strain hardening under the temperature-rate conditions of DSA is associated not with the dragging effect of dislocation atmospheres, but most likely with an increase in the rate of multiplication of dislocations under conditions of blocking of mobile dislocations. With an increase in the applied σ, previously inactive dislocation sources are activated. The weakening of the nanophase hardening of the zirconium alloy in the hcp Zr—Nb—Sn—nm ZrO_2 system [378] at low creep rates (10^{-6}-10^{-10} s^{-1}) is associated with the screening effect [388] caused by the preferential segregation of impurity oxygen atoms (0.15 % O_2) at dislocations by the Snoek-Cottrell mechanism. In this case, dense atmospheres are formed surrounding dislocations with a binding energy of 2.0 eV. The possibility of delocalizing the shear deformation and leveling the structure over the volume based on the formation of artificial additional sources of local microyielding — nanoparticles is one of the most important advantages of nanophase hardening.

There are a number of fundamental approaches and experimental techniques for identifying mechanisms that control the rate of plastic deformation. In this case, the activation energy (a.e. U*) is derived mathematically from experimental data on the microscopic mechanical properties of metal alloys. In particular, according to the Conrad concept [386], the activation parameters, a.e. U* and a.v. V*, and the vibration frequency of the dislocation segment, υ, can be calculated from the macrodeformation components, that is, partial derivatives, if a.e. as a function of stress does not depend on temperature. A straight line in theoretical coordinates indicates the presence of the force law of interaction in the form $\dot{\varepsilon} \cong \sigma^n$. In this case, there is no theoretical interpretation of this relationship within the framework of the dynamics of dislocations taking into account the density of defects, structure, impurity atoms and particles. In the case of plastic deformation, which is responsible for the macroscopic nature of the stress-strain dependence, the indicated partial derivatives according to Conrad should be determined with a constant fixed structure. However, this is only true for the initial yield stress. Since a change in the internal long-range stress correlates only with a change in the shear modulus with temperature, the calculated a.e. values U^* will exceed the true values and can be considered only as effective.

Thermal fluctuations assist the applied stress to overcome short-range (thermal) obstacles such as Peierls-Nabarro stress, i.e., crystal lattice resistance to dislocation motion, forest dislocations, jogs on screw dislocations (in slip planes), as well as cross-slip or climb (from slip planes) of edge dislocations. However, only short-range thermal obstacles are responsible for the dynamic aspects of creep deformation. The Pieirls-Nabarro stress is considered to be low in fcc and hcp crystals. It should be emphasized that the nonconservative motion of jogs and climb of dislocations occur with the participation of vacancies.

It is assumed that the a.e. for high-temperature creep deformation in metallic mono- and polycrystals coincides or agrees with the a.e. under the action of the applied creep stress. Moreover, according to Conrad, both of them correlate with their melting points. The limiting temperature of diffusion creep increases with deformation in this region. In this case, the thermally activated mechanism of dislocation climb is controlled by diffusion and becomes most likely a creep controlling mechanism in the temperature range $0.5\ T_m < T < T_m$. At lower temperatures ($0.2\ T_m < T < T_m$), the intersection of dislocations is considered as one of the most probable controlling mechanisms responsible for the rate of dislocation creep. Nevertheless, it cannot be considered proven that any of the mentioned mechanism is undoubtedly controlling with the exception of all the others. Hense, additional theoretical and experimental studies on this controversial issue are necessary for a more convincing identification of the controlling mechanisms of creep in zirconium alloys.

The Portevin-Le Chatelier effect is limited to a certain range of temperatures and strain rates, which can be described by the Arrhenius equation, similar to the equation in the domain of definitions of the lower yield stress, in the $\ln\dot{\varepsilon} - 1/T$ coordinates [428]. The anomaly $dG / d\dot{\varepsilon} < 0$ in this case is associated with the ambiguity of the function, which leads to local instability of the deformation [382]. Herein, it does not depend on the density of mobile dislocations, but depends on the total density of dislocations. This complicates a consistent theoretical interpretation of the most probable activated dislocation mechanisms.

The mechanical properties of the investigated alloys (Table 11.6) are significantly higher compared to alloys doped with niobium and tin [426, 428]. A characteristic feature of the Zr—Al—Nb alloys is that their yield stress at 293 and 673 K differ little, while when disordered alloys are heated, the elonation decreases significantly. There are certain difficulties in obtaining reliable information on the properties of nanoparticles and comparing them with each other due to differences in the valence, electronic structure, and chemical bond nature. Near the interface between the soft matrix and the solid phase, a higher density of dislocations is observed due to supersaturation at the boundary zones/interphase surfaces with vacancies, which increase the rate of diffusion climb of dislocations. The return of the yield point is mainly associated with local ordering in the stress field of dislocations by the Snoek-Schoeck mechanism.

There is evidence that the binding energy E_b for impurity interstitials in hcp transition metals can be as high as $Gb^3/6$ [428]. For α-Zr, under the data [108] the theoretical estimate ($Gb^3/6 \sim 1.55$ eV) is consistent with the measured dislocation depinning (with line tension of $0.5\ Gb^2$) from impurity interstitials (~1.47 eV). Besides, two additional peaks were revealed in the α-Zr relaxation spectrum of internal friction. They relate to the longtitutional pipe diffusion relaxation (at the 753K peak) with the bulk-diffusion coefficient D_L and to transverse core diffusion relaxation with coefficient D_T which is very close to the diffusion coefficient for oxygen in α-Zr. Since $D_L > D_T$, longitudinal core diffusion is much faster than transverse core diffusion.

With aid of the ε-T map [108], all of the complex and apparently anomalous results can be easily interpreted. The complex behavior of these relaxation peaks is similar to the behavior predicted theoretically by the Blair-Hutchison-Rogers concept and the Lucke-Schlipf model [108, 186]. It is shown that dislocations lose their solute atmospheres when they pass particles by the Orowan mechanism causing weakening effect [30]. In particular, some particles can be deformed by diffusion processes at the test temperatures due to the low partial pressure of oxygen present in zirconium alloys (up to 0.15% O). Its solute atoms cause a high concentration of oxygen vacancies in the oxide. This leads to significant creep below the threshold stress.

The high temperature and low frequency internal friction spectrum of deformed and annealed hcp α-Zr dominate at low strain amplitude at the 753 K peak, which is due to the thermally assisted depinning of dislocations from oxygen. The 803 K peak is believed to be caused by pipe core diffusion. The results obtained are consistent with those predicted by Blair-Hutchison-Rogers theory [108] based on the Teutonico-Granato-Lucke model of dislocation depinning [187].

There is evidence that the binding energy E_b for impurity interstitials in hcp transition metals can be as high as $Gb^3/6$. For α-Zr, $Gb^3/6 \cong 1.55$ eV so that peak P_o is consistent with depinning from an impurity interstitial. The TCD peak can be subsumed into the class of peaks attributed to the Snoek-Koster relaxation [427]. The deformation behavior of model zirconium-based alloys at 673K is assessed by tensile and creep testing.

11.7.2. Ordered Zirconium Alloys with Intermetallic Strengthening

Premises

Fuel elements in the form of a uranium oxide powder are placed in tube shells made of a zirconium alloy with additions of Nb and Sn and are used in power nuclear thermal reactors with a water coolant [429]. In connection with the technological requirements for increasing the temperature for the effective operation of the coolant up to 723 K, the known industrial alloys cannot be used under these conditions due to their insufficient strength and creep resistance. In this regard, the growing interest of specialists is aroused by a number of promising systems of zirconium alloys with a substantially continuous matrix consisting of Zr_3Al intermetallic compounds with an ordered structure of the $L1_2$ type [430-432]. In contrast to metal alloys, for example, with solid solution hardening caused by a sharp decrease in the yield stress with increasing temperature, the chemical compound Ni_3Al is characterized by an anomalous behavior of the temperature dependence of the yield stress due to the higher thermal resistance of its ordered structure. There is every reason to suppose a similar temperature dependence of the yield stress for the ordered compound Zr_3Al. Since Zr_3Al has a small thermal neutron capture cross-section, corrosion resistance and potentially high creep resistance studies of the structure of zirconium alloys based on Zr_3Al have been carried out at an advanced pace for many years [433-435].

Zirconium alloys with a substantially continuous matrix of the ordered intermetallic compound Zr_3Al have been patented in the USA [2]. These alloys in a cast state were subjected to hot deformation at 1273 K in the βZr—Zr_2Al two-phase region and then annealed at 1265 K. Noticeable improvements in short-term strength, creep resistance and corrosion resistance were found in zirconium grades containing from 7.5 to 9.5 mass% aluminum with intermetallic hardening according to the peritectoid reaction β-Zr + $Zr_2Al \leftrightarrow Zr_3Al$ (8.97% Al). The intermetallic compound Zr_3Al, which has an ordered fcc crystal structure of the Cu_3Au type, becomes the main phase in these cast alloys if its amount exceeds 50 vol%. Such alloys, unfortunately, have limited ductility (~3% δ at 293 K and ~10% δ at 573 K) and low manufacturability. They cannot yet be used as structural materials in new generation reactors, not only because of insufficient plasticity at room temperature, but also because of the amorphization caused by neutron irradiation. Some encouraging results were obtained on cast alloys in the Zr—Al—Nb system after prolonged annealing [436]. In this case, the morphology of the phases and the distribution of the Zr_3Al phase are associated with the activation of the controlling long-range (diffusion) mechanism.

Thus, the short-term and long-term mechanical properties of zirconium alloys with Zr_3Al intermetallic hardening have been studied insufficiently. This is especially true for the stress and temperature range corresponding to their potential applications. In this context, it becomes expedient to select the chemical compositions of alloys in the Zr—Al—Nb system that provide an optimal combination of high values of strength and ductility at 293 K and elevated temperatures (at least 673 K) using a new technological cycle of their thermomechanical and heat treatment.

Experimental techniques

Ingots of alloys Zr—8Al and Zr—8Al—1Nb were obtained using fusion of iodide Zr, Al grade A99 and Nb in an electric arc installation with a nonconsumable W-electrode in high-purity argon. The chemical (elemental) and phase

Table 11.7. **Modes of heat and thermomechanical treatment of zirconium alloys**

Grade	Type of treatment	Designation
Zr—8Al	Annealing at 1153 K: 4 hr	HT-1
Zr—8Al—1Nb	Annealing at 2153 K: 4 hr	HT-2
Zr—8Al	Hot forging 40% at 1237 K=>1173K	TMT
Annealing	at 1173 K: 10 min; annealing at 1153K: 4 hr	TMT: HT-3 and HT-1
Zr—8Al—1Nb	Hot forging 40% at 1237 =>1173 K	TMT: HT-4
Annealing	at 1273 K: 10 min.	
Zr—8Al—1Nb	Hot forging at 40% at 1237 K =>1173 K,	TMT
Annealing	at 1273 K: 10 min; annealing at 1153 K: 4 hr	TMT: HT-4 and HT-1

HT — heat treatment; TMT — thermomechanical treatment.

compositions of these alloys were determined using spectrographic and XRD findings. The obtained ingots were prepared for research in cast, deformed and annealed states by modes in the following combinations (Table 11.7).

At temperatures below 1261 K, Zr_3Al is formed by the peritectic reaction $\beta Zr + Zr_2Al \rightarrow Zr_3Al$, and below 1213 K — by the peritectoid reaction $\alpha Zr + Zr_2Al \rightarrow Zr_3Al$. This explains the choice of modes for thermomechanical and heat treatment (Table 11.7). After HT-1, the structure of the alloy consisting of 10% αZr and 90% of the Zr_3Al phase becomes difficult to deform (after 30% ε) with increased sensitivity through the local concentration of embrittling stresses. After severe deformation (from 40 to 75% ε), the alloys were subjected to heat treatment to isolate the maximum amount of the Zr_3Al phase at 1153 K. Due to the low manufacturability of Zr_3Al in the αZr matrix, some of the heat treatment modes were carried out at temperatures of 1173-1273 K, corresponding to a higher plasticity of βZr.

Tests for stress relaxation of zirconium alloys were carried out in the temperature range 673-973 K with an accuracy of ±0.25K. In order to exclude the influence of fluctuations in the ambient temperature, the measuring unit system was kept at a constant temperature and a load of ≈ 0.5 kgf for at least 3 hr. The relaxation tests of the samples were carried out at a strain rate of 10^{-4} s^{-1} according to the standard technique in a vacuum of 10^{-4} Torr. The growth of creep deformation was recorded for a rate of 10^{-7} s^{-1} (~1 μm in 10 min.). The elastic modulus E was calculated for unloading the sample with a rate of 10^{-3} s^{-1}.

Stress relaxation studies were carried out according to the method proposed by Sargent, with measurement of the parameters of the dependence of strain rate on the normalized stress in logarithmic coordinates and with an assessment of the sensitivity to the strain rate according to thermal activation analysis data.

Tensile tests were carried out at a strain rate of 10^{-4} s^{-1} in the area of uniform elongation in the temperature range 673-973 K. The values of elongation δ% under tension were recorded on the samples with special sensors with an accuracy of 1 μm.

Research results

In accordance with the phase equilibrium diagram (Fig. 11.19), the Zr—8Al alloy is in a two-phase region, which concludes a Zr-based solid solution and a Zr_3Al phase. The refractory intermetallic compound Zr_3Al is formed by the peritectic reaction $\beta Zr + Zr_2Al \rightarrow Zr_3Al$ at temperatures below 1261 K or by the peritectic reaction $\alpha Zr + Zr_2Al \rightarrow Zr_3Al$ below 1213K. It is an ordered superstructure with an fcc lattice of the Cu_3Al type ($L1_2$, cP 4) and with a lattice parameter a = 0.4372 nm at room temperature (Fig. 11.20). This type of ordered intermetallic compound Zr_3Al is formed during annealing at 1153 K for 4 hr in the course of peritectoid reaction. The XRD results for alloys Zr—8Al and Zr—8Al—1Nb are presented in Table 11.8.

According to these data, the volume fraction of the Zr_3Al phase in the deformed and annealed Zr—8Al—1Nb alloys is 80.6-84.5%. The rest of the volume is occupied

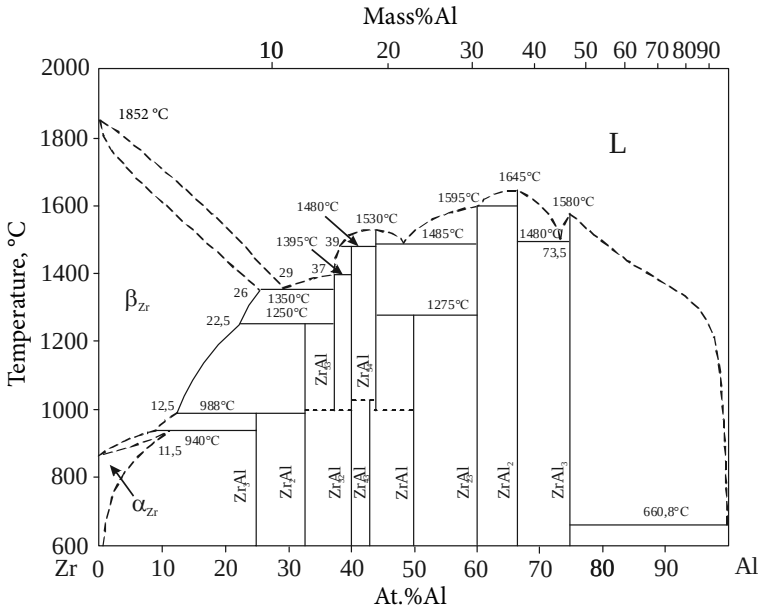

Fig. 11.19. Zr-Al binary equilibrium phase diagram [434]

Table 11.8. **Phase composition of deformed zirconium alloys**

Alloy	α_{Zr} (hcp lattice)		Zr_2Al (hexagonal lattice)	
	Lattice parameters, nm	Vol. fraction, %	Lattice parameters, nm	Vol. fraction, %
	A. Deformed state			
Zr—8Al	a = 0.32070 c = 0.1072 c/a = 0.15925	71.63	a = 0.49003 c = 0.59511	28.37
Zr—8Al—1Nb	a = 0.32091 c = 0.51145 c/a = 1,5937	80.39	a = 0.49003 c = 0.59498	19.61
	B. Deformed and annealed state			
	α_{Zr} (hcp)		Zr_3Al (fcc)	
Zr—8Al	a = 0.32250 c = 0.51575 c/a = 0.15937	7.36	a = 0.43761	92.64
Zr—8Al—1Nb	a = 0.32156 c = 0.51369 c/a = 1.5975	16.22	a = 0.43751	83.78

by the solid solution based on αZr. A decrease in the lattice parameter of the Zr—8 Al—1Nb alloy (compared to that of the Zr—8Al alloy) means that Nb with a smaller atomic radius dissolves in αZr. It is important to emphasize that Nb with an atomic radius smaller than that of the Zr atom and with a lattice parameter similar to that of Zr_3Al (a = 0.4372 nm), nevertheless, according to XRD data, does not dissolve in this ordered intermetallic compound, the lattice parameter of which practically does not change. It should be added that additional doping of Zr—8Al with niobium slows down the process of peritectoid transformation, reducing the volume fraction of Zr_3Al and increasing that of αZr.

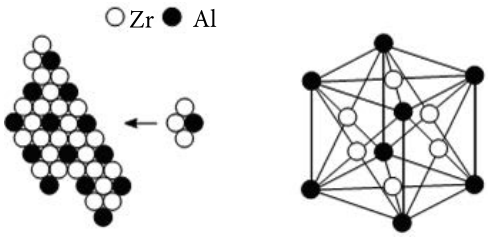

Fig. 11.20. Packing sequence of atoms and crystalline lattice of Zr_3Al

Cast ordered Zr_3Al alloys have limited ductility, not exceeding a few percent at 293 K (Table 11.9). Cast annealed alloys in the Zr—Al—Nb system are characterized by a low value of permanent deformation at 293 K. Thermomechanical treatment (TMT) of cast alloys, followed by annealing at 1153 K for 4 hr, leads to a significant increase in strength and ductility. During the thermomechanical treatment of these alloys, the concentration of vacancies increases sharply. The resulting increase in the diffusion mobility of atoms intensifies the formation of the Zr_3Al phase during the peritectoid transformation. A certain role in the formation of mechanical properties of alloys in the Zr—Al—Nb system belongs to zirconium-based solid solutions. In particular, with an increase in the volume fraction of a solid solution of Zr, when passing from the Zr—8Al alloy to Zr—Al—Nb, the permanent deformation also increases (Tables 11.9 and 11.10).

The deformation of alloys substantially ordered on the basis of the $L1_2$ superstructure Zr_3Al retains its features in a wide temperature range of 293-873 K. At the same time, they have important advantages: a) In the temperature range of 293-

Table 11.9. **Mechanical properties of substantially ordered Zr_3Al alloys in heat—treated cast and deformed states after tensile tests at 293 K**

Grade	E, GPa	$_{0.002}$, MPa	$_{0.2}$, MPa	$_{B}$, MPa	EL. %	RA, %
Cast state after annealing (HT—1)						
Zr—8Al	126	445	606	607	0.3	2.0
Zr—8Al—1Nb	122	345	601	845	3.6	6.4
Deformed state after annealing (HT—1)						
Zr—8Al	122	477	526	807	5.8	10.4
Zr—8Al—1Nb	106	510	618	950	7.9	13.0
Zr—8Al—1Nb	122	377	519	962	8.2	7.5

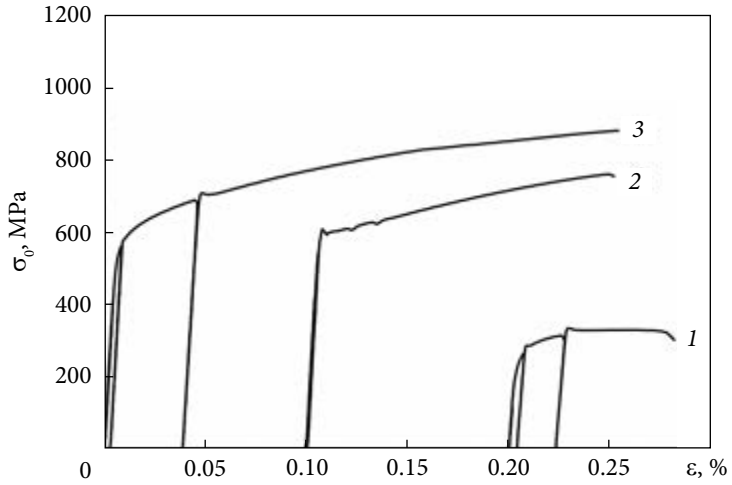

Fig. 11.21. Tensile curves for a zirconium alloy with nanophase and solution hardened strengthening (*1*) and essentially ordered Zr_3Al-based alloys (*2, 3*): (*1*) Zr—1Nb—1.5Sn—0.17Fe—1.5nmY_2O_3; (*2*) Zr—8Al after heat treatment at 1153 K for 4 hr; (*3*) Zr—8Al—1Nb after heat treatmentat 1153 K for 4 hr

773 K, these alloys retain uniform elongation from the onset of deformation to complete failure, i.e., do not show a tendency to localize shear deformation and neck formation. Moreover, the plasticity of these materials increases with increasing temperature (up to 873 K); b) A characteristic feature of the investigated ordered zirconium alloys with intermetallic Zr_3Al hardening is the actual absence of a clear temperature dependence of the yield stress, for example, for the Zr—8Al alloy (92% Zr_3Al) (Tables 11.9 and 11.10). This result is a sign of a more efficient thermal resistance of the ordered structure of the $L1_2$ intermetallic compound (Zr_3Al, Ni_3Al) compared to disordered alloys with solid solution hardening in the Zircaloy system, in which the yield stress decreases with increasing temperature. The retention of the yield stress of the Zr—8Al alloy with increasing temperature (606 MPa at 293 K and 604 MPa at 673 K, Tables 11.9 and 11.10) is associated with the appearance of hindered Keer-Wilsdorff complexes in the ordered structure of $L1_2$ [432, 433]. Moreover, all the mechanical properties of the investigated zirconium alloys Zr_3Al after hardening were found to be in an optimal combination significantly higher than the analogous properties of alloys in the Zr—Nb—Sn system and commercially acceptable

Table 11.10. **Mechanical properties of substantially ordered Zr_3Al alloys in the cast and annealed state after tensile tests at 763 K**

As-cast alloy after annealing (HT-1)	E, GPa	$_{0.002}$, MPa	$_{0.2}$, MPa	$_{B}$, MPa	EL. %	RA, %
Zr—8Al	106	383	604	776	14.4	24.8
Zr—8Al—1Nb	99	394	540	874	24.2	19.6

alloys EI 110, EI 635 [429]; c) Tension curves of zirconium alloys with different matrices show (Fig. 11.21) that in terms of strength and ductility characteristics, alloys substantially ordered on the basis of Zr_3Al are at least twice higher than similar characteristics of an alloy with solid solution ordering of a disordered matrix αZr. Niobium additionally increases the plasticity of ordered alloys after heat treatment at 1153 K, which changes the ratio of hard and soft phases, Zr_3Al / αZr, and increases the volume fraction of the soft component of αZr in the Zr—8Al—1Nb alloy. The presence of a yield point (at intermediate unloading) is associated with the multiplication of dislocations and the development of deformation aging caused by the formation of oxygen atmospheres at the cores of dislocations. Nevertheless, the fcc structure of Zr_3Al reduces the sensitivity of these ordered alloys to solid interstitial elements (H, O).

Strengthening Mechanism in Ordered Zirconium Alloys

In ordered alloys with the $L1_2$ superstructure, plastic deformation is carried out by superdislocations. Its mechanism is fundamentally different from that of disordered alloys [432, 436, 437]. In the course of deformation in the ordered structure $L1_2$, each helical superdislocation, in particular, with the Burgers vector <101> splits into superpartial/superparticle dislocations a/2 <101> connected in the octahedral plane by a band of antiphase boundaries [438]. In turn, each of the superparticle dislocations splits into partial dislocations a/2 <112>, connected by a complex stacking fault. It was found that in the process of deformation, the helical superdislocation splits into two superpartial/superparticle ones with antiphase boundaries between them. Each of them, in turn, splits into partial dislocations with a complex stacking fault between them.

Although the carriers of plastic deformation in intermetallic compounds with an ordered $L1_2$ structure are superdislocations, the peculiar plastic behavior of ordered alloys is nevertheless determined not only by the features of superdislocations and the structural transformations they undergo, but also by the specifics of barriers (for example, domain boundaries) which impede the movement of dislocations in these crystals. According to the model concepts [439, 440], at elevated temperatures, as a result of the activation of the transverse slip mechanism, a part of the thermally activated helical superdislocations passes from the {111} <101> octahedron plane to the {100} <100> cube plane and splits into two superpartial/ superparticle dislocations in a parallel plane with the formation of a hindered dislocation configuration blocked in the octahedron plane. In this case, a superparticle dislocation in the cube plane and a superpartial/superparticle dislocation in the octahedron plane form a hindered complex (step) — the so-called Keer-Wilsdorf barrier [431, 437, 439]. The number of these barriers increases with temperature. The transformation of gliding superdislocations into barriers is the main cause of temperature anomalies in the deformation characteristics of ordered alloys. With an increase in temperature, such alloys are self-strengthed due to an increase in deformation resistance, strain hardening coefficient,

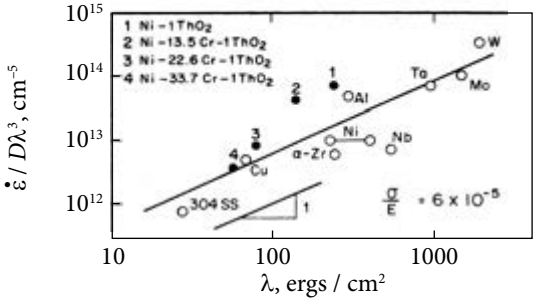

Fig. 11.22. Influence of stacking fault energy on the creep rate at constant stress over modulus for various pure metals (αZr, etc.)

and macroscopic yield stress. The power law $\dot{\varepsilon} \cong \sigma_n$ by its nature characterizes the athermal contribution of the force interaction of dislocations and the stages of deformation (dislocation) hardening at long-range distances (of about 300 interatomic distances). In particular, $n \cong 1$ (for the diffusion mechanism); $n \cong 3$ (for the mechanism of nonbasic slip of dislocation) and $n \cong 5$ (for the mechanism of dislocation climb).

For dislocation creep of alloys with intermetallic Zr_3Al hardening in the force mode, indicated by the strain hardening coefficient ($n \cong 5$ or 6 [430]), the activation volume V of the nonconservative motion of ledge jogs on screw dislocations cannot be lower than 100 b^3 due to annihilation of ledges formed by vacancies and interstitial elements [441]. Since V does not depend on the grain size, the transverse slip and climb of dislocations with a.v. $V \cong 10\text{-}50\ b^3$, which depends on the stacking fault energy (Fig. 11.22), can be considered as the most probable mechanism controlling creep rate of ordered alloys with intermetallic hardening. Some deviations of the activation parameters for this dominant mechanism are associated with a change in dislocation density, including during thermomechanical and heat treatment (from $10\text{-}10^{14}$ to $10^{15}\ m^{-2}$) during mechanical tests.

Ni—Cr dispersion hardened alloys and 304 stainless steel. Comparisons were made at constant diffusivity, D, and subgrain size, λ, by plotting the creep rate as $\dot{\varepsilon} / D\lambda^3$. The subgrain size for the dispersion hardening alloys was not measured; the λ used was the mean free path between particles which is oftentimes related to subgrain size [264]. The huge decrease in creep strain rate could be a decrease in the staking fault energy due to alloy age (Fig. 11.21). When subgrain effects are included, it is shown that the creep has been previously thought [264]. Further research in this area seems very much warranted.

The predominant contribution of the main Zr_3Al phase to the plastic deformation of zirconium alloys in the Zr—Al—Nb system is beyond doubt, since, in contrast to disordered alloys, the deformation of ordered intermetallic compounds occurs according to a fundamentally different mechanism. For example, the Ni_3 (Al, Ti) phase increases the ductility and fracture toughness of Ni—Cr alloys, since its ordered structure is disturbed by dislocations that have passed through the lattice of this phase. The restoration of order occurs as a result of diffusion, which reduces the increase in strength from the antiphase boundaries. The dislocation creep mechanism is cumu-

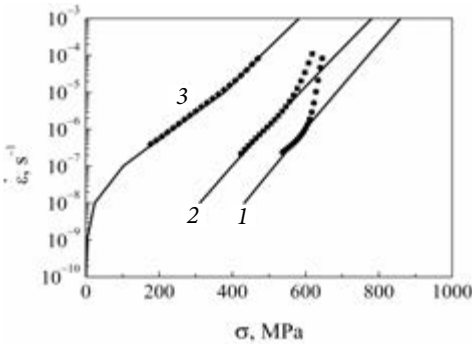

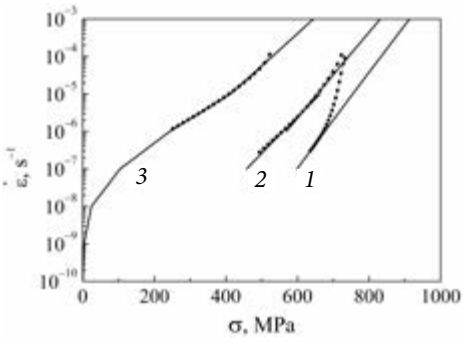

Fig. 11.23. Creep strain rate, $\dot{\varepsilon}$, as a function of stress at temperatures of 673 (*1*), 773 (*2*), and 873 K (*3*) for as-cast Zr—8Al—1Nb after heat treatment at 1153 K for 4 hr

Fig. 11.24. Creep strain rate, $\dot{\varepsilon}$ as a function of stress at temperatures of 673 (*1*), 773 (*2*), and 873 K (*3*) for as cast alloy Zr—8Al—1Nb deformed at 1273 K and annealed at 1153 K for 4 hr

lative and is accompanied by the formation of a defect structure. The critical defect density is formed when the critical stress is reached in the power mode n => ln n ln σ or the critical temperature (at σ = const) under conditions of thermally activated Arrhenius behavior $\ln\dot{\varepsilon}$ – 1 / T.

Under the preliminary data of thermal activation analysis (Figs. 11.23 and 11.24), the dislocation creep rate of substantially ordered Zr—8Al and Zr—8Al— 1Nb alloys at relatively low temperatures (773-873 K) and high stresses (5-7) × 10^{-3}σ / E is controlled by an a.e. of about 1.71-2.14 eV (0.25-0.33 Gb^3) with the a.v. 14.4-16.8 b^3, corresponding to the activation parameters required to activate the mechanism of solid solution hardening of α-Zr. In this case, the dissolved alloying element Nb increases the a.e. by 0.4 eV (from 1.7 to 2.1 eV) only after deformation of the Zr—8Al—1Nb alloy.

At higher temperatures (873-973 K) and the same stresses, the motion of dislocations at the steady-state stage of alloy creep is described by a higher a.e. 3.2...3.6 eV (0.50...0.74 Gb^3) with a.v. 13.4...18.7 b^3. And in this case, Nb increases the a.e. by 0.4 eV (from 3.2 to 3.6 eV) only after deformation of the ordered alloy Zr—8Al—1Nb. At low stresses (0.02...3.8) × 10^{-3} σ/E and elevated temperatures (873-973 K), the rate of dislocation creep is determined by a thermally activated process with a.e. 3.32 eV (0.7 Gb^3) and a.v. 5.3...8.8 b^3.

Thus, the calculated values of the a.e. turn out to be rather high, for example, in comparison with the energy of threshold formation on screw dislocations, especially since this mechanism requires large a.v. (100-300 b^3). In the periodical literature [433], two mechanisms are proposed that control the rate of dislocation creep at elevated temperatures. In accordance with these model concepts, the mechanism of climb of edge dislocations with a.e. 2.87...3.48 eV, increased in alloys with a higher Nb content, and a small activation volume in units of b^3 is considered dominant. In this context, there is every reason to assume that, at elevated temperatures, the creep rate is controlled by the thermally activated mechanism of disorder in the Zr_3Al interme-

tallic compound, the main component of this composite material. These observations are confirmed by the data [15], according to which the destruction and restoration of the order of the fcc lattice of Zr_3Al occurs as a result of sliding of the leading and trailing superdislocations. With this condition, strong Keer-Wilsdorf barriers increase in number with increasing temperature.

Concluding Remarks

A series of nanoreinforced hcp magnesium and hcp zirconium alloys in the Mg—Al—Ca and Zr—Nb—Sn systems, respectively, has been developed as nanophase materials with more excellent heat-resistance and higher long-term strength at elevated temperatures. Magnesium alloys of high purity in the hcp Mg—Al—Ca systems discontinuously nano-reinforced by nm Al_3Zr and ZrO_2 reveal the desirable increase in dislocation creep resistance and long-term strength over the unreinforced counterparts at 423 K (up to 70 MPa for 200 hr life).

Selected magnesium-based alloys reinforced by nano-precipitation hardening and nano-dispersion strengthening mechanisms were examined in the power law regime using long-term testing, strain-rate change measurements and constant structure steady-state creep tests to analyze the deformation and kinetic behavior of magnesium alloys in the hcp Mg—Al—Ca — nm Al_3Zr and Mg—Al—Ca—nm ZrO_2 systems at 423 and 673 K. The microstructures generated in these hardened alloys have been assessed by proper techniques aiming at controlling and understanding the composition modification in the nanophase-reinforced and nanophase-free hcp magnesium alloys. The experimental studies were employed to optimize the composition — processing — microstructure — strength property relationship of the Mg—Al—Ca nano-reinforced composite materials in terms of extended uniform strain concept:

• Nano-phase strengthening delays shear localization to much higher values of uniform microyield (creep for slow dislocations) and spreads a region of uniform tensile elongation from 0.5 to 30%. To be more uniform, a nanophase nanostructure is to be more thermally stable as regards its dynamic recovery. In this respect method of nm-dispersion strengthening takes precedence over age hardening when overcoming the concentrated sliding with localized shear. To illustrate, for nm Al_3Zr strengthened magnesium alloys, a transition from uniform to localized strain can exceed 1-2% at 423 K, while nm-particles of ZrO_2 can spread it up to 20-30%.

• The long-term strength of nano-reinforced hcp metal crystals in question is believed to be attributed to the GBs pinning by the nanoparticles embedded into their matrices. The thermally activated dislocation climb mechanism is suspected to be the rate-controlling mechanism responsible for the beneficial effect of nano-reinforced strengthening for hcp metal alloys under investigation.

• Magnesium alloys of high purity in the hcp Mg—Al—Ca systems discontinuously nano-reinforced by nm Zr_3Al reveal the desirable increase in the dislocation

creep resistance and long-term strength over the unreinforced counterparts at 423 K (up to 70 MPa for 200 hr life).

A series of hcp metal alloys in the Mg—Al—Ca system discontinuously nano-reinforced by Zr_3Al and ZrO_2 has been developed as crystalline nanophase materials with more excellent heat and creep resistance as well as higher long-term strength. The observations and findings suggest that the principles of nanophase strengthening should be considered as an effective means of obtaining desirable combinations of mechanical properties due to the nanoparticle-induced delaying of time-dependent shear localization.

A family of new experimental alloys based on hcp Zr—Nb—Sn—Fe systems and reinforced by nanooxides has been designed to improve their mechanical strength and dislocation creep resistance. To achieve this purpose, the effectiveness of their deformed and nanophase strengthening mechanisms was verified in as-cast, deformed, and annealed conditions. A new method for nanooxide particles injecting into the metal liquid was developed which provided more uniform distribution of nanoparticles. Nanosized refractory oxides, nm-yttria Y_2O_3 and nm-zirconia ZrO_2, were identified by proper electron microscopy technique. Stress relaxation and strain rate change tests were performed to optimize the specific properties of short- and long-term strengths at 293 and 673 K.

The present study is concerned with nanooxide-reinforced zirconium alloys in the Zr—Nb—Sn—Fe system containing up to 1.5% nm-Y_2O_3 and 1.2% nm-ZrO_2. They have been designed and examined mechanically and chemically using spectrographic, chemical and X-ray analyses as well as strain-rate sensitivity tests and isothermal tensile creep testing to reveal processing-chemistry-structure relations responsible for the strengthening effects. In this study, a series of new experimental alloys based on the hcp Zr—Nb—Sn—Fe system and reinforced by nanooxides has been designed to improve their mechanical strength and dislocation creep resistance.

The refractory nanooxide of yttrium (nm Y_2O_3) is shown to be more effective compared to nanozirconia (nm ZrO_2). Post thermomechanical treatment of as-cast zirconium alloys shows its beneficial influence on the better combination of strength and ductility of the nano-reinforced zirconium alloys. A yield point elongation and stress serrations due to deformed and dynamic strain aging were observed in hcp Zr—1.0Nb—0.6Zn—0.17Fe alloys nano-reinforced by nm Y_2O_3 and nm ZrO_2. Inevitable impurity oxygen atoms acting by an interstitial mechanism are likely to be responsible for the dragging of mobile dislocations to hinder their cross slip and to intensify the effect of DSA in the commercially pure Zr and its alloys. The observed strengthening effects of yield point elongation and dynamic strain aging appear to be caused by the interaction between dislocations and inevitable interstitial impurity of solute oxygen atoms (up to 0.15 %). Under the data of thermoactivation analysis, the steady-state creep strain rate is assumed to be controlled by a thermally activated dislocation by-pass mechanism with a.e. of 4.3 eV and a.v. of 31.5 b^3 as well as 3.4 eV and 22.5 b^3 for the as-cast and deformed Zr—1Nb—1.5Sn—0.17Fe—1.5nm Y_2O_3 al-

loys, respectively. The decrease in the activation parameters for deformed alloy state is likely to be associated with shortening of the activation length for mobile nanosegment and possible increase in the number of the jogs on dislocations.

As a result of these findings, the thermally activated overcoming of the nanooxides by dislocation climb appears to be a rate-controlling by-pass mechanism responsible for excellent optimal combination of short-range and long-range properties at 673 K including higher dislocation creep resistance by inhibiting of glide. The outcomes of trials indicate that the experimental data obtained are best of all consistent with those predicted by the Arzt-Wilkinson model. The discontinuously nanooxide-reinforced zirconium matrix composites should be considered as important innovations for materials engineering that provide an opportunity to combine the metallic properties with the ceramic ordered properties of strengthening nanooxides and thereby to improve the strength, modulus and thermal stability of the material as a whole. These materials are attractive for advanced structural and nuclear industrial applications as a conning material in nuclear fuel element.

The basic conclusions concerning the Zr—Nb—Sn—Fe system can be drawn from results obtained and may be stated as follows:

• A method of introducing refractory nanooxides into a liquid alloy in the Zr—1Nb—1.5Sn—0.17Fe—1.2ZrO_2 system based on a master alloy consisting of a powder composition of oxides and metal components (tin) has been proposed. According to the TEM data, such a technological solution provides a uniform distribution of nanooxides during the crystallization of a complexly alloyed zirconium matrix.

• Nanooxide strengthening discovers new possibilities for increasing the high-temperature strength and heat-resistance of hcp zirconium alloy crystals. In particular, at 673 K short-range strength of zirconium alloys is doubled in the hcp Zr—3.0 Sn—0.5nmZrO_2 system and increases threshold in the hcp Zr—1.5Sn—1Nb—1.2 ZrO_2 system. The promising results indicate that the useful increment of properties is believed to be caused by the preferential nanophase-pinning of grain boundaries. With the impeding of dislocation mechanisms, the systems can be expected to give a sounder result.

• Some deterioration of long-term strength is observed in the unrefined zirconium alloys in question upon slowing down the creep strain rates over the range from 10^{-6} to 10^{-9} s^{-1}. The change of dislocation damping with temperature in the hcp Zr matrix containing up to 0.15% O_2 gives the first evidence for the preferential segregation of oxygen on strain-produced dislocations to form Cottrell dense atmospheres pinning dislocations with strong binding energy of about 2.0 eV. The weakening of nano-dispersion strengthening of commercially available alloys in the hcp Zr—Nb—Sn—nm ZrO_2 system with slowing down the creep strain rates (10^{-6}-10^{-9} s^{-1}) is associated with the shielding effect due to a strong Cottrell locking of mobile dislocations by the large quantity of interstitial oxygen impurities which are assumed to inhibit the interaction between glide dislocations and solutes in the thermally activated range, as consistent with the Cottrell-Bilby theory.

• The unexpected behavior of commercially available zirconium alloys observed in the Zr—Nb—Sn—nmZrO_2 system might be well understood if properly provided for a shielding effect of impurity atoms of oxygen which inhibits the interaction of dislocations with substitutional solutes (Nb, Sn) and nm ZrO_2 particles. Unlike macroscopic changes in strain, evolution of microyielding in given zirconium alloys is sure to occur mainly through fast dislocations, while slow dislocations yield a small contribution to their interaction. The thermal nm ZrO_2 barriers remain, therefore, effective at 673 K only at higher strain rates (10^{-3}-10^{-5} s^{-1}). The oxygen contents should be kept very low to avoid any deleterious (detrimental) microscopic effects. It is reasonable to suppose that lowering of impurity interstitials and trace elements in raw materials in combination with nanophase strengthening which extends the uniform strain range may be considered as an effective means of impeding the shear localization in hcp crystals with sliding systems deficiency.

In this work, we selected the chemical compositions and processing modes of new experimental alloys in the Zr—8Al—1Nb system with intermetallic (Zr_3Al) hardening to further improve the mechanical properties of zirconium based on the formation of an ordered superstructure $L1_2$. The results of measurements at 293 and 673-973 K of various parameters of short-term and long-term mechanical properties are given for zirconium alloys Zr—8Al and Zr—8Al—1Nb, significantly ordered on the basis of Zr_3Al. It is found that their mechanical properties are mainly determined by the properties of the structure of the Zr_3Al intermetallic ordered to the $L1_2$ type (up to 92%). Alloying with niobium further increases the heat resistance, relaxation resistance, and dislocation creep resistance of the Zr—8Al—1Nb alloy. Since its macroscopic yield point practically does not change with increasing temperature, the high-temperature mechanical properties of the zirconium alloy with intermetallic Zr_3Al hardening are more than twice higher than those of zirconium alloys with solid solution hardening. The investigated modifications of essentially ordered zirconium alloys with intermetallic hardening are considered as a promising matrix for new generation composite materials with the highest performance characteristics.

The basic conclusions concerning the Zr—Al—Nb system can be drawn from results obtained and may be stated as follows:

• The results of short-term tests of cast, deformed and annealed zirconium alloys in the Zr—Al—Nb system at temperatures of 293 and 673 K, as well as long-term tests for stress relaxation in the temperature range 673-973 K, convince that the main role in the formation of mechanical properties of these alloys is performed by the Zr_3Al intermetallic compound with the ordered superstructure $L1_2$, which occupies up to 92% of the material volume.

Cast alloys based on an ordered intermetallic compound Zr_3Al with an fcc lattice and at least five independent slip systems are nevertheless characterized by relatively low plasticity at 293 K and limited deformability even at elevated temperatures. To increase the deformability and mechanical properties of cast alloys based on Zr_3Al, they must be subjected to thermomechanical treatment above 1260 K, followed by

heat treatment to 1210 K under conditions that provide the maximum amount of the Zr_3Al phase.

• Additional alloying of the two-phase Zr—8Al alloy with niobium (up to 1%), which dissolves in the primary αZr and does not interact with the ordered intermetallic compound, significantly increases the tensile strength and resistance to dislocation relaxation of the deformed alloy with an optimal combination of high technological values of their strength and plasticity (at 293 K).

• It has been established that the yield stress of these alloys with substantially intermetallic Zr_3Al ordering is practically independent of temperature, which indicates a high thermal resistance of their two-phase structure at 673-773 K. At the same time, the yield stress and heat resistance of alloys by intermetallic Zr_3Al hardening more than two times exceeds similar characteristics of zirconium alloys (Zircalloy type), which are distinguished by a strong temperature dependence of the macroscopic yield stress and its sharp decrease with increasing temperature.

• Diagrams of dislocation creep resistance of Zr-8Al and Zr—8Al—1Nb alloys were constructed in a wide range of normalized stresses $(0.02\text{-}7) \cdot 10^{-3}$ σ/E and temperatures 673–973 K. The presence of strain hardening (with multiplication of dislocations) limits the analytical capabilities of the thermal activation analysis performed. Therefore, it can only be assumed that the most probable mechanism for controlling the creep rate may be the difficult-to-activate deformation mechanism of thermal climb of screw dislocations with violation and restoration of order in the $L1_2$ structure of the Zr—Al—Nb alloys. The observed deviations of the activation parameters at various ratios of stresses and temperatures are determined by changes in the density of mobile dislocations of screw orientation in these alloys.

In the following we assume that science-based modifying a chemical composition and aligning the structure of defect metal crystal due to dispersion strengthening minimize the strain localization effects responsible for degradation of micromechanical properties. Nano-dispersion strengthening effects are considered as an effective means of assistance in promoting homogeneous microdeformation. In this respect, the method of nanophase strengthening takes precedence over age-hardening when overcoming the concentrated sliding with localized shear. Nanophase strengthening is most likely to extend an amount of uniform tensile strain responsible for the formation of dislocation creep resistance and the delayed effect of a premature fracturing. It thus appears that there may be considerable scope for further alloy development. Such an approach is believed to be a powerful starting point and considerable scope for further improvement of the newly developed alloys with minimal tendency to localized shear. The research is not only motivated by the basic science aspect but also the expectation that novel properties will lead to new technological and industrial applications. It is hoped that the basic information obtained can assist in the further development of new families of discontinuously nano-reinforced hcp magnesium and hcp zirconium alloys with the potential for technological applications at higher temperatures and stresses.

Section 4

SCOPES OF STRUCTURAL APPLICATIONS FOR CRYSTALLINE MATERIALS

Chapter

12 METAL MATRIX COMPOSITES

12.1. Prior Art

The need for high performance and light materials has led to extensive research and development efforts of metal matrix composites and cost-effective fabrication technologies [442-445]. The incorporation of thermally stable reinforcements into composite materials makes applications of magnesium matrix composites potential to the automotive industry including their use in disk rotors, piston ring grooves, gears, gearbox bearings, connecting rods and shift forks [446].

A number of papers have reviewed recent studies on the processing, microstructure and mechanical properties of metal matrix composites (MMCs) [443, 445, 446]. During the past decades, efforts to develop high temperature MMCs have led to the development of several new alloy systems on the basis of magnesium, aluminium and titanium [442, 447].

GKSS Research Center (Geesthachi, Germany) including Institute for Materials Research and Center for Magnesium Technology specializing in the development and licensing of advanced magnesium materials technology has announced several breakthroughs in the producing advanced magnesium alloys and their composites under the leadership of Prof. Dr. Karl U. Kainer [448]. However, the rapid chemical activity including instability of adjacent phases that are not in equilibrium threatens to frustrate the effective use of magnesium composite systems at high temperatures. Thus, this progress has not engendered extensive applications of these magnesium alloys in the automotive industry because of either insufficient high temperature strength or high cost.

The demand for reduced weight and increased stiffness in advanced materials application has generated strong interest in light metal matrix composite components. Since density of most ceramic reinforcements is higher than that of magnesium, use of magnesium alloys as matrix materials is particularly beneficial in produc-

Table 12.1. **The best properties of extruded silicon carbide particulate-reinforced magnesium alloys**

Code	SiC, vol%	Y.S. MPa	U.S. MPa	EL, %	Modulus, GPa
ZC7: (T6)	12	335	362	1.0	69
ZC7: (T6)	VNRF	320	350	6.0	44

ing a minimum weight composite. Wettability of the ceramic component is less of a problem with magnesium than with aluminum because of the magnesium ability to reach chemical equilibrium with any absorbed O_2 or N_2 on the ceramic surface.

Industry is turning to magnesium. Several companies have developed techniques for melt mixing magnesium alloys with particulate SiC or Al_2O_3 to produce composite materials that can be extruded or cast by a range of approaches [449, 450]. Magnesium Electron Limited (MEL) is concentrating upon the liquid metal route of production, employing particulate SiC. One of the advantages of this approach is that unlike the powder route, products are not restricted to wrought material but allow casting to be made. Some typical mechanical properties of the composites with greatly enhanced stiffness (up to 75 percent) are listed in Table 12.1.

To create more effective creep resistant and higher temperature long-term strength in the particulate-reinforced MMCs through nanophase structure, it is necessary to ensure at least the following conditions: (i) alignment of the local micromechanical properties, e.g., soft matrix, weak GBs and hard reinforcement; (ii) synergism of all the alloying elements; (iii) structural homogeneity and chemical uniformity of the components induced inside a composite material.

For alloy of monotectic systems, in the presence of the immiscibility gaps of metals, the dispersion phases are formed in a liquid state as a result of homogeneous melt emulsification. Combination of dispersion and composite strengthening can be one of the essentially new schemes of obtaining strengthened materials. Another approach to suppressing relative brittleness of reinforcing phases is to encapsulate them in a more ductile matrix for which its creep behavior need not be so stringent. Therefore, study of the fabrication methods and properties of the composite systems is clearly merited. There are two ways of increasing the strength of ceramics, (i) decreasing the crack size by careful quality control and (ii) increasing fracture toughness by alloying or making the ceramic into a composite which can absorb the energy of crack propagation. In spite of the numerous research investigations on fiber and particle reinforced metal-matrix composites, there have been very few experimental studies on the creep and only several attempts at theoretical analysis of composite creep. However, two useful conclusions have been drawn: 1) elevated temperature steady-state creep of composites with discontinuous fiber (particles) is controlled by creep of the matrix in the vicinity of them, and 2) elevated temperature steady-state creep of composites with continuous fibers is controlled by creep of the fibers.

12.2. Principles of Composite Strengthening

The well-known Hall-Petch and Mott-Stroch criteria are successfully used in the framework of the structural-impurity concept of fracture [451] for a comprehensive analysis of the brittle transition of single-phase polycrystalline objects. Their application for more complex heterophase systems will make it possible to analyze the interaction of brittle and plastic structural components, to single out the controlling mechanisms of deformation and fracture and to eliminate a number of contradictions in the description of strengthening of composites with high volume content of the phases [447]. However, unsuccessful attempts to obtain the usual linear Hall-Petch dependence for two-phase alloys containing two types of barriers to dislocations, namely grain boundaries and interphase surfaces of particles raised doubt about the validity of this empirical relation and the physical nature of its parameters [452, 453]. Moreover, due to the significant scatter of experimental data, the conclusions about the applicability of the Mott—Stroch criterion to heterophase systems cannot be considered convincing either [453].

In this work, an attempt is made to more thoroughly check the Hall-Petch and Mott-Stroch barrier models as applied to common two-phase alloys (eutectic origin) in the Al—Be—Mg system in order to confirm their validity for two-phase materials and on this basis to understand the relationship between local and macroscopic characteristics of deformation and fracture of these complex objects. The experiments were carried out on samples, which have in the initial state a two-phase structure consisting of a continuous plastic Al-matrix strengthened with Mg solute and reinforced with hard and brittle Be particles (at the level of 32.7 vol.%).

The research was performed using modern SEM and TEM techniques as well as optimization of physical experiment, in particular, by rotatable design [454]. In the temperature range 293-673 K, intense deformation of alloys in the AI—Be—Mg system is accompanied by the formation of a disoriented cellular structure in the Al-matrix with parameters α_C^{Al} and d_C^{Al} which are the disorientation angle and cell size, respectively. The latter linearly increases with increasing temperature up to 673K from 400 nm to 1.4 μm, providing substructural hardening Al and convergence of hardening characteristics of both phases. In this case, the yield stress of the alloy, σ_Y^{Al-Be}, obeys the linear Hall-Petch relationship with the parameters σ_0^{Al} and K_T^{Al} for the cellular structure (Fig. 12.1). The validity of this criterion is confirmed by the statistical analysis, which establishes a correlation between σ_Y^{Al-Be} and d_C^{Al}, which (at experimental correlation coefficient r = 0.995 and r_{cr} = 0.67) is determined by the following regression equation:

$$\sigma_Y^{Al-Be} = 14.0 + 1029.0(d_C^{Al})^{-1/2}. \qquad (12.1)$$

The existence of Eq. 12.1) confirms the universality of the concept [215, 216], according to which the structural sensitivity σ_Y of metals, along with the dependence of the resistance to dislocation movement in the lattice, is determined by the minimum mean free path of dislocations, λ, between the most effective barriers and does

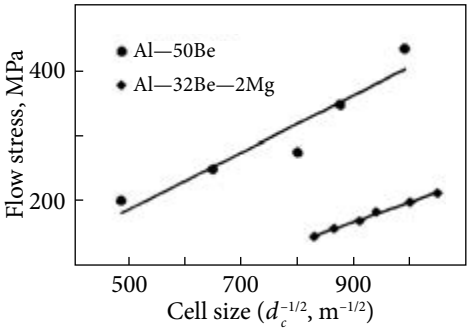

Fig. 12.1. Structural (barrier) Hall-Petch criterion for the cellular structure of the aluminium matrix in alloys of eutectic origin

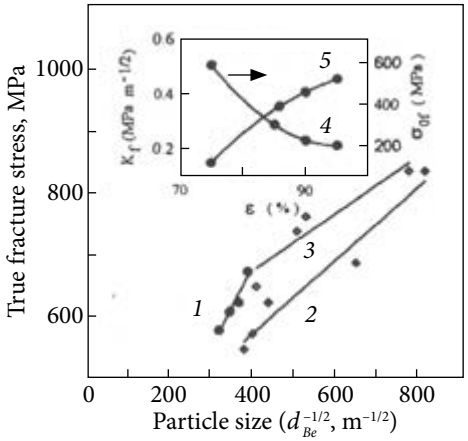

Fig. 12.2. Structural (barrier) Mott-Stroch criterion for the quasi-brittle particles of Be phase subjected to different degrees of deformation, ε: 75 (*1*), 85 (*2*) and 95% (*3*). Insert: the Mott-Stroch parameters σ_{of} (*4*) and K_f (*5*) as a function of preliminary deformation degree

not depend on their specific physical nature. With intense strain hardening of a two-phase alloy, the role of such barriers is played by the boundaries of A1 cells with supercritical disorientations $d_C^{Al} > 2^0$, which effectively limit the values of λ.

The strong correlation between the cell size and the tensile yield strength is indicated by the Hall-Petch relation (Fig. 12.1). At constant deformation ε, the true breaking stress σ_f^{Al-Be} of the A1—Be alloy is determined by the transverse (maximum) cross-section of Be-particles equal to the free path l_C^{Be} of cracks, which obey the Mott-Stroch criterion in the form

$$\sigma_f^{Al-Be} = \sigma_{of}^{Be} + K_f^{Al-Be} \cdot d_{Be}^{-1/2} \qquad (12.2)$$

with constant parameters K_f^{Al-Be} and $\sigma_{of}^{Be} > 0$ (Fig. 12.2). Here K_f^{Al-Be} is the coefficient of intensity of local stresses at the tops of transcrystalline cracks, which characterizes the resistance of the A1—Be interphase boundaries to the propagation of fracture; σ_{of}^{Be} is the resistance of the Be matrix to propagation of cracks. These observations are also confirmed by the regression analysis of the correlation between the size of the Be-particles, the interparticle distance d_{Al} and σ_f^{Al-Be} of the alloy at a confidence level of 95%. The detected correlations are described by the following regression equations:

$$\sigma_f^{Al-Be} = 459.50 + 13.2\, d_{Be}^{-1/2} \qquad (12.3)$$

for r = 0.89 and r_{cr} = 0.67 and

$$\sigma_f^{Al-Be} = 309.40 + 30.7\, d_{Al}^{-1/2} \qquad (12.4)$$

for r = 0.78 and r_{cr} = 0.67.

Fracture stress σ_f increases linearly with the reciprocal of a square root of a mean quasi-brittle Be particle size (Fig. 12.2). From a comparison of correlations (12.3) and

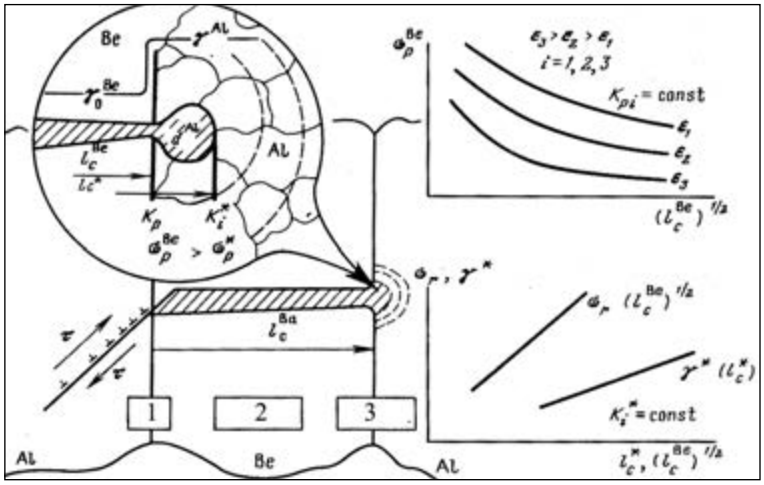

Fig. 12.3. A model of fracture for a two-phase alloy with plastic matrix in the Al—Be system

(12.4), it follows that σ_f^{Al-Be} of the alloy is controlled by the size of the Be-particles, and not by the distance between them. This means that Be particles behave in an Al-matrix like fibers in composite materials, i.e., take all the load that is distributed from fiber to fiber through the Al-matrix. In accordance with this, the macroscopic stress σ_f^{Al-Be} of the alloy, completely localized on Be particles, is equated to the microstructural (local) value of σ_f^{Be} for Be particles.

The features of alloy fracture are illustrated by the model shown in Fig. 12.3. The nucleation of brittle cracks occurs on the Al—Be interface as a result of the formation of dislocation pile-ups in the Al-matrix, which, like the "tangles" around the particles, are sources of high elastic energy.

First, microcracks propagate by an easily activated basic cleavage in the Be-particles and reach the values of l_{cr}^{Be}; then in the Al-matrix with $\gamma_{ef}^{Al} > \gamma_0^{Be}$ they pass into the stage of slow growth and merge with each other with the formation of micro-fractures of the Al-interlayers. The final fracture of the alloy is controlled by unstable critical cracks $l_{cr}^* > l_{cr}^{Be}$, satisfying the Griffiths-Orowan criterion. At higher values of σ_f^{Be}, micro fractures of A1-interlayers arise from cracks of ever shorter length l_C^*. The indicated mechanism of alloy fracture is consistent with the results of analysis of the Mott-Stroch equations, estimations of γ_{ef} and fractographic observations. First of all, the parameters σ_{of} and K_f change with deformation ε in opposite directions. From the dependence $\sigma_{o\rho}(\varepsilon) > 0$ it follows that brittle Be particles are destroyed in the Al-matrix with the manifestation of microplasticity, which increases with deformation. The accompanying weakening of the barrier action of the AI—Be interphase boundaries is associated with redistribution through the Al-matrix and the accumulation of residual elastic energy on the interface, which reduces γ_{ef} of alloy. The interaction of Be

particles with the A1 matrix is in better agreement with the Griffiths-Orowan concept, which is confirmed by the presence of the linear correlation $\gamma_f^{Al-Be} \cong \gamma_{ef}^{Al} = K_i^{Al} \cdot l_{cr}^{Be}$ and the critical values γ_{ef}^* obtained from the expression

$$\sigma_f^* = \left(\frac{2E\gamma_{ef}^*}{\rho l_c^*} \right)^{1/2}, \qquad (12.5)$$

where γ_{ef}^* is the critical fracture energy of Al interlayers; l_C^* is the critical length of Griffiths-Orowan cracks; σ_f^* is the critical Griffiths-Orowan stress; $K_i^{Al} \cong$ const. Here K_i^{Al} provides the activation of plastic relaxation of shear stresses at the crack tips and r_n^{Al} zone. Its value appears to be equated to the critical shear stress in Al polycrystals ($\tau_{Al} \cong 1$ MPa at 293 K).

The obtained regularities make it possible to establish the critical stage and local criterion for the fracture of two-phase A1—Be alloys. Under the conditions of plastic relaxation of σ_f^{ct} and substructural hardening of the A1 matrix, these alloys do not exhibit truly brittle behavior. Due to the alternation of phases with low (γ_0^{Be}) and high (γ_{ef}^{Al}) energies, the destruction of the alloy occurs from many sources-microcracks formed in the Be-particles, and is intermittently periodic in nature, due to their overcoming the activation barrier — the "jump" of energy $\Delta\gamma = \gamma_{ef}^{Al} - \gamma_0^{Be}$. Since γ_{ef} does not remain constant in the fracture process, the control (hard-to-activate) stage of fracture of two-phase alloys is crack propagation. In particular, in the A1—Be alloy, the development of this critical stage occurs under conditions of plastic relaxation by the mechanism of unstable growth and merging critical Griffiths-Orowan cracks in the A1-matrix with a cellular structure. According to Fig. 12.2 and electron fractography data (Fig. 8.21), it is the boundaries of the cells that cause additional dragging of microcracks attacking the Al-interlayer and determine the zone of plastic relaxation r_n^{Al} for values $l_{cr}^* > l_C^{Be}$ and $\sigma_f^* > \sigma_f^{Be}$. The corresponding local criterion for unstable fracture of the alloy is fulfilled when reaching, at a certain distance, a multiple of d_C^{Al}, the critical values σ_f^* (~420 MPa) and K_i^* (~1 MPa). In this case, the critical value of the fracture work (micro-fracture) of the Al-interlayers $\lambda_{ef}^* = K_i^* l_C^*$ becomes sufficient for the transformation of Be-cracks of length l_C^{Be} into Griffith-Orowan cracks of critical length $l_C^* > l_C^{Be}$, capable of further growth at $\gamma_{ef}^{Al} > \gamma_0^{Be}$, in full accordance with the model shown in Fig. 12.3.

12.3. Advantages of Magnesium Matrix Composites

The demand for reduced weight and increased stiffness in advanced materials application has generated strong interest in light metal matrix composite components [455]. Since density of most ceramic reinforcements is higher than magnesium, use of magnesium alloys as matrix materials is particularly beneficial in producing a minimum weight composite [446]. Wettability of the ceramic component is less of a problem with magnesium than with aluminum because of the magnesium

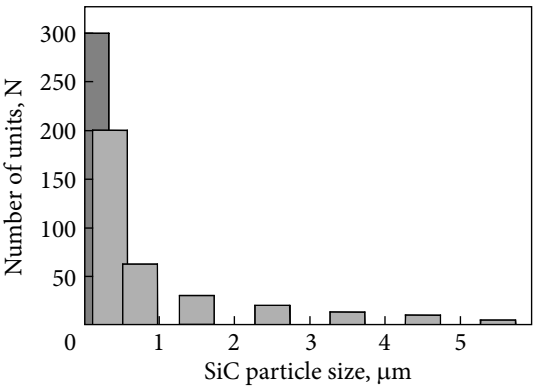

Fig. 12.4. Histograms of nano SiC particle distribution for Mg-5 vol.% SiC produced by rapid (liquid-phase) consolidation of the Mg based composites of the eutectic origin

ability to reach phase equilibrium with any absorbed O_2 or N_2 on the ceramic surfaces.

The beneficial effect of the oxide dispersoids in advanced high temperature ODS super alloys is well-known. Their advantages over conventional alloys are due to fine, uniformly dispersed and stable oxide particles which act as barriers to dislocation motion in Ni, NiCr, or Fe matrices. Nevertheless, their strength is limited because solid solution strengthening and precipitation strengthening are not or not fully exploited. Besides, they lack oxidation and corrosion resistance.

The concept of dispersion hardening originated with the sintered aluminum product, in which magnesium is additionally strengthened by the presence of particulate, has been successfully applied to other pure metals such as Cu, Bi, Al, Be, etc. in which the disperse phase is a hard inert refractory oxide (Al_2O_3, BeO, TiO_2, etc.) added mechanically. Al—Al_2O_3 alloys have shown excellent strength properties at room and elevated temperatures but the ductility is poor, because in dispersion strengthened alloys prepared by powder metallurgy the cohesion between the oxide particle and the matrix seems to be a mechanical one.

In order to overcome these problems, our laboratory develops metal alloy systems in which silicium carbide (Fig. 12.4) or a fine dispersion of yttrium oxide (about 2.5 and 3 vol%) is incorporated in the eutectic matrix by the alloying process. In the system the dispersoid imparts elevated temperature strength which superimposes on that contributed by the eutectic strengthening, thereby extending the useful strength of the alloy to well above 673 K. Yttria is one of the oxides with the highest negative free enthalpy of formation, attesting to its thermal stability, and consequently only negligible dispersoid coarsening occurs in alloyed composite materials. The average spacing between about 30 nm oxide dispersoids is expected to be approximately 100 nm. The desired uniformity of the dispersoid distribution has been confirmed at the level of TEM analysis [456].

The resulting microstructure of magnesium matrix nanophase particulate-reinforced composite is able to optimize uncorrelated (thermal, electrical and strength) parameters and cost efficiency. Optimum microstructural engineering in new experimental magnesium-based alloys of the Mg—Al, Ca system of eutectic origin (with larger ratio of Al/Ca) and their magnesium matrix composites reinforced by SiC and other particles as well as methods of their control in rapidly and

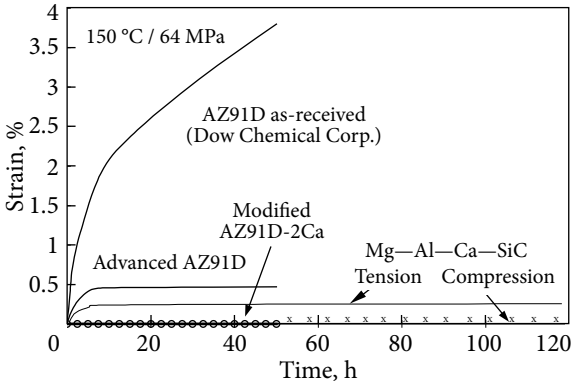

Fig. 12.5. Summarized creep data for the as-cast Mg AZ91D alloy and as-cast magnesium matrix composite material of the Mg—Al—Ca—SiC casting system at constant creep temperature and constant creep strength

directionally solidified ingots have been summarized and analyzed using electron microscopy characterization of magnesium alloys [457]. Unlike an AZ series of magnesium alloys with divorced eutectics (AZ91D etc.), the observed alloys in the Mg—Al,Ca—nmSiC system are expected to exhibit high creep resistance (at 423 K) and excellent creep fracture strength (60-80 MPa) (Fig. 12.5).

The practical interest in microstructures of eutectic origin from the chemical equilibrium of the two-phase alloys with constituents which are unaffected to chemical decay. Commercially available magnesium alloys such as AZ91D and the like are certain to be specified by divorced eutectic and laminated solid solution (Fig. 10.3) and as consequence low creep strength at higher temperatures. SiC particle as additional reinforcing agents were incorporated in order to improve the structured and thermal stability of AZ91D—2Ca and Mg—6Al—0.8Ca, X systems of eutectic origin. According to the previous experience with magnesium alloys, large ceramic particles are not wetted by molten magnesium if they are not exposed to pressure melting or squeeze casting under pressure. In this study, wettability of nano-dispersed SiC particles is marked in α_2-Mg—$Mg_{17}Al_{12-x}Ca_x$ eutectics. Besides, it should be noted that SiC dispersoids are mainly assimilated by GBs.

Several of the observations made in this study are expended to apply most generally to other eutectic systems, e.g., Al—Al_3Ni eutectic composite [458] which exhibit uniform microstructure or cell substructure and which are reinforced by a creep resistant phase such as nano SiC (Figs. 12.4 and 12.5). Time-dependent fracture mechanism identified in eutectic composites differs from normal tensile fracture through the substructure formation [458]. In this case, creep resistance of such a eutectic composite and its dispersion strengthening increase with increasing the solidification rate. Thermally stable microstructures of eutectic (Al—Be, Mg—Al—Ca— nano SiC, and Al—Ni_3Al) composites consisting of around 5-10 vol.% phase uniformly dispersed in the matrix retain under creep testing (for 100-200 hr) up to 90 % of their eutectic temperature. Thus, the idea of additional dispersion strengthening in eutectic systems having natural hardening is consistent with the model (Fig. 12.3) and the observed tendency of dislocations in the matrix-phase interface, as well as with resultant formation of cell substructure in areas of heavy deformation.

12.4. Nanocomposites

The creep results for nanocrystalline materials are conflicting [459, 460] seeing that there is an increased tendency of them to undergo localized shear. In many cases, nanocomposites exhibit mechanical or physical properties of special interest. In the production of nanocomposites, one of the key problems is to obtain a uniform distribution of two or more phases. In general, there are two approaches to the production of a uniform nanocomposite: (i) synthesis of a metastable homogeneous mixture and formation of the second phase after densification during sintering by precipitation and (ii) synthesis via the two phases blending during the step of particle formation. The ultimate uniformity of such a product can be obtained by coating the particles of the primary with second phase. Unfortunately, processes based on mechanical blending do not lead to powder homogeneous in the nanometer scale. GB strengthening of nanocrystalline materials with nanoscale powders may be disadvantageous when consolidation of powders to full density is considered. The problem may be partly overcome if higher consolidation temperatures are employed, as σ_i and K_y in the Petch-Hall equation decrease and the GB sliding increases with increasing temperature or if high pressure consolidation is employed at slightly elevated temperatures to full density [461]. However, consolidation at elevated temperatures may result in recrystallization and grain growth. At the same, in order to obtain thermally stable nanocrystallites and to retain their structures, an alternative processing route is required which provides consolidation of nanoscale powders below their recrystallization temperatures retaining the fine grain size.

The formation of nanoscale metal matrix composites is a technique that proved useful for consolidation of pre-alloyed and ultrafine elemental powders. In order to obtain thermally stable nanocrystalline structures an alternative processing route is suggested leading to the formation of nanoscale matrix composite materials with fine ceramic dispersions. Nanometric monodisperse powder and laser for gaseous phase reactions present a growing interest in ceramic processing leading to enhanced densification and improved thermomechanical properties of the final product.

Many intermetallic compounds show high yield strength, good stability and creep resistance up to relatively high temperatures. An interesting example is Ni_3Al, a material for which the increase in yield strength with increasing temperature is typical [462]. The major difficulty with intermetallic compounds, however, is their tendency to show brittle fracture or decreased ductility in polycrystalline form. The reasons for the mechanical behavior of intermetallics should be found in the chemical order, which reduces atomic mobility and which is also responsible for the presence of less mobile superdislocations [463].

The research in nanostructured materials and its success in improving the ductility of ceramics [464] have motivated research in nanostructured intermetallic compounds [465]. It is expected that the deformation behavior of nanostructural materials is a grain boundary diffusion-controlled mechanism, which does not involve

movement of dislocations. This means that materials which are brittle as coarse grained polycrystals because of an insufficient number of independent dislocation slip systems, can exhibit ductility in the nanocrystalline form owing to diffusion-controlled mechanism.

Thus, nanocomposites not only provide higher mechanical properties as compared to pure metals, but also have a better thermal stability due to the fine second phase nanoparticles preventing grain growth. In this case, strengthening by dispersed particles (oxides, carbides) may be more important than grain boundary strengthening. A further improvement of hardness, yield strength and thermal stability may be expected, if a very fine metal (or metal hydride) powder is added to the blend which will further react with the matrix to form an intermetallic for the production of intermetallic matrix nanocomposites, e.g., NiTi with hard ceramic particles.

A large fraction of atoms located at interfaces (about 50 at% for a 5 nm grain size) is expected to play an important role in determining the unique properties of nanocrystalline materials [459]. However, some fundamental subjects concerning their interfacial structure and structure-related properties are still controversial. So far, two major structural interface models have been proposed, i.e., the "gas-like" structure with neither long- nor short-range order by Gleiter [466] and similar to the common interfacial structure in polycrystals by Siegel et al. [467].

Using the molecular dynamics method and the empirical N-body potential for calculating radial distribution function, Peng and co-workers [468] have shown that in a relaxed nanocrustalline copper, the ordered structure of interface is formed, which similar to that in the coarse polycrystal. The initial computional system consists of seven spherical fcc-clusters of 3.18 nm in diameter and contains 10.293 Cu atoms. Clusters can relax sufficiently in three dimensions to reach a stable structure with low energy. The mean atomic cohesive energy of the nanocrystelline Cu is calculated to be 3.352 eV, much lower than the value for single crystal Cu (3.518 eV). Significant stress relaxation is observed for interfaces (GBs between two clusters or surface of individual clusters) as well as rotation of the cluster or dislocation motion through the cluster. Because of relatively high self-diffusion, atoms move to the voids at the triple junctions where three neighbor clusters intersect forming an ordered structure of small or high GB angle between the two clusters of common lattice orientation as well as the two-dimensionally coherent or semi-coherent boundary structure between the clusters of no common lattice orientation in the computed relaxed atomic structure. The significantly high diffusion and solid-like softening feature of the power spectrum of the interfacial component are closely related to the native characteristics of nanocrystalline materials, such as the higher energy states and smaller coordinate number of atoms at interfaces, and the rapid short-circuit diffusion along the interfacial network. Local atomic relaxation is observed which tends to provide a low energy configuration. Ordered GB structures are similar to those in polycrystals in spite of the existence of small localized disorder at or near interfacial planes, and the interfacial region is about three atomic layers wide.

Measurement of 110 nm grain rotation and plastic strain yielded clear evidence of dislocation activity responsible for GB sliding [469]. This can make significant contribution to the deformation of nanostructured metals (thin films) at low homologous temperatures. Nevertheless, nanocomposites not only provide higher mechanical properties as compared to pure metals, but also have a better thermal stability due to the fine second phase particles preventing grain growth. In this case, strengthening by dispersed particles (oxides, carbides) may be more important than GB strengthening.

12.5. Excellence for Advanced Materials

Polymer matrix nanocomposites are already used in various applications. Metal matrix nanocomposites can offer distinct advantages over polymer composites due to their inherent high temperature stability, excellent elastic modulus, long-term strength, high stiffness, wear resistance as well as thermal and electrical conductivity [470]. Magnesium matrix nanocomposites (MMNCs) reinforced with nm SiC, nm Al_2O_3, nm Al_3Zr, nm TiO_2, nm ZrO_2, carbon nanotubes etc. have been receiving attention in recent years as attractive materials for aerospace and automobile industries due to their good damping capacity, excellent castability and superior machinability. The principal dispersoids have been identified by proper electron techniques, in particular, by electron diffraction as 5 nm GB nanoparticles occurring in magnesium alloys (nm $Mg_{17}Al_6Ca_6$), beryllium alloys (nm Be_4C), and aluminum alloys (nm Al_3Sc). As described in Chapters 9-11, the superior properties of MMNCs can be retained at elevated temperatures of up to 523 K (for the best magnesium alloys). As a rule, the nanoparticles reduce the ductility of MMNCs by preventing their plastic deformation. With that, they can produce a grain refining effect to improve their ductility. The observed high modulus of elasticity and the relatively high cyclic threshold stress intensity factor are thought to result from the strong binding between the nanodispersoids and the matrix.

The major disadvantage of metallic nanocomposites is associated with the relatively high cost of these materials and the high cost of their fabrication. In practice the procedure is a compromise between cost considerations and product quality. In this context, advantages of magnesium alloys as structural materials are obvious. The next experimental magnesium alloys to be proposed and their nanoparticulate-reinforced magnesium matrix composites can compete with aluminium alloys and reinforced polymers, and offer great potential for industrial use in the future in different dynamical applications in the aeronautics, automobile and engineering industries. To exploit their potential, these alloys and nanocomposite materials made of them must be checked in industrial conditions. At present, these alloys were evaluated by extensive tensile and creep testing. It should be pointed out that Mg—Al—Ca alloys with know-how addition of Ti (≤ up 0.2%) and small addition of Sr (up to 1.7%) become heat-resistant ones opening new areas of industrial application. These new cost-effec-

tive engineering materials not containing expensive alloying additions at least in large amounts exhibit excellent castability, creep resistance and long-term strength at 423 K under 70 MPa, which are significantly superior to that of the commercially available magnesium alloys such as AZ91D, AS21, as well as AE42 containing large amount of expensive RE. They address the power train (dynamic) applications in the automobile industry.

It is however recognized that the demands for improved power drive system performance and overall efficiency are ever increasing. In answer to these demands, Magnesium Electron Ltd (MEL) has developed a new family of alloys based on the Mg—Y—Nd— RE system. Due to its combining superior temperature stability, inherent corrosion resistance and excellent mechanical properties, the alloy considered most suitable for aerospace applications is WE 43 (4% Y, 2.25 % Nd, 1 % HRE*, 0.6 % Zn). The envelope of long-term temperature capabilities has been increased to 523 K.

WE 43A-T6 competes with commonly used aerospace aluminum-based alloys, such as A355-T6, A3566, A201-T7 and A203, on the volume-to-volume basis, and can prove even better at elevated temperatures, with a dramatic potential weight saving of around 30%. Exposures for up to 10,000 hr at various temperatures up to 523 K have shown no significant reduction in r.t. tensile properties, while tensile properties of A201 and C355 fall quite drastically after long-term exposure.

In spite of the fact that magnesium has the lowest density and the best machinability of all engineering metals, it has only found restricted application as an engineering material due to limitations in the mechanical properties and corrosion resistance. It is reported that the main factor affecting the mechanical properties of more reactive magnesium alloys is the grain size. Novel material processes such as enhanced directional as well as rapid solidification technology (RST) including Free Jet Melt Spinning (MS) and Planar Flow Casting (PFC) expand the application of wrought (extrusion) reactive magnesium alloys with enhanced properties provided by structured refinement and solid solution extension. Rapid solidification processes (RSP) like Free Get Melt Spinning (MS) and Planar Flow Casting (PFC) result in substantial refinement of the microstructure giving a considerable increase in the mechanical strength of the alloys.

Rapidly solidified and then extruded AZ91 with additions of RE and silicon is characterised by week texture and a fine grain size of 0.3-1.0 μm and particle size of 0.2-0.7 μm (phase $Mg_{17}Al_{12}$) and 30-70 nm (phase MgRE) dependent on processing parameters like casting and consolidation conditions [471]. Rapid solidification process (RSP) is looked upon as a way of avoiding the limitations of traditional metallurgy in metals, and extensive work especially on aluminium alloys has resulted in promising improvement of the properties. Research Center (France) and PECHINEY NORSK HYDRO (Norway) have a joint program with objectives to develop new magnesium alloys with high strength and improved corrosion resistance using the

* Heavy Rare Earths, principally ytterbium, erbium, dysprosium and gadolinium.

RSP. Outstanding improvements in strength, equal compressive and tensile strength, and excellent corrosion resistance have been reported, in particular for new magnesium alloys of the Mg—Al, Zn, Zr, RE systems.

High strength Mg—Y alloys are now available with usable long-term properties to 523K. High strength nanocrystalline Mg—Al—Ca alloys [472] can be further reinforced using the GB pinning effect.

A further reduction of the density is attainable by alloying magnesium with Li, the lightest metallic element. Indeed, the production of magnesium alloys with densities down to 1.3 g/cm^3 and a higher specific elastic modulus than that of steel is possible. The high solubility in Li (nearly 90 mass%) leads to bcc magnesium alloys with remarkable deformation behavior. Some disadvantages of these alloys are reduced tensile strength, poor corrosion resistance and high cost. The mechanical properties of binary Mg—Li alloys can be improved by additions of aluminum. Increasing aluminum content results in solid-solution hardening and a rising volume fraction of the nanoscale phase Al—Li. The strength of these ternary alloys, for example, the specific strength of the Mg—Li8Al3 alloy is higher than that of the steel St 70.

Further improvements of mechanical properties are attainable by embedding fibres like nm SiC- whiskers for reinforcement of magnesium wrought alloys as well as glass, and Al_2O_3 and graphite fibres for reinforcement of magnesium cast alloys. In that way, an elastic modulus of up to 170 GPa is attainable in graphite reinforced Mg-alloys. Such fibers composites offer the advantage that their properties can be predicted and tailored to an application. In future it will be of interest to reduce the density of composites, for which Mg—Li alloys will be used for the matrix material. Another possibility for improving the mechanical properties is given by rapid solidification techniques. High solidification rates provide a very fine grain size, increased solubility and possibly metastable phases.

Recently the laser heating of surfaces has become more attractive. This process is partly in technical use for steel and aluminum, whereas laser treatment of magnesium and its alloys is relatively unknown. Thus, several conventional and Mg-Li alloys were laser heated and investigated. All of them showed a locally melted area with a fine microstructure, but no head affected zone. Hardness measurements confirm an improvement of the mechanical properties provided by grain refinement in the laser traces. Another method for rapid solidification is the melt spinning technique. With this method the production of semiproducts directly from the melt is possible.

12.6. Scopes of Structural Applications for HCP Crystalline Materials

Dimensional Stability

Development of dimensionally stable crystalline solids, their lightweight structures, high precision spacing systems and other critical instrumentation of diffraction-limited quality is one of the most important directions for severe ap-

plications. Beryllium with hcp lattice possessing an extremely high stiffness-to-weight ratio and attractive optical characteristics has been successfully used in precision aerospace navigational instrumentation and precision optical components (high quality gyroscopes and Be-mirrors) due to its high microyield strength and good dimensional (thermal and temporal) stability of beryllium optics [473, 474]. Conversion of military potential of hcp Be as a structural material and waste products from military technology opens the new possibilities in development of alloys of new generation in astrophysics, precision rocket and space navigation systems [474, 475]. Necessary level of their thermal and temporal stability should be provided with the complex treatment including annealing, aging and heat-cycling operations for the further stabilization of phase composition, residual concentration of the primary solid solution, integral dislocation vacancy structure as well as thermal (structural) elastic stresses.

Dynamic Structural Applications

Light alloys and their composites should be applied in conditions where microyield/creep resistance, low moment of inertia, stiffness and long-term strength are essential.

Magnesium is the lightest metal used for structural applications. Due to its low density, specific strength and stiffness, the material has been attractive to designers, and magnesium alloys have historically been used in a number of high-performance aerospace structural applications. Improvements in properties and castability (casting quality and complexity for thin walls) achieved by magnesium in the last 30 years have made magnesium alloys a prime choice for further application within the aerospace industry. However, because of low corrosion resistance and formability at room temperature as well as the moderate mechanical properties compared to improved aluminum alloys, this metal has not seen extensive use (market niches have decreased rather than increased). To address these problems and increase the use of light magnesium alloys, important development work has been carried out by Lockheed and Allied Signal in North America, MEL Shell in the United Kingdom, Norsk — Hydro / Pechiney in Europe (Norway, France).

Use of Mg as a design material is increased. Particularly, the motor industry has received an opportunity of manufacturing pieces from the unique (light, strong, resistant to corrosion) metal. Magnesium is well exposed to welding and is capable in many cases to exchange plastic used in automobiles, for example, light armchairs for passengers ensuring their increased reliability, Density of Mg (1.7-1.8 g/cm^3) is the least among all structural metals and alloys. At such density as the plastic, magnesium is more rigid by 10 times and is characterized by high specific strength. The application of magnesium, the basic competitor to aluminum, is also efficient from the economic point of view [476, 477].

These alloys were evaluated by extensive tensile and creep testing. It should be pointed out that Mg—Al—Ca alloys with addition of Ti (≤0.2%) and Sr (≤1.7%) be-

come heat-resistant opening new areas of industrial application. These new cost-efficient engineering materials not containing expensive alloying additions at least in large amounts exhibit excellent castability, creep resistance and long-term strength at 423 K under 70 MPa, which are significantly superior to that of the commercially available magnesium alloys such as AZ91D, AS21, as well as AE42 containing large amount of expensive REs. They address the power train (dynamic) applications in the industry.

We are also taking over the orders for modification of the chemical composition of the industrial, commercially available magnesium alloy AZ91D (Dow Chemical Corp., USA) to improve its creep behaviour. Development of the magnesium and aluminum alloys provides with highly improved creep resistance characteristics in line with remarkably low production cost via using micro-alloying, strengthening mechanisms and processing which do not call for use of expensive elements such as Y, Sc, RE, etc.

Thereby, with appropriate protection techniques, magnesium alloys offer aerospace engineers a valuable material choice now and during the 21st century. As aerospace designers continue to strive for overall efficiencies and power/drive system improved performance, the requirements are bound to be reduced with weight, improved with elevated temperature properties, and provided with more complex thin wall castings.

Damping Ability

The experimental magnesium alloys are particularly well adapted for use as die casting alloys and can be made by any standard die casting process. Having high damping ability investigated magnesium alloys with special ultrasonic properties attenuate a high level of elastic fluctuations and vibrations. Therefore, vibrations damping elements from magnesium alloys can be used in mobile units and systems of mechanical engineering testing vibrations.

CONCLUSIONS

Based on the fit to experimental data, conclusions are drawn with regard to the problems, potential, applications and prospects of cluster-assembled nanophase alloys and metal-matrix composite materials in the industry.

Metal-matrix composites are currently experiencing active development all over the world ranging from high-performance military and aerospace applications to big-volume low-cost commercial applications. While significant progress is being made, concerns of high cost and less-than-desired properties exist. Moreover, no one approach has yet been defined to optimize properties, cost, and technology of materials fabrication.

All of the best improvements in short-term and long-term strengths of nanophase metallic materials are associated mainly with the activation of nanodispersion strengthening mechanisms attributed to the GB pinning effect.

The novel magnesium alloys in the hcp Mg—Ca—Al system have 30% greater tensile and compression resistance than the commercial alloy AE42 (Mg—Al—RE) and corrosion resistance as good as that of the industrial alloy AZ91D (Dow Chemical Corp., USA). They have been estimated to cost less than the abovementioned alloys.

New Ukrainian magnesium alloys in the Mg—Al—Ca—Ti/Sr/Gd systems containing GB nanodispersoids (nm $Mg_{17}Al_6Ca_6$, nm SiC, etc.) have improved (by 30%) fluidity/castability, low-temperature ductility (4-5% elongation at r.t.), excellent performance of thermal resistance, and long-term strength, increased (by 423-473 K) heat resistance as well as higher creep resistance (at 70 MPa / 423 K for 200 hr) compared to the automotive industry alloys AZ91D, AS21, as well as the European alloy AE42 (Mg4Al2.5 RE), containing large additions of RE. They are corrosion resistant and estimated to cost less than the above metal alloy systems. Besides, the novel experimental magnesium materials demonstrate good castability in metal models which are usually used in permanent mold and die casting.

In many cases, nanocomposites exhibit mechanical or physical properties of special interest. In the production of nanocomposites, one of the key problems is to obtain a uniform distribution of two or more phases. In general, there are two approaches to obtaining a uniform nanocomposite: (i) synthesis of a metastable homogeneous mixture and formation of the second phase after densification during sintering by precipitation and (ii) synthesis of the two phases by blending during the step of particle formation.

Another important benefit appears to be enhanced corrosion resistance, offering the prospect of producing alloys of the system studied with equivalent corrosion resistance but higher specific strength as compared to aluminum alloys. There is a great interest in light alloys from the aeronautics, automobile and engineering industries. Looking ahead to the future, there are interesting prospects for magnesium research, such as further reduction of density, further improvement of mechanical (creep) properties and corrosion resistance as well as the development of new casting production technologies providing higher quality and cost-efficiency of magnesium. Advantages of using magnesium-based alloys as structural materials in different dynamic applications are available where a low moment of inertia, good stiffness and high resistance to time-dependent microplastic deformation are of importance. Novel magnesium alloys and their nanoparticulate-reinforced magnesium matrix composites can compete with aluminium alloys and reinforced polymers and manifest great potential for their industrial use in the future.

SUMMARY

This monograph analyzes and summarizes world achievements in the field of strength physics and materials science as well as the results of theoretical and experimental investigations of the physical nature and most probable strengthening dislocation mechanisms of microyielding, macroscopic deformation and thermally activated (quasi-brittle) fracture for hcp, fcc and bcc crystals with various Peierls barriers, as well as decaying solid solutions, ordered alloys with intermetallic strengthening, cluster-assembled nanophase and rapidly-hardening materials. Besides, it aims at studying possibilities of overcoming the brittleness and hydrogen embrittlement problems and to produce methods for thermally activated recovery of plasticity with restoration of resistance to fracture and strength for the most brittle metals of the periodic table of elements, in particular, chromium and beryllium.

In this case, we reviewed some recent trends and developments in high-strength materials rather than gave a detailed description of the present state of the art and the way it developed. On this basis, the alloying principles and strengthening methods have been developed for the formation of properties in metal alloy systems, which have a set of necessary technical characteristics in the critical temperatures range.

When publishing materials of a review nature, the author does not strive for the most complete description of the current state of scientific developments in this area of knowledge, limiting himself to the main areas of research and achievements in understanding the physical nature of phenomena and controlling mechanisms. The selection, systematization and generalization of the results and literature data reflect, of course, the scientific interests and viewpoints of the author on a number of the problems raised with the justification of approaches and their solutions.

The research identifies topical problems that hinder the further development of this direction in modern solid state physics. Based

on the published data and the results of original research, the main principles of the formation of the chemical compositions of multicomponent (binary, ternary and quaternary) alloys and the evolution of their structure are considered. In recent years, strength physics has made very significant progress but a large number of problems in the field are still open:

• Analysis of the jerky flow and serrated yielding reviews the high rate of strain-age hardening occurring in metal crystals with the formation of serrations on the stress-strain curve at elevated temperatures. This effect cannot be explained by the usual dislocation locking concepts in terms of Cottrell (elastic approximation) or Suzuki (chemical approximation) theories. Our approach gives access to mesoscopic systems and allows quantitative prediction of the activation of short-range rate-controlling mechanisms operating in rapidly solution hardened crystalline materials. These stress-induced ordering mechanisms (generally termed Snoek — Zener — Fleisher — Fisher and Schoeck — Seeger) require solute atoms to make only a single jump for dislocation locking affected according to Maxwell — Boltzmann's relationship.

• The transition of matter from the atomic to the solid state implies changes in cluster self-organization which turn out to be more complex than was originally supposed.

• Understanding the mechanical properties of nanophase alloys and their nanocomposites is a challenging issue. In this case, influence of large amount of grain boundaries is crucial. In nanocrystalline and nanophase materials the grain boundaries are certain to be responsible for most of the observed strengthening effects. Since their metastable structures have nets of misfit dislocations and coincidence superlattices, they are strongly dependent on the synthesis techniques, all based on driving the material far from equilibrium according to the Morris-Valiev-Sanders-Van Swygenhoven ideas, model considerations and computer simulations. Therefore, the activation energy and the dislocation activation volume are consistent with grain-boundary sliding and its strengthening mechanism.

• It should be pointed out that Cottrell's concept is assumed to be valid only beyond the dislocation cores due to macroscopic changes in diffusivity. Hence, the model would give marks that are too high when making calculations of the strength in terms of a long-range (diffusion-controlled) mechanism. A physics-based constitutive model of dislocation microyield/creep resistance has been put forward and applied to the attempt to describe and explain the physical nature of rate-controlling strengthening mechanisms responsible for the dragging of solutes on the dislocation cores by short-range mechanism.

• The first attempt to separate the contributions of plastic deformation and fracture using a kinetic creep curve belongs to Reed-Hill (1973). According to his ideas the usefulness temperature of strength corresponds to its maximum relative to the absolute melting temperature, T_{us}/T_m, at which a potential alloy can withstand a load of around 100 MPa without fracture. In our study, a quantitative (dislocation) criterion of useful long-term strength is formulated with reference to light metal alloy

systems. Such an approach is shown to be a reliable tool for studies of the structure and long-term strength in newly developed alloys.

• The main source of the rapid increase in yield stress and the rapid decrease in fracture stress for bcc and hcp metals and their alloys, respectively, is still a matter of controversy. A critical experimental examination of this topical problem depends on the preparation of high-purity single crystals and their micro alloys which are doped with controlled amount of interstitial impurities.

Thermoactivation analysis of quasi-brittle fracture opens up new possibilities for increasing fracture resistance and restoring the properties of semi-brittle crystals, hydrogenated metals, and difficult-to-machine alloys in a wider temperature range and determines the strategy for further research and applied developments. In connection with the development of the problem of overcoming the brittleness, recovery and formation of new properties of precision and light alloys for modern technology, special attention is paid to the search for dislocation fracture mechanisms that control the macroscopic parameters of these objects, as well as to check the unified composition-structure-properties relationship at all stages of their processing (at the dislocation, micro- and macroscopic levels). A more general dislocation theory of quasi-brittle dynamic fracture has been developed for crystals with various Peierls barriers under the action of applied stresses and thermal activation. This approximation makes it possible to calculate analytically the simultaneous contributions of plastic (dislocation) relaxation and thermal fluctuations at the tips of mobile microcracks to the fracture inhibition.

Great care should be taken when assessing the long-term operation of units and structures based on the results of short-term tests, since, in particular, with a decrease in the creep rate, their fracture can occur at any time due to the appearance of microyielding of grain boundaries and interfacial surfaces. The conventional creep limit is the stress at which deformation of a certain or required value is achieved in a given time, while the creep resistance depends on the nature of the interatomic bond, type of crystal lattice, energy of the stacking faults in the structure and the characteristics of dislocations.

At present, diagnostic techniques and methods have spread the field of applications, becoming very useful tools to approach many different problems in metal physics, chemistry and materials science from both fundamental and applied points. Since many aspects of the range of problems remain to be examined with the necessary criticism, a brief overview is given to reveal the internal inconsistencies of current approaches and concepts as well as disparities between model calculations and experimental data. Besides, the author reviews the present status of his own particular field, with emphasis upon the most important recent developments of diagnostic approaches and current practice. A newly developed diagnostic approach to material conditions preventing the premature fracturing of rapidly-hardened crystals has been proposed to improve reliability and extendin the service life of structural metal alloys and construction modules working under long-term loading below macroscopic yield stress.

A new first-order physical theory of useful long-term strength based on a dislocation model and analytical rate equations has been advanced for adequate describing dynamic (time-dependent) microyield/creep resistance responsible for a potentially useful measure of the uniform strain preventing a premature fracturing of rapid-hardening crystals. The theory based on mathematical modeling of the resistance to dislocation movement and Le Chatelier-Braun's physicochemical principle of shifting its mobile equilibrium furnishes an explanation of the above dragging effects at the early stage of their formation, including the onset of jerky flow. Besides, it describes the direct interactions between defects and solutes involving the jump-like movement of dislocations with increasing temperature. Interpretation of their relationships makes it possible to separate the time-dependent contributions of power and thermal components to the net activation energy needed for overcoming the short-range obstacles and to estimate the energy of thermal activation and dislocation activation volume. The theory also enables examination of the transition from uniform elongation to localized shear caused by loss of the shear stability for crystal lattice and, as a sequence, by microplastic instability. Such a diagnostic approach enables the short-range rate-controlling mechanisms to be identified for stressed crystals in terms of thermal activation numerical analysis of rapid strengthening using the constant structure steady-state creep tests and dislocation relaxation technique.

A more accurate (dislocation) criterion of useful long-term strength is formulated for quantitative assessment of the dragging effects preventing transition from the structurally uniform sliding to localized shear strain that governs the structural preparation of fracturing. In the context, a threshold dragging stress as a function of strain resistance is directly related to elastic (shear) stability of a dislocated crystalline lattice, line tension (excess energy), velocity and density of sliding dislocations.

Theoretical calculations of dislocation strength influenced by elastic stress fields of dislocations produced by mobile solutes paired with excess vacancies are in a reasonable agreement with the original and published experimental data. Such an approach might be applicable to the strain rate-sensitive materials permitting further generalization and is the most valid for precise measurements when tested under the constant structure and strain rate change conditions as well as stress relaxation tests and constant load creep testing. The proposed method can be expected to be appropriate in describing creep behavior of hcp metal alloy systems as a starting point for further development of the creep-resistant alloys with minimum of localized shear effects and rapid-hardening crystals thermally activated by a short-range mechanism.

Based on the fit to experimental data, conclusions are drawn with regard to the governing short-range mechanisms:

• Structure of a melt or a liquid mixture of reactants is the main source of a solid state clusterized structure. Measurements by mechanical spectroscopy have shown that separate peaks in hcp solid solutions are attributed to the presence of point defects pairs. These pre-cluster type complexes are believed to produce asymmetric elastic distortions in hcp anisotropic lattice and to cause short-range ordering around

moving dislocation. Besides, the pair defects are mobile enough to be responsible for the onset of jerky flow on the smooth region of stress-strain curve preceding serrations. The occurrence of pre-cluster pair associates is also supported by the deviation from classical (Arrhenius) behaviour in the Mg—Ba and Al—Li systems observed at high temperature. It should be stressed that they are caused by change in the diffusion-controlled mechanism in hcp interstitial solid solutions such as Be—C and Ti—H as well as in substitutional solid solutions such as alloys in the Mg—Ba and Al—Li systems oversaturated with excess vacancies. The formation of cluster compounds A_mB_n with own electronic structure is believed to occur by means of the chemical interaction between pair associates consisting of a solute and an excess vacancy due to their pair relaxation. The cluster compounds with strong chemical bonds can be a structural unit of cluster-assembled and nanophase materials.

• Pre-cluster separations of AE bound with excess vacancies are likely to change the chemical potential of a dislocation so that at high strain rate they are believed to cause the activation of a short-range (rapid) mechanism rather than a long-term mechanism. The interpretation is supported by estimates of lower values of the thermal activation energy (0.5-0.8 eV) for migration of an excess vacancy to be bound with AE. Thus, short-range ordering units could tentatively be suggested as being pre-cluster complexes which are responsible for the rate of rapid hardening based on the short-range mechanisms of dislocation dragging under the conditions of thermal activation.

• Physical principles of the precise alloying for the in situ bulk nanoclustering a structure of the condensed metal systems (metal melts and their extended solid solutions) are formulated in order to reveal the origin of the cluster-induced compounds responsible for the crucial increase (by two-three orders of magnitude) of quantum efficiency within the UV-spectrum range. The class of promising photoemission materials based on ternary Mg—Ba—Li and Al—Li—Ba alloy systems is being developed with the goal of applying them as pulse bulk photocathodes in high-current electronics including the next RF-guns of FELs and electron accelerators.

• Constitutive semi-logarithmic equations of strain rate are derived to carry out the numerical thermally activated analysis and reveal rate-controlling dislocation mechanisms accommodated by short-range diffusion of pair defects at $\tau^*T^* > kT$ and their repeated pinning of dislocation at $\tau^*T^* << kT$.

• Judging the results obtained, at least two underlying types of the dislocation dragging mechanisms were identified by using the new model-based analytical rate equations when evaluating the activation energies intrinsic to creep-resistant alloys in the hcp Mg—Al—Ca, Ti and fcc Fe—Ni—C systems:

(i) At higher stresses and lower temperatures ($V^*\tau^* > kT$), the movement of glide dislocations is most likely to occur jointly with their solute atmospheres so that for the case, the dynamic dragging of microyielding is provided by the resistance of mobile dislocation atmospheres with the a.e. for vacancy migration. Thermally activated drag dislocation mechanism operates with the thermal a.e. (about 0.8-0.9 eV) to be enough for rapid (short-range) pinning of an excess vacancy, eV in the stress field of

the moving dislocation atmosphere consisting of the pair defects EV-AE atom. In this case, thermally activated slip dragging by the pair defects having a high rapidity of the short-range pinning is believed to be the most likely rate-controlling drag mechanism responsible for the pre-yield resistance. When operated under limited mobility of slow dislocations it can slow down the rate strain to 10^{-10} s^{-1}. It is deduced that the above mechanism resembles closely the Shoeck-Fleisher ordering mechanism rather than solute locking by the Cottrell mechanism which could not operate in a multi-level defect structure by reason of preferential (short-range) interactions between excess structural defects.

(ii) At lower stresses and higher temperatures ($V^* \cdot \tau^* << kT$) the rate-controlling drag mechanism in the pre-yield region preceding jerky flow is thought to be essentially governed by the repeated thermal pinning and thermal depinning of mobile dislocations typical for the jump-like dislocation microyield resistance. In this case, mechanism is operating with the thermal a.e. (about 0.3-0.5 eV) to be enough for the jump-like pair relaxation of V_e-AE atom defects in the stress field around of a dislocation in terms of direct interchange of their positions. The dragging effect is believed to be due to the constant (discontinuous, repeated) interactions between mobile free dislocations and solutes by a jump-like mechanism. For the case, of point peculiar interest is an enhanced effect of dragging at the early stage of the jerky flow. It may be appropriate for improving the long-term strength of high-temperature alloys. Solute atmosphere dragging is expected from a Le Chatelier-Braun effect based on physical-chemical principles of shifting the mobile equilibrium by a mechanism of discontinuous (repeated) pinning and depinning of dislocation.

• Plastic deformation of a solid solution shows itself as a dynamical system of the short-range interactions between mobile defects and is mainly controlled by a certain thermally activated dislocation mechanism. In doing so the pair defects consisting of an excess vacancy and an alloying element are thought to be responsible for the essential slowing down dislocations. Rapid strengthening of metal crystals is associated with the activation of short-range rate-controlling mechanisms, as predicted by Fisher and Flinn. For rapid hardening crystals thermally activated by short-range mechanisms, rate equations are derived by assuming that the density of mobile dislocations remains unchanged.

Because of their crucial technological role, hcp metals such as Ti, Zr, Mg, Zn and Co, among others, have been intensively studied over the past 70 years. Zr-based alloys are used as cladding for nuclear reactor fuels. Ti-based alloys are applied to the aerospace technology and the aircraft industry. Mg-based alloys are intended for automobile, computer, communication and consumer electronic applications. At present, the future of Mg-based alloys is certain because of current and projected advantages of magnesium reactive element which is the lightest among structural industrial metals.

Considerable experimental effort over the world is being expended in developing long-term strength structural magnesium alloys containing, as a rule, light elements to operate in the transport (automobile, powertrain, etc.) industry at higher

useful temperature and larger stresses under service conditions. The main interest in magnesium for the automotive and aeronautic industries is due to its low density, compared with that of aluminum and steel, which can reduce vehicle weight and fuel consumption. Mg-Al based alloys (AZ or AM alloys) have been used widely as die casting alloys and have been considered as wrought magnesium alloys. These alloys exhibit good castability and have reasonable room temperature mechanical properties and corrosion resistance in many environments. However, Mg-Al based alloys have poor high temperature creep resistance, which is believed to be associated with the grain boundary (discontinuous) precipitation of the β-phase ($Mg_{17}Al_{12}$). In order to overcome and minimize the deterioration of high temperature physical properties, new alloy systems have been actively investigated which have stable microstructure and good mechanical properties such as high creep and corrosion resistance at high temperatures.

Advances in technology in many areas are placing greater demands concerning high-performing materials, their alloy composition and related processing techniques. By doing so innovations are essential if these demands are met.

The monograph also reports the results of tensile and creep testing on magnesium- and zirconium-based alloys including with the substantially ordered $L1_2$ structure of Zr_3Al intermetallic as well as their matrix composite materials reinforced by nanoparticles (nm $Mg_{17}Al_6Ca_6$, etc.) and nanooxides (nm Y_2O_3 and nm ZrO_2). A set of high creep-resistant and high temperature-strength light alloys are developed as structural materials for high-loaded parts and dynamic applications.

Design and microstructural analysis of magnesium alloys based on the Mg—Al—Ca system have been carried out in order to investigate for dynamical applications the influence of alloying elements on their microstructures as well as microchemistry-processing-microstructural relations using structure-sensitive techniques. Following the data obtained, there is a direct correlation of microstructure with creep properties of the new experimental magnesium alloys. The creep and heat-induced properties of the multicomponent magnesium alloys containing low range of inexpensive additions of titanium (0.07-0.2%) or strontium (about 1.8%) are defined by the resulting structure dynamically formed during creep strain (up to 200 hr). It is noteworthy that Ti as novel alloying element competes for creep resistance and cost with Sr and attracts as-cast desirable properties minimizing solute effects at ambient temperatures. This is due to the pinning of slowly moving dislocations with the binding energy no more than 0.3-0.4 eV as well as due to stress-induced self-strengthening. The creep resistance and long-term strength in the new experimental alloys are superior to those for the present commercial alloys AZ91D, AE42 and AS21 (creep strain ε_c less than 0.3-0.4 % at 423 K and 70 MPa for 200 hr; $\dot{\varepsilon}_c \sim 10^{-9}\ s^{-1}$) thanks to their novel microstructure having desirable engineering properties for structural applications The newly developed magnesium alloys with improved castability can be used in die-casting technology and automobile (powertrain) industry for manufacturing components and parts which are difficult to cast with a more desirable microstructure.

Magnesium alloys of high purity in the hcp Mg—Al—Ca, X system discontinuously nano-reinforced by nm Zr_3Al reveal the desirable increase in dislocation creep resistance and long-term strength over the unreinforced counterparts at 423 K up to 70 MPa for 200 hr life. The observations and findings suggest that the principles of nanophase strengthening should be considered as an effective means of obtaining desirable combinations of mechanical properties due to the nanoparticle-induced delay time-dependent shear localization.

In this study, a family of new experimental zirconium alloys based on hcp Zr — Nb—Sn—Fe system and reinforced by nanooxides has been designed to improve their mechanical response and dislocation creep resistance. To achieve this purpose, the effectiveness of their structural and nanooxide strengthening mechanisms was verified in as-cast, deformed and annealed conditions. Zirconium alloys discontinuously reinforced with nm Y_2O_3 and nm ZrO_2 nanooxides reveal the threefold increase in tensile (short-term) strength and two orders of magnitude gain in long-term strength due to the thermally activated by-pass mechanism. A set of high creep resistance and high temperature strength alloys is developed as structural materials for high-loaded parts and dynamic design application.

This research outlines a detailed study of mechanical properties of ordered zirconium alloys with intermetallic strengthening in the Zr—8Al and Zr—8Al—1Nb systems using strain rate change measurements and tensile tests in a wide temperature range to optimize their specific properties such as dislocation creep resistance, high temperature strength and low temperature ductility. In this approach, suitable combination includes melting, hot-working and annealing treatment of the Zr—8Al—1Nb alloy to produce a substantially continuous matrix of the L12-ordered intermetallic compound Zr_3Al (up to 92%). A series of mechanical tests has been carried out with the Zr_3Al-based alloys which should be considered as discontinuously reinforced composite materials by the very nature. Post thermomechanical treatment of as-cast Zr_3Al-based alloys indicates their unchangeable yield stress at 293 and 673-973 K.

Mechanical properties of the essentially ordered Zr_3Al based alloys are at least twice higher those that observed for solution-hardened zirconium alloys (Zircaloys). The Zr_3Al-induced structure developed by thermomechanical treatment with subsequent annealing improves the chemical and structural homogeneity of the composite material as a whole. The formation of inhibiting jog type obstacles on the screw dislocations is assumed to be the rate-controlling mechanism of Zr_3Al ordered alloy strengthening which is dependent on the dislocation density. The excellent combination of short-term mechanical properties at 293 K and relaxation strength at 673-773 K revealed in the Zr_3Al-based alloys leads to their ability for high performance applications.

The weakening of nano-dispersion strengthening of commercially available alloys in the hcp Zr—Nb—Sn—nmZrO_2 system with slowing creep strain rates (10^{-6}-10^{-10} s^{-1}) is associated with the shielding effect due to strong Cottrell locking of mobile dislocations by the large quantity of interstitial oxygen impurities. The change of dislocation damping with temperature in hcp Zr matrix containing up to 0.15 mass% of oxygen

gives the first evidence for the preferential segregation of oxygen at strain-produced dislocations to form Cottrell dense atmospheres with a strong binding energy of about 2.0 eV. The unexpected behavior of commercially available zirconium alloys observed in the Zr—Nb—Sn—nmZrO_2 system might be well understood if properly provided for a shielding effect of impurity atoms of oxygen which is assumed to inhibit the interaction of dislocations with substitutional solutes (Nb, Sn) and nm ZrO_2 particles. Unlike macroscopic changes in strain, evolution of microyielding in given zirconium alloys is sure to occur mainly through rapid dislocations, while slow dislocations yield a small contribution to the strain. The thermal nm ZrO_2 barriers remain, therefore, effective at 673 K only at higher strain rates (10^{-3}-10^{-5} s^{-1}). The oxygen amount should be kept very low to avoid any deleterious (detrimental) microscopic effects.

Shear strain localization observed under the age-hardening conditions is certain to occur with formation of a two-phase field as a result of structural decomposition of a supersaturated solid solution by the continuous precipitation of dispersoids coherent with matrix and particle-free zones free of precipitates near GBs. In this case, many of metal alloys age-hardenable suffer problems associated with low ductility, inadequate fracture toughness caused by strain localization. In particular, to overcome this problem, alloy development effort should be concentrated on addition of dispersoids to refine the grain size and to minimize strain localization. It is accepted that the nanocrystal may not disrupt shear bond propagation due to their small size. This leads to catastrophic failure without plastic deformation. However, science-based modifying a chemical composition and aligning the structure of defect metal crystal due to dispersion strengthening minimize the strain localization effects responsible for degradation of micromechanical properties. Nano-dispersion strengthening effects are considered as an effective means of alloying a structure and promoting homogeneous microdeformation. This type of strengthening delays shear localization to much higher uniform microyield (creep for slow dislocations) and spreads the region of uniform tensile elongation from 0.5 to 30%. To be more uniformly successful, a nanophase nanostructure is to be more thermally stable as regards its dynamic recovery. In this respect, the method of nm-dispersion strengthening takes precedence over age hardening when overcoming the concentrated sliding with localized shear. To illustrate, for nm Al_3Zr strengthened magnesium alloys, transition from uniform to localized strain can exceed 1-2% at 423 K, while nm-particles of ZrO_2 can spread it up to 20-30%.

Appointed physical principles of deep purification, rational microalloying, low temperature (substructural, cell-forming) strain-hardening, optimum heterogenation thermally activated restoration of the plasticity and restitution of the breaking strength are formulated for the most brittle metals of Periodical System of Elements. In accordance with this, methods for overcoming the brittleness and improvement of physicomechanical properties have been worked out for precise and light alloys possessing a complex of technical characteristics including low susceptibility to the stress concentration and the dimensional stability necessary for service in the critical temperature ranges, promising for technical applications.

It thus appears that there may be a considerable scope for further alloy development. Such an approach is believed to be a powerful stating point and considerable scope for further improvement of the newly developed alloys with minimal tendency to localized shear. The research is not only motivated by basic science aspect but also the expectation that novel properties will lead to new technological and industrial applications. The basic information obtained is expected to assist in the further development of new families of discontinuously nanophase strengthened hcp magnesium and hcp zirconium alloys with their potential for technological applications at higher temperatures and stresses.

In summary, therefore, the present theoretical study will hopefully stimulate further investigations that could lend a better understanding of the mechanisms responsible for the formation of dislocation creep resistance and long-term strength in metal crystals. The present newly developed diagnostic approach is believed to provide a physical basis not only for a proper understanding of dragging effects but also for alloy development. The proposed method can be expected to be appropriate in describing the creep behavior of metal alloy systems as a starting point for further development of the rapid-hardening and creep-resistant alloys with a minimum of localized shear effects. The physical fundamentals for formation and recovery of the mechanical properties of rare earth metals as well as their light and precise alloys can be used for the development of promising metal alloy systems of the next generation.

APPENDIX I

Derivation of the Equation for the Rate of Dislocation Resistance

Logarithmic differentiation of many functions, e.g., containing a number of multipliers is appreciably simplified and becomes useful if the mobile dislocation density ρ_m remains invariable. In this case, dislocation creep resistance due to the dynamic dragging of jump-like dislocations in the onset of jerky flow is described by the following relation for the dislocation dragging rate:

$$\dot{\varepsilon}_d = C\cdot\exp\left(-\frac{U^* + E_b - V^*\cdot\tau^*}{kT}\right) - C\cdot\exp\left(-\frac{U^* - E_b - V^*\cdot\tau^*}{kT}\right) =$$

$$= C\cdot\exp\left(-U^*/kT\right)\cdot\exp\left(-E_b/kT\right)\cdot\exp\left(V^*\cdot\tau^*/kT\right) -$$

$$-C\cdot\exp\left(-U^*/kT\right)\cdot\exp\left(E_b/kT\right)\cdot\exp\left(V^*\cdot\tau^*/kT\right) =$$

$$= C\cdot\exp\left(-U^*/kT\right)\cdot\exp\left(V^*\cdot\tau^*/kT\right)\cdot\left(e^{E_b/kT} - e^{-E_b/kT}\right) =$$

$$= C\cdot\exp\left(-\frac{U^* - V^*\cdot\tau^*}{kT}\right)\cdot 2\sinh(E_b/kT) \qquad (1.1)$$

or by the expression of closed form

$$\dot{\varepsilon}_d = 2\bar{\rho}_m\cdot b\cdot\bar{\lambda}\nu\cdot\exp\left(-\frac{U^* - V^*\cdot\tau^*}{kT}\right)\cdot\sinh\left(E_b/kT\right) \qquad (1.2.)$$

where U^* is the energy of thermal activation for overcoming the obstacle resistance to dislocation motion under serrated yielding conditions

$$\ell n\dot{\varepsilon}_d = \ell n(2\bar{\rho}_m\cdot b\bar{\lambda}\cdot\nu\ ) - \frac{U^*}{kT} + \frac{V^*\tau^*}{kT} + \ell n\cdot\sinh\left(E_b/kT\right). \qquad (1.3)$$

Since

$$\ell n\cdot\sinh(E_b/kT) = \ell n\left(\frac{1}{2}\cdot e^{E_{Cb}/kT} - \frac{1}{2}\cdot e^{-E_b/kT}\right) =$$

$$= \ell n\frac{1}{2} + E_b/kT - \ell n\frac{1}{2} + E_b/kT = 2E_b/kT \qquad (1.4)$$

after logarithmic differentiation (1.3.) one can obtain the power law in the steady-state of creep resistance

$$\frac{\partial \ell n \cdot \dot{\varepsilon}_d}{\partial \tau^*} = \frac{V^* \tau^*}{kT} \cong \frac{L_c b^2 \cdot \tau^*}{kT}. \tag{1.5}$$

As a first approximation, the values of the activation parameters can be calculated from the Eq.(1.5) through the experimental data of inelastic relaxation, creep testing or tensile tests. One can use Eqs. (1.2-1.5) for the development of more precise experimental technique to determine the effective a.v. V^* and the activation length L_c of a dislocation nanosegment by stepwise loading or creep curves (at constant temperature):

$$\frac{\partial \ell n \dot{\varepsilon}_d}{\partial \tau^*} => \frac{\partial \ell n \dot{\varepsilon}_d}{\partial \sigma} \approx \frac{\ell n(\dot{\varepsilon}_2 / \dot{\varepsilon}_1)}{\Delta \sigma} = \frac{V^*}{kT}. \tag{1.6}$$

and in Burger's vector units

$$\frac{\ell n(\dot{\varepsilon}_2 / \dot{\varepsilon}_1)}{\Delta \sigma} \cong \frac{L_c \cdot b^2}{T}. \tag{1.7}$$

Under such conditions, Eq. (1.6) coincides in essence with the Schoeck relation obtained in the terms of the thermodynamic approach for mobile dislocations [134, 282].

APPENDIX II

Solving a System of Equations for Weak Multiplication of Dislocations

For the more accurate evaluation of activation parameters under the weak dislocations multiplication conditions, it is necessary to take into account the contribution to deformation strengthening through the fixed and arrested dislocations, i.e. $\partial\rho_m / \partial\tau^*$.

$$\dot{\varepsilon}_{\min} = 2\rho_m b\lambda\nu \exp\left(-\frac{U^* + E_b - V^*\tau^*}{kT}\right) \tag{2.1}$$

Finding deferential of τ^* and equating (to zero) partial derivatives of ρ_m and λ with respect to τ^* for minimization of Eq.(2.1) one can obtain the following relation

$$\left(\frac{\partial\dot{\varepsilon}}{\partial\tau^*}\right)_T = 2b\cdot\lambda\cdot\nu\cdot\rho_m \frac{\partial}{\partial\tau^*}\cdot\exp\left(-\frac{U^* + E_b - V^*\tau^*}{kT}\right) + 2b\cdot\lambda\cdot\nu\frac{\partial\rho_m}{\partial\tau^*}\times$$

$$\times\exp\left(-\frac{U^* + E_b - V^*\tau^*}{kT}\right) + 2b\cdot\nu\cdot\rho_b\cdot\exp\left(-\frac{U^* + E_b - V^*\tau^*}{kT}\right)\cdot\frac{\partial\lambda}{\partial\tau^*}; \tag{2.2}$$

and

$$\frac{d\dot{\varepsilon}}{d\tau^*} = 2\exp\left(-\frac{U^* + E_b - V^*\tau^*}{kT}\right)\times$$

$$\times\left(b\lambda\nu\rho_m\cdot\frac{V^*}{kT} + b\lambda\nu\frac{d\rho_m}{d\tau^*} + b\nu\rho_m\frac{d\lambda}{d\tau^*}\right) = 0 \tag{2.3}$$

for any values of τ^*.

It follows that

$$\left(b\lambda\nu\rho_m\cdot\frac{V^*}{kT} + b\lambda\nu\frac{d\rho_m}{d\tau^*} + b\nu\rho_m\frac{d\lambda}{d\tau^*}\right) = 0 \tag{2.4}$$

and

$$\frac{V^*}{kT} = -\frac{1}{\rho_m} \cdot \frac{d\rho_m}{d\tau^*} - \frac{1}{\lambda} \cdot \frac{d\lambda}{d\tau^*}. \tag{2.5}$$

$$V^* = -kT\left(\frac{d\rho_m}{\rho_m} \cdot \frac{1}{d\tau^*} + \frac{d\lambda}{\lambda} \cdot \frac{1}{d\tau^*}\right) \tag{2.6}$$

$$V^* \approx -\frac{kT}{\Delta\tau^*}\left(\frac{d\rho_m}{\rho_m} + \frac{d\lambda}{\lambda}\right) \approx -\frac{kT}{\Delta\tau^*}\left(d \cdot \ell n\rho_m + d \cdot \ell n\lambda\right) \tag{2.7}$$

For small $\Delta\tau^*$

$$V^* \approx -\frac{kT}{\Delta\tau^*}\left(\Delta\ell n\rho_m + \Delta\ell n\lambda\right) \approx -\frac{kT}{\Delta\tau^*}\left(\ell n\rho_1 / \rho_2 + \ell n\lambda_1 / \lambda_2\right) \tag{2.8}$$

where $\Delta\tau^*$ is the increment of thermal component in shear stress; λ is a activation distance for successful jump of dislocation; $\Delta\rho_m$ and $\Delta\ln\rho_m$ are parts of the local density of mobile dislocations which have successfully overcome the thermal obstacles.

Since the a.v. $V^* = L_c \cdot b^2$, activation length L_c between the mobile nodes of pinning by alloying elements/impurities is determined from the relations

$$L_c = -\frac{kT}{b^2 \cdot \Delta\tau^*}\left(\partial\ell n\rho_m + \partial\ell n\lambda\right) \tag{2.9}$$

$$L_c \approx -\frac{kT}{b^2 \cdot \Delta\tau^*}\left(\frac{\Delta\rho_m}{\rho_m} + \frac{\Delta\lambda}{\lambda}\right) \tag{2.10}$$

At λ = const, the expression (2.10) relates to expression (2.11):

$$L_c = -\frac{kT}{b^2 \cdot \Delta\tau^*} \cdot \partial\ell n\rho_m \approx -\frac{kT}{b^2 \cdot \Delta\tau^*} \cdot \frac{\Delta\rho_m}{\rho_m} \tag{2.11}$$

REFERENCES

1. Frazier W.E. Long-term service of aluminum, magnesium and titanium at high temperatures. *Adv. Mater. Processes*. 1988. 134(5). P. 42-46.

2. Bhat M.A., Handa A., Nayak B.K., Lone I.H. Nanotechnology, Metal Nanoparticles, and Biomedical Applications of Nanotechnology. Ch. 5. Ed. M.A. Shah, M.A. Bhat, J. Paulo Davim. Pennsylvania: IGI Global Publishers. Hershcy, 2014.

3. Elorin S., Scott T. E. On the effect of work hardening on stress dependence of dislocation velocity. *Acta metal*. 1964. Vol. 12. No. 12. P. 1459-1470.

4. Starke E.A. Jr. The Application of the Fundamentals of Strengthening to the Design of N…W Aluminum Alloy. *J. of Metals*. 1981. Vol. 33. No. 8. 24 p.

5. Kumar K.S., Van Swygenhoven H., Suresh S. Mechanical behavior of nanocrystalline metals and alloys. *Acta Mater.* 2003. Vol. 51. P. 5743-5774. Doi: 10.1016/j. actamat. 2003.08.032.

6. Teutonico L. J., Granato A.V., Lucke K. Theory of the Thermal Breakaway of a Pinned Dislocation Line with Application to Damping Phenomena. *J. Appl. Phys.* 1964. Vol. 35. 220 p.

7. Taketomi S., Matsumoto R., Miyazaki N. Atomic study of the competitive relationship between edge dislocation motion and hydrogen diffusion in alpha iron. *J. Mater. Res*. 2011. Vol. 26. No. 10. P. 1269-1279.

8. Braun A.M., Ashby M.F. On the power-law creep equation. *Scripta Metallurg*. 1980. Vol. 14. Iss. 12. P. 1297-1302.

9. Rossouw C.J., Vehkatesan. J. *Electron Microscopy*. 2001. Vol. 50(5). P. 391-404.

10. Engelke H. in: Fundamental Aspects of Dislocation. Theory, Eds. Simmons J.A., de Wit R., Bullough R., Nat. Bur. Stand. Spec. Publ., 1970. Vol. 11. No. 317. P. 17-26.

11. McCormick P.G. Theory of flow localization due to dynamic strain aging. *Acta Metall*. 1988. Vol. 36(12). P. 3061-3067.

12. Hirth J.P., Lothe J. Theory of Dislocations. 2nd Ed. New York: Krieger Publishing Co, 1992. 857 p.

13. Sherby O.D., Klundt R.H., Miller AK. Flow stress and subgrain stability at elevated temperatures. *Metallurg. Trans*. 1977. A8. P. 843-850.

14. Jingyi Cheng, Sia Nemat-Nasser. A model for experimentally-observed high-strain-rate dynamic strain aging in titanium. *Acta Mater*. 2000. Vol. 48. P. 3131-3144.

15. Khantha K., Vitek V., Pope D.P. Strain rate dependent mechanism of cooperative dislocation generation; application to the brittle-ductile transition. *Mater. Sci. and Eng.* 2001. A319-321. P. 484-489.

16. Taketomi S., Matsumoto R., Miyazaki N. Atomistic study of the competitive relationship between edge dislocation motion and hydrogen diffusion in alpha iron. *Jour. Mater. Res*. 2011. Vol. 26. No. 10. P. 1269-1281.

17. Kennedy A.J., Sollars A.R. Magnesium and Aircraft Engineering: The Second of a Series of Articles Describing the Materials Used in Aircraft Construction. *Aircraft Engineering and Aerospace Technology*. 1993. No. 1. P. 16-22.

18. Aghion E., Bronfin B. Magnesium Alloys Development towards the 21st century. *Materials Science Forum*. 2000. Vol. 350-351. P. 19-28.

19. Garofalo F. Fundamentals of Creep and Creep-Rupture in Metals. New-York-London: Collier-Macmillan Ltd., 1965. 304 p.

20. Kassner M.E. Fundamentals of Creep in Metals and Alloys. 3rd ed. Butterworth-Heinemann Elsevier-Verlag., 2015. 338 p. https://doi.org/10.1016/C2012-0-0607-1.

21. Valeri S. Application of Auger-spectroscopy for structural investigations. *Riv. Nuovocim*. 1993. Vol. 16. No 5. P. 1-73.

22. Conrad H. Thermally activated deformation of metals. *J. of Metals*. 1964. Vol. 16. No. 7. P. 582-588.

23. Warren B.E. X-ray diffraction. Addison-Webslay Publ. Reading Mass., 1969.

24. Puskar A. Internal friction of materials. Cambridge International Science Publishing. 7 Meadow Walk, Great Abington, Cambridge CB1 6AZ, UK First published May., 2001. 342 p.

25. Koila M. Trapping effect in diffusion of interstitial impurity atoms in B.C.C. lattices. *Acta Metall*. 1974. 22. P. 1259-1268.

26. Li James C.M. Dislocation Dynamics in deformation and Recovery. *Canadian J. of Phys.* 1967. 45. P. 493-509.

27. Evans R.W., Wilshire B. Creep of Metals and Alloys. London: Institute of Metals, 1985. 314 p.

28. Gjestland H. et al. Stress-relaxation and creep behaviour of some rapidly solidified magnesium alloys. *Mat. Sci. Eng*. 1991. A134. P. 1197-1200.

29. Harries J.E. The Inhibition of Diffusion Creep by Precipitates. *Jour. Metal. Sci.* 1973. Vol. 7. Iss. 1. P. 1-6.

30. Kioussis N. G., Ghoniem N. M. Modeling of Dislocation Interfaces: A Multiscale Challenge. *J. Computational and Theoretical Nanoscience*. 2010. Vol. 7. P. 1-30.

31. Hashimoto E., Kino T. Hydrogen diffusion in aluminum at high temperatures. *J. Phys. F: Met. Phys*. 1983. Vol. 13. P. 1157-1165.

32. Basinski Z.S. Thermally Activated Glide in Face-Centered Cubic Metals and its Application to the Theory of Strain Hardening. *Phil. Mag.* 1959. Vol. 4. No.10. P. 393-432.

33. Ma E. Alloys created between immiscible elements, Progress in Materials Science, 2005, 413-509.

34. Sills R.B., Cai W. Solute drag on perfect and extended dislocation. *Phil. Mag*. 2016. Vol. 96. P. 895-921. DOI:10.1080/14786435.2016.1142677.

35. Mandal P.K. Study of hardening mechanisms in aluminum alloys. *Int. Journal of Engineering Research and Applications.* 2016. Vol. 6. Iss.1. P. 91-97.

36. Leyson G.P.M., Hector Jr.L.G., Curtin W.A. Solute strengthening from first principles and application to aluminum alloy. *Acta Mater*. 2012. Vol. 60. No. 9. P. 3873-3884.

37. Reed-Hill R.E. Physical Metallurgy Principles. New-York: Van D. Nostrand Company, 1973.

38. Braun A.M., Ashby M.F. On the power-law creep equation. *Scripta Metall.*1980. Vol. 14. Iss. 12. P.1298-1302.

39. Martin J.W., Doherty R.D., Cantor B. Stability of Microstructure in Matellic Systems (Cambridge Solid State Science Series) 2 nd Edition. London: Cambridge University Press, 1997, 442 p.

40. Williamson G.K., Hall W. X-ray line broadening from filed aluminium and tungsten. *Acta Metallurgica*. 1953. Vol. 1. Iss. 1. P. 22-31.

41. Valiev R.A. Langdon Terence G. Principles of equal-channel angular pressing as a processing tool for grain refinement. *Progress in Materials Science*. 2006. 51. P. 881-981.

42. Schaefer H.E., Wurschum R., Birringer R., Gleiter H. Structure of nanometer-sized polycrystalline iron investigated by positron lifetime spectroscopy. *Phys. Rev.* 1988. B38. Iss. 14. P. 9538-9545.

43. Schpack A.P. and Melnick A.B. On the existence of fcc clusters in liquid aluminum. *Nanostruct. Mater*. 1994. Vol. 4. No. 4. P. 485-489.

44. Cohen J.B., Fine M.E. Some aspects of short-range order. *Le journal de physique L1 Lh Radium*. 1962. Vol. 23. P. 749-759.

45. Sakata M., Cowlam N., Davies H.A. Chemical short-range order in liquid an amorphous Cu66Ti34 alloys. *J. Phys. F: Metal Phys.* 1981. Vol. 11. P. 157-162.

46.Van der Lugt W. Geertsma W.J. Of non-crystalline solids, liquid alloys with strong chemical interactions. 1984. 61-62. Pt. 1. P. 187-200.

47. Chieux P. Rappersberg. The observation of chemical short-range order in liquid and amorphous metallic systems by diffraction methods. *Journal of Physics*. 1980. Vol. 8. 41. P. 8-145.

48. Bityutskaya L.A., Mashkina E.S. System of kinetic parameters of the transition processes under melting of crystalline substances. *Phase Transitions*. 2000. Vol. 71. P. 317-330.

49. Tkachenko V.H., Kondrashev A.I., Maksimchuk I.N. Nanocluster-induced quantum photoyield of metal alloy systems. *Appl. Phys. B*. 2010. Vol. 101. P. 253-261.

50. Hashimoto E., Kino T. Hydrogen diffusion in aluminum at high temperatures. *J. Phys. F: Met. Phys*. 1983. Vol. 13. P. 1157-1165.

51. Tkachenko V.H., Kim K.H., Moon B.G., Vovchok A.S. Design and microstructural analysis of magnesium alloys for dynamical applications. *J. Mater. Sci*. 2011. 46. Iss.14. P. 4880-4895.

52. Tkachenko V.H. Proceedings of *Int. Conf. EUROMAT-2005, Csech R. Prague.* 2005.

53. Concustell A., Alcala G., Mato S., et al. Effect of relaxation and primary nanocrystallization on the mechanical properties of $Cu_{60}Zr_{22}Ti_{18}$ glass, Intermetallics 2005, 13, P. 1214-1219. DOI: 1016/j.Intermet.2005.04.003.

54. Mudry S., Shtablavyi T., Shcherba I. Liquid eutectic alloys as cluster solutions. *Arch. Mater. Sci. Eng.* 2008. Vol. 34. Iss.1. P. 14-18.

55. Koila M. Trapping effect in diffusion of interstitial impurity atoms in B.C.C. lattices. *Acta Metall*. 1974. Vol. 22. P. 1259-12688.

56. Mudry S., Prokhorenko V., Prokhorenko S., Bojar Z. Influence of structure state of melt on solidification process. *J. Achiev. Mater. Manuf. Eng*. 2006. 18. P. 159-162.

57. Haberland H. Clusters of Atoms and Molecules: Theory, Experiment and Clusters of Atoms. Berlin-Heidelberg: Springer-Verlag, 1994.

58. Ishikawa T., McLellan R.B. The diffusivity of hydrogen in aluminum. *Acta Metall.* 1986. Vol. 34. P. 1091-1095.

59. Bugaev V.M., Tatarenko V.A., Tkachenko V.G. Impurity-induced host-lattice vacancies in metals and interstitial alloys. *Int J. Hydrogen Energy*. 1999. 24. P. 135-140.

60. Tkachenko V.G. Contemporary Trends of the Development of Physics of Light Metals. *Progr. Phys. Metal*. 2009. Vol.10. P. 103-130.

61 Creiner W. Optical response of small magnesium cluster. *J. Phys.* 2004. B37. P. L137-L145.

62. Lualin A., Solovyov A.V., Brechignac C., Greiner W. Stability of small neutral and charged strontium clusters. *J. Phys.* 2005. B3. P. 8 L129-L135.

63. Koila M. Trapping effect in diffusion .of interstitial impurity atoms in B.C.C. lattices. *Acta Metall*. 1974. Vol. 22. P. 1259-12688.

64. Galaktionnova A.V., Emaletdinov A.K. Modeling of vacancy kinetics in nanostructured heat-resistant alloy at the thermal \fatigue. *Rev. Adv. Mater. Sci.* 2015. Vol. 43. P. 13-16.

65. Castleman A.W., Recent Jr. advances in cluster science Mass Eur. *J. Spectrom*. 2007. Vol. 13. P. 7-11.

66. Tkachenko V.G., Kondrashev A.I., Maksimchuk I.N. Nanocluster-induced quantum photoyield of metal alloy systems. *Appl Phys*. 2010. B 101. P. 253-261.

67. Rao T., Burrill A., Chang X.Y. Photocathodes for the energy recovery linacs, *Nucl. Instrum. Methods*. 2006. A557. P. 124-130.

68. Mudry S., Prokhorenko V., Prokhorenko S., Bojar Z. Influence of structure state of melt on solidification process. *J. Achiev. Mater. Manuf. Eng*. 2006. Vol. 18. P. 159-162.

69. Jackson M.J., Robinson G.M., Whitfield M.D. Manufacture of nanocrystalline metals by machining process. *J. Achiev. Mater. Manuf. Eng*. 2007. Vol. 20. P. 27-30.

70. Haberland H. Clusters of Atoms and Molecules, Theory, Experiment and Clusters of Atoms. Heidelberg, Berlin: Springer-Verlag, 1994.

71. Kreibig U., Vollmer M. Optical Properties of Metal Clusters. Berlin-Heidelberg: Springer-Verlag, 1995.

72. Shinde P.P., Yadav B.D., Kumar V. Evolution of atomic and electronic structure of magnetic Gd-doped gold clusters. *J. Mater. Sci*. 2012. Vol. 47. P. 7642-7652.

73. Brack M. Electronic Structure of Metal Clusters, Shells, Supershells and all that. Lecture presented at the Nordic Summer School on Clusters and Nanoparticles. Kristinberg. Sweden. 2014.

74. Tkachenko V.G., Khoruzhaya V.G., Meleshevich K.A. Phase equilibria in the Mg—Al—Ca system. *Powder Metall. and Met. Ceram*. 2003. Vol. 42. P. 268-275.

75. Nikitin K.V., Nikitin V.I., Timoshkin I.Yu. et. al. Melt treatment by pulsed magnetic fields at controlling the structure and properties of industrial silumin. *Russian J. Non-Ferrous Metals*. 2016. Vol. 57. Iss. 3. P. 202-210.

76. Jena A.K., Gupta A.K., Chaturvedi M.C. A differential scanning calorimetric investigation of precipitation kinetics in the Al-1.53 wt% Cu-0.79 wt% Mg alloy. *Acta Metall*. 1989. Vol. 37. P. 885-895.

77. Massalsky T.B., Binary Alloy Phase Diagrams .Vol. 1-3. American Society for Metals: Metal Park OH, 1986.

78. Tkachenko V.G., Maksimchuk I.N., Volosevich P.Yu. Creep Resistance and Long-Term Strength of Structural Magnesium Alloys. *High Temp. Mater. Processes*. 2006. Vol. 25. P. 97-101.

79. Pushkar A. Internal Friction of Materials. Cambridge-London: Int. Sci. Publ., 2001.

80. Cottrell A.H., Bilby B.A. Dislocation Theory of Yielding and Strain Ageing of Iron. *Phys. Soc*. 1949. A62. P. 49-62.

81. Samson J.A.R. Techniques of Vacuum Ultraviolet Spectroscopy. New York: Wiley, 1967.

82. Weissmann R. Muller K. Auger electron spectroscopy – a local for solid surfaces. *Surf. Sci*. 1981. Rep.1. P. 251-309.

83. Beevers C. J. Electrical resistivity observation on quenched and cold-work magnesium. *Acta Metall*. 1963. Vol. 11. P. 1029-1034.

84 Blaha P., Schwarz K., Luitz J., Wien A. Full Potential Linearized Augmented Plane Wave Package for Calculation Crystal Properties. Karlheinz Schwarz: Wien Techn. Univ., 1999.

85. Tkachenko V.G., Strongin B.G, Likhtorovich S.P. et al. Peculiarities of solid solution decay of hydride-forming and non-hydride-forming systems with close-packed crystal structure. *Int. J. Hydrogen Energy*. 1996. Vol. 21. P. 1091-1936.

86. Rudman P.S. A. theory of atom size difference induced short-range order. *Acta Metall*. 1965. Vol. 13. P. 387-389.

87. Hashimoto E., Kino T. Hydrogen diffusion in aluminum at high temperatures. *J. Phys. F: Met. Phys*. 1983. Vol. 13. P. 1157-1165.

88. Mott N.F., Nabarro F.R. Dislocation theory and transient creep. *Phys. Soc. Bristol. Conf*. 1948. P. 1-19.

89. Ismael J. Curie's principle. *Syntheses*. 1997. 110. P. 167-190.

90. Westphalen M., Kreibig U., Rostalski J., Liith H., Meissner D. Metal cluster enhanced organic solar cells. *Sol. Energy Mater. Sol. Cells*. 2000. Vol. 61. P. 97-105.

91. Tkachenko V.G., Kondrashev A.I., Maksimchuk I.N. Advanced metal alloy systems for massive high-current photocathodes. *Appl. Phys.* 2010. B98. P. 839-849.

92. Ferragut R., Somoza A., Torriani I. Pre-precipitation study in the 7012 Al—Zn—Mg—Cu alloy by electrical resistivity. *Mater. Sci. Eng.* 2002. A334. P. 1-5.

93. Han X.L., Wang Q., Sun D.L., Zhang H.X. First-principles study of the effect of hydrogen on the Ti self-diffusion characteristics in the alpha Ti—H system. *Scripta Mater.* 2007. 56. P. 77-80.

94. Shin D., Wolverton C. First-principles steady of solute-vacancy binding in magnesium. *Acta Mater*. 2010. Vol. 58. P. 531-540.

95. Buschow K.H.J. Short-range order and thermal stability in amorphous alloys. *J. Phys. F: Metal. Phys*. 1984. Vol. 14. P. 593-608.

96. Mandal P.K. Study of hardening mechanisms in alumin0um alloys. *Int. J. Eng. Res. Appl*. 2016. 6. Iss. 1. Pt. 6. P. 91-97.

97. Rudman P.S. An X-ray diffuse-scattering study of the Nb-Ti B.C.C. solution. *Acta Metall.* 1964. No. P. 1381-1388.

98. Tkachenko V.G., Kim K.H., Moon B.G., Vovchok A.S. Design and microstructural analysis of magnesium alloys for dynamical application. *J. Mater. Sci.* 2011. Vol. 46. P. 4880-4895.

99. Flinn P.A. Electronic Theory of Local Order. *Phys. Rev.* 1956. Vol. 104. P. 350-356.

100. Brounwer R.C., Griessen R. Heat of solution and site energies of hydrogen in disordered transition-metal alloys. *Phys. Rev*. 1989. B40. P. 1481-1494.

101. Lulay. J.,Wert C. Internal friction in Cd-Mg alloys. *Acta Metall*. 1956. Vol. 4. P. 627-631.

102. Seeger A. Dislocations and Mechanical Properties of Crystals. N.-Y.: J.C. Fisher John Wiley, 1965. 243 p.

103. Granato A., Lücke K. Theory of Mechanical Damping Due to Dislocations. *Journal of Applied Physics*.1956. Vol. 27. P. 583-593.

104. Granato A., Lucke K. Application of Dislocation Theory to Internal Friction Phenomena at High Frequencies. *J. Appl. Phys*. 1956. 27789-805./ https//doi. org/10.1063/1.1722485.

105. Teutonico L. J., Granato A. V., Lücke K. Theory of the Thermal Breakaway of a Pinned Dislocation Line with Application to Damping Phenomena. *Journal of Applied Physics*. 1964. Vol. 35. P. 220-233.

106. Stephenson E.T., Conrad G.P. Damping near the Snoek peak in Fe. *Acta Met*. 1968. Vol. 16. No. 10. P. 1253-1266.

107. Granato A.V., Lucke K. Temperature dependence of amplitude-dependent dislocation damping. *J. Appl. Phys*. 1981. Vol. 52. No.10. P. 7136-7142.

108. Blair D.G., Hutchison T.S., Rogers D.H. Theory of Damping due to Thermally Assisted Unpinning of Dislocations. *Canadian Journal of Physics*. 1971. Vol. 49. No. 6. P. 633-662.

109. Blanter M.S., Golovin I.S., Neuhauser H., Sinning H.-R. Internal Friction in Metallic Materials, Springer Berlin Heidelberg New York, 2007, 535 pages.

110. Snoeck G., Bisogni E., Shyne J. The activation energy of high temperature internal friction. *Acta Metall*. 1964. Vol. 2. P. 1466-1468.

111. Postnicov V.S. Mecanical relaxation in pure inorganic materials. *Reinststofe Wiss und Techn. Symposiusher* 1970 *Dresden.* Berlin. 1972. P. 129-154.

112. Teutonico L. J., Granato A. V. and Lücke K. Theory of the Thermal Breakaway of a Pinned Dislocation Line with Application to Damping Phenomena. *Journal of Applied Physics*. 1964. Vol. 35. P. 220-233. https://doi.org/10.1063/1.1713074

113. Read T.A. The Internal Friction of Single Metal Crystals. *Phys. Rev.* 1940. Vol. 58. 371 p.

114. Nowick A.S. Progress in Metal Physics. Ch.1. London: Pergamon Press, 1953. 357 p.

115. Carro J. A., Mondino M. Internal friction background and peaking effect. *J. Appl.Phys*. 1981. Vol. 52. No. 12. P. 7147-7154.

116. Tkachenko V.G., Strongin B.G., Maksimchuk I.N., Friesel V.V., Grechko V.P., Likhtarovich S.P. Peculiarities of sold solution decay of hydride-forming and non-hydride-forming systems with close-packed crystal structure. *Int. J. Hydrogen Energy.* 1996. Vol. 21. No.11/12. P. 1091-1096.

117. Rudman P.S. A theory of atom size difference induced short range order. *Acta Metall.* 1965. Vol. 13. No. 4. P. 2–11.

118. Bernal J.D. Structure of liquids. *Quantum Macrophysics*. Ed. V.T. Khozyainov. Moscow: Nauka, 1967. P. 117-127.

119. Cottrell A.H., Bilby B.A. Dislocation Theory of Yielding and Strain Ageing. of Iron. *Proc. Phys. Soc.* 1949. A62. P. 49-62. https://doi.org/10.1088/0370-1298/62/1/308

120. Cottrell A. H. Dislocations and Plastic Flow in Crystals. Oxford: Clarendon Press, 1953. 223 p.

121. Abramov A.A., Tkachenko V.G. Features of the Formation of Cluster Compounds in Metal Solid Solutions, *Ukr. J. of Phys.,* 2017, 62, 11, 961-969. 122. / Entel D., Kodan K., Mayer R. at al. Phase *Transitions*. 1998. B65. P. 79-108.

123. Gornostaev Yu.N., Katsnelson M.I., Kuznetsov A.R., Trefilov A.V. Modeling of martensitic transformations in crystals with dislocations of various types in bcc — Zr *FMM*. 2001. Vol. 91. No 3. P. 32-39.

124. Tkachenko V.H., Kondrashev O.I., Maksymchuk I.M. Physical foundations of metal crystal photoelectronics. Kyiv: Academperiodyka, 2009. 210 p.

125. Panin V.Ye. Hriniaev Yu.V., Danylov V.I. et al. Structural levels of plastic deformation and destruction. Novosibirsk: Nauka. Sib. Otdelenie. 1990. 225 p.

126. Lachenmann R., Schultz H. Inherent lattice hardening and interstitial solution hardening in tantalum. *Scripta Metall*. 1970. No. 9. P. 709-714.

127. Dorn J. E., Rajnak S. Nucleation of kink Pairs and the Peierls' Mechanism of Plastic Deformation Trans. *Met. Soc. AIME*. 1964. Vol. 230. No. 5. P. 1052-1064.

128. Frank W. Die kritische Schubspannug kubischer Kristalle mit Fehlstellen tetragonaler Symmetrie IV. Die untere Streckgrenze von α Eisen. *Phys. Stat. Sol.* 1967. Vol. 19. Iss. 1. P. 239-250.

129. Fleisher R.L. High-Temperature, High-Strength Materials: an overview. *JOM*. 1985. Vol. 37. P. 16-20.

130. Stein D.F, Low J.R. Effects of orientation and carbon on the mechanical properties of iron single crystals. *Acta Metall.* 1966. Vol. 14. Iss. 10. P. 1183-1194.

131. Ravi K.V, Gibala R. The strength of niobium-oxygen solid solutions. *Acta Metal.* 1970. Vol. 18. Iss. 6. P. 623-634.

132. Chambers R.H., Mason W.P. Physical Acoustics. Vol. II. New York: Academic Press, 1966. 123 p.

133. Fleisher R.L. Rapid Solution Hardening, Dislocation Mobility, and the Flow Stress of Crystals. *J Appl Phys.* 1962. Vol. 33. No. 12. P. 3504-3518.

134. Schoeck G., Seeger A. The flow stress of iron and its dependence on impurities. *Acta Metallurgica.* 1959. Vol. 7. Iss. 7. P. 469-477.

135. Frank W., Sestak B. A. United Model for the Interpretation of the Low-Temperature yield Stress, its Dependence on Crystals Orientation and of the Sleep Geometry of BCC Metals. *Scripta Metall.* 1970. Vol. 4. P. 451-453.

136. Seeger A. The Temperature and strain-rate Dependence of the Flow Stress of Body-Centered Cubic Metals: A Theory Based on Kink-Kink Interactions Zeitschrift fur Metallkunde. 1981. B72, No. 6. P. 369-380.

137. Feltham P. Stress relaxation in Copper and Alpha-Brasses at Low Temperatures. *J. Inst. Metals*. 1960. Vol. 61. 89. P. 210-218.

138. Trudeau M.L., Schultz R. High-resolution electron microscopy study of Ni-Mo nanocrystals prepared by high-energy mechanical alloying. *Materials Science and Engineering. 1*991. A134. No. 25. P. 1361-1367.

139. Ting-Sui Ke Experimental Evidence of the Viscous Behavior of Grain Boundaries in Meyals. *Phys. Rev*. 1947. Vol. 71. No. 8. P. 533-546.

140. Friedel J. Electron Microscopy and Strength of Crystals. New York: John Willy æ Sons, Inc., 1963. 605 p.

141. Physical Metallurgy. 3 rd Ed. Eds. Cahn R.W., Haasen P. Amsterdam: Elsevier Sci. Publ., 1973. 980 p.

142. Sickafus K.E., Sass S.L. Grain boundary structural transformations induced by solute segregations. *Acta Metall*. 1987. Vol. 35. No. 1. P. 69-87.

143. Meyers C.L., Jr., Onoda G.Y., Jr., Levy A.V., Kotfila R.J. Role of Grain Boundaries in the Ductile-Brittle Transition Behavior of Bcc Metals. *Trans. Metallurg. Soc. AIME*. 1965. Vol. 233. P. 720-728.

144. Liu X.D., Lu K., Ding B.Z., Hu Z.Q. Investigation of the lattice structure of nanophases in Fe-Cu-Si-B alloys. *Nanostr. Mater*.1993. No. 2. P. 581-586.

145. Lu K., Sui M.L., Lück R. Supersaturation of phosphorus in nanophase nickel crystallized from an amorphous Ni-P alloy. *Nanostr. Mater*.1994. No. 4. P. 465-473.

146. Mütschele T., Kirchheim R. Segregation and diffusion of hydrogen in grain boundaries of palladium. *Scripta Metallurgica*. 1987. Vol. 21. Iss. 2. P. 135-140.

147. Aulnier A. Etude Structurale du beryllium pur micrographie sur coupes minces. *Service des recherches de la Cie.* France. 1960. P. 299-309.

148. Gleiter H. Der Mechanismus des Korngrenzenglitens. *Acta Metall.* 1968. Vol.16. P. 1053-1067.

149. Siegel R. W. Nanostructured materials: mind over matter. *Nanostructured Material.* 1994. Vol. 4. No. 1. P. 121-138.

150. Meyers M. A., Mishra A., Benson D. J. Mechanical properties of nanocrystalline materials. *Progress in Materials Science.* 2006. Vol. 51. No. 4. P. 427-556.

151. Linga Murty K., Mohamed F.A. Dorn J.E. Effect of vacancy sinks and sources on serrated yielding due to solute locking. *Scripta Metall*. 1971. Vol.5. P. 1087-1092.

152. Cottrell A.H. Dislocations in metals: the Birmingham school. 1945. 55. *Proceedings of the Royal Society of London*. 1980. Vol. A371, No. 1744. P. 144-148.

153. Friedel J. Electron Microscopy and Strength of Crystals. Ed. G. Thomas, J. Washburn. New York: Interscience, 1963. 634 p.

154. Yoshinaga H. Morozumi S. A. Portevin-Le Chatelier Effect Expected from Solute Atmosphere Dragging. *Phil. Mag*. 1971. Vol. 23. 186. P. 1351-1366.

155. Dinhut J.E., Banou T., Moire P. Phenomene Portevin-Le Chatelier Dans Les Alliages Fe-Co Ordonnes et Desordonnes. *Acta Metall*. 1976. Vol. 24. P. 445-451.

156. Trojanova Z., Lukac P., Cizek L. Unstable Plastic Deformation in Mg alloys: Post Relaxation Effect. *Proc. 6th Int. Conf. Magnesium Alloys and Their Applications.* Ed. K.V. Kainer. Wolfsburg: WILEY-VCH, DGM, 2003. p. 495-500.

157. Westbrook J.H., Wood D.L. *Nature*. 1961. Vol.192. P. 78-79.

158. Hayes R.W., Hayes W.C. *Acta Metall*. 1982. Vol.30. No. 7. P. 1295-1301.

159. Yoshida H., Toma K., Abe K., Morozumi S. The Portevin-Le Chatelier Effect in Vanadium. *Phil. Mag.* 1971. Vol. 23. No. 186. p. 1387.

160. Alefeld G. Grouping of Pinning Points on dislocation lines. *Phil. Mag*. 1965. Ser. 8. Vol. 11. Iss. 112. P. 809-826.

161. Tkachenko V.H., Shulyak I.I., Strutinsky A.N., Friezel V.V., Krivik O.V. Activation Analysis of the structural clustering transformation in metal hydride-forming systems. *Hydrogen Materials Science and Chemistry of Metal Hydrides.* Ed. N. Veziroglu et al., Netherland: Kluwer Acad. Publish, 2002. P. 77-95

162. Inoue A., Takeuchi A., Zhang T. Ferromagnetic bulk amorphous alloys Metallurgical and Materials Transactions *Mater. Trems.* 1998. A29. P. 1779-1793.

163. Alefeld G. Grouping of Pinning Points on dislocation lines. 1965. 809 p.

164. Matteazzi P., Basset D., Miani F., Le Caer G.. Mechanosynthesis of nanophase materials. *Nanostructured materials*. 1993. Vol. 2. P. 217-229.

165. Pelton A.D., Decterov S.A., Eriksson G., Robelin C., Dessureault Y. *Metall.*

166. Gilman J.J. Creation of cleavage steps by dislocation. *Trans AIME*. 1958. Vol. 212. P. 310-315.

167. Hirth J.P., Lothe J. Theory of Dislocations. 2nd Ed. New York: Krieger Publishing Co., 1992. 857 p.

168. Fisher J.C., Johnston W.G., Thomson R., Vreeland T (Ed.). *Int. Conf. Dislocations and Mechanical Properties of Crystals*. New York: Wiley and Sons Inc., 1957.

169. Dupouy J.M. and Averbach B.L. *Acta Met.* 1961. Vol. 9. 755 p.

170. Tkachenko V.H. et.al. Structural clustering and relaxation effects in solid solutions of hydride forming systems, *Metallofiz. Noveishie Teknol.* 2001. Vol. 23. No. 3. P. 367-386.

171. Wilson D, Russel B. *Acta Metall*. 1959. Vol.7. P. 623.

172. Starke E.A. The Application of the Fundamentals of Strengthening to the Design of New Aluminum Alloy. *JOM*. 1981. Vol. 33. No. 8. P. 24-37.

173. Holt D.L. Dislocation Cell Formation in Metals. *J. Appl. Phys*. 1970. Vol.41. No. 8. P. 3197-3201.

174. Thompson A.W. Substructure Strengthening Mechanisms. *Metallurg. Trans A*. 1977. 8A. P. 833-842.

175 Lu K., Wang J. T., Wei W. D. A new method for synthesizing nanocrystalline alloys. *Appl J. Phys.* 1991. Vol. 69. P. 522-524. https://doi.org/10.1063/1.347698.

176. Gleiter H. The Interaction of Lattice Defects and Grain Boundaries. *Journal of the Less-Common Metals.*1972. Vol**.** 28. No. 2. P. 297-323.

177. Siegel R. W. Nanostructured materials: mind over matter. *Nanostructured Materials.* 1994. Vol. 4. No. 1. P. 121-138.

178. Hall E. O. The Deformation and Ageing of Mild Steel: III Discussion of Results. *Proc. Phys. Soc.* 1951. B64. P. 747–752.

179. Petch N. J. The cleavage strength of polycrystals. *J. Iron Steel Inst*. 1953. 174. P. 25-8.

180. Smith E. Stress produced at a barrier by a pileup of dislocations. *J. Appl. Phys.* 1970. Vol. 4. No. 6. P. 2736-2737.

181. Wolf. D., Yamakov V., Phillpot S.R., Mukherjee A.K. *Z. Metallk*. 2003. 94. 10. P. 1091-1097.

182. Tkachenko V.H. Contemporary Trends of the Development of Physics of Light. Metals. *Usp. Fiz. Met.* 2009. Vol. 10. No. 1. P. 103-130.

183. Smith E. Stress produced at a barrier by a pileup of dislocations. *J. Appl. Phys.* 1970. 41. No. 6. P. 2736-2737.

184. Rice J.R. Thomson R. Ductile versus brittle behsviour of crystals. *Phil. Mag.*1974. Vol. 29. No. 1. P. 73-97.

185. Tkachenko V.H., Kolesnik L.I., Maksimchuk I.N., Shklover V.V. Dislocation mechanism of embrittlement of metals and alloys with hcp and fcc crystal structure. *Int. J. Hydrogen Energy*. 1996. Vol. 21. No. 11/12. P. 12105-1113.

186. Lucke K., Schlipf J. *Proc. Conf. on the Interaction Between Dislocations and Point Defects.* Atomic Energy Research Establishment Report. 1968. AERE-R-5944. 1. 118 p.

187. Teutonico L.J., Granato A.V., Lücke K. Theory of the Thermal Breakaway of a Pinned Dislocation Line with Application to Damping Phenomena. *Journal of Applied Physics*. 1964. Vol. 35. P. 220 -233. https://doi.org/10.1063/1.1713074

188. Sargan G.F., Tkachenko V.H., Trefilov V.I., Firstov S.A. Dislocation substructure of foil made of chromium, *Izvest. Acad. Nauk USSR. Ser. Metals*. 1971. 2. P. 153-159.

189. Gleiter H. Nanocrystalline materials. *Progress in Materials Science.* 1989. Vol. 33. Iss. 4. P. 223-315.

190. Tyson W.R. Strengthening of hcp Zr, Ti and Hf by interstitial solutes – a review. *Can. Met. Quart*. 1967. Vol. 6. Iss. 4. P. 301-332.

191. Tkachenko V.H., Kolesnik L.I., Maksymchuk I.N., Shklover V.V. Dislocation mechanism of embrittlement of metals and alloys with HCP and FCC crystal structure. *Int. J. Hydrogen Energy*. 1996. 21. No. 11/12. P. 12105-1113.

192. Tkachenko V.H. Viscous grain boundary sliding and beryllium plasticity at low temperatures. *Fiz. Met. and Metalloved.*1981. Vol. 52. No. 3. P. 647-693.

193. Glazov A.P., Lashuk N.K., Kolesnik L.I., Tkachenko V.G. Structure and physical and mechanical properties of alloys of the Be-Co system. *Strength Problems*, 1983, № 5, 70-73.

194. James Li, Petch C.M. Relation and Grain Boundary Sources. *Trans. Metall. Soc. AIME*. 1963. Vol. 227. P. 239-247.

195. Gutmanas E.Y., Trusov L.I., Gotman I. Consolidation, microstructure and mechanical properties of nanocrystalline metal powder.s *Nanostr. Mater*. 1994. Vol. 4. Iss. 8. P. 893-901.

196. Kim D.K., Okazaki K. Nano-Crystalline Consolidation of MA Powders by EDC *Mat Sci Forum*. 1992. Vol. 88-90. P. 553-560.

197. Pande C.S., Masumura R.A., Armstrong R.W. Pile-up based hall-petch relation for nano-scale materials. *Nanostr. Mater*. 1993. 2. P. 323-331.

198. Chokshi A.H., Rosen A., Karch J., Gleiter. On the validity of the hall-petch relationship in nanocrystalline materials. *Scripta Met*. 1989. Vol. 23. Iss. 10. P. 1679-1683.

199. Liu X.D., Hu Z.Q., Ding B.Z. Hall-Petch relation in nanocrystalline Fe-Mo-Si-B alloys. *Nanostr. Mater.* 1993. 2. P. 545-552.

200. Coble R. L. A Model for Boundary Diffusion Controlled Creep in Polycrystalline Materials. *Journal of Applied Physics*. 1679. 34. 681; https://doi.org/10.1063/1.1702656.

201. Gleiter H. Nanocrystalline Materials Progress in Materials Science. 1989. Vol. 33. Iss. 4. P. 223-315.

202. Weller M., Diehl J., Schaefer H. E. Shear modulus and internal friction in nanometer-sized polycrystalline palladium. *Philosophical Magazine*. 1991. A Vol. 63. Iss. 3. P. 527-533.

203. Yamakov V., Wolf D., Salazar M., Phillpot S.R., Gleiter H. Length-scale effects in the nucleation of extended dislocations in nanocrystalline Al by molecular-dynamics simulation. *Acta Mater.* 2001.Vol. 49. Iss. 14. P. 2713-2722.

204. Terence G. L. Identifying creep mechanisms at low stresses. *Materials Science and Engineering*. 2000. Vol. 283. Iss. 1–2. P. 266-273.

205. Van Swygenhoven H., Derlet P. M., Hasnaoui A. Atomic mechanism for dislocation emission from nanosized grain boundaries. *Phys. Rev*. 2002. B 66. 024101024102.

206. Winterer M., Hahn H. Nanoceramics by chemical vapor synthesis. *Z. Metallk*. 2003. 94. No. 10. P. 1084-1090.

207. Stevens R.N. Grain Boundary Sliding in Metals. *Met. Rev*. 1966. 11. No. 108. P. 129-142.

208. StrochA.N.A Theory of the Fracture of Metals. *Adv. Phys*. 1957. 6. P. 418-465.

209. GriffithsA.A. The phenomena of rapture and flow in solids. *Trans. ASM*. 1968. Vol. 61. No. 4. P.871-906.

210. Petch N.J. The Ductile Fracture of Polycrystalline α-Iron. *Phil. Mag.* 1956. Vol. 1, No. 2. P. 186-190.

211. Armstrong R.W. Effects of microcracking and intrinsic obstacle strength on the Hall-Petch relation for ultrafine grain size polycrystals. Strength of Metals and Alloys. *Proc. 5th Int. Conf. Achen. Toronto e.a.* 1979. Vol. 2. P. 795-800.

212. Surgent G.A. Stress relaxation and thermal activation in niobium. *Acta Metall.* 1965.Vol. 13. P. 663-671.

213. Otsuka M., Horiuchi R. Ductility loss in Al—Mg alloys at high temperatures. *J. Jap. Inst. Metals*. 1984. Vol. 48. No7. P. 688-693.

214. Tkachenko V.G., Maksimchuk I.N., Trefilov V.I. Microkinetics and Stabilization of Dynamic Fracture of Semi-Brittle Crystals. *Doklady of USSR Academy of Sciences*. 1991. Vol. 320. No. 2. P. 330-333.

215. Tkachenko V.G., Maksimchuk I.N., Trefilov V.I. Physical Theory and New Scheme of Principle for Brittle Transition in Crystals. *Doklady of USSR Academy of Sciences*. 1991. Vol. 320, No. 3. P. 615-618

216. Tkachenko V.G., Maksimchuk I.N., Trefilov V.I. Dislocation Theory of the True Breaking Stress Formation in the Region of Brittle Transition in Crystals. *Doklady of USSR Academy of Sciences*. 1991. Vol. 320. No. 4. P. 873-876.

217. Fine M.E., Marcus H.L. Segregation to Interfaces and Brittle Fracture of Metals. *Metallurg. Trans*. 1971. Vol. 2. P. 1473-1474.

218. Jokl M.L., Kamed Jun, McMahon C.J., Vitek V. Solute segregation and intergranular brittle fracture in steels. *Metal Science*. 1980. Vol. 14. No. 8-9. P. 375-384.

219. Tkachenko V.G., Kim K.H., Moon B.G., Vovchok A.S. Design and microstructural analysis of magnesium alloys for dynamical applications. *J. Mater. Sci*. 2011.Vol. 46. Iss. 14. P. 4880-4895.

220. Roberts M.J., Owen W.S. Unstable Flow in Martensite and Ferrite.*Met. Trans*. 1970. No. 1. P. 320-323.

221. McMahon C.J. Intergranular brittleness. *Acta Metall.* 1966.Vol. 14. P. 839-845.

222. Wilcox B.A., Smith G.C. Intercrystalline fracture in hydrogen-charged nickel. *Acta Metall*. 1965. Vol. 13. P. 331-343.

223. Hayes R.W., Hayes W.C. On the mechanism of delayed discontinuous plastic flow in an age-hardened nickel alloy. *Acta Metall*. 1982. Vol. 30. No. 7. P. 1295-1310.

224. Amouzouvi K.F., Clegg L.J. Effect of Heat Treatment on Delayed Hydride Cracking in Zr—2,5Wt Pct Nb, *Metallurg. Trans. A*. 1987.Vol. 18. P. 1687-1694.

225. Schuh C.A., Argon A.S., Nieh T. G., Wadsworth J.The transition from localized to homogeneous plasticity during nanoindentation of an amorphous metal. *Phil. Mag*. 2003.Vol. 83. No. 22. P. 2585-2597.

226. Thomas G.,Westmacott K.H. Experiments in the High-Voltage Electron Microscope. *Phys. Stat. Sol. (a)*. 1979. Vol. 55. No. 2. P. 563-568.

227. Srivatsan T.S., Coyne Jr. E.J., Starke Jr. E.A. Microstructural characterization of two lithium-containing aluminium alloys. *J. Mater. Sci*. 1986. Vol. 2. P. 1553-1560.

228. Indenbom V.L., Orlov A.N. Problems of destruction in physics of strength. *Problemy prochnosti*. 1970. No. 12. P. 3-13 [in Russian].

229. Tetelman A.S. The effect of plastic strain and temperature on microcracks propagation in iron-3% silicon. *Acta Metall*. 1964. Vol. 12. No. 9. P. 993-1004.

230. Li J.C.M. Kinetics and dynamics in dislocation plasticity. *Dislocation dynamics*. Ed. A.R. Rosenfield et.al. N.Y.: McGraw-Hill Book Co., 1968. P. 87-116.

231. Thompson A.W. Substructure Strengthening Mechanisms. *Metallurg. Trans.* 1977. Vol. 8A. P. 833-842.

232. Li J.C.M. Generation of dislocations with grain boundary joins and Petch-Hall relation. *Trans. AIME,* 1961. Vol. 227. No 2. P. 239-247.

233. Sankaranarayanan, Jayalakshmi S., Gupta M. Effect of individual and combined addition of micro/nano-sized metallic elements on the microstructure and mechanical properties of pure Mg. *Materials and Design*. 2012. Vol. 37. P. 274-284.

234. Webster D., London G. Beryllium Science and Technology. N.Y.: L. Plenum Press, 1979. 14. 333 p.

235. Han X.L., Wang Q., Sun D.L., Zhang H.X. First-principles study of the effect of hydrogen on the Ti self-diffusion characteristics in the alpha Ti—H system. *Scripta Mater*. 2007. Vol. 56. P. 77-80.

236. Shin D., Wolverton C. First-principles study of solute-vacancy binding in magnesium. *Acta Materialia*. 2010. Vol. 58. P. 531-540.

237. Bilby B.A., Cottrell A.H., Swinden K.H. *Proc R. Soc. London Ser.* 1963. Vol. A 272. P. 304-316.

238. Tetelman A.S., Robertson W.D. The mechanism of Hydrogen Embrittlement Observed in Iron-Silicon Single Crystals.*Trans. Met. Soc. AIME*. 1962. Vol. 224. P. 775-783.

239. Chang S.J., Ohr S.M. Dislocation-free zone model of fracture.*J. Appl. Phys*.1981. 52. No. 12. P. 7174-7181.

240. Rice J.R., Thomson R. Ductile versus brittle behavior of crystals. *Phil. Mag*. 1974. 29.No. 1. P. 73-97.

241. Rice J.R.Effect of Hydrogen on Behavior of Materials. Eds. A.W. Thompson,I.M. Bernstein. New York: AIME, 1976. 155 p.

242. Argon A.S. Thermally activated crack growth in brittle solids. *Scripta Metall.* 1982. Vol. 16. P. 259-264.

243. ?Li, Wen and Vajo, John J. and Cimberland, Robert W. Liu, et al. Hydrogenation of Magnesium Nickel Boride for Reversable Hydrogen Storage. *J. Phys. Chem. Letters*. 2010. Vol. 1. No. 10. P. 69-72.

244. Roger Domenech-Ferrer, MadanaGurusamy Sridharan, Gemma Garcia, et al. Hydrogenation properties of pure magnesium and magnesium-aluminium thin films. *Journal of Power Sources*. 2007. Vol. 169. P. 117-122.

245. Peng Sgu-ke, Xiao Xue-Zhang, Xu Rui-Juan, et al. Hydrogen storage behaviors and microstucture of MF_3(M = Ti, Fe)-doped magnesium hydride. *Trans. Nonferrous Met. Soc. China*. 2010. Vol. 20. P. 1879-1884.

246. Inoue A., Masumoto T. Production and properties of light-metal-based amorphous alloys. *Mat. Sci. and Eng*. 1991. Vol. A 133. P. 6-9.

247. Abraschian R., Abraschian L., Reed-Hill R. Physical Metallurgy Principles. 4th ed. Stanford: Cengage Learning, 2009. 750.

248. Brown A.M., Ashby M.F. On the power-law creep equation. *Scripta Metal*. 1980. Vol. 14, Iss. 12. P. 1297-1302.

249. Kassner M.E. Fundamentals of Creep in Metals and Alloys. 3rd ed. Butterworth-Heinemann: Elsevier-Verlag, 2015. 338 p. DOI: 10.1016/C2012-0-0607-1.

250.Tkachenko V.H., Maksymchuk I.N., VolosevichP.Yu. Creep resistance and Long-Term Strength of Structural Magnesium Alloys. *High Temp. Mater. Processes*. 2006. 25. 97. DOI: 10.1007/s10853-011-5400-4.

251. Pekguleryuz M.O., Kaya A.A. Creep Resistant Magnesium Alloys for Powertrain Applications. *Adv. Eng. Mater*. 2003. 5. P. 74-93. DOI: 10.1002/adem.200300403.

252. Tkachenko V.G., Kim K.H., Moon B.G., Vovchok A.S. Design and Microstructural analysis of magnesium alloys for dynamical applications. *J. Mater. Sci.* 2011. Vol. 46. P. 4880-4895.DOI: 10.1007/s10853-011-5400-4.

253. Dinhut J.F., Bonou T., Moine P. PhenomenePortevin-Le Chatelier dans les alliages Fe—Co ordonnes et desordonnes. *Acta Metall.* 1976. Vol. 24. P. 445-451. DOI: 10.1016/0001-6160(76)90 065-1.

254. Van den Beukel A. Theory of the effect of dynamic strain aging on mechanical properties. *Phys. Stat. Sol*. 1975. Vol. A 30. P. 197-206. DOI: 10.1002/pssa.2210300120.

255. Mesarovich S.Dj. Dynamic strain aging and plastic instabilities. *J. Mechanics and Physics of Solids*. 1995. 43. P. 671-700. DOI: 10.1016/0022-5096(95)00010-G.

256.Fressengeas C., Beaudoin A.E., Lebyodkin. Dynamic strain ageing A. Coupled dislocation-solute dynamic model. *J. Mater. Sci. Eng.* 2005. Vol. A400-401. P. 226. DOI: 10.1016/j.msea.2005.02.073.

257. Cottrell A.H. Dislocations and Plastic Flow in Crystals, Univ Press, New-York, 1953, 551 p.

258. Yoshinaga H., MorozumiS. The Solute Atmosphere Round a Moving Dislocation and its Dragging Stress, *Phil. Mag.* 1971. A23. P. 1366-1385. DOI: 10.1080/14786437108217008.

259. Leyson G.P.M., Hector Jr.L.G., Curtin W.A Solute strengthening from first principles and application to aluminium alloy. *Acta Mater*. 2012. Vol. 60. P. 3873-3884. DOI: 10.1016/j.actamat.2012.03.037.

260. Sills R.B., Cai W. Solute drag on perfect and extended dislocation. *Phil. Mag.* 2016. Vol. 96. No. 1. P. 895-921. DOI: 10.1080/14786435.2016.1142677.

261. Mc Cormick P.G. Theory of flow localization due to dynamic strain aging.*Acta Metall*. 1988. Vol. 36. P.3061-3067. DOI: 10.1016/0001-6160(88)90043-0.

262. Hayes R.W., Hayes W.C. On the mechanism of delayed discontinuous plastic flow in an age-hardened nickel alloy. *Acta Metall*. 1982. Vol. 30. P. 1295-1301. DOI: 10.1016/0001-6160(82) 90148-1.

263. Sakamoto M. Diffusion equation and Cottrell Atmosphere Dragging of Edge Dislocation in High Concentration Solid Solution. *Mater. Trans*. 1989. Vol. 30. P. 337-344. DOI: 10.2320/matertrans 1989.30.337.

264. Sherby O.D., Klundt R.H., Miller A.K. Flow Stress and Subgrain Stability at Elevated Temperatures. *Metal. Trans.* 1977. Vol. 8. P. 843-852. DOI: 10.1007/BF02661565.

265. Mandal P.K. Study of hardening mechanisms in aluminum alloys.*Int. J. Engineering Research and Applications*. 2016. Vol. 6. P. 91-97. https://www.ijera.com/papers/Vol.6,issue1/Part%20-%206/M61069197 pdf.

266. Zhang F., Curtin W.A. Atomistically-informed solutes drag in Al—Mg. *Modelling Simul Sci in Mater. Eng.* 2008. No. 16. 1-22. DOI: 10.1088/0965-0393/16/5/055006.

267. Yoshinaga H., MorozumiS. A., Portevin-Le Chatelier. Effect Expected from Solute Atmosphere Dragging. *Phil. Mag.* 1971. Vol. A23. P. 1351-1366. DOI: 10.1080/14786437108217007.

268. Conrad H. Thermally activated deformation of α titanium below 0.4 T_m.*Canadian Journal of Physics*. 1967.Vol. 45(2). 581. DOI: 10.1139/p67-050.

269. Dorn J.E. Energetics in Metallurgical Phenomena. New York: Gordon and Breach, 1965. 241 p.

270. Nowick A.S., Berry B.S. Anelastic Relaxation in Crystalline Solids. N.Y.-London: Academic Press, 1972. 472 p.

271. Granato A.V., Lucke K. Temperature dependence of amplitude-dependent dislocation damping. *L. Appl. Phys*. 1981.Vol. 52. No. 10. P. 7136-7142.

272. Tkachenko V.G. Strength Physics of Less-Common Metals and Their Alloys. 2nd ed. London: Cambridge Int. Sci. Publish., 2002 (ISBN-1898326576). Kyiv: Nauk. Dumka, 1996. 359 p.

273. Yoshinaga H., Morozumi S. A., Portevin-Le Chatelier. Effect Expected from Solute Atmosphere Dragging. *Phil. Mag*. 1971. Vol. 23.No. 186. P. 1351-1366.

274. James C.M. Li. Dislocation Dynamics in Deformation and Recovery. *Canadian J. of Phys*. 1967. Vol. 45. P. 493-509.

275. Cottrell A.H. The ultimate mechanical properties of solids. *J. Birmingham Metallurg. Soc*. 1964. Vol. 44. P. 2-13.

276. Takeuchi S., Argon A.S. Glide and climb resistance to the motion of an edge dislocation due to dragging a Cottrell atoms sphere. *Phil. Mag*. 1979. Vol. 40. Iss. 1. P. 65-75.

277. Evans R.W., Wilshire B. Creep of Metals and Alloys. London: The Inst. of Metals. 1985. 14 p.

278. Gibbs G.B. Creep and stress relaxation studies with polycrystalline magnesium. *Phil. Mag.* 1966. 13. P. 317-329.

279. Heer J. The principle of Le ChatelierBraun. *J. Chem. Educ.* 1957. Vol. 34. No. 8. P. 375.

280. Conrad H. Thermally activated deformation of metals. 1964. 16. 7. 582. DOI: 10.1007. BF03378292.

281. Snoek J.L. Effects of small quantities of carbon and nitrogen on the elastic and plastic properties of iron. *Phys.* 1941.Vol. 8. P. 711-733. DOI: 10.1016/S0031-8914(41)90517-7.

282. Schoeck G. Moving dislocations and Solute Atoms. *Phys. Rev.* 1956. Vol. 102. P. 1458-1459. DOI: 10.1103/PhysRev.102.1458.

283. Fleisher R.L. High-Temperature, High-Strength Materials-An Overview. *J. Metals*. 1985. P. 37. P. 16-20. DOI: 10.1007/BF03259961.

284. Clapp P.C. A localized soft mode theory for martensite transformations. *Phys. Stat. Sol*. 1973. 57. P. 561-569. DOI: 10.1002/pssb.2220570213.

285. Arsenault R.J. An investigation of the mechanism of thermally activated deformation in Ta and Ta-base alloys. *Acta Metall.* 1966. Vol. 14. P. 831-838. DOI: 10.1016/0001-6160(66)90003-4.

286. Tkachenko V.G., Kim K.H., Moon B.G., Vovchok A.S. Design and microstructural analysis of magnesium alloys for dynamical applications. *J. Mater. Sci*. 2011.Vol. 46. Iss. 14. P. 4880-4895. DOI: 10.1007/s10853-011-5400-4.

287. Christian J.W. *Proceeding of the 2nd Int. Conf. on Strength of Metals and Alloys. ASM*. 1970. Vol. 1. 29. P. 117-125.

288. Christian J.W., Masters B.C. Low-Temperature Deformation of Body-Centred Cubic Metals. Pt. I. Yield and Flow Stress Measurements. *Proc. R. Soc. Lond*. 1964.Vol. A 281. No. 1385. P. 240-257.

289.Surgent G.A. Stress relaxation and thermal activation in niobium. *Acta Metall*. 1965.Vol. 13. P. 663-671. DOI: 10.1016/0001-6160(65)90129-X.

290. Gibbs G.B. Activation parameters for dislocation glide. *Phil. Mag*. 1967. Vol. 16. P. 97-107.

291. Nagarali S.S., Langdon T.G. Deformation mechanism in HCP metals at elevated temperatures. Pt. II. Creep behavior of a Mg—0.8%Al solid solution alloy. *Acta metal*. 1982. Vol. 30. P. 1157-1170.

292. Mordike B.L., Haasen P. The influence of Temperature and Strain Rate on the Flow Stress of α-iron Single Crystals. *Phil. Mag*. 1962. Vol. 7. No. 75. P. 459-474.

293. Hahn G.T., Rosenfield A.R. A modified double-pile-up treatment of the influence of grain size and dispersed particles on brittle fracture. *Acta Metall*. 1966. Vol. 14. P. 1815-1825.

294. Reed-Hill R.E. Physical Metallurgy Principles. New-York: D.V. Nostrand Company, 1973. 465 p.

295. Shukovsky H.B., Rose R.M., Wulff J.The low temperature electrical resistivity of lattice defects in deformed single crystals. *Acta Metall.* 1966. Vol. 14. P. 821-832.

296.Seeger A. The Temperature and Strain-Rate Dependence of the Flow Stress of Body-Centred Cubic Metals: A Theory Based on Kink-Kink Interactions. *Zeitschrift fur Metallkunde*. 1981. Vol. B72. No. 6. P. 369-380.

297. Gilman J.J. Micromechanics of Flow in Solids. New York: Mc Graw Hill, 1969. 249 p.

298. Tkachenko V.G. Physical Theory of Useful Strength of Metallic Crystals. *Strength of Materials*. 2013. Vol. 45. No. 5. P. 555-564. DOI: 10.1007/s11223-013-9493-7.

299. Jingyi Cheng, Sia Nemat-Nasser. A model for experimentally-observed high-strain-rate dynamic strain aging in titanium. *Acta Mater*. 2000. Vol. 48. P. 3131-3144.

300. Wilson D., Russel B. Stress induced ordering and strain-ageing in low carbon steels. *Acta Metall*. 1959.Vol. 7. P. 628-631.

301. Rose K.S.B., Glever S.G. A study of strain aging in austenite. *Acta Metall*. 1966. Vol. 14. P. 1505-1516. DOI: 10.1016/0001-6160(66)90172-6.

302. Rubiolo G.H., Bozzano P.B. Dynamic Interaction of Impurity Atmospheres with Moving Dislocations during Stress Relaxation. *Mater Trans*. 1995. Vol. 36. P. 1124-1133. DOI: 10.2320/matertrans 1989.36.1124.

303. Mukherjee K., May T., D'Antonio C., Maciag R.J. Serrated yielding in a 5005 aluminum alloy. *Met. Trans.* 1979. Vol. 1. P. 3233-3234. DOI: 10.1007/BF03038442.

304. Teutonico L.J., Granato A.V., Lucke K. Theory of the Thermal Break Way of a Pinned Dislocation Line with Application to Damping Phenomena. *J. Appl. Phys*. 1964. Vol. 35. No. 1. P. 220-234.

305. Saul R.H., Bauer C.L. Thermally Activated Dislocation Depinning in Dilute Copper Alloys. *J. Appl. Phys*. 1968. Vol. 39. Iss. 3. P. 1469-1477. DOI: 10.1063/1.1656382.

306. E. Aghion, B. Bronfin. Magnesium Alloys Development towards the 21st century. *Materials Science Forum*. 2000.Vol. 350-351. P. 19-28.

307. Bronfin B., Aghion E., BuchF., Schumann S., Friedrich H. Development of NewMagnesium Alloys for Advanced Applications. *Proc. of the 6th Int. Conf. Magnesium Alloys and Their Application.* Ed. K.U. Kainer. New-York: WILFY — VCH, 2003. P. 55-61.

308. Patent 5855697 US. Magnesium Alloy Having Superior Elevated-Temperature Properties and Die Castability, A. Luo, T. Shinoda. Impra America Inc. 1997.

309. Pekguleryuz M.O., Kaya A.A. Creep Resistant Magnesium Alloys for Powertrain Applications. *J. Advanced Mater.* 2003. Vol. 5. Iss. 12. P. 866-878.

310. Pekguleryuz M.O., Renaud J. Creep Resistance in Mg—Al—Ca casting alloys. *Magnesium Technology*. Eds. H. Kaplan, J. Hryn, B. Clow. NashvilleUSA: TN (TMS/AIME), Warrendale, 2000. P. 279-284.

311. Pekguleryuz M.O, Luo A.A. PCT WO 96/25529. Int. Cl. c22c 23/02. 22.08.96.

312. Patent 5, 855, 997 US. Magnesium Alloys Having Superior Elevated-Temperature Properties and Die Castability, A. Luo, T. Shinoda. 05.01.1999.

313.Pekguleryuz M.O., Baril E. Development of Creep Resistant Magnesium Diecasting Alloys. *Magnesium Alloys 2000, Materials Science Forum*. Eds. Y. Koyima., T. Aizawa, Kamado. Switzerland: Trans. Tech. Publication, 2000. P. 131-139.

314. King J.F. Development of Magnesium Diecasting Alloys. *Proc. of Intern. Conf. on Magnesium Alloys and their Applications*. Eds. B.L. Mordike, K.U. Kainer. Wolsburg, Germany: Werkstoff Information Gesellschaft, 1998. P. 37-47.

315. Nussbaum G., Gjestland H., Regazzoni G. Rapid solidification of magnesium alloys. *Light Metal Age*. 1986. August. P. 16-24.

316. Ryum N. The influence of a precipitate-free zone on the mechanical properties of an Al—Mg—Zn alloy. *Acta Metall.* 1968. Vol. 16. P. 327-332.

317. Wu R.Z., Deng Y.S., Zhang M.L. Microstructure and mechanical properties of Mg—5 Li—3Al—2Zn—*x*RE alloys. *J. Mater Sci*. 2009. Vol. 44. No. 15. P. 4132-4139.

318. Argo D., Pekguleryuz M.O., Labelle P. et al. Diecastability and Properties of Mg—Al—Sr Based Alloys. *Magnesium Technology*. Ed. J. Hryn. New Orleans: TMS, 2001. P. 131-145.

319. Tkachenko V.G., Khoruzhaya V.G., Meleshevich K.A., Karpets M.V. Phase equilibria in the Mg—Al—Ca system. *Power Metall. Met Ceram*. 2003. Vol. 42. No. 5-6. P. 268-275.

320. Tkachenko V.G., Kim K.H., Moon B.G., Vovchok S.A. Design and macroscopic analysis of magnesium alloys for dynamic applications. *J. Mater Sci*. 2011. Vol. 46. P. 4880-4895.

321. Liang G., Schultz R. Synthesis of Mg—Ti alloy by mechanical alloying. *J. Mater Sci*. 2003. 38. P.1179-1184.

322. Mott B.W. Immiscibility in liquid metal systems. *J. Mater. Sci*. 1968. Vol. 3. P. 423-435.

323. Kheilova M., Strunc M. Is the Le Chatelier-Braun Principle Valid in General in Linear Nonequilibrium Thermodynamics. *J. Non-Equilib.Thermodyn*. 1995. Vol. 20. P. 19-38.

324. Breinan E.M., Thompson E.R., Tice W.K. Creep behavior of Al—Al_3Ni eutectic composites. *Metallurgical and Materials Transactions.* 1972. Vol. B3. P. 211–219.

325. Hirsch P.B., Howie A., et al. Electron microscopy of thin crystals. London: Butterworth's, 1965. 549 p.

326. Keijser Th.H. De, Landford J.I., Mittemeijer E.J., Vogels A.B.P. Use of the Voigt function in a single-line method for the analysis of X-ray diffraction line broadening. *J. Appl Cryst*. 1982. Vol. 15. P. 308-314. DOI: 10.1107/S0021889882012035.

327. Taylor A. X-ray metallography. New York: John Wiley and Sons Inc., 1961. 587 p.

328. Krivoglaz M.A. X-ray and neutron diffraction in nonideal crystals. Berlin: Springer Verlag, 1996. 312 p.

329. Rossouw C.J., Bettles T.J., Davis C.T., Forwood P.R., Miller K. Venkatesan. Location of Zn within the $Mg_{12}(La_xCe_{1-x})$ lattice by X-ray incoherent channelling patterns. *Acta Crystallogr*. 2001.Vol. A57. Pt. 3. P. 321-32.

330. Su C.M., Ke T.S. Further Experiments on the High-Temperature Internal Friction Peak in High Purity Single Crystal Aluminum. *Phys Stat Sol*. 1986. Vol. A94. P. 191-202.

331. Read T.A. The Internal Friction of Single Metal Crystals. *Phys Rev*. 1940.Vol. 58. P. 371-380.

332. Lund R.W., Nix W.D. High temperature creep of Ni—20Cr—2ThO_2 single crystals. *Acta Metall*. 1976. Vol. 24. No. P. 469-481.

333.Tkachenko V.G. Strength physics of less-common metals and their alloys. 2nd ed. Cambridge-London: Metall. Mater. Trans, 2002. Kyiv: Naukova Dumka, 1996. 354 p.

334. Murty K., Mohamed F.A., Dorn I.E. Effect of vacancy sinks and sources on serrated yielding due to solute locking. *Scr. Metall*. 1971. Vol. 5. P. 1087-1091.

335. Patent 79413 Ukraine. Tkachenko V.G., Malka A.N., Maksimchuk I.N., et al. 2007.

336. Wilson D.V., Russel W. The contribution of atmosphere locking to the strainageing of low carbon steels. *Acta Met.* 1960. Vol. 8. No. 1. P. 36-45.

337. Murray J.L. Bull Alloy Phase Diagrams. 1982. 3. P. 335.

338. Massalski T.B. Physical Metallurgy. Ed. R.W. Cahn. Pt. III. Amsterdam, North-Holland. 1996. 2740 p.

339. Delaplace J., Nicoud J.C., Trabut L. Etude du frottement interieur dû aux joints de grains dans le magnesium. *J. Nuclear Mater*. 1970.Vol. 35. No. 2. P. 167-176.

340. Buzzichelli G. Activation energy-peak temperature relationship for the grain boundary relaxation in polycrystalline metals. *Solid State Commun*. 1969. Vol. 7. P. 1347-1349.

341. Tkachenko V.G., Tatarenko V.A., Schulyak I.I., et al. Structural Clustering and Relaxation Effects in Solid Solutions of Hydride-Forming Systems. *Metallofiz. Noveishie Teknol*. 2001.Vol. 23. No. 3. P. 367-386 [in Russian].

342. Pekguleryuz M.O., Kaya A.A. Creep Resistant Magnesium Alloys for Powertrain Applications, Magnesium Alloys and their Applications, *Deutche Gessschft fur Materialkunde*, Gamish (DGM) Germany, 2003, 74-93.

343. Uchida H., Shinya T. Estimation of creep deformation behavior in Mg—Al alloys by using θ projection method. *J. Jpn Inst Light Metals*. 1995. Vol. 45. P. 572-577.

344. Diqing Wan, Yajuan Liu. Low Frequency Mechanical Spectroscopy of High Damping Mg-3wt. % Ni Alloy. *Advanced Mater. Res*. 2011. Vols. 146–147. P. 1761-1764.

345. Woirgard J., Fouquet J. Mecanisme de relaxation du aux dislocations de joints de grains dans les metaux, *Scripta Met.* 1974. Vol. 8. P. 253-262.

346.Woirgard J. Modèle pour les pics de frottement interne observés a haute température sur les monocristaux. *Phil Mag*. 1976. Vol. 33. P. 623-637.

347. Hanaoui A., SuygenhovenH., Derlet P.M. On non-equilibrium grain boundaries and their effect on thermal and mechanical behaviour: a molecular dynamics computer simulation. *Acta Mater.* 2002. Vol. 50. P. 3927-3939.

348. Yoshinaga H., Morozumi S.A., Portevin Ch. Le effect expected from solute atmosphere dragging. *Phil Mag.* 1971. Vol. 23. P. 1351-1366.

349. Inoue A., Takeuchi A., Zhang T. Ferromagnetic bulk amorphous alloys. *Metallurgical and Materials Transactions.* 1998. Vol. A 29. P. 1779–1793.

350. Nabarro F.R.N., Devilliers H.L. The physics of creep. London: Taylor and Francis, 1995. 425 p.

351. Evans R.W., Wilshire B. Creep of metals and alloys. London:Institute of Metals, 1985.

352. Poirier J.P. Creep of crystals. High-temperature deformation processes in metals, ceramics and minerals. Cambridge — London — NewYork — New Rochelle — Melbourne — Sydney: Cambridge University Press, 1985. 145 figs. XII. 260 p.

353. He Lijia, Wang Jianzhong, Qi Jingang, et al. Influence of Electric Pulse on Solidification Structure of I. M. — 29Al—Si Alloy. *Research and Development*. 2010. Vol. 7. No. 2. P. 153-156.

354. Shukla A., Pelton A.D.Thermodynamic Assessment of the Al—Mn and Mg—Al—Mn Systems. *Journal of Phase Equilibria and Diffusion.* 2009. Vol. 30. P. 28-39.

355. Trojanova Z., Lukac P. Deformation behavior of ZC63 magnesium matrix composite. *Archives of Materials Science and Engineering.* 2007. Vol. 28. No. 6. P. 361-364.

356. Kassner M.E. Fundamentals of Creep in Metals and Alloys. 3rd ed. Butterworth-Heinemann: Elsevier—Verlag, 2015. 338 p.

357. Abraschian R., Abraschian L., Reed-Hill R. Physical Metallurgy Principles. 4th ed. Stamford: Cengage Learning, 2009.750 p. ISBN: 9780495438519.

358. Pekguleryuz M.O., Kaya A.A. Creep-Resistant Magnesium Alloys for Powertrain Applications. *Proc. 6th Int Conf*. Ed. K.U. Kainer. Wolfsburg, Germany: Wiley-VCA, 2003. P. 74-93.

359. Fleisher R.L. High-Temperature, High-Strength Materials-An overview. *J. Metals.* 1985. Vol. 37. P.16-20.

360. Mandal P.K. Study of hardening mechanisms in aluminium alloys. *Int. Journal of Engineering Research and Applications.* 2016. Vol. 6. Iss. 1. P. 91.

361. Tkachenko V.G.Contemporary Trends of the Development of Physics of Light Metals. *Uspekhi Fiz. Met.* 2009.Vol. 10. Iss. 1. P. 103-130 [in Russian].

362. Zeizinger H., Arzt E. The Role of Grain Boundaries in High Temperature Creep Fracture of an Oxide Dispersion Strength Superalloy. *Z. Metallkunde*. 1988. Vol. 79. P. 775–781.

363. Jayaram Jayakumar, Kaghunath B. K., Rao T.H. Recent Development and Challenges in Synthesis of Magnesium Matrix Nano Composites — A Review.*Int. J. of Latest Research in Science and Technology.* 2012. Vol. 1. Iss. 2. P. 164-171. ISSN (Online): 2278-5299.

364. Honeycomb R.W.K. The plastic deformation of metals. 2nd ed. Edward Arnold Publ. Itd., 1984. 483 p. ISBN 0713134682.

365. Swygenhoven H., Caro A.Plastic behavior of nanophase metals studied by molecular dynamics. *Phys. Rev. B*. 1998.Vol. 58. No. 17. P. 11246-11251.

366. Motta A.T., Couet A., Comstock R.J. Corrosion of Zirconium Alloys Used for Nuclear Fuel Cladding. *Annual Review of Materials Research*. 2015. Vol. 45. P. 311-343.

367. Hadjipanayis G.C., Siegel R.W.V. Nanophase Materials: Synthesis — Properties — Application. Dordrecht: KlumerNATO — AST, 1994. Ser. E. 260 p.

368. Gilman P.S. The physical metallurgy of mechanically-alloyed dispersion-strengthened Al—Li—Mg and Al—Li—Cu alloys. *Int. Conf. Aluminum Lithium Alloys*. Eds. T.H. Sanders, A.E. Starke. Monterey CA, 1983.

369. Luzzi D.E., Meshii M. Chemical disordering in amorphization. *J. Less-Common Metals*. 1988. Vol. 140. P. 193-210.

370. Sakata M., Cowlam N., Davies H.A. Chemical short-range order in liquid and amorphous $Cu_{66}Ti_{34}$ alloys. *J. Phys. F: Metal Phys*. 1981. Vol. 11. P. L157-162.

371. Schmid G. (Ed) Nanoparticles: From Theory to Applications. Wiley, 2004, Catalog #Z551376.

372. Clark J.B. Age hardening in a Mg-9 wt. % Al alloy. *Acta Metall.* 1968.Vol. 16. Iss. 2. P. 141-152.

373. Ryum N. The influence of a precipitate-free zone on the mechanical properties of an Al—Mg—Zn alloy. *Acta Metall.* 1968. 16. P. 327-332.

374. Gjesland H., Nussbaum G., Regazzoni G., Lohne O., Baugner O. Stress-relaxation and creep behavior of some rapidly solidified magnesium alloys.*Mater. Sci. Eng*. 1991. Vol. A134. P. 1197-1200.

375.Arzt E., Rösler J. The kinetics of dislocation climb over hard particles. II. Effects of an attractive particle-dislocation interaction. *Acta Metall.* 1988. Vol. 36. Iss. 4. P. 1053-1060.

376. Arzt E., Wilkinson D.S. Threshold stresses for dislocation climb over hard particles: the effect of an attractive interaction. *Acta Metall.* 1986. Vol. 34. No. 10. P. 1893-1898.

377. Rosler J., Arzt E. A new model-based creep equation for dispersion strengthened materials. *Acta Metal. Mater*. 1990. Vol. 38. No. 4. P. 671-683.

378. Tkachenko V.G., Kondrashev A.I., Malka A.N., Romanko P.M., Bondarchuk V.I. Resistance to microcreep and long-term strength of nanophase-strengthened Zr—based alloys. *Metallofizika I noveishietekhnologii*. 2017. No. 10. P. 1321-1334 [in Russian].

379.Granato A., Lücke K. Theory of Mechanical Damping Due to Dislocations. *Journal of Applied Physics*. 1956.Vol. 27. P. 583–593.

380.Vasudévan A.K., Ludwiczak E.A., Baumann S.F., Howell P.R., Doherty R.D., Kersker M.M. Grain boundary fracture in Al—Li alloys.*Mat. Sci. Techn*. 1986.Vol. 2.Iss. 12.P. 1205-1209.

381. Tkachenko V.G. Physical Theory of Long-Term Strength of Metallic Crystals. *Strength of Materials*. 2013. Vol. 45. No. 5. P. 555-564.

382. Cormick P.G.Theory of flow localization due to dynamic strain aging.*Acta Metall*. 1988. 36. Iss. 12. P. 3061-3067.

383. Schoeck G. Moving dislocations and Solute Atoms. *Phys. Rev*. 1956.Vol. 102. No. 6. P. 1458-1459.

384. Tkachenko V.G., Kim K.H., Moon B.G., VovchokA.S. Design and microstructural analysis of magnesium alloys for dynamical applications. *J. Mater. Sci.* 2011. Vol. 46. Iss. 14. P. 4880-4895.

385. Valiev R.Z., Alexandrov I.V., Zhu Y.T., Lowe T.C. Paradox of Strength and Ductility in Metals Processed by Severe Plastic Deformation. Cambridge: Cambridge University Press. 2011. P. 5-8.

386. Conrad H. Thermally activated deformation of metals. 1964. Vol. 6. No. 7.P. 582-588.

387. Ritchil I.G., Atrens A., So C.B.,Sprungmann K.W. Dislocation relaxation in a random array of solutes.*JournalPhysique*. 1981. Vol. 42. No. 10. P. 319-322.

388. Caillard D. DSA in iron alloys: the shielding effect of carbon. *Acta Mater*. 2016. Vol. 112. P. 273-284.

389. Srolovitz D.J., Lutton M.J., Petkovic-Luton R., et al. Diffusionally modified dislocation-particle elastic interactions.*Acta Metal.* 1984. Vol. 32. No.7. P. 1079-1088.

390. Kioussis N.G., Ghoniem N.M. Modelling of Dislocation Interfaces: A Multiscale Challenge. *J. Computational and Theoretical Nanoscience*. 2010. Vol. 7. P. 1-30.

391. Schroder J. H., Arzt E.Weak beam studies of dislocation/dispersoid interaction in a superalloy. *Scripta Metall.* 1985. Vol. 19. Iss. 9. P. 1129-1143.

392. Tkachenko V.G. Cluster compound formation in metal alloys crystals. *Materials Today Communication*. 2019. 21: 100662.

393. Zhu X., Birringer R., Herr U., Gleiter H. X-ray diffraction studies of the structure of nanometer-sized crystalline materials. *Phys. Rev*.1987. Vol. B35. P. 9085-9090.

394. Ti H., Keiser J.I., Landford E.J., Mittermeijer E.J., Vogels A.B.P. Use of the Voigt function in a single-line method for the analysis of X-ray diffraction line broadening. *J. Appl Cryst*. 1982. 15. No. 3. P. 308-314.

395. Matteazzi P., Basset D., Miani F., Le G. Caer. Mechanosynthesis of nanophase materials. *Nanostructured materials*. 1993. Vol. 2. P. 217-229.

396. Tkachenko V.G. Nanophase Strengthening of Hexagonal Metal Alloy Crystals. *Res Dev Material Sci*. 2020. Vol. 12. No. 5. P. 1344-1356.

397. Mott N. F.A Theory of Fracture and Fatigue. *J. Phys. Soc. Japan*. 1955.Vol. 10. No. 8. P. 650-655.

398. Nabarro F.R.N.Theory of Crystal Dislocation.London: Oxford Press, 1967. 535 p.

399. Kelly A., Fine M.E.The strength of alloy containing zones.*Acta Metall*. 1957. Vol. 5. P. 365-367.

400. Goodrum John W., Bruce G. Lefevre. Strengthening by ordered precipitates in a Ni—Ni_4Mo system. *Metallurg. Trans*. 1977. Vol. A8. P. 939–943.

401. Fischmeister H.F., Navara E., Easterling K.E. Effects of Alloying on Structural Stability and Cohesion between Phases in Oxide/Metalcomposites. *Metal Science Journal*. 1972. Vol. 6. Iss. 1. P. 211-215.

402. Nardone V.C., Tien J.K. Pinning of dislocations on the departure side of strengthening dispersoids. *Scripta Metallurgica*. 1983. Vol. 17. Iss. 4. P. 467-470.

403. Matteazzi P., Basset D., Miani F., Caer G. Mechanosynthesis of nanophase materials. *Nanostructured materials*. 1993. Vol. 2. P. 217-229.

404. Starke A.E. The Application of the Fundamentals of Strengthening to the Design of NewAluminum Alloy. *J. of Metals.* 1981. Vol. 33. No. 8. P. 24-31.

405. Sickafus K.E., Sass S. L. Grain boundary structural transformations induced by solute segregations. *Acta Metall.* 1987. Vol. 35, No. 1. P. 69-87.

406. Srivatsan T.S., Coyne E.J. Jr., Starke A.E. Jr. Microstructural characterization of two lithium-containing aluminum alloys. *J. Mater. Sci.* 1986. Vol. 21. P. 1553-1560.

407. Martin J.W., Doherty R.D. Stability of microstructure in metallic systems. 2nd ed. London — New York — Melbourn: Cambridge Univ. Press, 1997.

408. Zaimovski A.S., Nikitina A.V., Reshetnikov N.I. Tsirkonievyesplavy v yadernoyenergetike. Zirconium alloys in nuclear energetics. Moscow: Energoizdat, 1994. 564 p. [in Russian].

409. PortnoiK.I., Babich B.N. Dispersionstrengthenedmaterials. Ser.Uspekhisovremennogometallovedeniya. Moscow: Metallurgiya, 1974. 200 p. [in Russian].

410. Ko S., Lee J.M., Hong S.I. Out-of-pile mechanical performance and microstructure of recrystallized Zr—1.5Nb—O—S alloys. *Nuclear Engineering and technology*. 2011. Vol. 43. No. 5. P. 421-428.

411. Rezek J.,Childs R.G. Structure and properties of yttria-zirconium dispersions. *J. Nucl. Mater.* 1968. Vol. 26. Iss. 3. P. 285-299.

412. Berezina A.A., Segida E.A., Nosenko V.K., Kotko A.V. Elektronnayamikroskopiyaiprochnostmaterialov. Electron microscopy and strength of materials. 2007. Vol. 14. No. 57 [in Russian].

413. Kolobov Yu., Grabovetskaya R., Dudarev E.F., Ivanov V.T. *Voprosy materialovedeniya*. 2004. 1 (37). P. 56 [in Russian].

414. Sastry D.H., Prasad Y.V.K., Vasu K.I. An Evaluation of Rate-Controlling Obstacles for Low-Temperature Deformation of Zirconium. *J. Mater. Sci*. 1971. Vol. 6. P. 332-341.

415. Hadjipanayis G.C., Siegel R.W.V. (Eds) Nanophase Materials: Synthesis — Properties — Application. NATO — AST. Dordrecht: Klumer, 1994. Ser. E. 260 p.

416. Nam C., Kim K.H., Lee M.H., Jeong Y.H. Effect of Alloying Elements on the Thermal Creep of Zirconium Alloys.*Journal of the Korean Nuclear Society*. 2000.Vol. 32. No. 4. P. 372-378.

417. Tkachenko V.G., Nanophase Strengthening of Hexagonal Metal Alloy Crystals. *Res Dev Material Sci.* 2020. Vol. 12. No. 5. P. 1344-1356.

418. Kassner M.E. Fundamentals of Creep in Metals and Alloys. 3rd ed. Butterworth-Heinemann: Elsevier — Verlag, 2015. 338 p.

419. Novoselova A.V. Methody issledovaniya geterogennykh ravnovesii. Methods of investigation of geterogenous equilibria. Moscow: Vysshaya shkola, 1980. 387 p. [in Russian].

420. NovoselovaA.V. Geterophaseproblem of chemistry of semiconductors. *Vestnik AS USSR*. 1983. No. 3. P. 9-16. [in Russian].

421. ZubkovA.I., Ilinsky A.I., Podgornaya O.A., Sevruk V.I., Sokol-Prusskiy Ya.G. On possibility of a gingquick-hardened Cu—Mo alloys. *Fizika metallov I metallovedenie*. 1990. No. 10. P. 197-199 [in Russian].

422. Kane R.D., Ebert L.G. Creep deformation of TD-nickel chromium. *Metallurg. Trans. A*. 1976. Vol. 7. P. 133-137.

423. Sastry D.H., Prasad Y.V.K., Vasu K.I. An Evaluation of Rate-Controlling Obstacles for Low-Temperature Deformation of Zirconium. *J. Mater. Sci.* 1971. Vol. 6. P. 332-341.

424. Tkachenko V.G. Cluster compound formation in metal alloys crystals. *Materials Today Communication*. 2019. Vol. 21. 1000662. 1-8.

425. Antilla A., Raisanen J., Keinonen J. Diffusion of nitrogen in α-Ti. *J. Appl. Phys. Letters*. 1983. Vol. 42. No. 6. P. 498-500.

426. Charit I., Murty K.L. Creep behavior of niobium-modified zirconium alloys. *Journal of Nuclear Materials*. 2008. Vol. 374. Iss. 3. P. 354-363.

427. Ritchie I.C.Core diffusion, unpinning, and the Snoek-Koster relaxation. *Scripta Metall.* 1982. Vol. 16.P. 249-253.

428. Sleeswyk A.W., Verel D.J. The P-L effect and the density and activation entropy of moving dislocations. *Scripta Met*. 1972. Vol. 6. No. 9. P. 821-826.

429. Zaimovski A.S., Nikulina A.V., Reshetnikov N.I. Tsirkonievye splavy v energetike. Zirconium alloys in energetics. Moscow: Energoizdat, 1994. 256 p. [in Russian].

430. Patent 914, 829 US, Heat-treated zirconium alloy product. M. Erland, E. Schulson, J. Donald. Cameron. 1978.

431. Schulson E.M. Plastic flow of ordered Zr_3Al. *J. Nuclear Materials*. 1975.Vol. 57. No. 1. P. 98-102.

432. Grinberg B.A., Ivanov M.A. Intermetallidy $Ni_3AliTiAl$: mikrostruktura, deformatsionnoe povedenie. Intermetallics Ni_3Al and TiAl: microstructure, deformation behavior. Ekaterinburg: URO RAN, 2002. 311 p.[in Russian].

433. Tewari R., Tewari R., Dey G.K., Banerjee S., Prabhu N. Microstructural Evolution in Zr_3Al-based Alloys During Various Long-Terms. *Metallurgical and Materials Transactions A*. 2006. Vol. 37. P.49-58.

434. Tewari R., Day G.K., Banerjee S., Kutty T.R.G. A study on microstructural evolution, phase transformation, and high temperature properties of Zr_3Al and its ternary derivatives: Fu-

ture applications in Indian Pressurized Heavy Water reactors. *BARC newsletter*. 2009. No. 309. P. 90-100.

435. Li J.H., Gao Y., Li S., Mao L., Lhang F.S., Li Q.The effects of alloy composition and annealing time on microstructure and mechanical properties of Zr_3Al-based alloys. *Materials Research Innovations*. 2015. Vol. 19. No. 9. P. 55-57.

436. Tewari R., Dey G.K., Kutty T.R.G., Sengupta A.K., Prabhu N., Banerjee S. Deformation Behavior of Zr_3Al—Nb Alloys. Pt. II. Indentation Creep Studies. *Metallurgical and Materials Transactions A*. 2004. Vol. 35. No. 1. P. 205-216.

437. Takeuchi S., Kuramoto E. Temperature and orientation in Ni_3 Gasinglecrystals. *Acta Met.* 1973. Vol. 21. No. 4. P. 415-425.

438. Grinberg B.A., Ivanov M.A., Antonova O.V., et al. Blocking of dislocations without external stress: experiment and theory. *Uspekhi fiziki metallov*. 2013. 14. P. 107-227 [in Russian].

439. Kear B.H., Wilsdorf H.G.F. Dislocation configurations in plastically deformed polycrystalline Cu_3Au alloys. *Trans. Metall. Soc. AIME.* 1962. Vol. 224. No. 2. P. 382-386.

440. Grinberg B.A, Syutkina V.I. New methods for strengthening ordered alloys. Moscow: Metallurgia, 1985.175 p. [in Russian].

441. Chang K.I., Hong S.I. Effect of sulphur on the strengthening of a Zr—Nb alloy. *J. Nucl. Mater*. 2008.Vol. 373. P.16-21.

442. Jeng S.M., Yang J.M., Rosenthal D.G., Aksoy S. Mechanical behavior of SiCfibre-reinforced titanium/titanium aluminide hybrid composites. *J. Mater. Sci.* 1992. Vol. 27. P. 5113-5140.

443. Jayakumar Jayaram, Kaghunath B. K., Rao T.H. Recent Development and Challenges in Synthesis of Magnesium Matrix Nano Composites — a Review, *Int. J. of Latest Research in Science and Technology*. 2012. Vol. 1. Iss. 2. P. 164-171, ISSN online: 2278-5299.

444. Kassner M.E. Fundamentals of Creep in Metals and Alloys. 3rd ed. Butterworth—Heinemann: Elsevier-Verlag, 2015. 338 p.

445. Tkachenko V.G. Nanophase Strengthening of Hexagonal Metal Alloy Crystals. *Res Dev Material Sci.*, 2020. Vol. 12. No. 5. P. 1344-1356.

446. Hai Zhi Ye, Xing Yang Liu. Review of recent studies in magnesium matrix composites. *J. Mater. Sci*. 2004. Vol. 39. P. 6153-6171.

447. Tkachenko V.G., Kolesnik L.I., Maksimchuk I.N., Shklover V.V. Dislocation mechanism of hydrogen embrittlement of metals and alloys with HCP and FCC crystal structure. *Int. J. Hydrogen Energy*. 1996. Vol. 21. No. 11/12. P. 1105-1113.

448. Magnesium. *Proc. of the 6th Int. Conf. Magnesium Alloys and Their Applications*. Ed. K.U. Kainer, Weinheim: WILEY-VCH Verlag CmbH & Co. KGaA, 2004. 1064 p.

449. Albright D. L. *Proc. the 46th World Magnesium Conference (IMA),* Dearborn: MI, May 1989. 33 p.

450. Pekguleryuz M.O., Kaya A.A. Creep Resistant Magnesium Alloys for Powertrain Applications. *Proc. the 6th Int Conf.* Ed. K.U. Kainer. Wolfsburg, Germany: Wiley-VCA, 2003. P. 74-93.

451. Tkachenko V.G. Physical Theory of Useful Strength of Metallic Crystals. *Strength of Materials*. Vol. 45. No. 5. P. 555-564.

452. Lenel V.F. Ultrafine grain in metals. Moscow: Metallurgia, 1973. P. 11-40 [in Russian].

453. Fridlyander I.N., Yatsenko K.P. Metallovedeniei termicheskaya obrabotka metallov. 1970. No. 7. P. 50-55 [in Russian].

454. Nalimov V.V., Chernova N.A. Statistic methods for planning experiments. Moscow: Nauka, 1965. 325 p. [in Russian].

455. Isserow S., Rizzitano F.J. Titanium-Beryllium Microcomposites. A State of the Art. Review. *Composites.* 1974. Vol. 5. No. 4. P.141-150.

456. Kaya A.A., Yucel O., Eliezer D., Aghion E. An Electron Microscopy Investigation on As-cast AZ91D Alloy Modified with Nitrogen. *Proc. The 6th Int. Conf. Magnesium Alloys and Their Applications* Weinheim: WILEY-VCH Verlag GmbH & Co. KGaA, 2004. P. 151-157.

457. Troyanova Z., Lukac P. Deformation behaviour of ZC63 magnesium matrix composites. *Archives of Materials Science and Engineering*. 2007. Vol. 28. Iss. 6. P. 361-364.

458. Breinan E.M., Thompson E.R.,Tice W.K. Creep Behavior of Al—Al_3Ni Eutectic Composites. *Metallurg. Trans.* 1972.Vol. 3. P. 211-219.

459. Kumar. K.S., Swygenhoven H., Suresh S. Mechanical behavior of nanocrystalline metals and alloys. *Acta Mater.* 2003. Vol. 51. P. 5743-5774.

460. Meyers M.A., Misha A., Benson D. J. Mechanical properties of nanocrystalline materials. *Progress in Materials Science*. 2006. Vol. 51.No. 4. P. 427-556.

461.Gutmanas E.Y., Trusov L.I., Gotman I. Conclusion, microstructure and mechanical properties of nanocrystalline metal powders. *Nanostructured Materials*. 1994. Vol. 4. Iss. 8. P. 893-901.

462. Swygenhoven H., Grimmer H., Paschoud F., Victoria M., Hauert R. Nanostructured Ni_3Al layers and Ni_3Al/Ni multilayers obtained by magnetron sputtering. *Nanostruct. Mater*. 1994, Vol. 4. Iss. 4. P. 409-415.

463. Haasen P. Physical Metallurgy. Part ll. Eds. R. W. Cahn, P. Haasen. Amsterdam: Elsevier,1983. 1341 p.

464. Hahn H. Microstructure and properties of nanostructured oxides. *Nanostructured Materials.* 1993. Vol. 2. Iss. 3. P. 251-265.

465. Bohn R., Haubold T., Birringer R., Gleiter H. Nanocrystalline Materials. *Scripta Metall. Mater.* 1991. Vol. 25. P. 811-826.

466. Gleiter H. Nanocrystal line materials. *Progr. Mater. Sci.* 1989. Vol. 33. P. 223-247.

467. Siegel R.W. Cluster-Assembled Nanophase Materials. *Nanostruct. Mater*. 1994.Vol. 4. P. 121-134.

468. Peng B., Cai M., Li G., Wu X.J., Zhou F. Molecular dynamics study of the microstructure and properties of nanocrystalline copper. *Nanostruct. Mater.* 1994. Vol. 4. Iss. 4. P. 475-484.

469. Ke M., Hackney S.A., Milligan W.W., Aifantis E.C. Observation and measurement of grain rotation and plastic strain in nanostructured metal thin films. *Nanostruct. Mater.* 1995. Vol. 5. Iss. 6. P. 689-697.

470. Jayakumar J., Raghunath B.K., Rao T.H. Recent Development and Challenges in Synthesis of Magnesium Matrix Nanocomposites — A Review, *Int. J. Latest Research in Science and Technology*. 2012. Vol. 1. Iss. 2. P. 164-171.

471. Nussbaum G., Gjestland H., Regazzoni G. Rapid solidification of magnesium alloys. *Light Metal. Age.* 1986. P. 16-32.

472. Jayara J., Mendes C.L., Ohkubo T., Ohishi K., Hono K. Enhanced precipitation hardening of Mg—Ca alloy by Al addition. *Acta Mater*. 2010. Vol. 63, Iss. 8. P. 831-834.

473. Maringer R.E. Effects of processing on the dimensional stability of beryllium mirrors. US report DMIC Memo. 1970. No. 248, p. 6. Columbus, Ohio: Battelle Memorial Inst., *Nucl. Sci. Abstrs*. 1971. Vol. 25. No. 11. P. 2441-2446.

474. Beryllium Science and Technology. Ed. D. Webster. Vols. 1, 2. N.-Y.: Plenum Press, 1980. 333 p.

475. AzhazhaV.M., Babun A.V., Kovtun K.V., Sanin A.F. et al. Berillium — construction material of space engineering. Dnipro: ART-PRESb, 2005. 263 p.[in Russian].

476. Tkachenko V.G. Designing for Improved Creep Resistance in the RE-Free Magnesium Alloys. *Proc. the 6th Int. Conf. Magnesium Alloys and Their Applications.* Ed. K.U. Kainer. KGaA, Weiheim: WILEY-VCH Verlag GmbH & Co., 2004. P. 110-115.

477. Kaese V., Greve L., Jiittner S.,et al. Approaches to Use of Magnesium as Structural Material in Car Body. *Proc. the 6th Int. Conf. Magnesium Alloys and Their Applications*. Ed. K.U. Kainer. KGaA, Weiheim: WILEY-VCH Verlag GmbH & Co., 2004. P. 949-954.

Проаналізовано та узагальнено світові досягнення у галузі фізики міцності, фізичної металургії та матеріалознавства з основною метою вивчення потенціалу різних механізмів дислокаційного зміцнення рідкісних, кольорових, реактивних і надлегких металів (Be, Mg, Zr, Ti, Al, Mo, Cr), їх упорядкованих сплавів, нанофазних матеріалів з вмістом самозібраних кластерів та особливо важливих нанокомпозиційних матеріалів на основі металевих матриць. Книга охоплює всю тему — від тривимірних кристалів до напівфабрикатів, від наукових явищ до інженерних програм і від теоретичних міркувань до їх використання на практиці. Крім того, монографія має на меті забезпечити обмін та поширення основних ідей у цій галузі. Увагу акцентовано на оригінальних аналітичних і експериментальних дослідженнях, які постійно цікавлять науковців і інженерів-дослідників для активної роботи у відповідних галузях знань.

Книга призначена для вчених, інженерно-технічних працівників, що спеціалізуються у галузі фізики твердого тіла, фізичної металургії та обробки матеріалів, а також для навчання студентів і аспірантів відповідних спеціальностей.

Наукове видання

НАЦІОНАЛЬНА АКАДЕМІЯ НАУК УКРАЇНИ
ІНСТИТУТ ПРОБЛЕМ МАТЕРІАЛОЗНАВСТВА
ім. І.М. ФРАНЦЕВИЧА НАН УКРАЇНИ

ТКАЧЕНКО Володимир Григорович

ДИСЛОКАЦІЙНІ МЕХАНІЗМИ ТА МЕТОДИ ЗМІЦНЕННЯ МЕТАЛЕВИХ КРИСТАЛІВ

Англійською мовою

Редактор-коректор *Т.М. Ярмола*

Художнє оформлення *Є.О. Ільницького*
Технічне редагування і комп'ютерна верстка *О.А. Бурдік*

Підп. до друку 27.04.2021. Формат 70 × 100/16. Гарн. Minion Pro.
Ум. друк. арк. 24,21. Обл.-вид. арк. 26,91. Тираж 162 прим. (у т. ч. 150 прим. за державні кошти). Зам. № 6294.

Видавець і виготовлювач Видавничий дім «Академперіодика» НАН України
01024, Київ, вул. Терещенківська, 4

Свідоцтво про внесення до Державного реєстру суб'єктів
видавничої справи серії ДК № 544 від 27.07.2001